

Azərbaycan Milli Elmlər Akademiyası
Fizika-Riyaziyyat və Texnika Elmləri Bölməsi
Fizika İnstitutu

5

Fizika

Cild

XIII

2007

Bakı * Elm

LOCAL AND NONLOCAL CRITERIONS OF RUNAWAY ELECTRONS IN SOLID GASES AND DIELECTRICS UNDER ACTION OF HIGH VOLTAGE PULSES BY SHORT WAVEFRONT

E.D. GURBANOV, I.P.KUZHEKIN

Moscow Power Engineering Institute (Technical University)

Krasnokazarmennaya, 14, Moscow 111250 Russia

A.M. HASHIMOV, A.S. BONDYAKOV

Physics Institute of Azerbaijan National Academy of Sciences,

Az-1143, Baku, Javid str. 33

Present article is devoted to discharge processes in solid gases and dielectrics under influence on discharge gap the high voltage nanosecond pulses. Are considered the local and non-local criterions of run off electrons in gases and formation on the discharge gap the powerful electron beams. Are considered a conversion of diffusive volumetrical discharge to constricted discharge on different interelectrode distance and electrodes geometry, the physical processes in solid dielectrics under influence the high voltage nanosecond pulses. It is presented a quantitative correlations between the electrical pulse parameters, dielectrics properties and space-charge characteristics of pulsed discharges.

1. Introduction

Last time is given enormous attention to development of high voltage pulsed technique for realization of the different researches and applied purposes. At the most fields of industry and technique is observed transition from microsecond high voltage pulses to nanosecond ones. Nano and subnanosecond electrical pulses by on-peak power from MVt up to TVt are used in a number of the most areas of modern technique such as relativistic microwave electronics, super wide-band radio-location, electromagnetic reaction, research of electromagnetic compatibility of the complex systems, underground radio-location, lasers and accelerators power systems and so on [1]. Powerful short pulses are also used in a number of modern developmental physics areas such as controlled nuclear fusion and other large-scale physical experiments.

Particular interest presents study of high voltage nanosecond discharges and their influence on electro physical properties of solid dielectrics [2] and showing up the new phenomena earlier no metering in that materials under influence of high electrical fields.

Development of nanosecond pulsed discharge process is accompanied by infraction of electrons distribution function by energy and appearance of run off electrons capable to realize a collision ionization.

The run off electrons phenomenon in plasma is known a long time ago [3] were carried out the numerical computations [4,5] and analytic treatment for low fields [6]. This phenomenon has an essential importance for diagnostics and admixture's energy-balance in plasma of tokamacs [7].

2. Theory and experimental results in solid gases

Appearance of run off electrons in gases takes on special significance in view of getting the powerful subnanosecond electron beams with record big current amplitude [8].

Space structure of discharge gap's glow during the pulsed discharge process is defined by some factors such as the electrodes geometry, pressure and gas type, inductive and capacitive parameters of generator, disruption voltage of

discharger – peaker [9].

In spite of rapid growth of experimental researches and technical applications [10] of nanosecond gas discharges, transition to the new time scale doesn't entail the corresponding revision of fundamental positions of breakdown classical models developed for conditions near the static ones [10]. But in article [11] are determined the new understanding of nanosecond pulsed discharges.

An electrical breakdown models in solid gases differed in many respects from each other, sometime radically, nevertheless have general fundamental feature: they are local. It means that on given space time (r, t) the average statistical value such as an electrons energy - ε_e , ordered motion speed - v , Townsend ionization factor - α are determined by local field at the same point $E(r,t) = E_o + E_p(r,t)$, where E_o and $E_p = E_{p+} + E_{p-}$ - external field and space charge intensities.

To local models are related to Townsend avalanche generation with γ -processes on cathode and different modifications of single-avalanche streamer model that describes the breakdown processes in solid gases corresponding to right part of Paschen's curve ($pd \gg (pd)_{min}$), where the space charge Z_{cr} and time t_{cr} avalanche progress scales satisfy to correlations:

$$Z_{cr} = \alpha^{-1} \cdot \ln N_e^{kp} \leq d \quad (1)$$

$$t_{cr} \leq \frac{d}{v_-} \quad (2)$$

where N_e^{cr} - electrons quantity on the critical avalanche, d - interelectrode distance.

In classical streamer model can emphasize three main parts: an electrical field strengthening on electron avalanches front and streamers as result of their polarization ($E_f = E_o + E_p$); gas ionization by photons ahead of front; prevalent ionization processes in gas volume in comparison with cathode emission.

As result of field strengthening the electrons energy is become more than $\varepsilon(E_o)$, balanced intensity of external field E_o owing to which the ionization processes are intensified.

A volumetrical photoionization explains the streamers big propagation speed ($>> v_e(E_o)$) that is necessary for propagation of cathode streamer. Is opened to question the nature of radiation initiating the second ionization centers out of initial avalanche [12, 13]. On this article is considered all these questions.

In case of big interelectrode distance even for strong fields, where field intensity exceeds a critical value, Townsend's ionization mechanism is also true and is taking place the γ - processes on cathode and streamers formation by which are described the ionization processes in gases corresponding to right part on Pashen's curve ($pd > (pd)_{min}$).

At that for determination of an average energy E^* , it is necessary to take into account a number of electrons by $E > E_{cr}$, as is shown below:

$$\frac{d(N_e E^*)}{dx} = eEN_e - F(E^*)N_e \quad (3)$$

$$\frac{dN_e}{dx} = \alpha_i \cdot N_e \quad (4)$$

$$\frac{dE^*}{dx} = eE - F(E^*) - \alpha_i E^* \quad (5)$$

where α_i - a collision ionization factor, E^* - electrons average energy.

In formula (5) we can see that even by full neglect of electrons braking in gas $F(E^*)=0$, an average energy of electrons is restricted.

$$E^* < E_{max}^* = \frac{eE}{\alpha} \quad (6)$$

By sufficiently big over voltages ($\Delta > 1$) development of gas discharge process is differed from classical discharge forms in gases.

In strongly overstrained discharge gaps an avalanche-streamer transition is realized on the length of $z_{cr} \sim 100$ mcm. As a result of that is formed a plasma cloud by big conductivity. In strong electrical fields this cloud is polarized.. Then ionization is developed by electrons, escaped from cloud and accelerating in space charge zone. Part of these electrons have very big energy comparable with full kinetic energy $eU=eEd$ and uninterruptedly accelerated up to anode. These electrons efficiently radiate the brake quantum ionizing gas in whole discharge gap and beat out the electrons from electrodes. As a result of that number of the elementary "accelerators" is grown.

At that on fig.1 is shown the Pashen's curve division on three zone: space upper left part curve corresponds to the run off electrons, space between the left and right parts on curve corresponds to electrons multiplication and space below the right part corresponds to electrons drift those couldn't multiply

Were carried out the experiments in uniform and no uniform electrical fields [14] on big pressures and different

gases (nitrogen, air, helium, neon, argon, krypton) without ionization source.

In all gases in no uniform electrical field at the atmospheric conditions under influence of high voltage nanosecond pulses were received the high specific energy up to $1J/cm^3$ and electron beams by record current amplitude.

The run off electrons ensure the propagation speed of ionized field to anode and attendant X-radiation ionizes gas and causes a photoelectric effect on cathode stipulated for motion the cathode streamer.

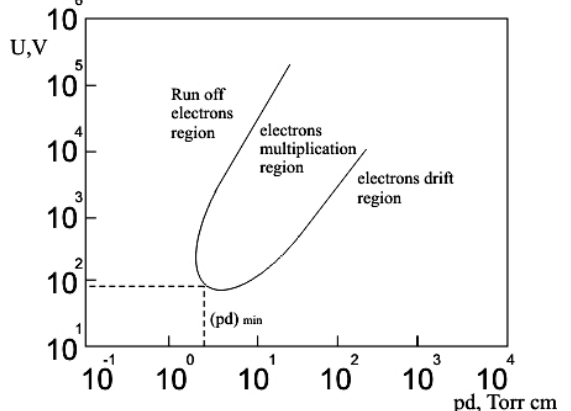


Fig. 1. Dependence of the critical breakdown voltage (U_{kp}) from multiplication an interelectrode distance between the electrodes – d on pressure – p (pd), Pashen's curve.

Our researches were carried out by means of high voltage nanosecond generator on 100 kV with short pulse front 2 ns. Block scheme of an experimental assembly is shown on fig.2.

Voltage pulse was supplied from generator 1 to high voltage electrode – cathode 3 inside of vacuum chamber 2 at atmospheric pressure – $P=760$ Torr and higher were used two cathodes by different radius of curvature – $r_c \sim 1-6$ mm. For getting a volumetrical pulsed discharge glow at atmospheric pressure and higher on cathode by diameter $\varnothing 1$ mm is installed fluoroplastic cap 6. As an anode is used a copperplate 4 and a metal screen 5. Interelectrode distance $\sim d$ is changed over the range $\sim 3-10$ mm. For photographing of the high speed pulsed discharge glow is used an electron-optical camera 7. The total current of pulsed discharge by current shunt 8 is registered on high-frequency oscilloscope TDS-5104. Electron beam's current by Faraday cup and current shunt 9 is also registered on high-frequency oscilloscope TDS-5104.

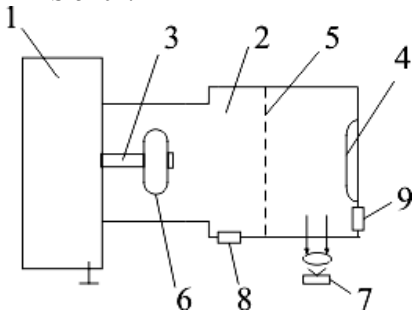


Fig. 2. Block scheme of an experimental assembly 1- high voltage nanosecond generator, 2- vacuum chamber, 3- cathode, 4 - anode, 5- metal screen, 6- fluoroplastic cap, 7- electron-optical camera, 8 – shunt for measuring of discharge total current, 9 – shunt for measuring of electron beam's current.

The cathode and cathode plasma are the sources of run off electrons in air at atmosphere pressure. Dispersion on gas molecules strongly influents on the space distribution of run off electrons. In case of pointed cathode, the interelectrode distance – d greatly influents on the width of run off electrons beams. By increase the - d up to 10 mm beam's diameter reaches $\varnothing \sim 3$ cm. If there are some channels in pulsed discharge taking place on developed work surface, the channels quantity are equal to beams quantity in electron stream behind the anode. The streams structure respond to emitting centers distribution. Plasma bunch on cathode is transformed into constricted channel growing deep into discharge gap by stream of run off electrons. By statistics of that interaction and also initiation of electron avalanches is explained a variety of discharges space forms. When overvoltages factor $\Delta \gg I$, the gas breakdown is initiated by auto electronic emission and the first avalanche reaches a critical size near the initialization point ($Z_{cr} \sim 100$ mcm<< d). As a result is happened the field strengthening of positive space charge E_{p+} and auto electronic emission. Therefore, when $\Delta > I$, the emissive processes play a fundamental role in ionization propagation towards cathode. The high penetrability of run off electrons and X-ray emission reduces to solid gas ionization far off the first ionization center and discharge loses its compact form and has diffusive or multi-channel character. By big overvoltages in solid gases in atmosphere pressure the complex space structure of the nanosecond volumetrical discharges as the constricted channels is explained by electrons acceleration in space charge field getting the possibility to accelerate up to anode.

These electrons radiate the quantum ionizing the gas in whole discharge gap and battered the electrons from electrodes. The space structure of discharge gap's glow as mentioned is determined by some parameters such as an electrodes geometry, interelectrode distance – d , gas pressure - p , parameters of generator. The photography of discharge gap's glow for different distance value – d and electrodes geometry are presented on figures 3-7. On figures a flat copperplate and the metal screen is as an anode and as a cathode is a metal rod by different radiuses of curvature – $r_k \sim 1-6$ mm. On fig. 3 is shown that in atmosphere pressure, $U_{gen}=100$ kV and $d=10$ mm is realized the diffusive volumetrical discharge



Fig.3. $r_k=6$ mm, anode - copperplate, $U_{gen}=100$ kV, $P=760$ Torr, interelectrode distance $d=10$ mm



Fig.4. $r_k=6$ mm, anode - metal screen, $U_{gen}=100$ kV, $P=760$ Torr, interelectrode distance $d=5$ mm

On the cathode are formed the plasma bunches by visible dimension $l_p \sim 2$ mm<< d , but remaining space up to anode is filled up by diffusive glow. The cathode plasma formations significantly are not uniform.

On fig. 4 is shown that at atmosphere pressure and interelectrode distance – $d=5$ mm there are some plasma bunches on the cathode and is realized transition from diffusive volumetrical discharge to constricted discharge and constricted channels quantity is equal to plasma bunches quantity on cathode

We have to note, when we decrease an air pressure, the plasma bunches dimension on cathode is grown and luminosity is decreased.

When $P < 0.5$ Torr the discharge phenomena on the case of planar electrodes with developed work surface aren't observed, but if cathode is a metal rode by different radiuses of curvature, the plasma bunches are appeared on its surface and their size is significantly smaller in comparison with atmosphere conditions - $P=760$ Torr.

On Fig. 5 when the cathode radius of curvature is smaller $r_k \sim 1$ mm, an interelectrode distance $d=10$ mm, $U_{gen}=100$ kV and $P=760$ Torr, an intergrowth of the bright constricted channel and overlap of whole discharge gap is observed.



Fig.5. $r_k=1$ mm, anode- metal screen, $U_{gen}=100$ kV, $P=760$ Torr, interelectrode distance $d=10$ mm



Fig.6. $r_k=1$ mm, anode- metal screen, $U_{gen}=100$ kV, $P=760$ Torr, interelectrode distance $d=3$ mm

On Fig. 6 by decrease of an interelectrode distance up to $d=3$ mm the enlargement of discharge channel is observed. Diffusive cover in that case is not appeared.

In case of sharply no uniform field is fixed only one bright channel and plasma bunch. By increase of the field uniformity the channels and plasma bunches quantity are grown.

On fig. 7 is shown a glowing ball, formed by pressures more than atmospheric ($P=3.5$ atm) and interelectrode distance – $d=3$ mm. By means of fluoroplastic cap, put on etal rod by diameter $\varnothing 1$ mm and high pressure in vacuum chamber the pulsed discharge channel looks like glow ball.

By multiple overvoltages in volumetrical discharges in air ionization emission reaches the light speed and the current pulse with a high rate of pulse rise ~ 10 TA/s is realized. In that case a pulse front is $\tau_l < 0.5$ ns and upper bound of current is $I_m \sim 1.5$ kA. By decrease of the interelectrode distance – d the volumetrical discharges pass into constricted channel and the current amplitude I_m and channels conductivity are grown.

Also we have to note the importance of the breakdown delay time parameter – t_d relatively to moment of voltage pulse supply from generator that characterizes a speed of ionization processes development.

When $d < 10$ mm and $U_{gen} > 180$ kV independently from cathode geometry in solid gases a big conduction current is already appeared on the front of voltage pulse and $t_d < \tau_l < \tau_{gen} < 0.6$ ns, where τ_l is an acceleration time of voltage pulse at the discharge gap.



Fig. 7. $r_k=1$ mm, anode - metal screen, $U_{gen}=100$ kV, $P=3.8$ atm, interelectrode distance $d=10$ mm

So speed of ionization propagation $V_I > d/t_d > d/\tau_{gen} > 2.5 \cdot 10^9$ cm/s is more than speed of streamers propagation [15, 16]. When $U_{gen} < 180$ kV in relatively uniform field we can register the breakdown delay interval parameter – $t_d \sim 2$ ns for cathodes radius of curvature $r_c \sim 20$ mm. By decrease of pressure this parameter t_d is grown.

Thus the mechanism of discharge development in solid gases by big overvoltages can be presented in the following way. As a result of auto electronic emission the initial electrons from cathode form an avalanche that on pulse front during some picoseconds on the length $Z_{cr} \sim 100$ mcm transforms into anode streamer. Before the voltage pulse reaches the maximal value, an electrical field intensity on the streamer front reaches the critical value E_{cr} . On that time on streamer front are formed the run off (high power) electrons and is realized the mechanism of polarized self-acceleration reducing to generation the powerful subnanosecond pulses of electrons by anomalous energy (100-200 keV). These electrons ionize a gas and form the volumetrical discharges on discharge gap in relatively weak non-uniformity field. In strongly no uniform fields the volumetrical discharge is only formed as a result of gas ionization by run off electrons stream. Because an interelectrode distance – $d > Z_{cr}$ the cathode discharge is caused only by photoelectric effect. Local field strengthening on cathode by positive space charge reduces to formation of plasma bunch during $t_d < 1$ ns on the first avalanche place. From this moment are begun formation and development of cathode spot and exploding processes on cathode by transition to exploding electronic emission. On sufficiently small interelectrode distance the plasma bunch is constricted and advanced over ionized gas by run off electrons. As result the high local intensity of electrical field on the channel head where is concentrated a negative space charge, this channel is accelerated as a single whole. In spite of the fact that reached power density, input in discharge gap is ~ 100 MVt/cm³ plasma is remained low-temperature, weakly ionized in all discharges development stages because there is the weak coupling of run off electrons with gas.

Thus on big overvoltages the run off electrons effect plays a fundamental role in breakdown mechanism of pulsed discharges in solid gases. Participation of run off electrons in breakdown process in solid gases is determined by displacement of minimum on Pashen's curve $U(pd)$ to right by overvoltage growth (shortening the pulse front τ_{gen}) for big pd.

3. Pulsed discharge researches in solid dielectrics

By influence of high voltage nanosecond pulses on solid dielectrics is also observed a formation process of high power electrons. During an influence of powerful short pulses it is necessary to note the propagation speed of pulsed discharge, parameters of plasma condition in discharge channel, its geometrical sizes and others. Already it is insufficient to know only parameters of discharge gap and high voltage pulse.

The direct measurement of propagation speed of discharge channel by electron-optical chronogram was determined that the sonic speed is a limit for propagation speed of discharge channel from cathode and anode i.e. $v_c < c_o < v_a$ where v_c – discharge speed from cathode, v_a – discharge speed from anode, c_o – sonic speed in solid dielectrics [17].

Change of that boundary "from above" and "from below" by change the pulse parameters (U , dU/dt) were unsuccessful.

Transition mechanism from subsonic initial channel to supersonic anode channel demands an especial study.

Discharge speed from anode - v_a is mainly determined by origin discharge voltage U_0 and corresponding momentary value dU/dt , but discharge speed from cathode - v_c depends only on U_0 . In that case an influence of interelectrode distance – d and momentary value dU/dt is absent. This can be related with instability of dielectrics phase boundary with its melt. Supersonic speed of change of boundary curvature under influence of very high electrical fields reduces to formation the shock wave that is result of turbulent energy-release by electron injection from valence band to conducting band and formation the complex "shock wave + energy-release zone" named as electron detonation.

Run off electrons took part in collision ionization of valence band in solid dielectrics have anomalous energy and just only they explain the physical mechanism of turbulent electron injection to conducting band under influence of high voltage nanosecond pulses on these materials. As result of this is formed dense non-ideal plasma by big pressure on self-destruction which is liberated energy accumulated in an ionic subsystem.

Ionization degree of electron injection will be determined by correlation [18],

$$\chi_e = \omega \frac{\Delta}{v_a} \quad (7)$$

where $\omega = \frac{n}{N}$ - ionization probability c^l , n – quantity of electron-hole pairs formed in time unit and volume unit, N – valence electrons quantity. Ionization probability ω depends from forbidden gap and defined as

$$\omega = \frac{n}{N} = \frac{(eEd^*)^2}{2\pi\hbar E_D^*} \exp\left(\frac{Ed^*}{eEd^*} \ln \frac{1}{\alpha}\right) \quad (8)$$

where α - ratio of valence band to conducting band, E_D^* and d^* - accordingly an effective value of forbidden gap and lattice constant by shock compressing.

By compressing of solid dielectrics dependence between forbidden gap and plasma pressure is presented by following formula:

$$E_D^* = E_{D_0} - a_p \cdot p \quad (9)$$

where $a_p = \gamma \cdot \kappa$ - pressure factor $J^* Pa^{-1}$, κ – compressibility factor, γ - proportionality factor.

These expressions allow to quantitatively estimating the dependence of plasma pressure P , ionization factor ω and E_D^* from speed of an electron detonation wave in solid dielectrics.

Ascertained regularities allow us to use conceptions and methods of high-density energy physics for description the dynamics and matter state parameters in discharge channel on transition front from subsonic to supersonic speed.

It is evident that speed of this process at the different dielectric mediums and its initial parameters (U_0 , dU/dt) present a big interest.

It is necessary to carry out a number of experiments and theoretical study for proper quantitative consideration an influence of compressibility on electron injection process in solid dielectrics. First of all it is concerned to study an influence of plasma pressure on electron structure of large band dielectrics. It will allow to more rigorous determination of pressure factors value a_p . Can say that here this dependence will be nonlinear in a large pressure interval.

So were determined the quantitative correlations between the electrical parameters of process, physical properties of dielectrics, matter parameters in energy-release zone and space-charge characteristics of pulsed discharges under influence of high voltage nanosecond pulses on solid dielectrics.

4. Conclusion

In presented article are considered the physical processes in pulsed nanosecond discharges in solid gases and dielectrics. The local and non-local criterions of run off electrons (high power) in solid gases are shown.

To produce the pulsed discharge figures by different electrodes geometry and interelectrode distance. Is shown transition of volumetrical diffusive discharge to constricted discharge formed due to run off electrons created on cathode plasma bunches.

The electrical breakdown process in solid dielectrics under influence of high voltage nanosecond pulses, electron injection process from valence band to conducting band by run off electrons by anomalous energy were considered.

Was determined the quantitative correlations between the pulse electrical parameters and physical properties of solid dielectrics and their interference on each other. Consideration of that interference can produces to correction of existent and detection the new before no registering phenomena in solid dielectrics.

-
- [1] I.V. Grekhov, G.A.Mesyats: Usp.Fiz.Nauk, 175, 2005, № 7, 735.
 - [2] Yu.N.Vershinin: Proceedings of RAS, 2, 2003, 152.
 - [3] R.G. Giovanelly: Philos. Mag. 40, 1949, 206.
 - [4] H. Dreicer: Phys.Rev. 115, 1959, 238.
 - [5] R.M. Kulsrud: Phys.Rev. Lett. 31, 1973, 690.
 - [6] A.V. Gurevich: IETP, 39, 1960, 1296.
 - [7] V.S. Marchenko, S.I. Yakovlenko: PP, 5, 1979, 590.
 - [8] V.F. Tarasenko, S.I. Yakovlenko: UFN, 174, 2004, № 9, 954.
 - [9] L.P. Babich, T.V. Loyko, V.A. Tsukerman: Usp. Fiz. Nauk, 160, 2004, № 7, 49.
 - [10] G.A.Mesyats, Yu.I. Bichkov, V.V. Kremnev: Usp. Fiz. Nauk, 107, 1972, 301.
 - [11] L.B. Loeb: Fundamental processes of electrical discharge in gases. (New York, 1939)
 - [12] Yu.L. Stankevich: JETP Lett, 40, 1970, 1476.
 - [13] K. Yoshida, H. Tagashira: J.Phys.Ser.D 9, 1976, 491.

- [14] *I.D. Kostyrya, V.S. Skakun, V.F. Tarasenko, A.M. Tkatchev, S.I. Yakovlenko:* JETP Lett., 30, 2004, №10, 31
- [15] *G. Reter:* Electron avalanches and breakdown in gases. Mir. Moscow, 1968.
- [16] *E.D. Lozansky, O.B. Firsov:* Spark theory. Atomizdat, Moscow, 1975.
- [17] *A.M.Gashimov, R.N. Mekhtizadeh, E.J.Gurbanov, A.S. Bondyakov:* Int. Conference “Physics-2005”, Baku, 2005, 450.
- [18] *Yu.N.Vershinin, A.M.Gashimov, E.J.Gurbanov:* SEAE, 2005, №.6, 72.

E.D. Qurbanov, İ.P. Kujekin, A.M. Həşimov, A.S. Bondyakov

**YÜKSƏK GƏRGİNLİKLİ QISA İMPULSLARIN BƏRK CİSİM HALINDA OLAN DİELEKTRİKLƏRƏ VƏ
YÜKSƏK SIXLIQLI QAZLARA TƏSİRİ ZAMANI ELEKTRONLARIN HƏRƏKƏTİNİN LOKAL VƏ
QEYRİ-LOKAL KRİTERİYALARI**

Məqale yüksək sixlıqli qaz mühiti və bərk cisim halında olan dielektriklərdə, qazboşalması aralığına yüksək gərginlikli nanosaniyə impuls gərginlikləri vasitəsilə təsir etdikdə, qazboşalması proseslərinin tədqiqinə həsr olunmuşdur. Elektronların qaz mühitində hərəkətinin lokal və qeyri-lokal kriteriyalarına və qazboşalması aralığında güclü subnanosaniyə elektron dəstinin əmələ gəlməsinə baxılmışdır. Bərk cisim halında olan dielektriklərdə katod və anod yaxınlığında plazma kanalında və oxun dinamikasının əmələ gəlməsi şərtləri müəyyənləşdirilmişdir. İmpuls qazboşalmasının elektrik parametrləri, dielektrikin xüsusiyyətləri və termodinamik xarakteristikaları arasında əlaqələr təqdim olunmuşdur.

Э.Д. Курбанов, И.П. Кужекин, А.М. Гашимов, А.С. Бондяков

**ЛОКАЛЬНЫЙ И НЕЛОКАЛЬНЫЙ КРИТЕРИИ УБЕГАНИЯ ЭЛЕКТРОНОВ В ПЛОТНЫХ ГАЗАХ И
ТВЕРДЫХ ДИЭЛЕКТРИКАХ ПРИ ВОЗДЕЙСТВИИ КОРОТКИХ ИМПУЛЬСОВ ВЫСОКОГО
НАПРЯЖЕНИЯ**

Настоящая статья посвящена разрядным процессам в плотных газах и твердых диэлектриках при воздействии на разрядный промежуток высоковольтных наносекундных импульсов высокого напряжения. Рассмотрены локальный и нелокальный критерии убегания электронов в газах и формирование в газовом промежутке мощных субнаносекундных электронных пучков. Анализируются случаи перехода диффузного объемного разряда в контрагированный разряд при различных конфигурациях электродов и расстояниях между ними. Сформулированы условия образования плазменного канала и его динамики у катода и анода в твердых диэлектриках. Представлена количественная связь между электрическими параметрами импульсного разряда, свойствами диэлектрика и термодинамическими характеристиками.

Received: 17.08.07

SPECTRAL CHARACTERISTICS OF ANTIREFLECTIVE OPTICAL COATINGS WITH COMPLEX REFRACTIVE INDEX

R.A. KARAMALIYEV

Baku State University, Z. Khalilov str., 23, AZ-1148, Baku, Azerbaijan

R.M. KASIMOV

*Institute of Chemical problems of National Academy of Sciences,
H.Javid av., 29, AZ-1143, Baku, Azerbaijan*

Spectral characteristics of reflection of optical waves by system an absorbing coat-metal at the selective thickness of coating corresponding requirements of a total absorption of incident radiation in it are considered.

1. Introduction

Last years the optics of antireflecting coatings represents the significant practical interest. The problem of the full suppression of reflection of optical waves from absorbing coatings is especially actual one. However, known computational methods of antireflecting coatings are valid only when optical media are completely transparent. As is known, in this case refractive indices of all media can have only real values [1-3].

One of the interesting problems in thin-film coatings optics is that of analysis of the spectral characteristics of a multilayer whose optical constants and thickness are known. For microwave region of spectrum the effect of reflectionless absorption in layered system an absorbing dielectric-metal both theoretically and experimentally was investigated in [4,5]. This method of investigation was extended to include optical wavelengths in [6].

In the present paper we have developed the research technique of antireflective absorbing optical coatings presented in [6] for to investigate their spectral characteristics.

2. Reflection characteristics of a two-layer dielectric-metal structure

In order to find a formula for the reflectance of a two-layer dielectric-metal structure illuminated by a parallel beam

of light at wavelength λ , we must consider the multiple reflections of light at each surface of the structure and perform a multiple beam summation. Incident light is considered normally and plane polarized. The reflected complex amplitude R^* is given by

$$R^* = \frac{r_1 e^{i\varphi_1} + r_2 e^{i\varphi_2 - 2ikl}}{1 + r_1 r_2 e^{i(\varphi_1 + \varphi_2) - 2ikl}} \quad (1)$$

where l is the thickness of the absorbing coating; r_1, r_2 , φ_1, φ_2 are modules and phases of reflection coefficients for first and second surfaces of the layer, respectively; k is complex wave number and for materials with complex refractive index equals

$$k = \frac{2\pi(n - i\chi)}{\lambda} \quad (2)$$

where n is the refractive index of the layer material, χ is the extinction coefficient of the material. Modules and phases of reflection coefficients are given

$$n = \sqrt{\frac{(1-n)^2 + \chi^2}{(1+n)^2 + \chi^2}}, \quad \varphi_1 = \pi - \arctg \frac{2\chi}{1-n^2 - \chi^2}, \quad r_2 = 1, \quad \varphi_2 = \pi. \quad (3)$$

The expression for energy reflectance may be obtained from equation (1)

$$R^2 = \frac{\left(r_1 - r_2 e^{-\frac{4\pi\chi l}{\lambda}}\right)^2 + 4nr_2 e^{-\frac{4\pi\chi l}{\lambda}} \cos^2\left(\frac{2\pi nl}{\lambda} + \frac{\varphi_1 - \varphi_2}{2}\right)}{\left(1 - nr_2 e^{-\frac{4\pi\chi l}{\lambda}}\right)^2 + 4nr_2 e^{-\frac{4\pi\chi l}{\lambda}} \cos^2\left(\frac{2\pi nl}{\lambda} - \frac{\varphi_1 + \varphi_2}{2}\right)} \quad (4)$$

We shall introduce the suggestion that the specified zero minimum of function $R(l)$ is realized at thickness of a layer of the absorbing substance a little differing from quantities of multiple $\lambda/4n$

$$\frac{l}{\lambda} = \frac{1}{n} \left(\frac{2N-1}{4} + \Delta \right) \quad (5)$$

where N is ordinal number of the minimum of $R(l)$ dependence corresponding to the antireflective absorption, Δ is the quantity to be determined by optical parameters of absorbing coating material.

One can see from equation (1) that the condition $R=0$ will be realized if we get

$$\ln \frac{r_2}{r_1} = \frac{\chi}{n} [\pi(2N - 1) + \varphi_2 - \varphi_1] \quad (6)$$

$$\frac{l}{\lambda} = \frac{1}{n} \left(\frac{2N - 1}{4} + \frac{\varphi_2 - \varphi_1}{4\pi} \right) \quad (7)$$

$$\Delta = \frac{\varphi_2 - \varphi_1}{4\pi} \quad (8)$$

From equations (6)-(8) one can see that to obtain non-reflective absorption on the coating layer for the selective wavelength, layer thickness and its optical parameters are required.

The dispersion theory gives us the connection between optical parameters n , χ and complex dielectric constant ε . The real ε' and imaginary ε'' parts of ε may be expressed by relations

$$\varepsilon' = n^2 - \chi^2, \quad \varepsilon'' = 2n\chi \quad (9)$$

In the first approximation we can obtain the next relation between ε' and ε''

$$(\varepsilon' - n_\infty^2)^2 + (\varepsilon'' - b)^2 = b^2 \quad (10)$$

where

$$b = \frac{2\pi q^2 N_0}{m\gamma\omega_l}, \quad \omega_l^2 = \omega_0^2 - \frac{4\pi q^2 N_0}{m} \quad (11)$$

n_∞ is refractive index far from the resonance frequency ; q, m are charge and mass of electron , N_0 is concentration, γ is damping coefficient, ω_0 and ω_l are frequencies.

In this approximation the frequency ω which the effect of non-reflective absorption takes place may be determined from the next equation

$$\frac{\varepsilon''}{\varepsilon' - n_\infty^2} = \frac{\gamma}{2(\omega_l - \omega)} \quad (12)$$

Let us illustrate the results of this approach for dye solution of rhodamine. The absorption spectrum of rhodamine presented in fig.1.

Using optical parameters of dye solution $\gamma, N_0, \omega_l, n_\infty$ we can calculate layer thickness l_0 , refractive index n and extinction coefficient χ for a given incident optical wavelength. The Table of these selective parameters was presented in [6].

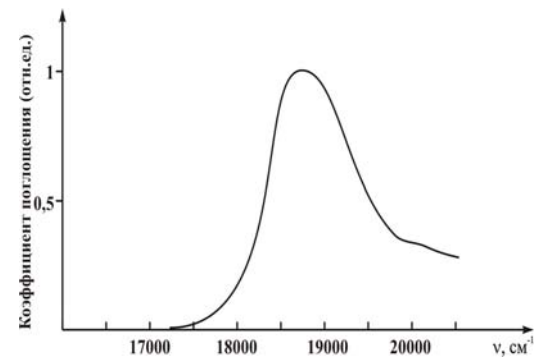


Fig.1. The absorption spectrum of rhodamine.

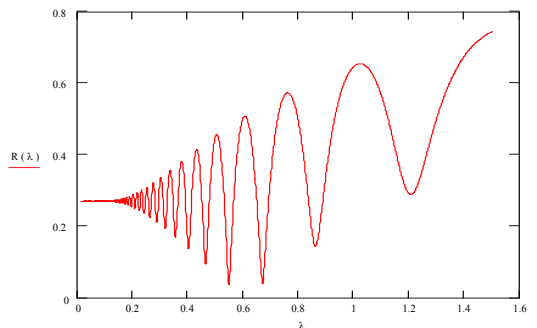
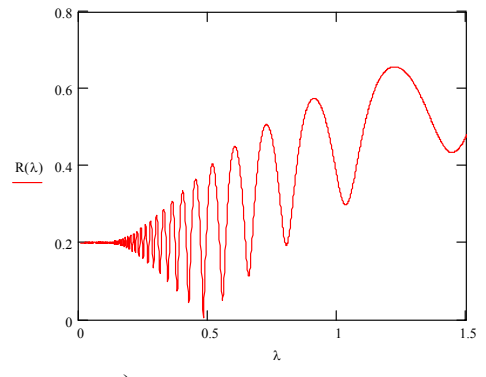
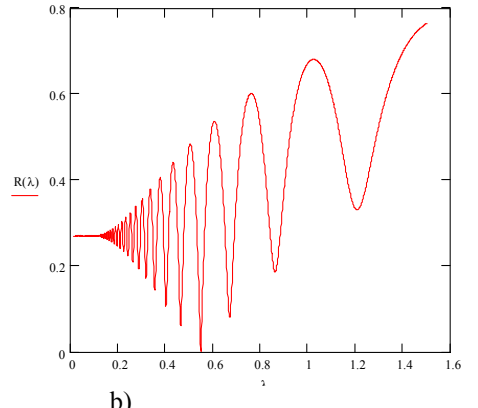


Fig.2. Absolute value of reflection coefficient R vs. of wavelength in the two-layer dielectric-metal structure: layer thickness l and wavelength λ is given in mcm, $r_2=1$, $\chi=0.08$, $n=1.7$, $l=0.68..$



a)



b)

Fig.3. Absolute values of reflection coefficient R vs. of wavelength in the two-layer dielectric-metal structure: layer thickness l and wavelength λ is given in mcm, $r_2=1$, a) $\chi=0.08$; $n=1.73$; $l=0.724$; $N=5$; b) $\chi=0.07$; $n=1.72$; $l=0.884$; $N=6$

In fig.2 we represent dependence of reflection coefficient amplitude R on incident wavelength λ for non-selective values of optical parameters of the rhodamine. One can see that reflection coefficient R is an oscillating function of incident wavelength which asymptotically approaches its limit value $R=1$. There are two regions in the $R(\lambda)$ dependence which differ by character of changing of extrema in increasing of wavelength of incident light. In the left domain decreasing of wavelength lead to a decreasing maxima and increasing minima of function R up to the complete coincidence of these parameters with limit R at large value of layer thickness. Unlike this case, in the right domain of function $R(l)$ we observe increasing both maxima and minima of function R which approaches to 1. It is clear that a proper choice of dielectric properties of the optical coating, the boundary of the left and right regions may coincide with one of the minima of function $R(l)$ taking zero value. It follows from this that existence conditions for this so-called zero minimum of function R will determine conditions for the total (non-reflective) absorption of the optical radiation by the coating-metal structure under study.

The method of computation of selective values of l , n and χ for to arise non-reflective absorption in the optical coating was presented in [6]. Using these optical parameters calculated for dye solution of rhodamine we have obtained spectral characteristics of this optical coating (fig.3a,b). They are gained at thickness of a layer $l = 0.724$ (a) and $l = 0.884\text{mkm}$ (b) corresponding to the fifth and sixth zero minimums of function $R(l)$. To these specified selective values of layer thickness of a coating correspond selective values of optical coefficients of a coating $n=1.73$, $\chi=0.08$ (a) and $n=1.72$, $\chi=0.07$ (b).

3. Conclusion

As follows from the analysis of the gained spectral characteristics of the rhodamine a total or non-reflective absorption of optical radiation may be observed for a frequency band where the wave dispersion of this substance takes place. Thus, the total absorption may be realized at the infinite number of discrete values of a layer thickness of a coating.

-
- | | |
|--|--|
| <p>[1] <i>L.M. Brebovskih.</i> Waves in layered media, M., 1957(Russian)</p> <p>[2] <i>M. Born, E.Volf.</i> Principles of optics, M., 1970.</p> <p>[3] <i>Sh.A. Furman, A.V. Tikhonravov.</i> Basics of Optics of Multilayer Systems, Editions Frontieres, <i>Gif – sur – Yvette</i>, France, 1992</p> <p>[4] <i>R.M. Kasimov, M.A. Kalafi, Ch.O. Kajar, E.R. Kasimov.</i> J. Engineering-physics, v.71, 2, 1998, pp.282-285 (Russian)</p> | <p>[5] <i>R.M. Kasimov, M.A. Kalafi, E.R. Kasimov etc.</i> J. Technical physics, v.66, №5, 1996, pp.167-171 (Russian)</p> <p>[6] <i>R.M. Kasimov, R.A. Karamaliyev, V.M. Salmanov.</i> Trans.of Acad.of Science of Azerb., ser. of phys-tech. and math.sciences v.26, №5, 2006, pp.118-123 (Russian)</p> |
|--|--|

R.Ə. Kərəməliyev, R.M. Qasımov

KOMPLEKS SINDIRMA ƏMSALLI ƏKS ETDİRMƏYƏN OPTİK ÖRTÜKLƏRİN SPEKTRAL XARAKTERİSTİKALARI

Udan örtük-metal sistemində düşən şüalanmanın örtükdə tam udulması şərtlərinə uyğun seçilmiş qalınlıqları üçün optik dalğaların əks olunmasının spektral xarakteristikaları öyrənilmişdir.

Р.А.Карамалиев, Р.М.Касимов

СПЕКТРАЛЬНЫЕ ХАРАКТЕРИСТИКИ АНТИОТРАЖАЮЩИХ ОПТИЧЕСКИХ ПОКРЫТИЙ С КОМПЛЕКСНЫМ ПОКАЗАТЕЛЕМ ПРЕЛОМЛЕНИЯ

Рассмотрены спектральные характеристики отражения оптических волн системой поглощающее покрытие-металл при избирательных толщинах покрытия, соответствующих условиям полного поглощения в нем падающего излучения.

Received: 09.09.07

RAMAN SPECTRA IN HETEROSTRUCTURES Ge/Ge_{1-x}Si_x

Sh.M. ABBASOV

Institute of Radiation Problems, NAS Azerbaijan, Az141 Baku, F.Agayev st. 9

A.S. BAYTSAR

Lvov National University named after I.Franko. Ukraine, Lvov, Bender st. 12/13

Z.A. IBRAHIMOV, K.T. AGAVERDIYEVA, L.A. TAIBOV, U.F. FARAJOVA

National Academy of Aviation

The structure studied in this work has been obtained by the method MLE on Ge substrates. The parameters of the samples were determined by method of x-ray structure analysis. The method of combined light scattering spectroscopy was used for the regulation of the content.

At modern stage of scientific and technological revolution special emphasis is placed on the advancement of those fields of science the achievements of which define the wide prospect of technological development. These fields of science include semiconductor physics, one of the main tasks is search, study and modification of crystal properties with high values of applied-physics characteristics in order to develop new materials promising different technological applications.

Solid solutions of Ge and Si are of great interest from scientific and technological aspect. This interest is conditioned by multiple unique properties: complete solubility, continuity of electrical properties' change, resistance against thermal actions, large energy gap width, high fusion temperature, mechanical strength, resistance against the effect of high-energy particle bombardment and others.

At present it was experimentally showed that Ge and Si really form solutions not only in liquid state but also in solid state and the quantity of lattice parameter of Ge_{1-x}Si_x solid solutions change almost linearly with the change of solution and alloy composition.

The interest to the study of defectless films of Ge_{1-x}Si_x solid solutions at substrates of Ge is connected with practical significance of such structures for developing of transistors with high charge carrier mobility in channel. In such devices the channel has thin (10 nm) stressed layer of Si and Ge grown in buffer layer from solid solution. At the result of significant mechanical stress stretching for Ge (constriction for Si) leading to splitting of valley, charge carrier mobility can increase for several times the value of unstressed material [1]. As vibration spectrum of lattice depends substantially on atomic composition of films and amount of mechanical deformation in them and are considered relevant for Raman spectroscopy (RS) to evaluate these parameters.

Raman spectroscopy is a rapid, informative and nondestructive technique. The first analysis of the composition and mechanical stress in Ge_{1-x}Si_x solid solutions were carried out in the 60s of the last century, the technique improved and developed [1-3] but there still remain methodical difficulties bringing to ambiguity in interpreting of obtained results.

So the purpose of the work is formulation of refined parameter description of the dependence of intensity and position of Raman scattering peaks on the composition and permanent and mechanical deformation in the films of

Ge_{1-x}Si_x solid solutions on the substrates of Ge with orientation (100).

Experimental samples were developed with application of molecular beam epitaxy (MBE) on the substrates of Ge with orientation (100). After standard procedure of chemical cleaning the substrate of Ge charged into growing vessel MBE. Disposal of protective and chemically applied germanium was conducted at the temperature 650-700°C in low flow of Ge (0.02nm/s). The next stage was growing of buffer layer of Ge the thickness of which was 50 nm with the purpose of obtaining of maximum pure surface of Ge (100) and this had superstructure transformation such as 2x1. After observing such surface transformation film growth of Ge_{1-x}Si_x solid solutions was realized with the help of DBE, for the obtaining of which the method of low-temperature MBE had been used [4,5]. Growth rate of Ge_{1-x}Si_x solid solutions was about 0.1nm/s. The thickness of the films varied between 250 and 500 nm. The composition and residual mechanical stress in obtained structures were checked by the method of X-ray diffraction. Analysis of rocking curves of X-ray diffraction taken in several allowed reflections for Ge (for example, (113) and (004)) was used for this purpose.

Peculiarity series were detected during thermal treatment of deposited Ge_{0.85}Si_{0.15}. Films of solid solutions Ge_{0.85}Si_{0.15} are extremely resistant against thermal annealing. Condensates obtained at the temperature $T_n=490\text{K}$ carried quasi-amorphous character. At the temperature range 350-450K they carry semiconductor character of conductivity with thermal activation energy which equals to 0.052eV. This value was determined according to inclination of graphics $\lg \sigma=f(1/T)$ constructed for experimental values, at the temperature regions 450-550K, 550-680K semiconductor character of conductivity remains unchanged but activation energy slightly increases and reaches to 0.096eV. At these temperature regions three sections are observed with more abrupt change of electrical conduction (350-420K, 510-540K, 590-620K) which are responsible for crystallizing process realized in condensates.

Crystallization kinetics and thermal stability were studied by heating amorphous films directly in electron microscope column UEMV-100K using adapters PRON-2 (fig.1). At the same time thermal stability of amorphous state was determined with the appearance of diffuse maximums of amorphous phase on the background which are more

intensive than diffraction reflections of crystalline phase. Films formed at the substrates in the process of deposition at the room temperature and at the temperature 490K.

For example, in Fig. 1 sequential stages of structural transformations in amorphous films were given. Amorphous films Ge_{0.85}Si_{0.15} don't be in equilibrium in initial state but they relax to metastable state. At that with the increase of temperature annealing of defects, change of free volume and short-range topological order occur too, but composite order remains unchanged.

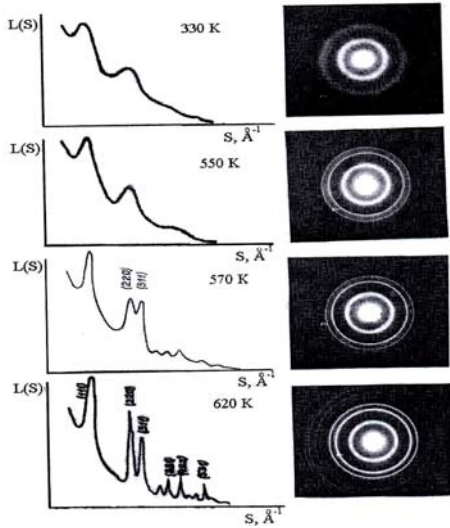


Fig. 1. Crystallization kinetics of films of solid solutions Ge_{1-x}Si_x (x=0.15).

In order to study thin films Ge_{1-x}Si_x by the method of Raman scattering it would be better to use wave-lengths of laser radiation of blue-green range in consequence of light absorption's shallow depth (less than 10nm). But Raman spectra have data only on upper layer.

Raman spectra were registered at room temperature with the help of automatic plant on the basis of spectrometer DFS-52 using lines of Ag-laser 514.5 nm.

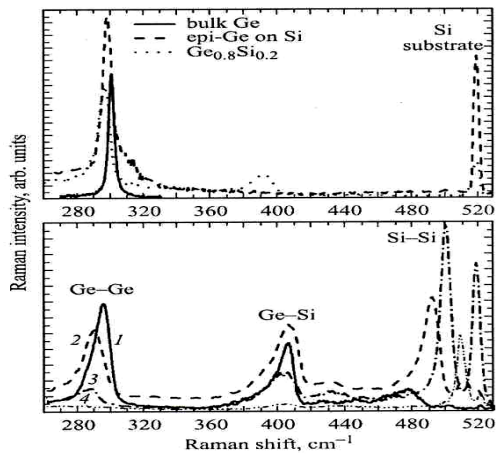


Fig. 2. Raman spectra of relaxed germanium films (dashed line) and solid solutions Ge_{1-x}Si_x (dots) are shown above. For comparison spectrum of bulk germanium (full line) are shown too. Raman spectra of the films of solid solutions Ge_{1-x}Si_x are given below.

In fig.2 Raman spectra of pure germanium films and germanium-silicon solid solutions were shown at frequency

ranges of optical oscillations Ge-Ge (about 300 cm⁻¹), Ge-Si (about 400 cm⁻¹) and Si-Si (about 500 cm⁻¹).

It is seen that peaks of Raman scattering on oscillations Ge-Ge –coupling films of silicon grown on germanium substrate shift to the side of low frequency (approximately for 2cm⁻¹) and broadened. For silicon and germanium tensile stress shifts phonons' frequency to the side of low frequency. Tensile stress in the films of silicon and germanium may occur at cooling of heterostructures due to different coefficients of thermal expansion of germanium and silicon. If structural stress was relaxed in growth process at epitaxial temperature, then tensile stress may occur in the film at cooling of the sample. Observed high-frequency arm may be conditioned by the presence of local mechanical compression stress near dislocations. On spectrum of Ge_{1-x}Si_x films you can see peaks from scattering to coupling vibration Ge-Si (~395cm⁻¹).

In some works authors tried to determine the composition of films according to the state of Raman scattering peaks [4-6]. The basic difficulty of this technical approach is that state of peaks depends on mechanical stress (shift may reach 17cm⁻¹ for the peak of Ge-Ge and 35cm⁻¹ for the peak of Si-Si). Another difficulty is that if the composition of silicon is small in heterostructures, Raman scattering peaks can't be seen in coupled vibrations of Si-Si and its state can't be determined.

Numerous simulations of Raman spectra were conducted to determine the dependence of peaks' state. Due to cyclic and boundary conditions natural frequency and eigenvectors of oscillation were calculated in Ge-Si solid solutions basing on Bohr model, then according to the obtained data Raman spectra were calculated basing on Wolkenstein's additive bond polarizability model [6]. Coupling constants of hardness for germanium in Bohr model were determined by approximation of computational phonon dispersion in bulk material to experimental data obtained according to the one on neutron scattering [7]. As phonon dispersion both for germanium and silicon are very identical, mass substitution method was used to construct Ge-Si heterostructure. Solid solution was simulated on the basis of random filling of unit cell by germanium and silicon atoms with necessary relationship x. In order to avoid the influence of periodical boundary conditions quite big unit cell containing 432 atoms was chosen for calculations.

Relation of derived coupling polarizability for germanium and silicon was defined on normalized relationships of Raman scattering intensity to scattering volume for germanium and silicon. More detailed calculations were given in the works [8-10].

According to literary data state of Raman scattering peaks on optical phonon for bulk germanium are 300-302cm⁻¹. As for the germanium GES-40 studied by us, the state of the given peak was 300.3 cm⁻¹. Dispersion of optical phonons has such character that localization effects make their frequencies decrease. Phonons having frequencies peculiar to optical coupling oscillations Ge-Ge scatter and damp by more light atoms and become local ones.

It was established that electrical conduction of the films of Ge_{0.85}Si_{0.15} solid solutions at high temperature (300-500K) carries band-to-band conductivity character.

At the result by determination of parameters and by the method itself it was shown that the composition and mechanical stress in heterostructures Gt/Ge_{1-x}Si_x can be defined on the basis of Raman scattering data.

- [1] *Sh.M. Abbasov.* The influence of irradiation on electrophysical, optical and photoelectrical properties of GE-Si solid solutions. Baku. Edit. "Science" 2003. 208p.
- [2] *M.I. Alonso, K. Winer.* Phys. Rev., 1989 iss.39, p.10056.
- [3] *J.C. Tsang, P.M. Mooney, F. Dacol,* J.Appl. Phys. 1994, 75, p.8098.
- [4] *L.S. Palatnik, M.Y. Fuks, V.M. Kosevich.* Formation mechanism and structure of condensed films. Moscow. Science., 1972. 319 p.
- [5] *V. Srivastava, K. Joshi,* Phys. Rev. 1973. Iss.8.p. 4671.
- [6] *M.M. Wolkenstein.* DAN. The USSR. 1971. 32. 185.
- [7] *Sh.M. Abbasov, Y.T. Agaverdiyeva, T.I. Kerimova, U.F. Farajova.* Semiconductor Physics. Quantum Electronics, Optoelectronics, 2006. v. 9, №3, p.22-24.
- [8] *V.A. Volodin, M.D. Efremov, A.I. Nikiforov, D.A. Orehov, O.P. Pchelyakov, V.V. Ulyanov.* FTP, 2003. 37. p.1220.
- [9] *G.Kh. Azhdarov, R.Z. Kazimzadeh, V.V. Mirbagirov.* FTP. 1992. v. 26. iss3. p.553.
- [10] *Sh.M. Abbasov, A.I. Klimovskaya, R.I. Baytsar, E.P. Krasnozhonov.* Growth form of $Ge_{1-x}Si_x$ filamentary crystals of p-type obtained by chemical transport reaction method. Edit. NAS Azerbaijan. Baku. Edit."Science", 2000. v.20. №2, p 117-121.

Ş.M. Abbasov, A.S. Baysar, Z.A. İbrahimov, G.T. Ağaverdiyeva, L.A.Taibov, U.F. Fərəcova

Ge/ $Ge_{1-x}Si_x$ GETEROSTRUKTURLARINDA KOMBİNASİON SƏPİLMƏ SPEKTRLƏRİ

Ge_{1-x}Si_x əsasında Ge altlıq üzərində molekulyar dəstədən səpilmə yolu ilə alınmış heterokeçidin parametrləri rentgenstruktur analiz və rekombinasiya olunmuş işığın səpilmə metodu ilə təyin olunmuşdur.

Qüsursuz Ge/Ge_{1-x}Si_x nazik təbəqənin alınması yüksək yürüklüyə malik tranzistorun hazırlanmasında böyük əhəmiyyət kəsb edir.

III.М. Аббасов, А.С. Байцар, З.А. Ибрагимов, Г.Т. Агавердиева, Л.А. Таибов, У.Ф. Фараджова

СПЕКТРЫ КОМБИНАЦИОННОГО РАССЕЯНИЯ В ГЕТЕРОСТРУКТУРАХ Ge/Ge_{1-x}Si_x

Структуры, исследованные в настоящей работе, получены методом МЛЭ на Ge подложках. Параметры образцов определены методом рентгеноструктурного анализа. Метод спектроскопии комбинационного рассеяния света использовался для контроля состава.

Received: 24.07.07

BEHAVIOR OF PHASE TRANSITION IN NEAR INVERSION ZONE OF $\text{Pb}_{1-x}\text{Sn}_x\text{Te}$

A.A. AQASİYEV, E.S. GARAYEV, S.N. SARMASOV

Baku State University

Baku, Az-1145, Z. Khalilov str.23

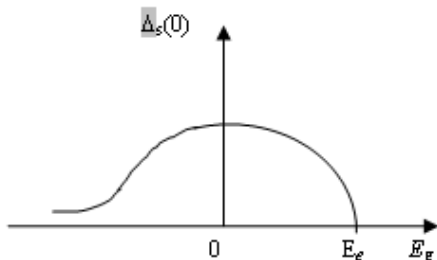
The correlation of temperature of phase transition of the heterojunction $\text{Pb}_{1-x}\text{Sn}_x\text{Te}$ in a vicinity of inversion tone were observed. The temperature dependence of resistivity on the composition with low carrier concentration ($\rho < 10^{19} \text{ cm}^{-3}$) has been investigated. The interzone interaction on the basis of model of seqnetoelectrics, observed from coulomb model of interzone interaction is considered.

The surface structure of crystals is interesting in most respects. For example, it is interesting to know the crystals compound between the structural surface of pure and nature, and the forming energy surface complexes adsorbent-adsorbate. The special interest, surface property represents in compound with high concentration of carriers in chalcogenides of lead (Pb).

We have observed the correlation of temperature dependence of ferroelectrical phase transition T_n and the width of band gap E_g in composition of $\text{Pb}_{1-x}\text{Sn}_x\text{Te}$ in near inversion zone ($x=0,4 \div 0,6$). The temperature dependence of resistivity ρ in composition with low concentration of carriers ($\rho < 10^{19} \text{ sm}^{-3}$) and range of $x=0,2 \div 0,75$ was investigated. The investigations were carried out by horizontal method with alternating current at temperature of 120 K in a vicinity of T_n anomaly increase of ρ takes place, which is more clearly observed in the samples with low concentration of carriers. Correspondence of anomaly ρ of ferroelectrical phase transition in these compositions was convince showed by Kobayashy and others [1,2], where simultaneously with the measuring was fixed the softening of ferroelectrical mode by the method of non-elastic scattering of neutrons. According to anomaly in the temperature dependence ρ was determined T_n .

The non - monotonic dependence of T_n on the composition (minimum in the region of inversion zone) was revealed. Results obtained from the inversion zone correspond to well-known published data.

Interpretation of results was made on the basis of interzone models of ferroelectricity. Due to work [3], it is necessary to take into account the coulomb pair of electrons from different zones which becomes essentially at $E_g \leq E_l$ in the near inversion side by side with the electron-phonon interaction. This leads to effective overregulation of E_g and as the result of that, to non-monotonic dependence T against x .



As a rule the coulomb interzone interaction in the model of ferroelectricity isn't considered. As the fixed slit $E_g > E_l$, where E_l - is the energy of coulomb exciton, and electron-hole pair is impossible [3], and the consideration of coulomb interaction doesn't lead to new effects, but simply result in the overregulation of interzone electron-phonon

bond constants [4]. If $E_g \leq E_l$, then electron-hole pair leads to reorganization of spectrum in a vicinity of \min_l and \max_{l_2} . All zones of exciton slits appreciably become inessential for structural transition. Exclusion may be the incident of small values of E_g , or may be in $\text{Pb}_{1-x}\text{Sn}_x\text{Te}$ where exciton slit is $\Delta_s \geq E_g$ [5]. This coulomb interaction may lead to qualitative changes. Over $E_g \leq E_l$, the interzone coulomb interaction leads to exciton pair and reorganization of spectrum ($T=0$) [4];

$$E(p) = \pm [\varepsilon^2(p) + \Delta_s^2(p)]^{1/2} \quad (1)$$

where $\varepsilon(p) = \varepsilon_1 = -\varepsilon_2$, but Δ_s - exciton slit. Considering, that $\varepsilon(p) = \varepsilon_{g/2} + p^2 / 2m$ and $\Delta_s(p)$ is the function of E_g , and in a vicinity $p=0$ can be defined for $E_g \neq 0$, $E_g < E_l$.

$$2\Delta_s(0) = E_l [2(I - E_g / E_l)]^{1/2} \quad (2)$$

where $\varepsilon_l = 6,8 (me^4 / m_0 e_0^4) \vartheta B$; e_0 and m_0 - are the mass and charge of free electrons. In solid solutions of chalcogenides $m \ll m_0$, usually $m \approx 10^2 m_0$, and ℓ_{can} appreciably increase ℓ_0 [6], that is E_l can reach some tens of electron-volt. In a vicinity $E_g=0$ $\Delta_s(0) = 5,5 (m_l / m_0 \varepsilon_0) \text{ eV}$; and over $E_g < 0$ (semi-metal) $\Delta_s(0)$ exponentially diminish with the growth of $|E_g|$. Qualitative dependence of $\Delta_s(0)$ on E_g is represented in the figure 1. Without account coulomb interaction of temperature of transition can be represented in the form [7].

$$T_c(E_g) = T_c(0) - \alpha E_g^n, \quad (3)$$

where $T_c(0)$, α and n uniquely are defined with the structure of spectrum.

As seen, in $E \rightarrow 0$ T_l increases reaching maximum values of $E_g=0$. Thus, over $E_g > E_l$, $E_g \rightarrow E_l$ and T_c increase, reaching maximum values over $E_g = E_l$. The further diminishing of E_g connects with the coulomb interaction and T_c must decrease, accepting minimum values over $E_g = 0$. Over $E_g < 0$ takes place inversion of zone and E_g is always over zero, Δ_s quickly decreases, T_c increases. Consequently, in a vicinity of non-slit conditions T_c adopts minimum not

maximum values. In chalcogenides $Pb_{1-x}Sn_xTe$ is the width of forbidden zones-function of x , consequently, in solid solutions $T_c(x)$ must behave itself appreciably non-monotonous.

Of course, detail investigations (concentration and temperature dependence, forms to right and left from $E_g \approx 0$) represent a great interest for arrangement and development of interzone models of ferroelectricity.

-
- [1] *M. Grin. Poverkhnostniye svoystva tvyordikh tel.* Izd. «Mir», Moskow, 1972, s.432. (in Russian).
 - [2] *B.A. Akimov, V.A. Bogoyavlenskiy, L.I. Ryabova, V.N. Vasilkov.* FTP, 2001, t.35, vip.5, s. 524-527. (in Russian).
 - [3] *E.V. Bursian, Ya.G. Girshberg, N.N. Trunov.* Mejzonnaya model segnetoelektrichestva. Teoriya i eksperiment. Izv. VUZ-ov, Fizika, 1981, №8, s.91-109. (in Russian).
 - [4] *A.N. Kozlov, L.A. Maksimov.* JETF, 1965, t.48, s.1184. (in Russian).
 - [5] *Yu.I. Ravich, S.A. Nemov.* FTP, 2002, t.36, vip.1, c.3-23. (in Russian).
 - [6] *H.Kawamura.* Proc. III Int. Conf. On Physics of Narrow cap Semicond., p.7. Warszama, 1977.
 - [7] *Ya.G. Girshberg, E.V. Bursian.* Sb. segnetoelektri. lek., s.8, 1978. (in Russian).

A.A. Ağasiyev, E.S. Qarayev, S.N. Sərməsəv

İNVERSİYA ZONASINDA $Pb_{1-x}Sn_xTe$ HETEROQURULUŞLARIN FAZA KEÇİDİ

İnversiya zonasında $Pb_{1-x}Sn_xTe$ heteroquruluşların fazaya keçidinin temperatur korrelyasiyasına baxılmışdır. Birləşmənin ($Pb_{1-x}Sn_xTe$) xüsusi müqavimətinin konsentrasiyadan asılılığı tədqiq olunmuşdur.

A.A. Ağasiyev, E.S. Qarayev, S.N. Sərməsəv

ПОВЕДЕНИЕ ФАЗОВОГО ПЕРЕХОДА В $Pb_{1-x}Sn_xTe$ В БЛИЗИ ИНВЕРСИИ ЗОН

Найдена корреляция температуры фазового перехода в составах $Pb_{1-x}Sn_xTe$ в окрестности инверсии зон. Исследована температурная зависимость удельного сопротивления составов с малой концентрацией носителей ($\rho < 10^{19} \text{ см}^{-3}$). Рассмотрено межзонное взаимодействие в модели сегнетоэлектричества, исходя из модели кулоновского межзонного взаимодействия.

Received: 23.07.07

EFFECT OF HUMIDITY ON OPTICAL AND ELECTRICAL PROPERTIES OF FREE STANDING POROUS SILICON FILMS

T.D. DZHAFAROV^{a,b}, S. AYDIN^b, C. ORUC LUS^b

^a Institute of Physics, Azerbaijan National Academy of Sciences, AZ-1143 Baku, Azerbaijan

^b Department of Physics, Yildiz Technical University, 127 Davutpasa, 34210 Istanbul, Turkey

The PS films were prepared on n-type Si substrates by anodic etching under the white light illumination. Free standing PS films of thickness 5-10 μm and porosity (30-90) % were obtained by electropolishing. The main results of this investigation are the following, (a) The rising of film porosity (from 30% to 90%) results in both the increase of band gap of PS (from 1.4 to 1.9 eV) and resistivity (from $2 \cdot 10^4$ to $4 \cdot 10^4 \Omega \text{ cm}$), (b) The resistivity of films along pores approximately 2-4 times as large as than that in across direction, (c) The band gap of films in humid ambient in the range of 40-95 %RH increases from 1.6 to 1.9 eV. The observed porosity-stimulated and humidity-stimulated changes optical and electrical characteristics were discussed on the base of model including the quantum confinement of charge carries in the PS microcrystallites and chemical activity of PS surfaces.

Keywords: Porous silicon; Optical band gap; Resistivity; Humidity.

1. Introduction

The discovery of visible photoluminescence from porous silicon (PS) has attracted considerable interest due to its potential application in the development of silicon-based optoelectronic devices. However, the origin of photoluminescence in PS is still controversial. A few models are suggested for explanation mechanism of photoluminescence. According model proposed by Canham [1,2] radiative recombination of electron-hole pairs occurs within nanometer silicon wires and their energy gaps become larger than that of bulk Si (quantum confinement effect). This model modified by Koch et al. [3] suggests that electron-hole pairs are photo-excited in nanometer silicon particles and radiatively recombined via Si intrinsic surface states. Another model [4, 5, 6] suggests that luminescence from PS was caused by some special luminescence materials, such as SiH_x complexes, polysilanes, or SiO_2 rather than an intrinsic property of nanometer Si. A third model believes that excitation of charge carriers occurs in nanometer silicon particles and the photoexcitated carriers transfer into the luminescence centers (defects and impurities) in the surrounding SiO_x layers [7].

In general, main models proposed for explaining the origin and mechanism of visible photoluminescence in PS can be divided on three groups. The first group comprises intrinsic effects in nanometer Si, whereas the second group of model is related with processes proceeding an external surfaces of nanocrystals, i.e. on surfaces of PS. These processes are determined with composition and structure of materials on PS surfaces. The third group combines models of the first and second group. The structure of PS is characterised by an extremely large surface area to volume ratio (up to $10^3 \text{ m}^2 \text{ cm}^{-3}$). It is known that surface bonds, in particular Si-H and Si-O bonds play an important role in regulating optical, electrical and gas sensing properties of PS. These properties of PS are very sensitive to humidity of ambient. Investigations of optical properties of the free standing PS films can promote understanding mechanism of photoluminescence. The optical and electrical characteristics of free standing films depending on porosity are rarely considered [8]. Xu et al. [9] have measured evolution of the optical absorption of free standing PS films during thermal oxidation in air and decreasing of the gap have explained due to the Si-O bonds formation. Sagnes et al. [10] have

measured the absorption spectra of the free standing PS films with porosity in a range of 45-79 % and observed a blue-shift of curves with an increase of the porosity. As far as our knowledge goes, data on effect of humidity on optical absorption spectra of free standing PS films are absent in literature.

In this work optical transmission spectra of the free standing PS films with porosity in a range of 30-85 % were measured and the increase of energy band gap of PS films with rising in the porosity have observed. Further, humidity-stimulated changes of optical absorption spectra and band gap of PS films have discovered.

2. Experimental Procedure

PS films were formed by anodization of (111)-oriented n-type silicon wafers ($0.01 \Omega \text{ cm}$) in HF-ethanol solution at constant current density under the white light illumination [11]. The PS films were then detached from the Si substrates by electropolishing at a current density of about 0.8 A/cm^2 . The free standing PS films were characterized by porosity, thickness, resistivity and optical measurements. Average porosity of films was determined by gravimetry. Free standing PS films of thickness 5-10 μm and porosity of $P=30\text{-}90\%$ were analysed in this work.

The transmission spectra of free standing PS films were measured from 300 to 1000 nm at room temperature by using 'UV/VIS Lambda 2S' (Perkin Elmer) spectrometer. Resistivity measurements were performed along and across of pores. Optical and electrical measurements of PS films were examined at the normal room conditions ($T=300\text{K}$, 40%RH) and in the measuring cell at different ambient humidity (water vapour) in the range of 40-95%RH. The relative humidity in cell was measured by using 'Extech-444701' Hygro-Thermometer.

This investigation focuses on the analysis of the transmission spectra and resistivity in dependency on both porosity of PS films (for normal room conditions) and relative humidity of ambient (for PS films with given porosity). Time-dependence transmission spectra and time-dependence resistivity measurements under humidity exposition in cell were carried out after 5-or 10-min intervals of humidity exposition.

The absorption coefficient (α) was determined from the measurements of transmission spectra of two porous silicon films of same porosity with different thickness by using the relation [12]

$$\alpha = (d_1 - d_2)^{-1} \ln(T_1 / T_2) \quad (1)$$

Here T_1 and T_2 are the transmission of films with thickness d_1 and d_2 respectively.

3. Results and Discussion

Measuring of transmission spectra at room conditions ($T=300$ K, 40%RH) were carried out for free standing PS films with porosity of 46%. fig.1 shows the absorption coefficient spectrum for PS film. Analysis of measured curves of absorption coefficient (α) versus photon energy ($h\nu$) for PS films with porosity in range of 30-90% showed that spectra discovered behaviour expected for direct semiconductors

$$\alpha^2(h\nu)^2 = A(h\nu - E_g) \quad (2)$$

Here E_g is energy gap and A is constant. Absorption coefficient curves for PS films discovered a continuous blue-shift with porosity increase in range of 30-90 %.

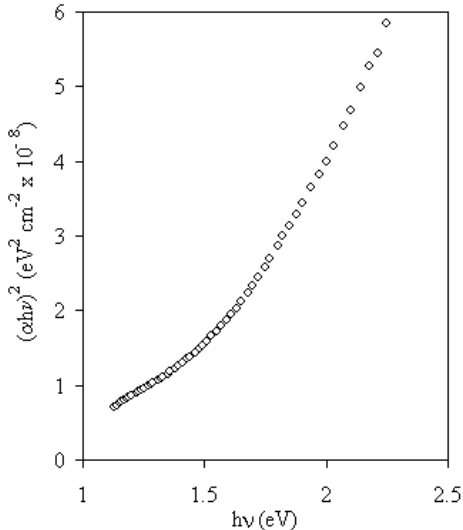


Fig. 1. Optical absorption spectrum of PS film of $P= 46 \%$ porosity (40 %RH).

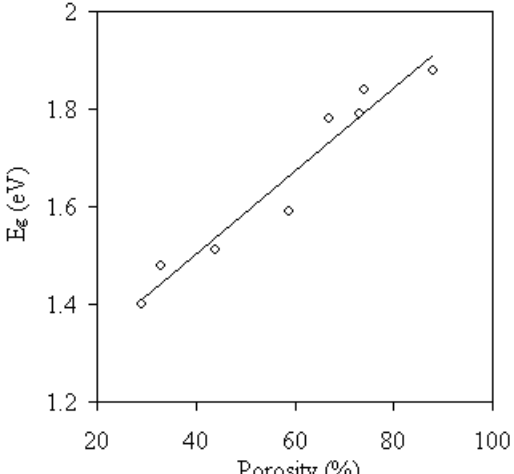


Fig. 2. Energy gap of PS films in dependency on porosity (40%RH).

Fig. 2 shows energy gap in dependency on porosity of the free standing PS films, calculated from extrapolation of the high energy part of $(\alpha^2 - h\nu)$ spectra. Near linear increase of band gap from 1.4 to 1.9eV with rising of porosity of PS films in the range of 30-90 % is observed.

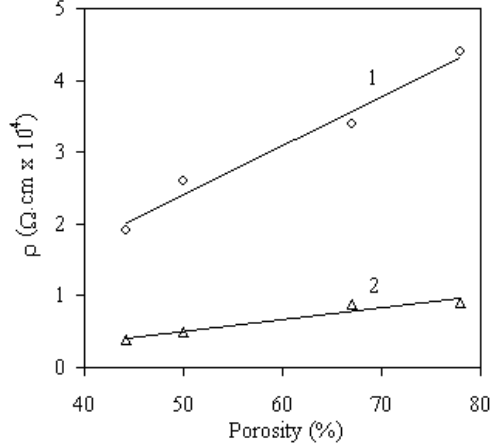


Fig. 3. Resistivity of PS films (1) along and (2) across of pores (40 %RH).

Fig. 3 presents resistivity along and across of pores for free standing PS films with porosity in a range of 45-78%. Increase of resistivity with increase of porosity is observed for both directions. These data on resistivity - porosity dependence (fig.3) correlate with increase of energy band gap of PS films with rising in porosity (fig.2). Lower values of resistivity across of pores can be related with presence of lower-porosity layer along PS film-Si substrate interface.

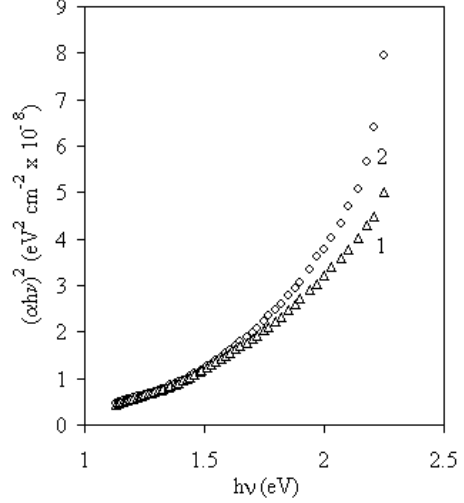


Fig. 4. Optical absorption spectra of PS film at (1) 40 %RH and (2) 90 %RH ($P=68 \%$).

Data on absorption spectrum of PS films with different porosity at normal room ambient above have been presented. Data on the absorption spectra of PS films in dependency on humidity will be below considered. The absorption spectra of PS film with a porosity $P= 68 \%$ for normal room conditions ($T=300$ K, 40%RH) and under exposition in humid ambient (90 %RH) are shown in fig.4. The blue-shift of the absorption curves with increasing the relative humidity is observed. Energy gap of PS films in humid atmosphere ($E_g=1.9$ eV for 90%RH), calculated from the absorption spectra is considerable larger than that for normal room conditions ($E_g=1.6$ eV for 40 %RH).

It will be noted that optical absorption spectra of PS films at once after placing in humid ambient are changes and then after exposition in humid during approximately 20-25 min these changes are ended. Fig. 5 shows evolution of the energy band gap of PS film with porosity of 68% at once after placing the sample in humid atmosphere of 90 %RH ($t=0-20$ min) and after removal from humid ambient to normal room conditions with 40%RH ($t=20-45$ min). It will be noted that evolution of resistivity of PS films (with porosity 64%) on placing in humid ambient with 90%RH and the further removal from humid ambient showed behaviour which is similar to ($E_g - t$) curve presented in Fig. 5. Increase of energy gap of PS film from 1.6 to 1.9eV under humid exposition at first 20min can be tentatively explained by diffusion hydrogen or oxygen from humid atmosphere (water vapour) and formation Si-H and Si-O bonds on PS surfaces. Further decrease of energy gap as result of removal PS film from humid ambient in normal room conditions, can be caused by rediffusion of hydrogen or oxygen atoms or molecules from PS surfaces out of sample. We believed that increase of energy gap in humid atmosphere is mainly caused by hydrogen diffusion into PS films, rather than oxygen diffusion [13]. The indirect confirmation of this suggestion can be data of Xu et al. [9] on decrease of energy gap of PS films with an increase in oxygen termination atoms. Further, hydrogen diffusion coefficient in PS is larger than oxygen diffusion coefficient [13] and therefore formation of Si-H bonds under humid exposition is more preferably. On accepting hydrogen-stimulated model of increasing of energy gap of PS films, rate of increase in energy gap is determined by diffusion coefficient of hydrogen in PS films. Then estimation of diffusion coefficient of hydrogen in PS films at room temperature for 90 %RH results in $D \sim 2 \cdot 10^{-10} \text{ cm}^2/\text{s}$ [14].

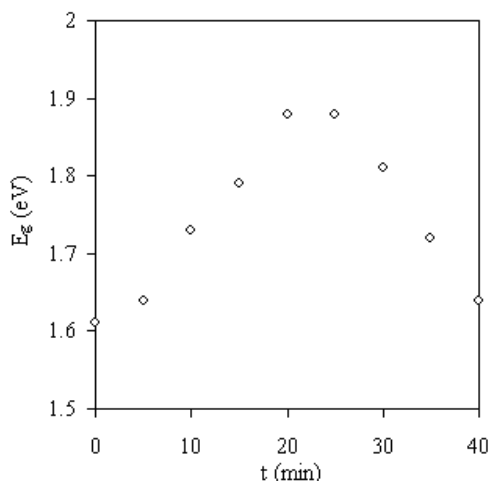


Fig.5. Change of energy gap of PS film ($P= 68 \%$) during exposition in humid (90%RH, $t=0-20$ min) and subsequent removal of PS film from humid atmosphere ($t= 20-40$ min).

Fig. 6 presents the energy band gap of PS films (with porosity of 68%) in dependency on the relative humidity. These data were received from optical transmission measuring carried out after exposition of PS film in humid ambient for 30 min. As it is seen from fig. 6, $E_g - RH$ dependence as a energy gap versus porosity ($E_g - P$) curve (fig.2), shows nearly linear increasing of energy gap.

Data on fig. 2 and Fig. 6 concerning a increase of the energy gap in dependency on porosity of PS films and ambient humidity respectively, can be explained by a model including the quantum confinement of carriers in the PS microcrystallites and the formation of the Si-H bonds on pore surfaces in humid atmosphere.

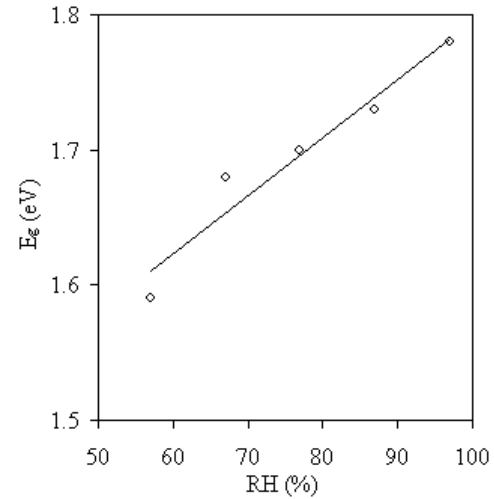


Fig. 6. Energy gap of PS film in dependency on relative humidity ($P=68 \%$).

Visible light emission photoluminescence in PS, as it is known is closely related with the band gap of PS. Therefore data on the band gap-porosity and the band gap-humidity dependencies (fig.2 and fig.6) can be further for understanding of mechanism of photoluminescence in PS films. As it is mentioned above, two main groups of models were suggested for explanation of photoluminescence in PS. The first group of models [1,2,3] suggest that the luminescence in PS is related with quantum confinement of charges in nanostructures, causing the widening of the Si band gap. The second group of models believes [4,5,6,7] that the visible luminescence was caused by some special luminescence materials (such as SiH_x complexes, polysilanes etc) forming on PS surfaces. Data of present investigation on increase of the band gap with the rising of porosity of PS films (fig. 2) can be support of the quantum confinement model of luminescence, since the rising of porosity is accompanied by decrease of nanocrystals sizes. At the same time, data on increase of band gap of PS films with increase of humidity can be evidence of realization of luminescence in SiH_x -type complexes on PS surfaces, since the surface concentration of these complexes must increase in humid ambient. This, in turn, can cause the chance of composition of complexes on PS surfaces.

In conclusion, data on increase of the band gap of PS in dependency on porosity and humidity, received in this work, can be support for both quantum confinement based and the surface complexes based models of luminescence in PS respectively.

Acknowledgement

This work was supported by STCU Grant no: 3819.

- [1] *L.T. Canham.* Appl. Phys. Lett. 57, 1990, 1046.
- [2] *M.S. Hybersen.* Phys. Rev. Lett. 72, 1994, 1514.
- [3] *F. Koch, V. Petrova, T. Muschik, A. Nikolov and V. Gavrilenko.* Mater. Res. Soc. Symp. Proc. 283, 1993, 197.
- [4] *M.S. Brandt, H.D. Fuchs, M. Stutzman, J. Weber and M. Cardona.* Solid State Commun. 81, 1992, 307.
- [5] *C. Tsai, K.H. Li, J. Sarethy and S. Shik.* Appl. Phys. Lett. 59, 1991, 2814.
- [6] *S.M. Prokes, O.J. Glembocki, V.M. Bermudes and R. Kaplan.* Phys. Rev. B45, 1992, 13788.
- [7] *G.G. Qin and Y.Q. Jie.* Solid State Commun. 86, 1993, 559.
- [8] *O. Bisi, S. Ossicini and L. Pavesi.* Surface Science Reports, 38, 2000, 1-126.
- [9] *D. Xu, G. Guo, L. Gui, Y. Tang and G. Qin.* Pure Appl. Chem. 72, 2000, 237.
- [10] *Sagnes, A. Halimaoui, G. Vincent and P. A. Badoz.* Appl. Phys. Lett. 62, 1993, 1155.
- [11] *T.D. Dzhafarov, C. Oruc, S. Aydin.* J. Phys. D: Appl. Phys. 37, 2004, 404.
- [12] *T.D. Dzhafarov and M. Caliskan.* J. Phys. D: Appl. Phys. 40, 2007, 4003.
- [13] *T.D. Dzhafarov and B. Can.* J. Mater. Sci. Lett. 19, 2000, 287.
- [14] *G.B. Abdullaev and T.D. Dzhafarov.* Atomic Diffusion in Semiconductor Structures, Harwood Academic Publishers, New York, 1987.

T.C. Cəfərov, S. Aydın, C. Oruc Lus

NƏMİŞLİYİN NAZİK TƏBƏQƏLİ MƏSAMƏLİ SİLİŞİUMUN OPTİK VƏ ELEKTRİK XASSƏLƏRİNƏ TƏSİRİ

Məsaməli Si nasik təbəqələrin (5-10) μm optik və elektrik xassələrinin nəmişlik və nümunələrin məsaməlilikdən asılılığı araşdırılmışdır. Göstərilmişdir ki, məsaməli Si təbəqələrin məsaməliliyi 30%-dən 90%-ə qədər artdıqda, onların qadağan olunmuş zolağı 1.4 eV-dan 1.9 eV qədər yüksəlir və xüsusu müqaviməti 2×10^4 -dən 4×10^4 Ohm sm qədər artır. 40-95% nəmişlik ortamında məsaməli Si təbəqələrin qadağan olunmuş zolağı 1.6eV-dan 1.9 eV qədər artır. Müşahidə edilən nəticələr yüksəkşiyicilərinin kvant similans modeli ilə və məsaməli səthin kimyəvi aktivliyi ilə izah edilmişdir.

Т.Д. Джадаров, С. Айдын, Дж. Орудж Лус

ВЛИЯНИЕ ВЛАЖНОСТИ НА ОПТИЧЕСКИЕ И ЭЛЕКТРИЧЕСКИЕ СВОЙСТВА ТОНКИХ ПЛЕНОК ПОРИСТОГО КРЕМНИЯ

На пленках пористого кремния (5-10 мкм) с различной пористостью выполнены измерения оптического пропускания и электропроводности. Показано, что увеличение пористости пленок от 30% до 90% приводит к возрастанию ширины запрещенной зоны от 1.4 эВ до 1.9 эВ, а также сопровождается увеличением удельного сопротивления от 2×10^4 до 4×10^4 Ohm см. Под действием влажности в интервале 40 - 95% RH ширина запрещенной зоны возрастает от 1.6 эВ до 1.9 эВ. Наблюдаемые изменения оптических и электрических свойств пористого кремния, стимулированные пористостью или влажностью, объяснены на основе модели квантово-размерного эффекта ограничения носителей заряда и модели химической активности поверхности пор.

Received: 20.09.07

THE EFFECT OF UV LIGHT ON PIGMENTED IN BIOLOGICAL SYSTEMS AND THE ROLE OF PIGMENT

R.B. ASLANOV, R.L. MAMEDOVA

*Institute of Physics of the National Academy of Sciences of Azerbaijan
H. Javid ave., 33. Baku, Azerbaijan*

The accumulation kinetics of free – Radicals (FRs) in white and pigmented keratin arc determined by UV light and arc found to obey the same law. The ESR signal in pigmented keratin has two components. These are the signals appearing in white wool due to pigment and UV light. For both $g=m$ 2.0054 and $H_m = 0.6\text{--}0.8\text{mT}$ for the central line.

We conclude that the events in melanin can be explained by the theory of Brillouin zones and pigments save the biological systems from the effect of IV light by behaving like a trap for FRs

1. Introduction

In previous publications the role of pigment epithelia was clearly studied (1)-(3) and it was found that the natural pigment in biological systems is more active hen being only a passive screen. However, these researches are not complete for the blowing reasons: 1) the suggested mechanism was not tested for other biological systems having pigment; 2) the role of pigment in FR processes was not it tidied, that is TR processes were not analyzed in systems having different degrees of pigmentation. The Lest system to lie used for these two purposes is the wool keratin which has a different pigment (t. e. different color). The FR processes funned by the effect, of UV radiation has been explained for white keratin [4]. However, we should make some more points clear and solve some other problems For example, in FR processes, the function of the sulphur atoms has not yet been understood (as is known, the amount of the amount of sulphur in keratin is 12% cystein + cystin). For this purpose although the method of recombination-kinetics, for some proteins, has been suggested (5)-(9) in this paper we prefer to me the accumulation and annihilation reactions of FR formed in wool keratin having various degrees of pigmentation due to the UV radiation effects.

2. Materials and methods

Keratin was taken up from the wool of white (albino) rabbits and sheep with van oust colors. The wool was cleaned by stirring it slowly in a chloroform-methilalcohol mixture (in a ratio 2 to 1) for 6 hours. Later the wool was dried at room temperature. Two different kinds of samples were used: wet and dry ones. We placed the wet samples in a parts ampoule and poured distilled water. The dry samples having a mass of 4-5gr were placed in a quartz ampoule having an inker diameter of 2mm. The air was taken out under a pressure of 1.3N/m during 30 minutes and the basin was closed.

The samples were irradiated through a glass ray filter UFS 2. a ray filter of thickness 0 cm and a high pressure Hg tube of power 500 Watt. First, at 77 K. the ESR spectrum of wool keratin subjected to UV was recorded and later the sample being left at different temperatures during 5 minutes intervals was radiated again and measured. The process was repealed 8 times.

3. Discussion

As in (4), a triplet signal for white wool keratin was observed in the dry samples and the extreme components

belonged to FR. As the temperature increased, the integral intensity of the signal increased. This might be due to either the recombination of FR or the migration of free electrons. From the kinetics we saw that the total concentration of FR was proportional to temperature (fig. 1) and two kinds (fast and slow) of reactions occurred. The same phenomenon happened in silk fibroin and college (9)-(10). An Increase in temperature lowered the relative concentration of FR. (Fig.1): while in the fast and slow reactions it increased the concentration of FR respectively. In the interval between 333 and 393 K the concentration of paramagnetic centers increased and the concentration of FR in slow reactions remained constant (30 %).

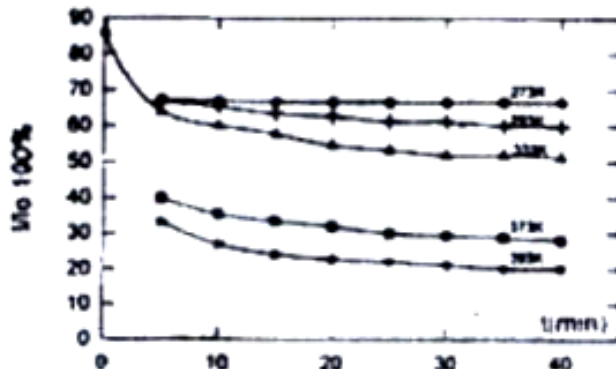


Fig.1. The recombination kinetic corves of FR, formed by the effect of UV radiation, in while wool keratin. 1 and 1 are the integral intensities of ESR spectrum in the standard and experimental samples, respectively.

In the wet samples, the change of the thermal reactions of FR, were the same as in the dry samples but 20% more FRs were added in the reactions. However, the recombination rate of FRs became lower and the reactions stopped at lower temperatures. Wetting might increase the portion of regular regions in proteins.

Using the kinetic proportionality in fig 1 all the basic beat treatment curves are plotted in fig.2. The treatment was initiated at temperatures below 273K and completed at 423K. In the dry samples, the slow reaction was initiated at 273K and completed at 333K (fig.3 (b)). In these samples the amount of the slow reactions increased up to 333K with a percentage of 30 ± 3 then it stayed constant as the temperature increased. The fast reaction increased starting from 273K and was completed at 393K. Thus in the wool keratin the thermal treatment of FRs formed by the effect of UV, occurred at temperatures in a wide range (fig.2). Comparison of our

experimental results with those for globular and other fibroin proteins, yields: 1) The FRs in keratin, subjected to the effect of UV, have two recombination reactions. 2) This can be explained by the existence of regular and irregular regions, as well, including the *a*-spiral. The FR reactions in irregular regions completed at 393K in the dry samples whereas in the wet samples it completed at 243K. The total reactions of FR forming in the regular regions occur at 393K in the dry samples and at 273K in the wet samples. In the slow recombination, the amount of FR is 30%. The amount of the peptide chains in the wool keratin not belonging to the *a*-structure is 30%. The remaining 70% expresses the amount of the peptide chains belonging to the *Q*-structure. A highly intense singlet signal, with $g=2.0054$ and $H_m = 0.6\text{--}0.8\text{mT}$, is observed for wool keratin having various degrees of pigmentation in the absence of UV effect. The amount of spins (unpaired electrons) increases as the degree of pigmentation increases. The ratio of the high spin concentration showed a 10 fold increase, from white to black wool.

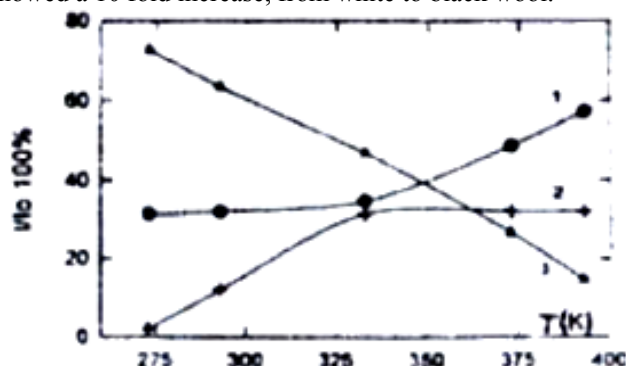


Fig.2. At 77 K, in white wool keratin, the initial amount of FR formed by UV radiation is proportional to temperature:: 1 - stable FR, 2 - FR in slow reaction, 3 - fast reaction.

This ratio might be different for different wool. In our previous investigations, we stated two mechanisms for the formation of the signal in the biological systems: 1) "Developed Zone Theory", restricted for amorphous semiconductors, might be applied to melanines. For the unpaired electrons near the valance and conduction band boundaries, the theory of zone to zone transition is valid. 2) It is assumed that as a result of the absorption of light quanta, FRs form in monomer unit of keratins. Thus, melanin (pigment) having both too many FRs and electron traps protects the biological systems against photochemical destruction. In addition, melanin plays the role of deactivator for the chemical protector. Although the FR concentration belonging to melanin increases with the amount of pigment in wool keratin, the amount of FR emerging due to the UV - radiation and its speed of formation decrease efficiently. In fig. 3, the accumulation kinetics of

FRs by the effect of UV in both white (1) and black (2) wool keratin and the increasing curve belonging to the pigment, are shown. From this we end up with the following two conclusions: a) The signal of the pigment and the kinetics of FR accumulation with UV in keratin form through a two-stage process in all proteins, that is, each of the paramagnetic centers is spread throughout the crystal - like and amorphous regimes of the biopolymer. In this case, it is possible, using recombination- kinetic method, to determine the amounts of the polymer chains both belonging and not belonging to spiral, b) As seen from fig. 3. the accumulation speed of FR in the pigment keratin is as low as it can be. According to the calculations, passing from the low pigment keratin to the high pigment one decreases this speed to its half. This event proves the protective role of pigment for electrons in biological systems.

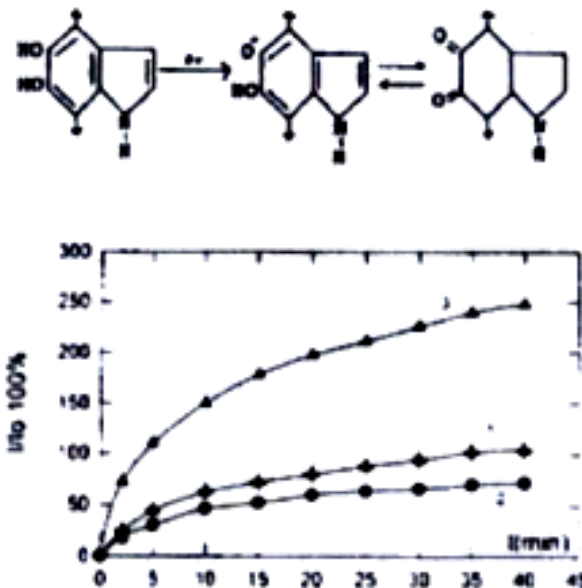


Fig.3. The accumulation kinetics of FR in pigmented wool keratin: 1 - white wool. 2-black wool formed by UV, 3 - paramagnetic renters of pigment.

The intensity of the ESR signal can determine the amount of the pigment in biological systems. But, in the wool samples containing man-made dyes, an ESR signal which is not proportional to the degree of pigmentation is observed. In this case, by the effect of UV we find out that the accumulation-recombination kinetics of FR is similar to that in white wool. Thus, we conclude that man-made dyes only play the role of screening the pigment but never play the biological protective role.

-
- [1] G.B. Abdullaev, Sh.V. Mamedov, A.I. Jafarov and V.V. Perelygin. DAN Azerb. SSR, 29, 25, 1973.
 - [2] G.B. Abdullaev, Sh.V. Mamedov, A.I. Jafarov and N.M. Magamedov. DAN Azerb. SSR, 31, 31, 1975.
 - [3] Sh.V. Mamedov. Avtoreferat of Ph. D. Dissertation, Baku, 1986, 40.
 - [4] R.B. Aslanov, S.R. Gassymov, S.R. Nuriyev and Sh.V. Mamedov. Fizika, 1, 5, 1995.
 - [5] K.M. I'vov. DAN Azerb. SSR, 177, 971, 1967.
 - [6] K.M. I'vov and In.A. Kim. Studiobiophysica, 33, 193, 1972.
 - [7] I.P. Kayushin, K.M. I'vov, M.K. Pusatova. "Issledovaniye Paramagnitnykh Sistem Obuchennykh Belkov.", Nauka, 1970, 263.
 - [8] K.M. I'vov and In.A. Kim. Biopolymers, 14, 83, 1975.
 - [9] K.M. I'vov, R.B. Aslanov and Sh.V. Mamedov. Biophysika, 29, 537, 1989
 - [10] K.M. I'vov, R.B. Aslanov and N.G. Yesipova. Biophysika, 31, 154, 1986.

THE EFFECT OF UV LIGHT ON PIGMENTED IN BIOLOGICAL SYSTEMS AND THE ROLE OF PIGMENT

R.B. Aslanov, R.L. Məmmədova

BİOLOJİ SİSTEMLƏRDƏ UB ŞÜALARIN PİQMƏNTƏ TƏSİRİ VƏ PİQMƏNTİN ROLU

UB şüanın təsiri ilə ağ və rəngli yun keratinində sərbəst radikalların toplanma kinetikası eyni qanuna əsaslanır.

Rəngli keratində UB şüanın təsiri ilə alınan EPR siqnalı iki komponentli $g=2.0054$ və $\Delta H_m=0.6-0.8\text{mT}$ olan mərkəzi siqnaldan ibarətdir. Belə nticə çıxarılır ki, melanində baş verilənlər Brillion zonalar nəzəriyyəsi ilə izah oluna bilər və bioloji sistemlərdə piqment UB şüalanmanın təsirini azaldır və köhnəlmədən qoruyur.

Р.Б. Асланов, Р.Л. Мамедова

ВОЗДЕЙСТВИЕ УФ СВЕТА НА ПИГМЕНТ В БИОЛОГИЧЕСКИХ СИСТЕМАХ И РОЛЬ ПИГМЕНТА

Накапливание кинетики свободных радикалов (СР) в белом и пигментном кератине шерсти определяется УФ светом и основывается на подчинении тому же закону. В пигментном кератине ЕПР сигнал имеет два компонента: $g=2.0054$ и $\Delta H=0.6-0.8\text{мТ}$ для центральной линии. Мы сделали вывод, что происходящее в меланине может быть объяснено теорией зоны Брюллиэна и пигментов, спасающих биологические системы от воздействия УФ света, ведущие себя подобно ловушке для СР.

Received: 21.09.07

MESONS DISTRIBUTION FUNCTIONS IN THE “NAIVE-NON-ABELIANIZATION” APPROXIMATION AND POWER-SUPPRESSED CORRECTIONS TO $F_K(Q^2)$

Y.V. MAMEDOVA

*Baku State University, Institute for Applied Mathematics
AZ 1148, Z. Khalilov st., 23*

Power suppressed corrections to the kaon electromagnetic form factor $F_M(Q^2)$ is estimated by means of the running coupling constant method. In calculating the mesons distribution amplitudes (DAs) found, the “naive non-abelianization” approximation is used. Comparisons are made with $F_M(Q^2)$ obtained using the “ordinary” DAs and running coupling constant method, as well as with frozen coupling approximation’s results.

1. Investigation of mesons electromagnetic (e.m.) form factors (ffs) $F_M(Q^2)$ is one of the interesting and long-standing problems in perturbative QCD (pQCD) [1-3]. The form factors are a source of information on the structure of mesons, on their DAs $\Phi_M(x, \mu_F^2)$, which are universal, nonperturbative quantities characterizing meson M . These DAs can be used to explain and compute other exclusive processes involving M . Therefore, comparing the calculated form factors with experimental data, one can deduce the information concerning the shape of DA. But before inferring such information and making conclusions about a meson DA, one has to be sure that all corrections, at least those calculable in the context of pQCD, are taken into account. There are some sources of such corrections to the meson e.m. form factor $F_M(Q^2)$, considered in the literature [4-8]. First of all, these are the next-to-leading order correction to the hard-scattering amplitude $T_H(x, y; Q^2, \mu_F^2, \mu_R^2)$ of the subprocess $q\bar{q}' + \gamma^* \rightarrow q\bar{q}'$ found in [4], the two-loop correction to the Brodsky-Lepage evolution kernel $V[x, y; \alpha_s(Q^2)]$ and to the distribution amplitude itself

obtained in [5]. The form factor $F_M(Q^2)$ with effects of transverse momenta of the meson constituents on the one-gluon exchange hard scattering amplitude T_H and on the distribution amplitude, including the Sudakov form factor and unconventional helicity components ($h_1 + h_2 = \pm 1$) of the meson wave-function, has been computed in [6-8].

Another source of contributions to the form factor $F_M(Q^2)$ is the power-suppressed corrections, which in the present experimentally-accessible regime of momentum transfer ($Q^2 \sim \text{a few GeV}^2$), may play an important role in explaining the experimental data. In order to estimate these corrections in [9] and [10], the running coupling constant method and infrared matching scheme have been used.

In this letter we calculate the hard-scattering e.m. form factor of the kaon using the running coupling constant method and the mesons DAs, recently obtained in [11] in the “naive non-abelianization” (NNA) approximation.

2. It is well known that at large momentum transfer the meson M electromagnetic form factor $F_M(Q^2)$ is given by the expression [1]

$$F_M(Q^2) = \int_0^1 \int_0^1 dx dy \Phi_M^*(y, \mu_F^2) T_H(x, y; Q^2, \mu_F^2, \mu_R^2) \Phi_M(x, \mu_F^2), \quad (1)$$

where $Q^2 = -q^2$ is the momentum transfer in the process (q^2 is the square of the four-momentum of the virtual photon γ^*), μ_R^2 , μ_F^2 are the renormalization and factorization scales, respectively.

At the leading order of pQCD the hard-scattering amplitude $T_H(x, y; Q^2, \mu_R^2, \mu_F^2)$ does not depend on the factorization scale μ_F^2 and depends on μ_R^2 only through the running coupling constant $\alpha_s(\mu_R^2)$. At the next-to-leading order, T_H depends on μ_R^2 , μ_F^2 explicitly due to terms proportional to $\ln(Q^2/\mu_F^2)$ and $\ln[(1-x)(1-y)Q^2/\mu_R^2]$ (see [4]). The proper choice of these scales, i.e. the choice which minimizes the higher-order corrections to $F_M(Q^2)$ and at the same time allows one to estimate the power-suppressed corrections to $F_M(Q^2)$, is an important problem in pQCD

[4,9,10,12]. For the factorization scale μ_F^2 a natural choice is $\mu_F^2 = Q^2$ which eliminates the logarithms of Q^2/μ_F^2 . In Ref.9 the renormalization scale μ_R^2 has been chosen as

$$\mu_R^2 = (1-x)(1-y)Q^2, \quad \bar{\mu}_R^2 = xyQ^2, \quad (2)$$

and in [10] as

$$\mu_R^2 = (1-x)Q^2/2, \quad \bar{\mu}_R^2 = xQ^2/2. \quad (3)$$

Equation (2) describes the case with two running variables (x, y) , whereas in (3) we freeze one of the variables by taking its mean value. In (3), we take $\langle y \rangle = 1/2$, x is the running variable. Alternatively, one can take $\langle x \rangle = 1/2$, and y as the running variable or the mean value of the sum of the form factors, calculated using both of

these possibilities; due to symmetry of T_H and (1) with respect to x, y , one will obtain the same result. In all cases the choice of $\mu_R^2, \bar{\mu}_R^2$ depends on the Feynman diagram for T_H under consideration. Of course, the second choice, (3), leaves in the NLO correction some logarithmic terms, but it

$$T_H(x, y; Q^2, \alpha_s(\mu_R^2)) = \frac{16\pi C_F}{Q^2} \left[\frac{2}{3} \frac{\alpha_s(\mu_R^2)}{(1-x)(1-y)} + \frac{1}{3} \frac{\alpha_s(\bar{\mu}_R^2)}{xy} \right], \quad (4)$$

where $C_F = 4/3$ is the color factor.

3. An important moment in our study is the choice of the mesons DAs $\phi_M(x, Q^2)$ in Eq.(1). The meson DAs are phenomenological model functions, the information about shapes of which should be taken either from experimental data, or from nonperturbative calculations. The evolution of $\phi_M(x, Q^2)$ as a function of the factorization scale Q^2 can be found by means of pQCD methods [1]. In the literature for the pion, kaon and ρ_L -meson various model DAs have been proposed [2,14,15]. They have been obtained using QCD sum rules method. But from the very beginning these DAs, enhanced in the endpoint region (for example, the Chernyak-Zhitnitsky DA of the pion) have been met with criticism [16], intensified recently in the light of new experimental data on the transition form factor $F_{\pi\gamma}(Q^2)$ reported by CLEO collaboration [17]. In [18] and [19] the authors have

allows us to compare our predictions with results obtained by means of the infrared matching scheme [13], and also leads to better agreement with experimental data [10]. Therefore, we shall use (3) in our computations.

At the leading order of pQCD, T_H has the following form:

concluded that these data can be explained by the pion asymptotic or asymptotic-like DA and that model DA from [2] (Chernyak-Zhitnitsky DA) disagrees with the data. At the same time an asymptotic-like pion DA employed for computation of the electromagnetic form factor $F_\pi(Q^2)$ in the hard-scattering approach (1) gives result lying below the experimental data on $F_\pi(Q^2)$. As it was proven in [9] and [10], the power-suppressed corrections, estimated using the running coupling constant method, enhance the “ordinary” pQCD result approximately by a factor 2 and can help in solution of problems with $F_\pi(Q^2)$.

Recently, in [11] the authors have calculated the contribution of “bubble chain” diagrams to the Brodsky-Lepage evolution kernel $V[x, y; \alpha_s(Q^2)]$ in the “naive non-abelianization” (NNA) approximation and, as a result, have got new, infrared (ir) renormalon improved DA for the meson

$$\phi_M(x, Q^2) = f_M [x(1-x)]^{1+\alpha} \sum_{n=0}^{\infty} b_n(Q^2) A_n(\alpha_s) C_n^{3/2+\alpha}(2x-1), \quad (5)$$

where $\{C_n^{3/2+\alpha}(2x-1)\}$ are the Gegenbauer polynomials, $A_n(\alpha_s)$ are normalization constants, $b_n(Q^2)$ define the evolution of $\phi_M(x, Q^2)$ with Q^2 and $\alpha \equiv \alpha_s(Q^2) \beta_0 / 4\pi$. Here, the n takes odd values in the case of the kaon, because the kaon DA contains an antisymmetric under replacement $2x-1 \leftrightarrow 1-2x$ [2]. In (5) f_M is the meson M decay constant, for the kaon it equals to $f_K = 0.112 \text{ GeV}$. In accordance with this normalization of DA and decay constant f_M , which differs from that of [11], $A_n(\alpha_s)$ are given by the expression

$$A_n(\alpha_s) = \frac{\Gamma(3+2\alpha)}{\sqrt{3}\Gamma(1+\alpha)\Gamma(2+\alpha)} \frac{n!}{(2+2\alpha)_n} \frac{3+2\alpha+2n}{2+2\alpha+2n}, \quad (6)$$

where $\Gamma(z)$ is the Euler gamma function, $(\alpha)_n$ is the Pochhammer symbol, $(\alpha)_n = \Gamma(\alpha+n)/\Gamma(\alpha)$.

In this work we neglect the dependence of $\phi_M(x, Q^2)$ on the factorization scale Q^2 , therefore we do not write down the expression for $b_n(Q^2)$. It is worth noting that (5)

and (6) are valid for both even and odd values of n .

4. As it has been emphasized above, here we choose the renormalization scale μ_R^2 as in (3). But the electromagnetic form factor (see (1) and (4)) with $\alpha_s[(1-x)Q^2]$ (and $\alpha_s(xQ^2/2)$) suffers from ir singularities associated with the behavior of α_s in the soft regions $x \rightarrow 1; 0$. Thus, the form factor $F_M(Q^2)$ can be found after regularization of $\alpha_s(\mu_R^2)$ in this endpoint regions. To solve this problem it is convenient to express the running coupling constant $\alpha_s(\lambda Q^2/2)$ in terms of $\alpha_s(Q^2/2)$, which can be done by means of the renormalization group equation [20]

$$\alpha_s(\lambda Q^2/2) = \frac{\alpha_s}{1 + \ln \lambda/t} - \frac{\alpha_s^2 \beta_1}{4\pi \beta_0} \frac{\ln[1 + \ln \lambda/t]}{[1 + \ln \lambda/t]^2}. \quad (7)$$

Here, $t = 4\pi/\beta_0 \alpha_s(Q^2/2)$, $\alpha_s \equiv \alpha_s(Q^2/2)$ is the one-loop QCD coupling constant and β_0, β_1 are the QCD beta-function one- and two-loop coefficients, respectively,

$$\alpha_s(\mu^2) = \frac{4\pi}{\beta_0 \ln(\mu^2/\Lambda^2)}, \quad \beta_0 = 11 - \frac{2}{3} n_f, \quad \beta_1 = 102 - \frac{38}{3} n_f, \quad (8)$$

where n_f is the number of quark flavors, Λ is the QCD parameter $\Lambda = 0.2 \text{ GeV}$.

For our purposes it is convenient to rewrite the meson DA in the following form:

$$\phi_M(x, Q^2) = f_M [x(1-x)]^{1+\alpha} \sum_{n=0}^{\infty} K_n(\alpha_s) x^n. \quad (9)$$

The explicit expressions of new coefficients $K_n(\alpha_s)$ can be found in the Appendix.

Substituting (4), (7) and (9) into (1), performing integration over x using the inverse Laplace transformations [21]

$$\frac{1}{(t+z)^\nu} = \frac{1}{\Gamma(\nu)} \int_0^\infty \exp[-u(t+z)] u^{\nu-1} du, \quad \text{Re } \nu > 0 \quad (10)$$

and

$$\frac{\ln(t+z)}{(t+z)^2} = \int_0^\infty \exp[-u(t+z)] (1 - C - \ln u) u du, \quad (11)$$

where $z = \ln(1-x)$, and after integration over y we find the following expressions for the e.m. form factor for the kaon:

$$\begin{aligned} [Q^2 F_M(Q^2)]^{res} &= \frac{(16\pi f_K)^2}{9\beta_0} \{ 2 \sum_{n=0}^4 K_n B(2+n+\alpha, 1+\alpha) \\ &\times \sum_{l=0}^3 K_l \int_0^\infty \exp(-tu) R(u, t) B(2+l+\alpha, 1+\alpha-u) du \\ &\quad + \sum_{n=0}^3 K_n B(2+\alpha, 1+n+\alpha) \\ &\times \sum_{l=0}^4 K_l \int_0^\infty \exp(-tu) R(u, t) B(2+\alpha, 1+l+\alpha-u) du \}, \end{aligned} \quad (12)$$

with $R(u, t)$ defined as

$$R(u, t) = 1 - \frac{\beta_1}{\beta_0^2} u (1 - C - \ln t - \ln u).$$

In (12), $B(x, y) = \Gamma(x)\Gamma(y)/\Gamma(x+y)$ is the Beta function, $C \approx 0.577216$ is the Euler-Mascheroni constant.

As it was demonstrated in [9] the integration in (1) in the framework of the running coupling constant method using the inverse Laplace transforms allows us to obtain the Borel transforms $B[Q^2 F_M](u)$ and the resumed expressions for $Q^2 F_M(Q^2)$.

The inverse Borel transformation (12) have the infinite number of infrared renormalon poles at the points $u = N + \alpha$ in the Borel plane. Indeed, this is evident from the following formula for $B(\alpha, \beta)$

$$B(\alpha, \beta) = \frac{\alpha + \beta}{\alpha\beta} \prod_{k=1}^{\infty} \frac{k(k + \alpha + \beta)}{(k + \alpha)(k + \beta)}, \quad (13)$$

and $N = 1; k+1, k+l+1$.

After regularization of these ir renormalon poles in accordance with the principal value prescription (see Refs. 20 and 22) Eq. (12) became the resummed form factor $[Q^2 F_M(Q^2)]^{res}$.

It is instructive to compare our recent result with its obtained in the context of the same method, but using the “ordinary” DA ($\alpha \equiv 0$, in (5)) [9,10],

1) we have the infinite number of ir renormalon poles, instead of finite one,

2) each infrared renormalon pole in (12) is shifted to a value α .

It is known [9, 10] that an ir renormalon pole at $u = u_0$ corresponds to a power-suppressed contribution $\sim (\Lambda^2/Q^2)^{u_0}$ to the form factor. Even if the pole is located at $u = u_0 + \alpha$, its contribution is of order $(\Lambda^2/Q^2)^{u_0}/e$. Therefore, our formula (12) take into account the power-suppressed corrections $C_p(Q^2)(\Lambda^2/Q^2)^p$, $p = 1, 2, 3, \dots$ to the meson e.m. form factor $Q^2 F_M(Q^2)$, the coefficients $C_p(Q^2)$ of which depend on the meson DA under consideration. It is worth noting that the principal value prescription itself produces the higher twist ir renormalon ambiguities $\delta C_p(Q^2)(\Lambda^2/Q^2)^p$ which has to be canceled exactly by uv-renormalon ambiguities of higher twist corrections to $Q^2 F_M(Q^2)$. In our work we neglect these effects and do not estimate $\delta C_p(Q^2)$.

5. In this section we compare our result for the kaon electromagnetic ff $F_K(Q^2)$ obtained in the context of the running coupling constant method using the ir renormalon improved (9) and the ordinary DAs with each other, as well as with $F_K(Q^2)$ found by means of the frozen coupling approximation. It is worth noting that in this approximation $F_M(Q^2)$ with new DAs (9) can be easily calculated.

Equation (12) together with (13) is our final expression, which can be used for computation of power-suppressed corrections to $F_M(Q^2)$. In numerical calculations we have used $N = 120$ ir renormalon poles in (13); this is enough for correct estimation of integrals in (12). Our results for the kaon electromagnetic form factor $F_K(Q^2)$ are depicted in Figs. 1 and 2. It is interesting to compare ffs found by means of the ordinary and ir renormalon improved DA. The same DAs in the framework of the frozen coupling approximation lead to predictions shown also in Fig.1. In this approximation the ir renormalon effects reduce the perturbative QCD contribution to $F_K(Q^2)$. The kaon electromagnetic ff $F_K(Q^2)$ found by means of different model DAs are plotted in Fig.2.

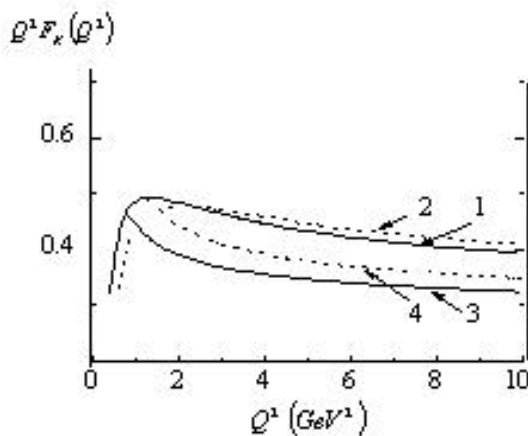


Fig. 1. The kaon electromagnetic form factor $F_K(Q^2)$ as a function of Q^2 . All curves are found using the asymptotic DA. Curves 1, 2 correspond to ff obtained using the running coupling constant method; curve (1) – by means of infrared renormalon improved DA, curve (2) – using the ordinary DA. Curves 3 and 4 describe ff calculated in the framework of the frozen coupling approximation, with (curve 3) and without (curve 4) ir renormalon corrections.

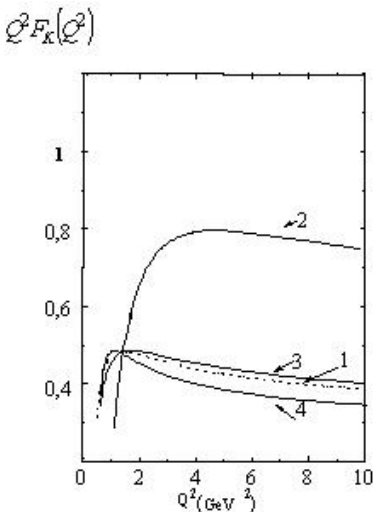


Fig.2. The kaon em formfactor $F_K(Q^2)$, computed in the context of the running coupling constant method and ir renormalon improved DAs vs Q^2 . Curve 1 is found using the asymptotic DA, curve 2- by means of the Chernyak-Zhitnitsky DA, curve 3 corresponds to DA with parameters $b_0 = 1$, $b_2 = 0.1$, curve 4 – to DA with parameters $b_0 = 1$, $b_2 = -0.2$.

Appendix

The coefficients $K_n(\alpha_s)$ of DA in (9) are given as

$$K_0(\alpha_s) = A_0(\alpha_s) - b_1 A_1(\alpha_s)(3+2\alpha) + b_2 A_2(\alpha_s)(2+\alpha)(3+2\alpha) - \frac{1}{3} b_3 A_3(\alpha_s)(2+\alpha)(3+2\alpha)(5+2\alpha) + \frac{1}{8} b_4 A_4(\alpha_s)(3+2\alpha)(5+2\alpha) \left[1 + \frac{1}{3}(3+2\alpha)(7+2\alpha) \right],$$

$$K_1(\alpha_s) = 2b_1 A_1(\alpha_s)(3+2\alpha) - 2b_2 A_2(\alpha_s)(3+2\alpha)(5+2\alpha) + 2b_3 A_3(\alpha_s)(3+\alpha)(3+2\alpha)(5+2\alpha) - \frac{2}{3} b_4 A_4(\alpha_s)(3+\alpha)(3+2\alpha)(5+2\alpha)(7+2\alpha),$$

$$K_2(\alpha_s) = 2b_2 A_2(\alpha_s)(3+2\alpha)(5+2\alpha) - 2b_3 A_3(\alpha_s)(3+2\alpha)(5+2\alpha)(7+2\alpha) + 2b_4 A_4(\alpha_s)(4+\alpha)(3+2\alpha)(5+2\alpha)(7+2\alpha),$$

$$K_3(\alpha_s) = \frac{4}{3} b_3 A_3(\alpha_s)(3+2\alpha)(5+2\alpha)(7+2\alpha) - \frac{4}{3} b_4 A_4(\alpha_s)(3+2\alpha)(5+2\alpha)(7+2\alpha)(9+2\alpha),$$

$$K_4(\alpha_s) = \frac{2}{3} b_4 A_4(\alpha_s)(3+2\alpha)(5+2\alpha)(7+2\alpha)(9+2\alpha).$$

Y.V. MAMEDOVA

- [1] *G.P.Lepage, S.J.Brodsky.* Phys.Rev., 1980, D22, 2157; *A.V.Efremov, A.V.Radyushkin.* Phys.Lett., 1980, B94, 245; *A.Duncan, A.H.Mueller.* Phys.Rev., 1980, D21, 1636.
- [2] *V.L.Chernyak, A.R.Zhitnitsky.* Phys.Rep., 1984, 112, 173.
- [3] *G.Sterman, P.Stoler.* Ann.Rev. Nucl.Part.Sci., 1997, 47, 193.
- [4] *R.D.Field, R.Gupta, S.Otto, L.Chang.* Nucl. Phys. B186, 1981, 429; *F.-M.Dittes, A.V.Radyushkin.* Sov.J.Nucl.Phys., 1981, 34, 293; *E.Braaten.* S.-M. Tse. Phys.Rev., 1987, D35, 2255.
- [5] *F.-M.Dittes, A.V.Radyushkin.* Phys.Lett., 1984, B134, 359; *M.H.Sarmadi.* Phys.Lett., 1984, B143, 471; *S.V.Mikhailov, A.V.Radyushkin.* Nucl. Phys. 1985, B254, 89; *D.Muller.* Phys.Rev. 1995, D51, 3855.
- [6] *H.-N. Li, G.Sterman.* Nucl. Phys., 1992, B381, 129.
- [7] *R.Jakob, P.Kroll.* Phys.Lett., 1993, B315, 463; 1993, B319, 545(E).
- [8] *W.Wang, L.S.Kisslinger.* Phys.Rev., 1996, D54, 5890.
- [9] *S.S.Agaev.* Phys.Lett., 1995, B360, 117; 1996, B369, 379 (E); Mod.Phys.Lett., 1995, A10, 2009; 1996, A11, 957; 1998, A13, 2637.
- [10] *S.S.Agaev.* Proc.of the Conference on QCD 98, Nucl. Phys. B (Proc. Suppl.) , 1999, 74, 155.
- [11] *P.Gosdzinsky, N.Kivel.* Nucl.Phys. 1998, B521, 274.
- [12] *S.J.Brodsky, G.P.Lepage, P.B.Mackenzie.* Phys.Rev. 1983, D28, 228.
- [13] *B.R.Webber.* JHEP , 1998, 9810, 012.
- [14] *G.R.Farrar, K.Huleihel, H.Zhang.* Nucl.Phys., 1991, B349, 655; *V.M.Braun, I.E.Filyanov.* Z.Phys., 1989, C44, 157.
- [15] *P.Ball, V.M.Braun.* Phys.Rev., 1996, D54, 2182.
- [16] *N.Isgur, C.H.Llewellyn Smith.* Phys.Rev.Lett.1984, 52,1080; Nucl.Phys., 1989, 317, 526.
- [17] *J.Gronberg et al.* CLEO collab., Phys.Rev. 1998, D57, 33.
- [18] *P.Kroll, M.Raulfs.* Phys.Lett., 1996, B387, 848.
- [19] *S.J.Brodsky, C.-R. Ji, A.Pang, D.G.Robertson.* Phys.Rev., 1998, D57, 245; *A.V.Radyushkin.* Jefferson Lab. Preprint, JLAB-THY-97-29, hep-ph/9707335.
- [20] *H.Contopanagos, G.Sterman.* Nucl.Phys. 1994, B419, 77.
- [21] *A.Erdelyi.* Tables of Integral Transforms (Mc-Graw-Hill, 1954), vol.1.
- [22] *M.Beneke.* Phys.Rep., 1999, 317, 1.

Y.V. Məmmədova

“ZƏİF QEYRİ-ABELİZASIYA” YAXINLAŞMASINDA MEZONLARIN PAYLANMA FUNKSIYALARI VƏ $F_K(Q^2)$ -Ə ÜSTLÜ DÜZƏLİŞLƏR

İşdə kaonun $F_K(Q^2)$ elektromagnit formfaktoruna dəyişən qarşılıqlı təsir sabiti üsulu çərçivəsində üstlü düzəlişlər qiymətləndirilmiş, hesablamalar zamanı “zəif qeyri-abelizasiya” yaxınlaşmasında təpilmüş paylama funksiyasından istifadə olunmuşdur. Alınmış nəticələr “adi” paylanma funksiyası və dəyişən qarşılıqlı təsir sabiti, eləcə də fiksə olunmuş qarşılıqlı təsir sabiti üsulunun və digər model paylanma funksiyalarının köməyi ilə təpilmüş nəticələrlə müqayisə olunmuşdur.

E.B. Mamedova

ФУНКЦИИ РАСПРЕДЕЛЕНИЯ МЕЗОНОВ В ПРИБЛИЖЕНИИ «НАИВНОЙ НЕАБЕЛИЗАЦИИ» И СТЕПЕННО-ПОДАВЛЕННЫЕ ПОПРАВКИ К $F_K(Q^2)$

В работе оценены степенно-подавленные поправки к электромагнитному форм фактору $F_K(Q^2)$ каона, полученного с помощью метода бегущей постоянной взаимодействия. В вычислениях использована функция распределения мезонов в приближении «наивной неабелизации». Полученные результаты сравниваются как с результатами, полученными с помощью обычных ФР и метода бегущей постоянной взаимодействия, так и с использованием приближения фиксированной постоянной и различных модельных функций распределения.

Received: 20.09.07

FAZA KVAZİSXRONİZM REJİMİNDE İŞLƏYƏN YÜKSƏKEFFEKTİLİ LAZER TEZLİK ÇEVİRİCİLƏRİ

Z.H.TAĞIYEV, N.V. KƏRİMOVA

Azərbaycan Tibb Universiteti

R.C. QASIMOVA, Q.Ə. SƏFƏROVA, M.Ə. MƏMMƏDOV

Bakı Dövlət Universiteti, Bakı, Az-1145, Z. Xəlilov, 23

İşdə faza kvazisinxron rejimində lazer tezlik çeviricilərinin işi sabit intensivlik yaxınlaşmasında araşdırılmışdır. Göstərilmişdir ki, nizamlı domen strukturunda domenlərin uzunluğunun optimal (koherent) uzunluğa bərabərliyində çevrilmənin effektiviyi maksimuma çatır. Sabit amplitud metodundan fərqli olaraq, sabit intensivlik yaxınlaşmasında koherent uzunluq əsas dalğanın intensivliyindən asildir. Domenlərin sayı artıqca onların koherent uzunluğu da artmış olur.

Qeyri-xətti optik proseslərdə tezlik çeviricilərinin effektivliyini artırmaq üçün dalğaların qarşılıqlı təsiri zamanı onların faza sürətlərinin bərabərlik şərtini təmin etmək tövbə olunur. Bu şərt daxilində dalğalar mühitdə yayıldığı zaman onların arasında faza sürüşməsi meydana çıxmır. Dalğaların qarşılıqlı təsiri zamanı meydana çıxan faza sürüşməsini kompensasiya etmək üçün müxtəlisf sxemlər mövcuddur. Təcrübi nöqtəyi nəzərdən ən səmərəli üsul - birinci kristaldan keçən optik dalğaların, əvvəlki kristal-dan yalnız spontan polaryazasiyasının istiqamətilə fərqlənən ikinci kristaldan da keçirilməsidir.

Praktikada bu hal ikinci kristalin optik oxunu birinci kristalına nəzərən π qədər sırlatmaqla əldə edilir. "Firladılmış" belə kristallarda üç ranqlı qavrayıcılıq tensorun işarəsi əksinə çevrilir. Bu fikir, ilk dəfə bir-birindən asılı olmayaraq iki qrup alımlar - Blombergen və əməkdaşları [1] və Frankenlə, Uord [2] tərəfindən irəli sürülmüşdür. Ardıcıl qoyulmuş periodik polaryazəlmış kristallar nizamlı domen (təbəqə) quruluşlu (NDQ) kristallar adlanır. Bircinsli qeyri-xətti mühitlərdən fərqli olaraq, belə nizamlı quruluşlu kristallarda qarşılıqlı təsirdə olan dalğaların faza uyğunluğu, domenlərin uzunluğunun koherent qarşılıqlı təsir məsafəsinə bərabərliyindən yaranır ki, bu da faza kvazisinxronizminə uyğundur. Başqa sözlə, kvazisinxronizm - qeyri-xətti optik qarşılıqlı təsir zamanı faza uyğunluğu yaratmaq metodudur ki, qarşılıqlı təsirdə olan dalğalar arasında fazalar münasibəti periodik quruluşa malik qeyri-xətti mühitlərin hesabına korreksiya olunur [3, 4].

Kvazisinxronizm qeyri-xətti qarşılıqlı təsir hesabına qeyri-xətti optikada istifadə olunan kristallar sınıfını genişləndirir. Bura həm adı sinxronizmə malik olmayan izotrop kristallar, və həm də sinxron qarşılıqlı təsirdə istifadə oluna bilməyən effektiv qeyri-xətti tensor komponentli kristallar aididir [5].

Bircinsli kristallardan fərqli olaraq NDQ - kristallarının üstünlüyü həm də ondadır ki, bir kristalda eyni zamanda bir neçə harmoniyanın generasiyasını almaq mümkündür. Dalğaların ardıcıl qarşılıqlı təsiri zamanı ikinci və üçüncü harmoniyaların generasiyası eyni zamanda [6] -ci işdə alınmışdır. Bu zaman nakaçka rolunda dalğa uzunluğu $\lambda=1.230\text{mkm}$, davametmə müddəti 9ns olan impuls lazerindən istifadə olunmuşdur. Bu yolla impulsun davametmə müddəti 100 ns, təkrarlanma tezliyi 1 kHz və orta gücü 1 Vt tərtibində Nd: YAG şüalanmasının üçüncü harmoniyaya generasiyası da alınmışdır [7].

Periodik qeyri-xətti strukturlarda kvazisinxron qarşılıqlı təsirin nəzəriyyəsinə, xüsusən ikinci harmoniyanın generasiyasına, bir çox işlər həsr olunmuşdur [5-9]. Bu

işlərdə məsələlər əsasən ya sabit amplitud yaxınlaşmasında, ya da ki, dəqiq hesablama yolu ilə həll edilmişdir. Son zamanlar dalğaların qeyri-xətti qarşılıqlı təsirini xarakterizə edən tənliklərə müyyəyen sadələşdirmələr aparmaqla, sabit intensivlik yaxınlaşması da tətbiq edilmişədir [5].

Bu işdə sabit intensivlik yaxınlaşmasında [10] mühitdəki itgini və qarşılıqlı təsirdə olan bütün dalğaların faza dəyişmələrini nəzərə almaqla, ikinci harmoniyanın generasiyası zamanı kvazisinxron qarşılıqlı təsir prosesi araşdırılmışdır. Sabit amplitud yaxınlaşmasından fərqli olaraq, baxılan yaxınlaşmada ikinci harmoniya dalğasının əsas dalğaya əks təsiri nəzərə alınır.

Sabit intensivlik yaxınlaşmasında analitik təhlil zamanı [5]-ci işdən fərqli olaraq əsas dalğanın intensivliyinin ayrı-ayrı domenlərdə dəyişdiyi və domen hüdudunda isə sabit qaldığı nəzərdə tutulur. [5] işdə isə, bütün domenlər struktur boyunca əsas dalğanın intensivliyinin sabit qaldığı götürülür.

Məlumdur ki, domen strukturunda ikinci harmoniya prosesini xarakterizə edən tənliklər aşağıdakı kimidir

$$\begin{aligned} \frac{dA_1}{dz} + \delta_1 A_1 &= -i\gamma_1 A_2 A_1^* \exp(-i\Delta z), \\ \frac{dA_2}{dz} + \delta_2 A_2 &= -i\gamma_2 A_1^2 \exp(i\Delta z), \end{aligned} \quad (1)$$

burada $A_{1,2}$ - ω_1 və ω_2 ($\omega_2=2\omega_1$) tezliklərinə uyğun əsas və ikinci harmoniya dalğalarının kompleks amplitudları, δ_j , γ_j - uyğun olaraq ω_1 və ω_2 tezlikli dalğaların udma əmsalları və qeyri-xətti əlaqə əmsalları, $\Delta=k_2-2k_1$, - dalğaların faza sürüşməsidir.

Başlanğıc halda qəbul edilir ki, birinci domenin girişində ancaq ω_1 tezliyinə uyğun dalğanın kompleks amplitudu sıfırdan fərqlidir, yəni

$$A_1(z=0) = A_{10} \exp(i\varphi_{10}), \quad A_2(z=0) = 0, \quad (2)$$

harada $z=0$ birinci domenin girişinə uyğundur, φ_{10} -əsas dalğanın başlanğıc fazasıdır.

Domendən domenə keçərkən sərhəd şərtləri aşağıdakı kimi götürülür

$$A_{1,2}^n(z=0) = A_{1,2}(l_{n-1}) \exp(i\varphi_{1,2}(l_{n-1})), \quad n = 2, 3, \dots \quad (3)$$

burada $A_{1,2}^n(z=0)$ n -ci domenin girişində, $A_{1,2}(l_{n-1})$ - $(n-1)$ -ci domenin çıkışında ω_1 və ω_2 tezlikli dalğaların kompleks amplitudlarıdır, $\varphi_{1,2}(l_{n-1})$ - $(n-1)$ - tərtibli

domendən n - tərtibli domenə keçid zamanı ω_1 və ω_2 tezlikli dalğaların faza döyişilməsidir.

(2) və (3) sərhəd şərtləri daxilində (1) sistemin ardıcıl yerləşdirilmiş dörd domen üçün həlli ($\delta_2=2\delta_1$):

$$\eta_2(l_4) = \eta_2(l_3) \left[\left(\cos \lambda_4 l_4 + c_a \gamma'_2 \frac{\sin \lambda_4 l_4}{\lambda_4} \right)^2 + \left(c_b \gamma'_2 + \frac{\Delta_4}{2} \right)^2 \frac{\sin^2 \lambda_4 l_4}{\lambda_4^2} \right] \exp(-2\delta_2 l_4), \quad (4)$$

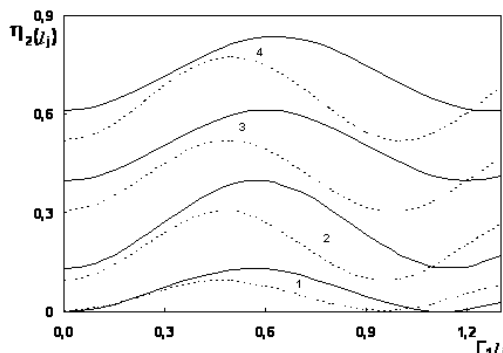
Burada iki qonşu domenlərdə qeyri-xətti qavrayıcılığın işarələri bir birinin əksinədir $\gamma_{1,2}/\gamma'_{1,2} = -1$ və

$$\lambda_4^2 = 2\Gamma_4^2 + \Delta^2 / 4,$$

$$\Gamma_4^2 = \gamma'_1 \gamma'_2 I_1(l_3),$$

c_a, c_b - əmsalları birinci üç domenin uzunluğundan, Δ - dalğaların faza sürüşməsindən, $\gamma_{1,2}(\gamma'_{1,2})$ - qeyri-xətti əlaqə və $\delta_{1,2}$ - udma əmsallarından və qarşılıqlı təsirdə olan dalğaların intensivliklərindən asılıdır. c_a, c_b üçün ifadələr nəhəng olduğuna görə burada verilir.

(4) düsturuna daxil olan $l_1(l_3)$ vuruğu üçüncü domenin çıkışında əsas dalğanın intensivliyidir.



Səkil. Sabit intensivlik yaxınlaşmasında hesablanmış ikinci harmoniyanın η_2 çevrilmə effektivliyinin domenlərin gətirilmiş uzunluqlarından $\Gamma_1 l_j, j=1-4$ asılıqları $\eta_2(l_1, l_2, l_3, l_4)$: $\delta_{1,2}=0$, $\tilde{\Delta}=2.4$ (bütöv xəttlər) və $\tilde{\Delta}=3$ (nöqtəvi xəttlər) ($\tilde{\Delta}=\Delta/2\Gamma_1$). Burada $\Gamma_1 l_{1,opt} = 0.5639$, $\Gamma_1 l_{2,opt} = 0.5742$, $\Gamma_1 l_{3,opt} = 0.6015$ (bütöv xəttlər üçün) və $\Gamma_1 l_{1,opt} = 0.4736$, $\Gamma_1 l_{2,opt} = 0.4777$, $\Gamma_1 l_{3,opt} = 0.4890$

(nöqtəvi xəttlər üçün).

Şəkildə ikinci harmoniyanaya çevrilmənin effektivlik əyriləri göstərilmişdir. Burada, $\eta_2(l_1)$ effektivliyin birinci domenin l_1 uzunluğundan, $\eta_2(l_2)$ ardıcıl götürülmüş iki domen olduğu halda, effektivliyin ikinci domenin l_2 uzunluğundan, $\eta_2(l_3)$ ardıcıl götürülmüş üç domen olduğu halda, effektivliyin üçüncü domenin l_3 uzunluğundan, və nəhayət, $\eta_2(l_4)$ ardıcıl götürülmüş dörd domen olduğu halda, effektivliyin dördüncü domenin l_4 uzunluğundan asılılıqları verilmişdir.

Öyrilər faza sürüşməsinin gətirilmiş $\tilde{\Delta}$ ($\tilde{\Delta}=\Delta/2\Gamma_1$) iki qiymətlərində, yəni $\tilde{\Delta}=2.4$ (bütöv xəttlər) və $\tilde{\Delta}=3$ (nöqtəvi xəttlər) qurulmuşdur. Öyrilərdən görünür ki, effektivliyin domenlərin uzunluqlarından asılılığı $\eta_2(l_1)$ maksimumlara malikdir. Domenin uzunluğu koherent uzunluğa bərabər olduqda, effektivlik $\eta_2(l_1)$ maksimuma çatır və harmoniya dalğası o biri domenə daxil olur. İkinci domendə də harmoniyanın effektivliyi ikinci domenin koherent uzunluğuna qədər artmış olur, və s. Beləliklə, nizamlı domen strukturunda harmoniya dalğasının intensivliyi domenlərdə get-gedə artaraq, çıkışda maksimuma çatır. Araşdırımlar göstərir ki, domenlərin sayının az olduğu halda belə ikinci harmoniyanaya çevrilmənin effektivliyini nəzərə çarpacaq dərəcədə artırmaq olur.

Qeyd edək ki, sabit amplitud metodunun nəticəsindən fərqli olaraq (4) düsturunda λ_4 - ün ifadəsinə əsas dalğanın intensivləyindən asılı hədd Γ_4 daxil olur. İntensivlikdən asılı olan bu həddin daxil olması ikinci harmoniyanın faza döyünmələrinin minimumlarının yerini dəyişir və məsələnin optimal parametrlərinin qiymətlərinə təsir edir. Ona görə də əsas dalğanın intensivliliyindən asılı olan faza münasibətlərinin müntəzəm domen strukturlarında nəzərə alınması vacib məsələlərdəndir.

- [1] J.A. Armstrong, N.Bloembergen, J.Ducuing, and P.S.Pershan, Phys.Rev., 1962, 127, 1918-1939.
- [2] P.A. Franken and J.F. Ward, Rev.Mod.Phys., 1963, 35, 23-39.
- [3] M.M. Fejer, G.A. Magel, D.H.Jundi, and R.L. Byer, IEEE J. Quantum Electronics, 1992, 28, No.11, 2631-2654.
- [4] R.L. Byer, Nonlinear Opt. Phys. Materials, 1997, 6, 549-553.
- [5] A.V. Boxin, V.Q. Dmitriev, Kvantovaş elektronika, 2002, 32, №3, 219-222.
- [6] M.Gu, M. Makarov, Y.J. Ding, J.B. Khurgin, W.P. Risk, Opt. Letts., 1999, 24, 127-131; M.Gu, B.Y. Korotkov, Y.J. Ding S.V. Kang, J.B. Khurgin, Opt. Commun., 1999, 155, 323-326.
- [7] A.S.Çirkin, V.V. Volkov, Q.D. Laptev, E.Ö. Morozov, Kvantovaş elektronika, 2000, 30, №10, 847-858; V.Q. Dmitriev, Cinqx, Kvantovaş elektronika, 2004, 34, №10, 933-940.
- [8] O. Phister, J.S. Wells, L. Hollberg, L. Zink and others, Opt.Lett., 1997, 22, 1211-1215.
- [9] R.L. Byer, Nonlinear Opt.Phys.Materials.1997, 6, 1211-1220.
- [10] Z.A. Tağıev, A.S. Çirkin, CGTF, 73, 1271-1282,(1977); Z.H. Tagiev, R.J. Kasumova, R.A. Salmanova, and N.V. Kerimova, Quantum Semiclassic. Opt. 3, 84-87, 2001.

**HIGH EFFICIENCY LASER RADIATION FREQUENCY CONVERTERS IN
QUASI-PHASE -MATCHED REGIME**

There is made an analysis of quasi-phase-matched interaction of light waves of the process of doubling frequency in regular domain structure in the constant-intensity approximation. The analytical expression of the frequency conversion efficiency for the case of four domains has been obtained. It has been shown that in the constant-intensity approximation, in contrast to the constant-amplitude approximation, the account of the dependence of the phase relationships from the pump intensity influences on the characteristics of conversion process of nonlinear waves in regular domain structure.

З.А. Тагиев, Р.Дж. Касумова, Г.А. Сафарова, М.А. Мамедов, Н.В. Керимова

**ВЫСОКОЭФФЕКТИВНЫЕ ПРЕОБРАЗОВАТЕЛИ ЧАСТОТЫ ЛАЗЕРНОГО ИЗЛУЧЕНИЯ В
РЕЖИМЕ ФАЗОВОГО КВАЗИСИНХРОНИЗМА**

В приближении заданной интенсивности рассмотрен режим квазисинхронного взаимодействия световых волн в регулярных доменных структурах на примере процесса удвоения частоты. Дано выражение для эффективности преобразования в случае четырех доменов. Показано, что в отличие от результатов приближения заданного поля в приближении заданной интенсивности учет зависимости фазовых соотношений от интенсивности основного излучения влияет на характеристики процесса преобразования нелинейных волн в регулярной доменной структуре.

Received: 17.08.07

AQAR GELİNİN ÖZLÜ-ELASTİK XASSƏLƏRİNİN REBİNDER ÜSULU İLE ÖYRƏNİLMƏSİ

E.Ə. MƏSİMOV, A.R. İMAMƏLİYEV, K.M. BUDAQOV

Baki Dövlət Universiteti, Fizika Problemləri İnstitutu

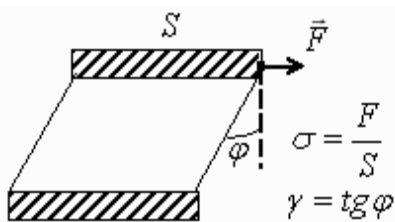
Bakı, Az-1145, Z. Xəlilov.23

Bu işde sürüşmə deformasiyası həndəsəsində aqar gelinin ani elastiklik və yüksək elastiklik sabitlərinin, həmcinin statik özlülük əmsalının mexaniki gərginlikdən asılılığı öyrənilmişdir. Möhkəmlik həddindən aşağı gərginliklərdə ani elastiklik sabiti, demək olar ki, dəyişmir, yüksəkelastiklik sabiti zəif artır. Möhkəmlik həddindən yuxarı gərginliklərdə isə hər iki sabit azalır. Alınan nəticərin keyfiyyətçək izahı verilmişdir.

Bərk cisimlər üçün Huk qanununa tabe olan elastiklik, mayelər üçün isə Nyuton qanununa tabe olan özlü axın xassəsi xarakterikdir. Özlü-elastik materiallarda bu xassələrin kombinasiyası müşahidə olunur [1]. Özlü-elastik materiallar Debər ədədi (De) adlanan ədədlə xarakterizə olunur. Bu ədəd material üçün xarakterik olan relaksasiya (və ya gecikmə) müddətinin proses üçün xarakterik olan deformasiya müddətinə (deformasiya sürətinin tərs qiyməti) olan nisbətinə bərabərdir

$$De = \frac{t_{material}}{t_{proses}} \quad (1)$$

Mayelər üçün $De << 1$ (sirf özlü maddələr üçün $De \rightarrow 0$), bərk cisimlər üçün isə $De \gg 1$ (mükəmməl elastik bərk cisimlər üçün $De \rightarrow \infty$) şərti ödənir. $De \approx 1$ şərtini ödəyən materiallar özlüelastik materiallar adlanır. Belə materiallar bir çox reoloji xüsusiyyətlərə malik olur ki, bunların arasında normal gərginlik effekti (Kuit axını zamanı Vaisenbenrq effekti, Puazeyl axını zamanı Barus effekti), gərginlik relaksasiyası, gecikən reaksiya, sürünənlilik və s. göstərmək olar [2].



Søkil 1.

Bir çox polimerlər, o cümlədən, bioloji təbiətli polimerlər, su mühitində dispersiya və ya həll olunduqda özlü-elastik sistem əmələ gətirə bilirlər. Sırf özlü sistemdən elastik gelin yaranması (zol-gel keçidi) həm kimyəvi, həm də termik yolla həyata keçə bilər. Termik yolla gel əmələ götürən təbii polimerlərə, aqaroza, aqar və karraginan kimi aqaroidləri göstərmək olar.

Gellər daha çox bərk hala yaxın xassələr göstərilərlər. Gelə tətbiq olunan gərginlik həm bərpa olunan, həm də bərpa olunmayan deformasiya (axın) yarada bilər. Bu cür özlü-elastik xassələri modelləşdirmək üçün müəyyən qayda ilə birləşdirilmiş yay və özlü mayedə hərəkət edən porşendən ibarət sistemə baxılır [3]. Məsələn, sürüşmə deformasiyası halında gelə sabit gərginlik tətbiq

olunduqda yaranan deformasiyanın zamandan asılılığını tapmaq üçün

$$\sigma = G\gamma + \eta \dot{\gamma} \quad (2)$$

tənliyi ilə xarakterizə olunan sadə Kelvin-Foyqt modeli (yay və porşen paralel birləşdirilir) doğrudur [3]. Burada

$\sigma = \frac{F}{S}$ - mexaniki gərginlik, $\gamma = tg\varphi$ - sürüşmə de-

formasiyası, - sürüşmə sürəti, G - elastiklik modulu, η isə özlülükdür (şəkil 1).

$$v_1 = v_1 \left(I - e^{-t/\tau} \right) \quad (2)$$

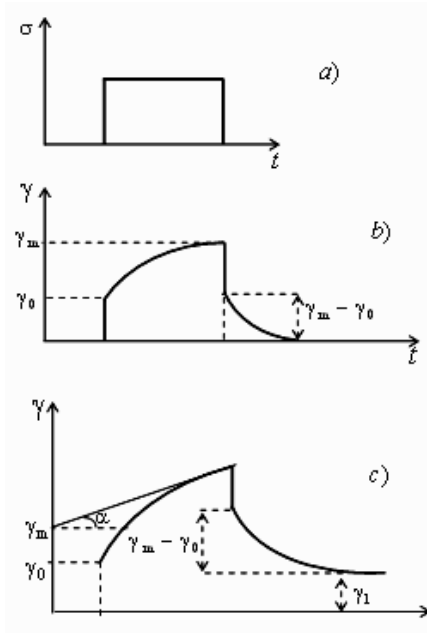
¹ 1990-91, 1991-92, 1992-93, 1993-94, 1994-95, 1995-96, 1996-97, 1997-98, 1998-99.

$$\gamma = \gamma_0 e^{-t/\tau} \quad (4)$$

düsturu ilə ifadə olunur. Burada γ_m - maksimal deformativə

$$\tau = \frac{\eta}{G} \quad (5)$$

ise gecikme müddətidir



Səkil 2.

AQAR GELİNİN ÖZLÜ-ELASTİK XASSƏLƏRİNİN REBİNDER ÜSULU İLƏ ÖYRƏNİLMƏSİ

Ölçmələr göstərir ki, alınan nəticələr (2)-(5) düsturlarının təsvir etdiyindən fərqli olur (şəkil 2). Birinci fərqli ondan ibarətdir ki, elastik deformasiya ani və yüksək-elastik adlanan iki hissədən ibarətdir. İkinci isə ondan ibarətdir ki, özlü axın müəyyən σ_k gərginliyindən sonra başlayır.

Ani elastiklik (Huk elastikliyi) geldəki polimer molekullarının valent rabitələrinin və bucaqlarının məhdud dərəcədə deformasiyası ilə, yüksəkelastiklik (gecikmiş elastiklik) isə ayrı-ayrı seqmentlərin sərbəst şəkildə yerdəyişməsi ilə əlaqədardır. Geldə makromolekullar arasında fəza torunun mövcud olması nisbətən kiçik gərginliklərdə onların bütövlükdə bir-birinə nəzərən yerdəyişməsinə mane olur. Bu halda verilən gərginliyi götürdükdə gel-nümənə əvvəlki vəziyyətinə qaydır və əvvəlcə ani olaraq makromolekullarda əvvəlki valent rabitələri və bucaqlar, sonra isə müəyyən gecikmə ilə molekulun əvvəlki konformasiyası bərpa olunur (şəkil 2b). Nümunəyə verilən gərginliyi artırmaqdə davam etsək, müəyyən gərginlikdən başlayaraq (bu gərginlik plastik deformasiyanın və ya özlü axının başladığı gərginlik olub gelin möhkəmlik həddi σ_k adlanır) fəza toru qırılmağa və molekullar özləri bir-birinə nəzərən yerini dəyişməyə başlayır. Bu gelin dönməyən deformasiyasıdır və gərginlik götürüldükdə qismən bərpa olunur (şəkil 2c).

Bu işdə aqar gelinin özlü-elastik xassələri Rebinder üsulu ilə (tangensial sürüşmə deformasiyası həndəsəsində) öyrənilmişdir. Aqar təbii biopolimer olub təbabətdə yeyinti sənayesində, əczaçılıqda geniş tətbiq olunur [4]. Bütün istifadə etdiyimiz aqar (Precoldia, Saxalin) kifayət qədər güclü geləmələğətirmə qabiliyyətinə malikdir. Gelin hazırlanması aşağıdakı texnologiya üzrə həyata keçirilmişdir. Yarpaq şəklində olan aqar tərəzidə çəkilərək təmiz (distillə) suyuna əlavə olunur, suyun qaynama temperaturuna yaxın temperatura qədər qızdırılır və bir neçə saat bu vəziyyətdə saxlanılır. Bu zaman yarpaqdakı aqar tamamilə suya keçir. Məhlul kiçik məsaməli süzgəcdən keçirildikdən sonra soyudulur və 35-40°C intervalında gel halına keçir. Ölçmə, gel bir gün saxlanıldıqdan sonra $t=20^\circ\text{C}$ -də aparılır. Gel nümunə təxminən $20\text{mm} \times 15\text{mm} \times 10\text{mm}$ ölçüsündə götürülmüşdür. Nümunəyə verilən gərginlik diskret yüksəklər tərəfindən yaradılır. Sürüşmə deformasiyası fotoelementin köməyi ilə elektrik siqnalına çevrilir və qrafikcəkən Y girişinə verilir.

Qrafikcəkən yuxarıda qeyd olunan əyirləri (şəkil 2b və 2c) verir. Bu əyirlərə əsasən həm elastiklik modullarını həm də özlülüyü tapılmışdır:

$$G_0 = \frac{\sigma}{\gamma_0} \quad (6)$$

$$G_1 = \frac{\sigma}{\gamma_m - \gamma_0} \quad (7)$$

$$\eta = \frac{\sigma - \sigma_k}{\dot{\gamma}} = \frac{\sigma - \sigma_k}{\operatorname{tg} \alpha} \quad (8)$$

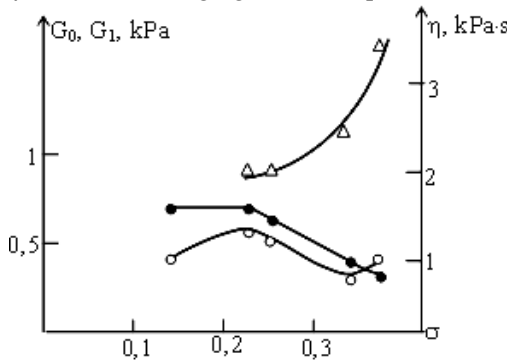
Şəkil 3-də 1%-li aqar gelinin ani (dolu dairələr) və gecikmiş elastiklik modulların (içibos dairələr), həmçinin statik özlülüğünün (üçbucaqlar) tətbiq olunan mexaniki gərginlikdən asılılıq qrafikləri göstərilmişdir. Nəticələri

aşağıdakı kimi şərh etmək olar:

1. σ_k kritik gərginliyindən aşağı gərginliklərdə ani elastiklik modulu G_0 demək olar ki, dəyişmir, bu gərginlikdən yuxarıda isə gərginlik artıqca azalır;

2. G_1 yüksəkelastiklik modulu σ_k kritik gərginliyindən aşağıda gərginlik artıqca artır, σ_k -dən yuxarıda isə azalır;

3. η özlülük əmsali gərginlik artıqca artır.



Şəkil 3.

Kiçik gərginliklərdə ani elastiklik modulunun demək olar ki, sabit qalması valent rabitələrinin və bucaqlarının gərginliklə mütənasib olmasının nəticəsidir. Yüksək elastiklik modulunun zəif artması isə göstərir ki, gərginlik artıqca polimer zəncirlərinin dərtiləşməsi çətinləşir. Lakin müəyyən gərginlikdən (σ_k) başlayaraq fəza toru əmələ gətirən rabitələr qırılmağa başlair və bu andan başlayaraq G_0 və G_1 kəskin azalmağa başlayır. 1%-li gel üçün möhkəmlik 20°C -də, qrafikdən göründüyü kimi 240Pa ətrafında olur. Gelin möhkəmliyini digər sadə üsulla da qiymətləndirmək olar. Bunun üçün gel nazik uzun şaquli bordan porşenlə sıxıb çıxarmaq lazımdır. Müəyyən uzunluqda (l_k) gel sütunu öz ağırlığı ilə qırılır [5]. Bu uzunluğu özcməklə gelin möhkəmliyi $\sigma_k = \rho gl_k$ düsturunun köməyi ilə hesablamaq olar. Qeyd edək ki, aqarın konsentrasiyasının artması gelin möhkəmliyinin kəskin artmasına səbəb olur. Məsələn, möhkəmliyin sonuncu üsulla qiymətləndirməsi 1%-li aqar gel üçün $\sigma_k \approx 270\text{ Pa}$, 2%-li aqar gel üçün isə $\sigma_k \approx 1,6\text{ kPa}$ verir.

Əksər qeyri-Nyuton mayelərində mexaniki gərginlik artıqca özlülüğün azalması müşahidə olunur. Çünkü gərginliyin artması axına (molekulların bir-birinə nəzərən yerdəyişməsinə) mane olan faktorların aradan qalxmasına səbəb olur. Lakin bəzi mürəkkəb mayelərdə (dispersiyyalarda, genişləndiricilərdə) əksinə xassə – mexaniki gərginlik artıqca özlülüğün azalması mümkünür [2]. Geldə də oxşar xassə müşahidə olunur (şəkil 3). Bunun səbəbini gelin mürəkkəb quruluşu ilə izah etmək olar. Geldə fəza toru müxtəlif səviyyəli assosatlardan - ikiqat spirallardan, supraliflərdən və ssosiatlaşmadan iştirak etməyən makromolekullardan ibarətdir. Özlüelastik xassələrdə bunların hər birinin öz payı vardır [6]. Belə mürəkkəb sistemlərdə gərginlik (və ya axın sürəti) artıqca axının çətinlişməsi mümkünür. Məsələn, gelə verilən gərginliyin bir hissəsi aqreqatların dağılmasına, digər hissəsi isə onların qarşılıqlı yerdəyişməsinə sərf oluna bilər. Bu versiyanın yoxlanması əlavə təcrübələr qoyulmasını tələb edir.

- [1] *E. Gregorova, W. Pabst, J. Stetina.* "Theory of Linear Viscoelasticity" Chekh. Journ. "Ceramics – Silikaty", 48(3), 2004, p.93-99
- [2] *S.A. Khan, J.R. Royer, S.R. Raghavan.* "Rheology: Tools and Materials" – Aviation Fuels with Fire Safety: A Proceedings, 1997, p.31-46
- [3] *Q.M. Bartenev, S.Ya. Frenkel.* Fizika polimerov, Leninqrad. "Химия ", 1990, 430 с.(Rusca).
- [4] *C.M. Dea I.* "Industrial Polysaccharides" ş Pure & Appl. Chemistry, v.61, No7, pp.1315-1322
- [5] *S. R. Raghavan, B.H. Cipriano.* "Gel formation: phase diagrams using tabletop rheology and calorimetry" – Molecular Gels: Materials with self-assembled fibrillar networks, ed by R.G.Weiss & P.Terech, 233-244, 2005 Springer

E.A. Masimov, A.R. Imamaliyev, K.M. Budagov

THE INVESTIGATION OF ELASTOVISCOUS PROPERTIES OF AGAR GELS BY REBINDER'S METHOD

In this work the dependence of instantaneous and high-elastic modules, as well as static viscosity of agar gels on applied stress in a tangential shear geometry has been studied. At the stresses lower than yield stress the instantaneous modulus almost doesn't change, but the high-elastic modulus increases slowly. If the applied stress exceeds the yield stress both quantities decrease by increasing of the stress. The obtained results are explained qualitatively.

Э.А. Масимов, А.Р. Имамалиев, К.М. Будагов

ИЗУЧЕНИЕ УПРУГОВЯЗКИХ СВОЙСТВ ГЕЛЕЙ АГАРА МЕТОДОМ РЕБИНДЕРА

В работе изучена зависимость мгновенной и высокоэластичной модулей упругости, а также статического коэффициента вязкости агаровой гели от приложенного механического напряжения в геометрии сдвиговой деформации. Ниже предела прочности геля мгновенный модуль почти не меняется, а высокоэластичный модуль слабо увеличивается с ростом напряжения, а при напряжениях выше предела прочности обе величины уменьшаются с ростом напряжения. Приводится качественное объяснение полученных результатов.

Received: 17.04.07

**PAYLANMA ƏMSALI VAHİDDƏN BÖYÜK OLDUQDA YENİ ÜSULLA DÜZƏLDİLMİŞ
XƏLİTƏNİN BAŞLANĞICININ QİDALANDIRICININ BAŞLANĞICI GÖTÜRMƏKLƏ
BƏRK MƏHLUL MONOKRİSTALLARININ ALINMASI**

V.İ. TAHİROV

Bakı Dövlət Universiteti, Bakı, Az-1145, Z. Xəlilov. 23

Z.Ə. AĞAMALIYEV, Z.Y. HƏSƏNOV

AMEA Fizika İnstitutu, AZ 1143, Bakı, H. Cavid pr., 33

Ə.F. QULİYEV, N.F. QƏHRƏMANOV

Sumqayıt Dövlət Universiteti

İşdə göstərilmişdir ki, yeni üsulla alınmış binar bərk məhlul xəlitəsinin, ikinci komponentin birincidə paylanması əmsali vahiddən böyük ($k>1$) olduqda, başlanğıcını qidalandırıcının başlanğıcı kimi istifadə etməklə bərk məhlulun sabit tərkibli monokristallarını yetişdirmək mümkündür. Bu zaman qidalandırıcının və kristalın yerdəyişmə sürətləri bir-birinə bərabər seçilməlidir. Beləliklə, Ge-B binar sistemi üçün ($k=17$) kəsilməzlik tənliyinin həllindən istifadə edilərək germaniumun borla aşqarlanmış sabit tərkibli monokristalları yetişdirilmişdir.

Binar bərk məhlulların monokristallarını yetişdirmək üçün, adətən, qidalandırıcı xəlitədən istifadə olunur. Biz [1]-də bu məqsəd üçün yararlı olan yeni üsulla alınmış

xəlitə boyunca tərkib paylanmasıının aşağıdakı kimi olduğunu göstərmışik:

$$C_1(t) = \begin{cases} C_0 \left\{ 1 - (1-k) \exp\left(-\frac{kvt}{l}\right) \right\}, & 0 \leq t \leq t_1 = \frac{L-l}{v} \text{ olğugda} \\ C_0 \left\{ 1 - (1-k) \exp\left(-\frac{kvt_1}{l}\right) \right\} \cdot \left(\frac{l-v(t-t_1)}{l} \right)^{k-1}, & t \geq t_1 \text{ olğugda} \end{cases} \quad (1)$$

Burada C_0 - xəlitədə ikinci komponentin orta konsentrasiyası, k - onun paylanması əmsali, L - xəlitənin uzunluğu, l - ərimiş zonanın eni, v - onun yerdəyişmə sürəti, t - zamanıdır.

Qatı binar bərk məhlulların monokristallarını almaq üçün $k>1$ olduqda bu cür xəlitənin sonunu, $k<1$ olduqda - başlanğıcını qidalandırmanın başlanğıcı kimi istifadə etmək lazımdır. Çünkü, bu halda kristallaşma cəbhəsində baş verən ifrat soyumanın qarşısını almaq mümkün olur. Bununla belə, bir sira hallarda binar bərk məhlul monokristallarının alınmasında yeni üsulla alınmış xəlitənin başlanğıcını $k>1$ halında qidalandırıcının başlanğıcı kimi seçməklə də uğurlu nəticələr almaq olar. Bu, kristallaşma cəbhəsində ifrat soyumanın nəzərə alınmayacaq dərəcədə kiçik olduğu tərkiblərdə mümkündür. Zəif bərk məhlullarda doğrudan da bu cür imkan yaranır. Əgər yada sal-saq ki, məsələn, yarımkərıcı monokristalların aşqarlanması məhz zəif bərk məhlulların monokristallarının alın-

ması deməkdir, onda bu variantın həyata keçirilməsinin nə qədər aktual olduğu aydın görünər. Ona görə də biz hazırkı işdə həmin variati araşdıracaqıq. (1) paylanmasıının birinci və ikinci sətinə uyğun olaraq prosesi iki mərhələdə həyata keçirəcəyik.

Qidalandırıcıya, yetişdirilən kristala, və kəsik konus şəkilli putadakı ərintiyə aid olan parametrləri uyğun olaraq 1,2 və 3 indeksləri ilə göstərəcəyik.

Birinci mərhələdə kristallaşma rejimini bu şərtlərə uyğun seçəcəyik:

$$S_1 = S_2 = S, \quad v_1 = v_2 = v \quad (2)$$

S_1, S_2 - xəlitənin və kristalın en kəsiyinin sahəsi, v_1 və v_2 - onların yerdəyişmə sürətləridir.

Birinci mərhələdə uyğun həcmələr və onların törəmələri belə olar:

$$\begin{aligned} V_2(t) &= V_1(t) = Svt, & V_3(t) &= V_3(0) + \eta(V_1(t) - V_2(t)) = V_3(0) \\ \dot{V}_2(t) &= \dot{V}_1(t) = Sv, & \dot{V}_3(t) &= 0 \end{aligned} \quad | \quad (3)$$

Burada vahid zamanda qidalandırıcıdan ərintiyə daxil olan maddənin miqdəri həmin müddətdə putadakı ərintidən kristallaşmaya sərf olunan maddənin miqdərinə bərabərdir. Ona görə ərintinin səthinin səviyyəsi dəyişməz

| qalır ($v_3=0$).

Kəsilməzlik tənliyindəki P və Q parametrlərinin ifadələrini yazaq [2]:

$$\left. \begin{aligned} P(t) &= \frac{\dot{V}_3(t) + k \dot{V}_2(t)}{V_3(t)} = \frac{kSv}{V_3(0)} \\ Q(t) &= \frac{\dot{V}_1(t)C_1}{V_3(t)} = \frac{C_0Sv}{V_3(0)} \left[1 - (1-k) \exp\left(-\frac{kvt}{l}\right) \right] \end{aligned} \right\} \quad (4)$$

İkinci komponentin konsentrasiyası üçün kəsilməzlik tənliyinin həllini yazaq [2]:

$$\begin{aligned} C_3(t) &= \exp\left(-\int P(t)dt\right) \left\{ \int Q(t) \exp\left(\int P(t)dt\right) dt + A_4 \right\} = \\ &= \exp\left(-\int \frac{kSv}{V_3(0)} dt\right) \left\{ \int \frac{SvC_0}{V_3(0)} \left[1 - (1-k) \exp\left(-\frac{kvt}{l}\right) \right] \cdot \exp\left(\int \frac{kSv}{V_3(0)} dt\right) dt + A_4 \right\} = \\ &= \exp\left(-\frac{kSvt}{V_3(0)}\right) \cdot \left\{ \int \frac{SvC_0}{V_3(0)} \left[1 - (1-k) \exp\left(-\frac{kvt}{l}\right) \right] \exp\left(\frac{kSvt}{V_3(0)}\right) dt + A_4 \right\} = \\ &= \exp\left(-\frac{kSvt}{V_3(0)}\right) \left\{ \frac{SvC_0}{V_3(0)} \left[\int \exp\left(\frac{kSvt}{V_3(0)}\right) dt - (1-k) \exp\left[kSv\left(\frac{1}{V_3(0)} - \frac{1}{Sl}\right)t\right] dt + A_4 \right\} = \\ &= \exp\left(-\frac{kSvt}{V_3(0)}\right) \left\{ \frac{C_0}{k} \left[\exp\left(\frac{kSvt}{V_3(0)}\right) - (1-k) \frac{IS}{IS - V_3(0)} \cdot \exp\left[kSv\left(\frac{1}{V_3(0)} - \frac{1}{Sl}\right)t\right] \right] + A_4 \right\} = \\ &= \frac{C_0}{k} \left[1 - (1-k) \frac{IS}{IS - V_3(0)} \exp\left(-\frac{kvt}{l}\right) \right] + A_4 \exp\left(-\frac{kSvt}{V_3(0)}\right) \end{aligned} \quad (5)$$

A_4 - integrallama sabitidir. Onun qiymətini başlanğıc şərtində istifadə etməklə tapacaqıq.

Burada başlanğıc şərtin seçilməsinin müxtəlif variantları ola bilər. Ancaq hələlik biz başlanğıc şərti elə seçəcəyik ki, prosesin başlanğıcında putadakı ərintidə ikinci komponentin konsentrasiyası sıfır bərabər olsun:

$$t = 0 \text{ -da } C_3(0) = 0 \quad (6)$$

Bu şərt daxilində (5)-dən alarıq:

$$\frac{C_0}{k} \left(1 - \frac{IS}{IS - V_3(0)} \right) + A_4 = 0$$

Buradan:

$$A_4 = -\frac{C_0}{k} \left[1 - \frac{IS(1-k)}{IS - V_3(0)} \right] \quad (7)$$

A_4 -ün qiymətini (5)-də yerinə yazaq:

$$\begin{aligned} C_3(t) &= \frac{C_0}{k} \left[1 - \frac{IS(1-k)}{IS - V_3(0)} \exp\left(-\frac{kvt}{l}\right) \right] - \frac{C_0}{k} \left[1 - \frac{IS(1-k)}{IS - V_3(0)} \right] \cdot \exp\left(-\frac{kSvt}{V_3(0)}\right) = \\ &= \frac{C_0}{k} \left\{ 1 - \exp\left(-\frac{kSvt}{V_3(0)}\right) + \frac{IS(1-k)}{IS - V_3(0)} \left[\exp\left(-\frac{kSvt}{V_3(0)}\right) - \exp\left(-\frac{kvt}{l}\right) \right] \right\} \quad 0 \leq t \leq t_1, \quad t_1 = \frac{L-l}{v} \end{aligned} \quad (8)$$

Kristal boyunca ikinci komponentin konsentrasiyasının paylanması isə belə olar:

$$C_2(t) = kC_3(t) = C_0 \left\{ 1 - \exp\left(-\frac{kSvt}{V_3(0)}\right) + \frac{IS(1-k)}{IS - V_3(0)} \cdot \left[\exp\left(-\frac{kSvt}{V_3(0)}\right) - \exp\left(-\frac{kvt}{l}\right) \right] \right\}, \quad 0 \leq t \leq t_1 \quad (9)$$

Yeni üsulla alınmış qidalandırıcının son l uzunluğunda ikinci komponentin konsentrasiyasının paylanması qanunu başqa cür olur. Ona görə bu hissə üçün kəsilməzlik tənliyi ni yenidən həll etmək lazımdır. Doğrudur, qidalandırıcı-nın son l uzunluğunun təyinatı başqadır və ondan praktiki olaraq kristal yetişdirmək üçün istifadə olunmur. Bununla

belə l -in kifayət qədər böyük qiymətlərində onun müəyyən hissəsindən kristal yetişdirmə prosesində istifadə etmək olar. Ona görə biz burada ikinci mərhələyə də baxacaqıq.

Yenə də:

$$S_1 = S_2 = S, \quad v_1 = v_2 = v \quad (10)$$

götürəcəyik.

Həcmərin yeni ifadələrini yazaq:

$$\left. \begin{aligned} V_1(t) &= V_1(t_1) + Sv(t-t_1) \\ V_2(t) &= V_2(t_1) + Sv(t-t_1) \\ V_3(t) &= V_3(0) + \eta(V_1(t) - V_2(t)) = V_3(0) \end{aligned} \right| \quad (11)$$

Həcmərin zamana görə birinci tərtib törəmələri isə bələ olar:

$$\dot{V}_1(t) = \dot{V}_2(t) = Sv, \quad \dot{V}_3(t) = 0 \quad (12)$$

P və Q parametrlərini də yazaq:

$$\left. \begin{aligned} P(t) &= \frac{kSv}{V_3(0)} \\ Q(t) &= \frac{C_0Sv}{V_3(0)} \left\{ 1 - (1-k) \exp\left(-\frac{kvt_1}{l}\right) \right\} \left(\frac{l-v(t-t_1)}{l} \right)^{k-1}, \quad t \geq t_1 \end{aligned} \right| \quad (13)$$

İkinci mərhələ üçün kəsilməzlik tənliyinin həllini tapaq:

$$\left. \begin{aligned} C_3(t) &= \exp\left(- \int P(t) dt\right) \left\{ \int Q(t) \exp\left(\int P(t) dt\right) dt + A_4 \right\} = \exp\left(- \int \frac{kSv}{V_3(0)} dt\right) \left\{ \int \frac{C_0Sv}{V_3(0)} \left[1 - (1-k) \exp\left(-\frac{kvt_1}{l}\right) \right] \right. \\ &\quad \cdot \left. \left(\frac{l-v(t-t_1)}{l} \right)^{k-1} \cdot \exp\left(\int \frac{kSv}{V_3(0)} dt\right) dt + A_4 \right\} = \exp\left(- \frac{kSvt}{V_3(0)}\right) \left\{ \int \frac{C_0Sv}{V_3(0)} \left[1 - (1-k) \exp\left(-\frac{kvt_1}{l}\right) \right] \right. \\ &\quad \cdot \left. \left(\frac{l-v(t-t_1)}{l} \right)^{k-1} \cdot \exp\left(\frac{kSvt}{V_3(0)}\right) dt + A_4 \right\} \end{aligned} \right. \quad (14)$$

k -nın ixtiyari tam qiyməti üçün sonuncu integrallı analitik şəkildə ifadə etmək mümkün deyil. Lakin biz təqribi hesablamadan istifadə etməklə $k>1$ olan ümumi hal üçün

integrallı hesablayacaq. Bunun üçün integrallaltı ifadədə bəzi dəyişikliklər aparaq:

$$\left(\frac{l-v(t-t_1)}{l} \right)^{k-1} = \left(1 - \frac{v(t-t_1)}{l} \right)^{k-1} \approx \left(1 - (k-1) \frac{v(t-t_1)}{l} \right) \quad (15)$$

Burada ikinci hədd 0-dan başlayaraq vahidə qədər dəyişir, bu dəyişmə intervalının başlangıcında $\frac{v(t-t_1)}{l} \ll 1$ olur. Biz (15)-i məhz bu başlangıç intervalı

fürən yazdıq. Əslində, praktiki olaraq, onun yalnız başlangıç intervalından istifadə etmək olar. (15)-i (14)-də istifadə edək. Özü də integrallı (J_4) ayrıca həll edib sonra yerinə yazaq:

$$\begin{aligned} J_4 &= \int \left(\frac{l-v(t-t_1)}{l} \right)^{k-1} \exp\left(\frac{kSvt}{V_3(0)}\right) dt \approx \int \left(1 - (k-1) \frac{v(t-t_1)}{l} \right) \exp\left(\frac{kSvt}{V_3(0)}\right) dt = \\ &= \int \left[\left(1 + (k-1) \frac{vt_1}{l} \right) - (k-1) \frac{vt}{l} \right] \exp\left(\frac{kSvt}{V_3(0)}\right) dt = \\ &= \left[\frac{V_3(0)}{kSv} \left(1 + (k-1) \frac{vt_1}{l} \right) \exp\left(\frac{kSv}{V_3(0)}\right) - (k-1) \frac{v}{l} \int t \exp\left(\frac{kSvt}{V_3(0)}\right) dt \right] = \\ &= \left[\frac{V_3(0)}{kSv} \left(1 + (k-1) \frac{vt_1}{l} \right) \exp\left(\frac{kSvt}{V_3(0)}\right) - (k-1) \frac{v}{l} \left(\frac{V_3(0)}{kSv} t \exp\left(\frac{kSvt}{V_3(0)}\right) - \frac{V_3(0)}{kSv} \int \exp\left(\frac{kSvt}{V_3(0)}\right) dt \right) \right] = \\ &= \frac{V_3(0)}{kSv} \left[\left(1 + (k-1) \frac{vt_1}{l} \right) - (k-1) \frac{v}{l} \left(t - \frac{V_3(0)}{kSv} \right) \right] \exp\left(\frac{kSvt}{V_3(0)}\right) \end{aligned} \quad (16)$$

J_4 -ü (14)-də yerinə yazaq:

$$\begin{aligned}
 C_3(t) &= \exp\left(-\frac{kSvt}{V_3(0)}\right) \left[\frac{C_0Sv}{V_3(0)} \left[1 - (1-k)\exp\left(-\frac{kvt_1}{l}\right) \right] \cdot \right. \\
 &\quad \cdot \frac{V_3(0)}{kSv} \left[\left(1 + (k-1)\frac{vt_1}{l} \right) - (k-1)\frac{v}{l} \left(t - \frac{V_3(0)}{kSv} \right) \right] \cdot \exp\left(\frac{kvt}{V_3(0)}\right) + A_4 \Big] = \\
 &= \frac{C_0}{k} \left[1 - (1-k)\exp\left(-\frac{kvt_1}{l}\right) \right] \left[\left(1 + (k-1)\frac{vt_1}{l} \right) - (k-1)\frac{v}{l} \left(t - \frac{V_3(0)}{kSv} \right) \right] + \\
 &\quad + A_4 \exp\left(-\frac{kSvt}{V_3(0)}\right), \quad t \geq t_1
 \end{aligned} \tag{17}$$

A_4 integrallama sabitini tapmaq üçün ikinci mərhələnin başlangıcını birinci mərhələnin sonu ilə üst-üstə sal-

maq lazımdır. Bu o deməkdir ki, $t=t_1$ anında (17) və (8) bir birləşmə bərabər olmalıdır. Bu şərti yazaq.
 $t=t_1$ -dən (17)-dən:

$$C_3(t_1) = \frac{C_0}{k} \left[1 - (1-k)\exp\left(-\frac{kvt_1}{l}\right) \right] \cdot \left[\left(1 + (k-1)\frac{vt_1}{l} \right) - (k-1)\frac{v}{l} \left(t_1 - \frac{V_3(0)}{kSv} \right) \right] + A_4 \exp\left(-\frac{kSvt_1}{V_3(0)}\right)$$

(8)-dən isə:

$$C_3(t_1) = \frac{C_0}{k} \left\{ 1 - \exp\left(-\frac{kSvt_1}{V_3(0)}\right) + \frac{(1-k)lS}{lS - V_3(0)} \left[\exp\left(-\frac{kSvt_1}{V_3(0)}\right) - \exp\left(-\frac{kvt_1}{l}\right) \right] \right\}$$

alariq. Son iki bərabərliyin sağ tərəflərini bərabərləşdirək:

$$\begin{aligned}
 &\frac{C_0}{k} \left[1 - (1-k)\exp\left(-\frac{kvt_1}{l}\right) \right] \left[\left(1 + (k-1)\frac{vt_1}{l} \right) - (k-1)\frac{v}{l} \left(t_1 - \frac{V_3(0)}{kSv} \right) \right] + A_4 \exp\left(-\frac{kSvt_1}{V_3(0)}\right) = \\
 &= \frac{C_0}{k} \left\{ 1 - \exp\left(-\frac{kSvt_1}{V_3(0)}\right) + \frac{(1-k)lS}{lS - V_3(0)} \left[\exp\left(-\frac{kSvt_1}{V_3(0)}\right) - \exp\left(-\frac{kvt_1}{l}\right) \right] \right\}
 \end{aligned}$$

Buradan A_4 -ü taparıq:

$$\begin{aligned}
 A_4 &= \frac{C_0}{k} \left\{ 1 - \exp\left(-\frac{kSvt_1}{V_3(0)}\right) + \frac{(1-k)lS}{lS - V_3(0)} \left[\exp\left(-\frac{kSvt_1}{V_3(0)}\right) - \exp\left(-\frac{kvt_1}{l}\right) \right] - \left[1 - (1-k)\exp\left(-\frac{kvt_1}{l}\right) \right] \cdot \right. \\
 &\quad \cdot \left. \left[\left(1 + (k-1)\frac{vt_1}{l} \right) - (k-1)\frac{v}{l} \left(t_1 - \frac{V_3(0)}{kSv} \right) \right] \right\} \exp\left(\frac{kSvt_1}{V_3(0)}\right)
 \end{aligned} \tag{18}$$

A_4 -ün bu qiymətini (17)-də yerinə yazmaq lazımdır.

İkinci mərhələdə kristal boyunca paylanma bələ olacaq:

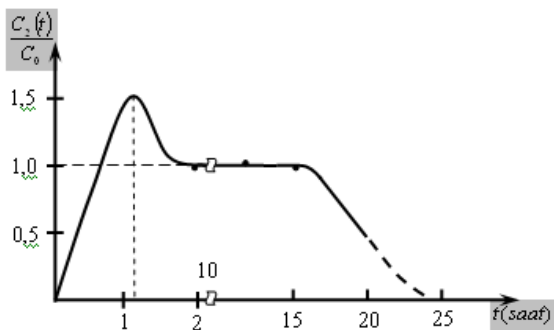
$$\begin{aligned}
 C_2(t) &= kC_3(t) = C_0 \left[1 - (1-k)\exp\left(-\frac{kvt_1}{l}\right) \right] \left[\left(1 + (k-1)\frac{vt_1}{l} \right) - \right. \\
 &\quad \left. - (k-1)\frac{v}{l} \left(t - \frac{V_3(0)}{kSv} \right) \right] + kA_4 \exp\left(-\frac{kSvt}{V_3(0)}\right)
 \end{aligned} \tag{19}$$

A_4 -ün (18) ifadəsini burada yerinə yazmaq lazımdır. Bütün kristal boyunca ikinci komponentin konsentrasiyasının dəyişmə qanununu almaq üçün (9)-ilə (19)-ı birləşdirmək lazımdır:

$$C_2(t) = \begin{cases} C_0 \left\{ 1 - \exp\left(-\frac{kSvt}{V_3(0)}\right) + \frac{lS(1-k)}{lS - V_3(0)} \cdot \left[\exp\left(-\frac{kSvt}{V_3(0)}\right) - \exp\left(-\frac{kvt}{l}\right) \right] \right\}, & 0 \leq t \leq t_1 \\ C_0 \left\{ \left[1 - (1-k) \exp\left(-\frac{kvt_1}{l}\right) \right] \left[\left(1 + (k-1) \frac{vt_1}{l} \right) - \left(k-1 \right) \frac{v}{l} \left(t - \frac{V_3(0)}{kSv} \right) \right] + \frac{k}{C_0} A_4 \exp\left(-\frac{kSvt}{V_3(0)}\right) \right\}, & t \geq t_1 \end{cases} \quad (20)$$

A_4 -ün (18) ifadəsini burada yerinə yazmaq lazımdır.

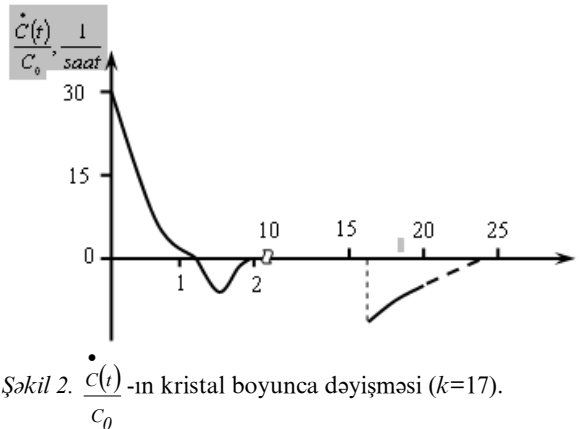
Qeyd edək ki, burada biz birinci mərhələ üçün $C_2(t)$ -nin kristal boyunca dəyişmə qanununu alarkən k -nın qiymətinə heç bir məhdudiyyət qoymadıq. O, vahiddən həm böyük, həm də kiçik ola bilər. İkinci mərhələdə isə k -nın qiymətinin vahiddən böyük olması şərtini qoymuşduq. Bu məhdudiyyəti kəsilməzlik tənliyində iştirak edən integralların analitik şəkildə ifadə oluna bilməsi üçün qoymuşduq. İkinci mərhələ üçün digər məhdudiyyət qidalandırıcıını uyğun hissəsinin yalnız az bir qisminin istifadə oluna bilməsi imkanından irəli gəlir.



Şəkil 1. Ge-B sistemi üçün (20)-dən hesablanmış $\frac{C_2(t)}{C_0}$ -in kristal boyunca dəyişməsi.

Şəkil 1-də germaniumda bor aşqarı üçün (borun Ge-də paylanması əmsali $k=17$ -dir [3]). (20)-dən kristal boyunca hesablanmış konsentrasiya dəyişməsi göstərilmişdir. Bu halda da ikinci komponentin konsentrasiyası sıfırdan başlayaraq artır. Ancaq burada artım daha kəskindir. Özü

də bu kəskin artım iti maksimumdan keçir və sonra azalaraq sabit qiymətə (C_0 -a) yaxınlaşır. Kristalın sonunda (yəni qidalandırıcının son l uzunluğuna uyğun gələn hissəsində) konsentrasiya azalmağa başlayır. Onu da qeyd etməliyik ki, burada ərintidə (daha doğrusu, kristallaşma cəbhəsində) ikinci komponentin konsentrasiyası kiçik ($10^{15} \div 10^{16} \text{ sm}^{-3}$ tərtibində) olduğu üçün ikinci komponentin konsentrasiyasının başlangıçda xeyli kəskin artması və maksimumdan keçməsi kristallaşma cəbhəsində ifrat soyumanın yaranmasına səbəb olmur. Ona görə bərk məhlül monokristallarının alınması üçün mövcud olan əlverişli şərait pozulmur.



İkinci komponentin konsentrasiyasının kristal boyunca dəyişmə sürətinin necə olduğunu müəyyən etmək üçün $C_2(t)$ -nin zamana görə birinci tərtib törəməsini almaq lazımdır. Birinci mərhələ üçün (20)-in birinci sətirindən alarıq:

$$\begin{aligned} \dot{C}_2(t) &= C_0 \left\{ \frac{kSv}{V_3(0)} \exp\left(-\frac{kSvt}{V_3(0)}\right) + \frac{lS(1-k)}{lS - V_3(0)} \cdot \left[-\frac{kSv}{V_3(0)} \exp\left(-\frac{kSvt}{V_3(0)}\right) + \frac{kv}{l} \exp\left(-\frac{kvt}{l}\right) \right] \right\} = \\ &= C_0 \frac{kSv}{lS - V_3(0)} \left\{ \frac{kSl - V_3(0)}{V_3(0)} \exp\left(-\frac{kSvt}{V_3(0)}\right) + (1-k) \exp\left(-\frac{kvt}{l}\right) \right\}, \quad 0 \leq t \leq t_1 \end{aligned} \quad (21)$$

$\dot{C}_2(t)$ -ni sıfıra bərabər etməklə əyrinin maksimumuna uyğun gələn $t=t_{max}$ -u tapa bilərik:

$$C_0 \frac{kSv}{lS - V_3(0)} \left\{ \frac{kSl - V_3(0)}{V_3(0)} \exp\left(-\frac{kSvt}{V_3(0)}\right) + (1-k) \exp\left(-\frac{kvt}{l}\right) \right\} = 0$$

Buradan alarıq:

$$\frac{kSl - V_3(0)}{(k-1)V_3(0)} \exp\left(-\frac{kSvt}{V_3(0)}\right) = \exp\left(-\frac{kvt}{l}\right) \quad (23)$$

Hər iki tərəfi l əsasından loqarifmalayıb t -ni tapaqq:

$$\ln \frac{kSl - V_3(0)}{(k-1)V_3(0)} - \frac{kSvt}{V_3(0)} = -\frac{kvt}{l} \quad (22)$$

Təcrubi parametrlərin qiymətləri belə seçilmişdir: $l=18mm$, $V_3(0)=900mm^3$, $r=4mm$, $S=\pi r^2=50,24mm^2$, $v=2\frac{mm}{saat}$,

$k=17$ (borun Ge-da paylanma əmsalı).

(23)-dən t_{max} -un ədədi qiymətini tapaqq:

Buradan $t=t_{max}$ -u belə alarıq:

$$t_{max} = \frac{18 \cdot 900}{17 \cdot 2(18 \cdot 50,24 - 900)} \ln \frac{18 \cdot 50,24 \cdot 17 - 900}{16 \cdot 900} = 100,95 \cdot 0,01 = 1,01(\text{saat})$$

$$t_{max} = 1,01 \text{ saat}$$

$\dot{C}_2(t)$ -nin kristal boyunca dəyişməsi şəkil 2-də göstərilmişdir. Göründüyü kimi, $\frac{\dot{C}_2(t)}{C_0}$ başlangıçda ən böyük qiymətə malikdir, sonra o, tədricən azalaraq t_{max} -da sıfır-

dan keçir, işarəsinə dəyişir, minimum qiymətdən keçərək, yenidən sıfıra yaxınlaşır. Sonuncu qiymət $t=t_1$ anına qədər davam edir.

İkinci mərhələdə (yəni $t>t_1$ olduqda) $\dot{C}(t)$ -ni bələ alarıq:

$$\dot{C}(t) = C_0 \left\{ - (k-1) \frac{v}{l} \left[1 + (k-1) \exp\left(-\frac{kvt_1}{l}\right) \right] - \frac{k}{C_0} \cdot \frac{kSv}{V_3(0)} \cdot A_4 \cdot \exp\left(-\frac{kSvt}{V_3(0)}\right) \right\} \quad (24)$$

İkinci mərhələ üçün $\dot{C}_2(t)$ mənfi qiymət alır və kristalın sonuna yaxınlaşdıqca sıfıra yaxınlaşır (təcrübədə

alinması mümkün olmayan hissə qırıq xətlə verilmişdir).

- [1] V.I.Tahirov, Z.O.Ağamaliyev, S.R.Sadixova, Ə.F.Quliyev, N.F.Qəhrəmanov «Tərkibi qeyri-müntəzəm paylanmış qidalandırıcı xəlitənin tətbiqi ilə binar bərk məhlul monokristallarının alınması» SDU Xəbərləri №1 2007 səh. 3-13
 [2] V.I.Taqirov. Poluprovodnikoviye tvyordiyе rastvorı

- [3] Ge-Si. İz-v. «Elm», Baku, 1983.(Rusca).
 S.A. Medvedev. Vvedeniye v texnologiyu poluprovodnikovix materialov. İzd-v. «Visşaya şkola», Moskva, 1970.(Rusca).

V.I. Tagirov, Z.A. Agamalyev, Z.Y. Hasanov, A.F. Quliyev, N.F. Qahramanov

OBTAINING OF BINARY SOLID SOLUTION SINGLE CRYSTALS USING THE BEGINNING OF THE FEEDING INGOT AS REPLENISHMENT BEGINNING AT K>1 BY NEW METHOD

Binary solid solutions single crystals with permanent content distribution have been grown using ingots made by new method and truncated cone crucible. When second component distribution coefficient is more than unit the end of the ingot is taken as the beginning of the feeding ingot. The velocities of replacement of the feeding ingot and the grown crystal are taken the same.

The method applied to Ge-B binary system.

В.И. Тагиров, З.А. Агамалыев, З.Й. Гасанов, А.Ф. Гулиев, Н.Ф. Гахраманов

ПОЛУЧЕНИЕ БИНАРНЫХ ТВЁРДЫХ РАСТВОРОВ МОНОКРИСТАЛЛОВ ИСПОЛЬЗОВАНИЕМ НАЧАЛА НОВЫМ МЕТОДОМ ПОЛУЧЕННОГО ПОДПИТЫВАЮЩЕГО СЛИТКА КАК НАЧАЛА ПОДПИТКИ ПРИ k>1

В работе решением уравнения непрерывности показано, что использованием начала слитка, полученного новым методом, когда коэффициент распределения второго компонента больше единицы, можно получать монокристаллы бинарных твёрдых растворов с постоянным составом. При этом скорости перемещения подпитки и монокристалла нужно выбирать одинаковыми.

Таким образом, получены монокристаллы германия, легированные бором ($k=17$) с различными постоянными концентрациями.

Received: 21.09.07

**THE CURRENTS, LIMITED BY THE SPACE CHARGES IN
CHALCOGENIDE VITREOUS SEMICONDUCTORS OF $\text{Se}_{95}\text{As}_5$ SYSTEM, CONTAINING
THE SAMARIUM IMPURITIES**

A.I. ISAYEV, S.I. MEKHTIYEVA, N.Z. JALILOV, R.I. ALEKPEROV, V.Z. ZEYNALOV

Physics Institute of Azerbaijan National Academy of Sciences,

Az-1143, Baku, Javid str. 33

It is established, that transition of charge (holes) carriers transfer in $\text{Al}-\text{Se}_{95}\text{As}_5-\text{Te}$ structure is carried out by the current mechanism of monopolar injection, limited by the space charges at the participation of two groups of shallow traps (shallow E_{t1}), corresponding to charged intrinsic defects C_1 , caused by selenium broken bonds and deep (E_{t2}), corresponding also to charged intrinsic defects P_2^- , created by arsenic atoms with the broken coordination. It is shown that samarium impurities strongly influence on the mechanism of current-going and on the parameters of shallow traps (energy state and concentration); in which connection mainly influence on the deep traps.

Such peculiarities of chalcogenide vitreous semiconductors (CVS), as structure change and electric properties under the light action, in particular, the change of index of light refraction, optical absorption edge, and also the appearance of unpaired spins, which are registered by the electron spin resonance, photoluminescence with Stokes shift, fatigue and etc. make the given materials perspective for the use in the different electric switches, storage devices, infrared technique, and also in the different acousto-optic devices [1-3]. CVS of $\text{Se}_{95}\text{As}_5$ system differs by the crystallization stability [4] and has the improved parameters of the electric charge transition at the introduction of halogen impurity (Cl, Br), and also high photosensitivity [5-6], that makes given CVS more attractive material.

The states, caused by the 4f states of rare earth element ions, form at the use of rare earth elements (REE) in the capacity of the impurities in the forbidden band CVS and in this case the optic width of the forbidden band CVS will be covered on the energy at most possible transition number, allowed for REE ion (Sm), that leads to the essential change of its optic, photoelectric and electric properties [7-10]. For the understanding of electron process mechanisms, which are responsible for above mentioned peculiarities it is necessary to define the energy spectrums of localized states in the forbidden band, for which the current investigation, limited by space charges (CLSC) is the one from the certain methods, to which the given work is dedicated.

The experiment and sampling techniques

The CVS synthesis of $\text{Se}_{95}\text{As}_5$ with samarium impurity is carried out by the melting of the corresponding quantities of chemical elements of high purity in evacuated quartz ampoules up to 10^{-6} millimeter of mercury at temperatures, higher 900°C into rotating stove with the further cooling in the mode of out stove. The impurity introduces in the synthesis process, its concentration is in the limits $0,001\div 1\text{at\%}$.

The volt-ampere characteristics (VAC) are measured in the stationary mode on the standard technique. The samples present themselves structure "sandwich" with aluminic and telluric electrodes. The samples for the measurements are produced by the method of thermal vacuum evaporation $\sim 10^{-6}$ millimeter of mercury. The film width is measured by interferometer method and varied in the range $0,2\div 8\text{mcm}$.

VAC of $\text{Al}-\text{Se}_{95}\text{As}_5-\text{Te}$ structure with samarium impurity are investigated at the applying of electric field of both

polarities. CLSC mode is observed at the application of positive potential to Te, and at the reversal polarity VAC of N-type is observed.

The results and their discussion

VAC of $\text{Al}-\text{Se}_{95}\text{As}_5-\text{Te}$ structure with samarium impurity at the application of the positive (fig.1a) and negative (fig.1b) potentials to Te at room temperature is shown on the fig.1. VAC of VAC of Al-amorphous selenium-Te structure is also presented on the fig.1a. It is seen, that VAC of the given structures at the application of positive potential to Te consists in several regions.

The dependence $I\sim V^n$ where $n\leq 1$ is observed in the most samples at small voltages. Further, the dependence $I\sim V^n$, where n in the different regions of VAC has the different values, evidences, that transition of charge carriers (holes) in the given structure is carried out by the current mechanism of monopolar injection, limited by space charges at the participation of shallow traps of charge carriers, is observed. The investigation shows, that the voltage, at which the nonlinear dependence of current intensity on the voltage begins, quadratically depends on the sample width that proves the CLSC mechanism embodiment once again. As it is shown from the fig.1,a, VAC of amorphous selenium at small values of applied voltages with voltage increase is obeyed to ohmic law, which transfers to quadratic law, after which the current begins to strongly increase with the increase of applied voltage, the region, called by "total trap filling" is observed [11]. Further this region is replaced by another one, in which the current quadratic dependence on voltage, $I\sim V^2$ is observed. Such VAC behavior corresponds to CLSC mechanism, controlled by small traps [11]. VAC of $\text{Al}-\text{Se}_{95}\text{As}_5-\text{Te}$ structure differs from VAC of amorphous selenium by the fact, that region, corresponding to power law, i.e. $I\sim V^n$, where n exceeds 2 goes after the region, which is obeyed to ohmic law. Further, the region, where $I\sim V^2$ is observed. Finally, the quadratic region is changed by the other one, in which VAC slope increases again. The VAC peculiarities of $\text{Al}-\text{Se}_{95}\text{As}_5-\text{Te}$ structures, investigated by us prove about the fact, that transition of electric charge in the given material is controlled by the two groups of trap centers with the depths of occurrence E_{t1} and E_{t2} , situated in the different sides of Fermi level. Simultaneously, voltage values, at which the region, corresponding to strong current increase, i.e. to the mode, corresponding to limit trap filling is observed, shifts to high voltages, that proves about the

increase of the concentration of local states, being the shallow traps of the main charge carriers. The samarium impurities quite complicated influence on VAC forms and on the values of voltage transient between different regions. The concentration growth of samarium atoms up to 0,005 at% leads to gradually reconstruction of VAC form,

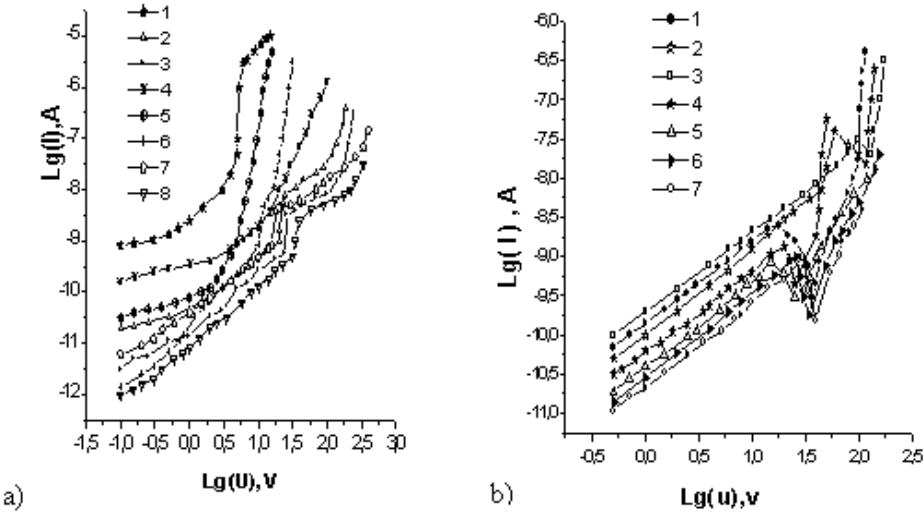
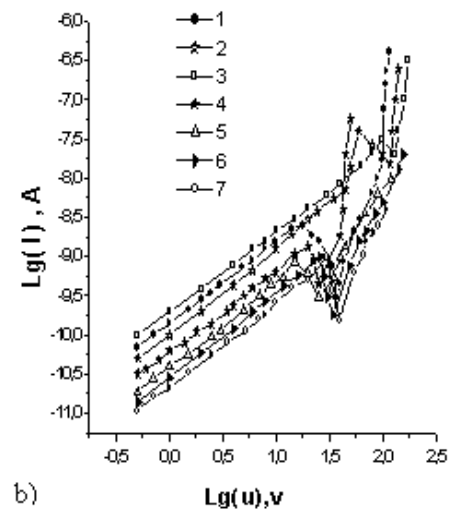


Fig.1. Volt-ampere characteristics (VAC) of Al-Se₉₅As₅-Te structure with samarium impurity at applied positive (fig.1,a) and negative (fig.1,b) potentials to Te at room temperature.

The influence of chemical composition and samarium impurities on the VAC behaviors allows us to say the some thoughts about the nature of local states and their energy position in the forbidden band relatively to equilibrium position of Fermi level, controlling current going in the investigated materials. The shallow traps of the charge main carriers (holes) in amorphous selenium are small (E_{tl}), i.e. are situated below, than value of equilibrium Fermi level. It is supposed, that local states, which control VAC in amorphous selenium are connected with charged intrinsic defects C_1^- , caused by broken selenium bonds. It is supposed, that the charged intrinsic defects P_2 , created by arsenic atoms with violated coordination exist parallel with defects of C_1^- type in CVS of Se₉₅As₅ system. The existence possibility of such defects in CVS, containing arsenic is also informed in the ref [12]. According to forms of VAC, the energy state of local states, corresponding to given defects should be higher Fermi level, i.e. are deep ones.

At low voltages the holes, injected in Se₉₅As₅ system from tellurium contact are captured by deep traps (E_{tl}), but the conductivity stays ohmic one because of the presence of equilibrium holes. The filling of E_{tl} centers takes place with voltage increase and simultaneously the concentration of free hole concentration increases and the moment when concentration of injected free holes exceeds the concentration of equilibrium holes, the current strongly increases with voltage increase, i.e. the so-called region of "limit trap filling" is observed. After it the current is controlled by the E_{tl} traps, moreover the trap square-law is observed still Fermi quazi-level stays higher, than E_{tl} level. The slope increase of VAC on the last region probably is connected with thermofield hole emission from trap levels. In the proof of the last said the fact evidences, that strong current increase takes place at the same values resistance of applied field at the inverse polarity of applied field, when CLSC mode isn't

corresponding to CLSC in the amorphous selenium. Further the concentration growth of samarium atoms, lead to the fact, that VAC becomes the same, as in CVS of Se₉₅As₅ system. Analogically, the halogen impurities influence on the drift mobility of charge carriers that is successfully explained in the limits of the model of charged intrinsic defects [5-6].



observed, that also is connected with field trap emptying (fig.1,b). The influence of rare earth element impurities on VAC can be explained, if the submissions, developed in the model limits of charged intrinsic defects [12] could be involved.

According to this model, the transition of charge carriers in CVS is controlled by U -centers, presenting themselves the charged defects D^+ and D^- , which form from initial neutral defects D^0 on the reaction:



Where D^+ and D^- -centers are traps for electrons and holes. It is supposed, that role of C_1^- and P_2 centers, connected by broken centers of selenium and arsenic atoms with violated coordination play in our case the role of D^- -centers, correspondingly.

The electric neutrality law should be carried out at the introduction of positive charged impurity A^+ into CVS (it is supposed, that samarium mainly reveals in the form of positive charged ion Sm⁺³):

$$[A^+] + [D^+] = [D^-] . \quad (2)$$

According to the law of mass action, the quantitative relation between concentrations of charged centers is expressed by the expression:

$$[D^+] [D^-] = [D^0]^2 = const . \quad (3)$$

According (2) and (3), at the introduction of positive charged A^+ impurity the concentration of D^+ -centers should decrease, and concentrations of D^- -centers should increase, that should influence on the current-going mechanisms. If we

take into consideration that hole transition in CVS of Se₉₅As₅ system is controlled by the local states, connected by D⁻ centers, then it is possible to explain the changes, taking place in VAC at the concentration change of samarium atoms. Indeed, the voltages, at which the region, corresponding to limit trap filling is observed, shifts to high value of applied voltage, that evidences about growth of trap concentration of hole shallow at relatively big concentrations (0,6 1at%). The influence of samarium impurities on VAC at small concentrations doesn't take place in the limits of the model of intrinsic charged defects, i.e. the region, corresponding to the filling of deep centers disappears; in the result of participation of samarium impurity in VAC, i.e. the concentration of deep states decreases. The halogen impurities take an effect the same influence on D⁺ and D⁻ centers, i.e. halogen impurities in the small concentrations decrease the concentrations of intrinsic defects of both signs [5-6]. The analogous influence is observed in the present paper and probably, is caused by chemical activity of REE atoms, which are able to form the chemical compounds with selenium and arsenic, in the result of which the concentration of initial intrinsic defects decreases, too.

The some parameters, characterizing the transition of electric charge in CVS of Se₉₅As₅ system, and also parameters of hole shallow traps are defined, using the known CLSC theory [11].

The film specific resistance is calculated from the ohmic region of VAC and using these values, the concentration of equilibrium free holes (table) from the formula $\rho = (e\rho_0\mu)^{-1}$, where e is elementary charge and μ is mobility of free carriers in the allowed band $\mu=10\text{cm}^2/\text{V.s.}$ is estimated. Using this formula

$$\rho_0 = N_v \exp\left(-\frac{F_0 - E_v}{kT}\right) \quad (4)$$

Fermi level in the forbidden band (F_0-E_v) (table №1), where N_v is effective state density in the valency band, kT is thermal energy, is defined. At calculations N_v was equal to 10^{19}cm^{-3} [12].

The concentration (p_{t02}) of traps, initially disengaged by the holes with E_{t2} energy is calculated from the equation:

$$V_{FCT} = \frac{ep_{t02}L^2}{\epsilon} \quad (5)$$

and is presented in the table №1, where V_{FCT} is voltage, at which the region of total filling of E_{t2} traps begins. As it is seen from the table $p_{t02} \gg p_0$. As it was mentioned above, the deep levels in the investigated materials are connected with D⁻(P₂⁻). Taking into consideration the concentration of P₂⁻ centers (N_{t2}) in 10^{16}cm^{-3} order [18], on the formula

$$p_{t02} = \frac{N_{t2}}{1 + g_A \exp(\frac{E_{t2} - F_0}{kT})} \approx \frac{N_{t2}}{g_A} \exp(\frac{F_0 - E_{t2}}{kT}). \quad (6)$$

The energy position of E_{t2} level (table №1) is calculated. G_A is the coefficient of spin degeneration of E_{t2} level in the formula (6). It is considered, that $g_A=2$.

Taking into consideration, that Fermi quasi-level for the holes (F) coincides with E_{tl} with accuracy up to kT on the region, where trap quadratic law (TQL) begins, the energy position of E_{tl} level, where P_{FCT} is concentration of free holes, injected into the sample at the voltage, corresponding to beginning of TQL (V_{FCT}) regions, is estimated.

$$E_{tl} - F_0 \approx F - E_v = kT \ln \frac{N_v}{p_{FCT}} \quad (7)$$

The ρ_{FCT} values are calculated from the formula:

$$V_{FCT} = \frac{ep_{FCT}L^2}{\epsilon}. \quad (8)$$

The estimation results of E_{tl} also are presented in the table №1.

Table №1

	F ₀ -E _v , eV	P _{t02} , Sm ⁻³	E _{t2} , eV	E _{tl} , eV
Se	0,7	-	-	0,26
Se ₉₅ As ₅	0,79	$4,256 \times 10^{14}$	0,856	0,23
Se ₉₅ As ₅ Sm _{0,001}	0,8	$5,9 \times 10^{14}$	0,847	0,23
Se ₉₅ As ₅ Sm _{0,005}	0,75	-	0,875	
Se ₉₅ As ₅ Sm _{0,01}	0,78	-	0,887	
Se ₉₅ As ₅ Sm _{0,1}	0,79	$1,22 \times 10^{14}$	0,89	
Se ₉₅ As ₅ Sm _{0,6}	0,8	$3,33 \times 10^{14}$	0,859	0,24
Se ₉₅ As ₅ Sm ₁	0,8	$4,34 \times 10^{14}$	0,86	0,21

As it is seen from the table the energy state of E_{tl} level corresponds to the activation energy of the hole drift mobility in the amorphous selenium, that also evidences about the connection of the given states with the charged intrinsic defects C₁⁻, caused by the broken selenium bonds. This fact allows to accept the value 10^{19} cm^{-3} [12], which corresponds to the density of localized states, controlling the hole drift mobility for center concentrations with energy $E_{tl}(N_{tl})$.

Conclusion

In the result of the carried investigations it is established, that transition of charge carriers (holes) in Al-Se₉₅As₅-Te structure is carried out by the mechanism of currents of monopolar injection, limited by space charges at the participation of two group of shallow traps (small E_{tl}),

corresponding to charged eigen defects C₁⁻, caused by the broken selenium bonds and deep (E_{t2}), corresponding to charged eigen defects P₂⁻, formed by arsenic atoms with violated coordination. It is shown that samarium impurities strongly influence on the mechanism of current going and on the parameters of shallow traps (energy state and concentration); moreover, mainly influence on deep traps, connected by charged intrinsic defects P₂⁻, formed by arsenic atoms with violated coordination. The small content of Sm impurity (till 0,01 at%) increases their energy deep, decreasing the concentration of deep traps, and big concentrations of the given impurities (more than 0,01 at%) decrease their energy deep, increasing the concentrations of these traps. The behavior of Sm impurity in small concentrations is explained by chemical activity of REE,

which are able to form the chemical compounds with selenium and arsenic, in the result of which the concentration of initial intrinsic defects decreases. The behavior of samarium impurity in big concentrations takes place according to the model of charged intrinsic defects [12], i.e. if

it is taken into consideration, that samarium impurities mainly reveal in the form of positively charged ions, then in the result of their presence the concentration of U -centers should change: concentration of D^+ -centers decreases, and D^- -centers increases, that indeed is observed in experiments.

- [1] *A. Meden, M. Sho. Fizika i primenie amorfnykh poluprovodnikov.* Mir, M., 1991, 670 s.
- [2] K. Shimakawa, A. Kolobov. *Adv. Phys.*, 1995, 44, 475.
- [3] *K.L.Bhatia, G. Parthasarathy, E.S.P. Gopal.* *J.Non – Crist. Sol.*, 1985, 69, 189.
- [4] *A.I. Isaev, L.P. Kazakova, E.A. Lebedev, S.I. Mekhtieva, I.I. Yatlinko.* *Sposob polucheniya khalkogenidnikh etekloobraznikh poluprovodnikov na osnove Se – As.* A. S. №1512015, Moskva, 1989.
- [5] *L.P. Kazakova, E.A. Lebedev, A.I. Isaev, S.I. Mekhtieva, N.B. Zakharova, I.I. Yatlinko.* FTP, 1993, 27, 959.
- [6] *L.P. Kazakova, E.A. Lebedev, N.B. Zakharova, I.I. Yatlinko, A.I. Isayev, S.I. Mekhtiyeva.* *J. of Non-Cristalline solids*, 1994, 167, 65.
- [7] *S.A. Kozyukhin, A.R. Fayrushin, E.N. Voronkov.* FTP, 2005, 39, 1012.
- [8] *H. Harada, Tanaka Keiji.* *J.Non – Crist. Sol.* 1999, 246, 189.
- [9] *A. Zakery, S.R. Ellion.* *J.Non – Crist. Sol.*, 2003, 330.
- [10] *S.G. Bishop, D.A. Turnbuli, B.G. Aitker.* *J.Non – Crist. Sol.*, 2000, 266-269, 867.
- [11] *M. Lampert, P. Mark.* *Injektionnie toki v tverdikh telakh.* M., 1973, 416 s.
- [12] *N.F. Mott, E.A. Devis.* *Elektronnie protsessi v nekristallicheskikh veshestvakh* (M., Mir, 1982) (Per. s anql. Mott N. Davis E., *Electronic processes in non-cryst. Solids*).
- [13] *P.W. Anderson.* *Phys. Rev. Lett.*, 1975, 37, 953.
- [14] *N.F. Mott, E.A. Davis, R.A. Street.* *Phil. Mag. B*, 1975, 32, 961.
- [15] *R.A. Street, N.F. Mott.* *Phys. Rev. Lett.*, 1975, 35, 1293.
- [16] *M. Kastner, D. Adler, H. Fritzsche.* *Phys. Rev. Lett.*, 1976, 37, 1504.
- [17] *H. Fritzsche, M. Kastner.* *Phil. Mag. B*, 1978, 37, 285.
- [18] *L.P. Kazakova, K.D. Tsendin.* FTP, 1999, 33, 866 .

A.İ. İsayev, S.İ. Mehdiyeva, N.Z. Cəlilov, R.İ. Ələkbərov, V.Z. Zeynalov

TƏRKİBİNDƏ SAMARIUM AŞQARI OLAN $\text{Se}_{95}\text{As}_5$ - ŞÜŞƏVARİ HALKOGENİD YARIMKEÇİRİCİ SİSTEMLƏRİNDE FƏZA YÜKLƏRİ İLƏ MƏHDUDLANMIŞ CƏRƏYANLAR

Müəyyən olunmuşdur ki, $\text{Al}-\text{Se}_{95}\text{As}_5-\text{Te}$ strukturunda yüksələnməsi iki qrup zəptetmə tələsinin iştirakı olduqda (qırılmış selen rabişələri ilə bağlı olan C_1^- məxsusi yüksələn defektlərə uyğun gələn dayaz (E_{1l}) və arsen atomları tərəfindən yaradılan $-P_2^-$ məxsusi yüksələn defektlərə uyğun gələn dərin (E_{12}) fəza yüksələri ilə məhdudlanmış monopolyar injeksiya cərəyanları ilə baş verir. Göstərilmişdir ki, samarium aşqarları cərəyanın keçmə mehanizmində və zəptetmə tələsinin parametrlərinə (energetik vəziyyəti və konsentrasiyası) nəzərə çarpan səviyyədə təsir göstərir. Lakin qeyd olunmuşdur ki, samarium aşqarları əsasən arsen atomları ilə yaradılan $-P_2^-$ məxsusi yüksələn defektlərlə bağlı olan dərin zəptetmə tələlərinə təsir edir.

А.И. Исаев, С.И. Мехтиева, Н.З. Джалилов, Р.И. Алексперов, В.З. Зейналов

ТОКИ, ОГРАНИЧЕННЫЕ ПРОСТРАНСТВЕННЫМИ ЗАРЯДАМИ В ХАЛЬКОГЕНИДНЫХ СТЕКЛООБРАЗНЫХ ПОЛУПРОВОДНИКАХ СИСТЕМЫ $\text{Se}_{95}\text{As}_5$, СОДЕРЖАЩИЕ ПРИМЕСИ САМАРИЯ

Установлено, что перенос носителей заряда (дырок) в структуре $\text{Al}-\text{Se}_{95}\text{As}_5-\text{Te}$ осуществляется по механизму токов монополярной инъекции, ограниченных пространственными зарядами, при участии двух групп ловушек захвата (мелкие E_{1l} , соответствующие заряженным собственным дефектам C_1^- , обусловленные оборванными связями селена и глубокие E_{12} , соответствующие также заряженным собственным дефектам P_2^- , создаваемыми атомами мышьяка с нарушенной координацией). Показано, что примеси самария сильно влияют на механизм токопрохождения и на параметры ловушек захвата (энергетическое положение и концентрация); в основном, на глубокие ловушки.

Received: 18.09.07

THE DOPING INFLUENCE OF NEAR-SURFACE REGIONS OF PHOTOSEMICONDUCTOR MICROPARTICLES BY ANNEALING IN CHLORINE ATMOSPHERE ON THE ELECTROPHOTOGRAPHICAL (EF) PARAMETERS OF TRIGONAL Se LAYERS IN THE BONDING SOLUTION

N.I. IBRAGIMOV, V.G. AGAYEV

Institute of Physics of NAS of Azerbaijan

Az 1143, Baku, H.Javid av., 33

The introduction of chlorine impurity in the near-surface region of microparticles ($\approx 15 \text{ mcm}$) of trigonal Se by diffusion annealing increases the integral photosensitivity of EF layers.

The electrophotography (EPh), for the development of which the perfection necessity of existing and the search of new materials, useful for the photoreceptor formation appears, is the one of operative methods of information recording and duplication. Moreover, the change possibility of their properties purposefully is considered of no small importance one.

Nowadays, the amorphous Se and its alloys, chalcogenides and organic semiconductors, multi-layer composition structures and etc are widely used. The use of amorphous Se is caused by correspondence of its photoelectric properties to demands of Eph process. Besides, Se is manufacturable, comparatively easily comes to purification, doping and it is relatively inexpensive one.

EPh layers on the base of amorphous Se have the high photosensitivity ($S_{int} \approx 0,8 (\text{Lk} \cdot \text{s})^{-1}$) in the visible region of spectrum, well charge up to initial potential $U_0 \approx 600 \text{ V}$, have the long duration of dark half-decay of surface potential $\tau_{1/2}$. However, they have the significant disadvantage: they crystallize under the influence of many factors and fail in the result of exploitation and storage. Moreover, the technology of their manufacture is complex, requires the vacuum equipment, high temperatures, big power inputs. EPh layers on the base of trigonal Se in the bonding solution are stable on the structure, have enough high photosensitivity ($S_{int} \approx 0,4 (\text{Lk} \cdot \text{s})^{-1}$), the complex and power-consuming equipment isn't required for their manufacture.

Se by SF-17 type, which is treated by thermal processing in the extracted quartz ampoules at 700 during 3 hours with the further quick cooling up to 250°C in the flowing water, is the initial material. At such thermal processing in Se the initial molecular and submolecular structure (thermal prehistory) destroys and the stabilized new one, which corresponds to the given conditions of thermal processing forms [1]. Moreover, at such thermal processing the chemical oxygen fixation and other impurities and their transition into electro-inactive state take place [2].

Se, obtained by such way, crystallizes at 210°C during 40 hours. The measurements show, that trigonal Se has the dark conductivity $\approx 10^7 (\text{Om} \cdot \text{cm})^{-1}$. This trigonal Se is crushed in a ball mill up to average size of particles $\approx 15 \text{ mcm}$, is filled up into quartz ampoules, in which the gaseous chlorine is filled with the help of a la carte tap after degassing ($\rho \approx 10^{-2} \text{ Pa}$).

The pure chlorine is obtained by the way of interaction of MnO_2 with HCl [3]. The chlorine pressure in ampoules varies in the interval $5 \cdot 10^3 \div 10^5 \text{ Pa}$. After chlorine filling the trigonal

Se is treated to diffusion annealing at $T_{tr} = 90 \div 170^\circ\text{C}$ during $0,5 \div 5$ hours. In the result of such thermal processing the chlorine molecules diffuse in the near-surface region of trigonal Se particles up to depth $\approx 1 \text{ mcm}$, i.e. in fact that region of photosemiconductor dopes, where the light quantum can penetrate at exposure of EPh layer.

The solvent (ETOH) and the bonding solution (polivinilbutiral of III type) are added to obtained by such way powder of trigonal Se with chlorine impurity and after combined dispersion the emulsion is marked on the aluminum substrate (foil by width 150 mcm) by method of swimming roll. The substrate preliminary is degreased, dipped in 10% solution of KOH, thoroughly washed and conserved in acetone up to emulsion marking.

The width of manufactured EPh layers is $20 \div 30 \text{ mcm}$ in the dependence on the relation trigonal Se – bonding solution. Further, EPh layers are dried in the common conditions during the day.

Their main EPh parameters are measured on the electrometric installation with vibrating electrode near layer surface. The charging of EPh layers is carried out in the corona discharge. The light characteristics are measured by exposure through shutter with the use of lamp glowing and neutral color filters after dark adaptation of EPh layers during 15 minutes.

The newly-made EPh layers from the trigonal Se, annealed in chlorine atmosphere in bonding solution charge only up to initial potential $U_0 \approx 100 \text{ V}$, have the duration of dark half-decay of surface potential $\tau_{1/2} \approx 15 \text{ s}$ and integral photosensitivity $S_{int} \approx 0,04 (\text{Lk} \cdot \text{s})^{-1}$. The essential improvement of all parameters of the same layers after drying at $T_d = 70 \div 150^\circ\text{C}$ with further slow cooling is observed. Thus, S_{int} increases almost in 10 times at $T_d \approx 120 \div 150^\circ\text{C}$. The improvement of other parameters is observed. The obtained results are tabulated in the table, from which it is seen, that powder annealing of trigonal Se in chlorine atmosphere ($P_{Cl} = 5 \cdot 10^3 \div 10^5 \text{ Pa}$) essentially influences on the parameters of EPh layers.

The further growth $T_d > 150^\circ\text{C}$ leads to the parameter degradation and thus, the drying at $T_d \approx 120 \div 150^\circ\text{C}$ is necessary for the formation of optimal sizes. The parameter degradation of EPh layers at $T_d > 150^\circ\text{C}$ is probably caused both by penetration of chlorine impurity deep into particles of trigonal Se and beginning of thermo-destruction process of bonding solution.

The introduction of chlorine impurity into trigonal Se is caused by the fact, that chlorine increases the dark conductivity of photosemiconductor on several orders. Situating on the edges of Se chains, the chlorine molecules decrease the height of potential barriers and promote to mobility of current carriers. Simultaneously with it both acceptor impurity and the chlorine increase the carrier concentrations. The photosensitivity of trigonal Se increases because of the given reasons. However, the growth of dark conductivity of photosemiconductor strongly decreases the charge quantity of EPh layer. The chlorine impurity makes degradation the dark characteristics, improving the light ones. Thus, it is necessary to introduce the impurity so, that it can wrap up the surface layer of particles of trigonal Se up to the depth of light penetration at exposure (≈ 1 mcm at $\lambda \lesssim 0,7$ mcm). The impurity shouldn't penetrate into internal regions

of powder particles in order the conductivity of main mass of trigonal Se stays low one. Only at that case the slow relaxation of surface charge in the darkness will be promoted. The diffusion annealing of powder of trigonal Se in chlorine atmosphere is carried out especially with realization aim of such situation.

From the table it is seen, that the parameter improvement of EPh layers is observed with the increase of annealing time t_{tr} up to 1 hour. At the further increase t_{tr} their degradation is observed, i.e. the annealing during $t_{tr} \approx$ during 1 hour is optimal one.

The result analysis (see table) allows us to confirm that annealing of photosemiconductor microparticles in chlorine atmosphere at the given T_{tr} and t_{tr} promotes the increase of integral photosensitivity of EPh layers of trigonal Se in bonding solution.

Table

PCl ₂ , Pa	T_{tr}, h	$S_{int}, (\text{Lk} \cdot \text{s})^{-1}$					U_0, V					$\tau_{I/2}, \text{s}$				
		0,5	1	2	3	5	0,5	1	2	3	5	0,5	1	2	3	5
$5 \cdot 10^3$	90	0,23	0,21	0,24	0,26	0,27	293	288	282	262	251	41	40	38	37	36
	120	0,23	0,25	0,31	0,34	0,37	290	286	272	254	244	39	38	37	36	34
	135	0,24	0,28	0,33	0,35	0,38	284	274	266	248	235	38	36	35	34	33
	150	0,25	0,31	0,34	0,37	0,39	275	265	262	242	232	36	34	32	29	28
	170	0,25	0,30	0,33	0,35	0,38	270	262	258	240	228	34	31	28	26	25
10^4	90	0,24	0,24	0,27	0,29	0,31	292	288	278	256	246	41	39	37	36	36
	120	0,25	0,30	0,37	0,40	0,41	285	280	272	250	238	39	37	36	34	33
	135	0,26	0,32	0,38	0,41	0,42	280	272	265	244	232	37	35	34	33	32
	150	0,27	0,37	0,40	0,42	0,43	275	264	258	240	228	36	34	32	30	30
	170	0,28	0,35	0,38	0,43	0,43	268	260	255	235	224	33	30	28	26	25
$5 \cdot 10^4$	90	0,25	0,28	0,28	0,31	0,32	290	285	274	250	236	40	38	37	36	36
	120	0,26	0,32	0,38	0,40	0,44	282	278	265	242	230	38	37	35	33	32
	135	0,28	0,34	0,40	0,42	0,45	276	270	258	235	224	36	35	34	32	32
	150	0,32	0,43	0,50	0,50	0,49	270	264	254	231	220	35	34	33	31	30
	170	0,33	0,44	0,48	0,47	0,47	260	258	250	226	216	32	28	26	25	24
10^5	90	0,26	0,27	0,27	0,30	0,30	288	280	270	246	230	39	37	34	31	28
	120	0,27	0,31	0,36	0,40	0,42	282	274	263	238	225	37	35	31	29	28
	135	0,28	0,34	0,40	0,41	0,44	275	266	256	232	217	35	32	29	27	26
	150	0,34	0,45	0,47	0,44	0,47	265	253	248	228	213	32	30	26	22	21
	170	0,35	0,42	0,45	0,41	0,40	258	256	246	224	210	30	28	24	20	19

[1] N.I. Ibragimov. Nekotoriye zakonomernosti formirovaniya strukturi i svoystv selena. Azerbaycan Respublikasının Prezidenti H.Ə. Əliyevin 80-illik yubileyinə həsr olunmuş etmi konfransın materialları. XXI YNE, Bakı, 2003, s.15.

[2] G.B. Abdullayev, N.I. Ibragimov, Sh. V. Mamedov. Phys. Selenium and Tellurium, Pergamon Press, 1969, p.321.

[3] B.M. Yavorskiy, A.A. Detlov. Spravochnik po fizike, M., Nauka, 1985, s. 512. (in Russian).

N.İ. İbrahimov, V.H. Ağayev

FOTOYARIMKEÇİRİCİNİN MİKROZƏRRƏCİKLƏRİNİN SƏTHƏ YAXIN OBLASTININ XLOR ATMOSFERİNDƏ TERMİK İŞLƏMƏKLƏ LEQİRƏ EDİLMƏSİNİN TRİQONAL Se-NİN ƏLAQƏLƏNDİRİCİDƏ EF LAYLARININ PARAMETRLƏRİNƏ TƏSİRİ

Triqonal Se-nin mikrozərrəciklərinin (≈ 15 mkm) səthə yaxın oblastının xlorla aşqarlanması EF layların integrallı fotohəssashığını artırır.

H.I. İbragimov, B.G. Ağayev

ВЛИЯНИЕ ЛЕГИРОВАНИЯ ПРИПОВЕРХНОСТНЫХ ОБЛАСТЕЙ МИКРОЧАСТИЧЕК ФОТОПОЛУПРОВОДНИКА ОТЖИГОМ В АТМОСФЕРЕ ХЛОРА НА ЭЛЕКТРОФОТОГРАФИЧЕСКИЕ (EF) ПАРАМЕТРЫ СЛОЁВ ТРИГОНАЛЬНОГО Se В СВЯЗУЮЩЕМ

Введение примеси хлора в приповерхностную область микрочастичек (≈ 15 мкм) тригонального Se диффузионным отжигом увеличивает интегральную светочувствительность EF слоёв.

Received: 17.09.07

THE INFLUENCE OF TEMPERATURE –TIME CRYSTALLIZATION MODE ON THE MECHANICAL STRENGTH AND ON THE STRUCTURE OF POLYMERIC MAGNETIC NANO-COMPOSITES ON PVDF+Fe₃O₄ BASIS

P.B. AGAKISHIYEVA, S.A. ABBASOV, R.A. ALI-ZADE

*Institute of Physics of NASA,
AZ-1143 Baku, Azerbaijan, H. Javid ave. , 33*

M.A. RAMAZANOV

Baku State University

Baku, Az 1145, Z.Khalilov str.23

The investigation results of the influence of temperature-time crystallization mode on the microstructure and on the strength properties of compositions on PVDF+Fe₃O₄ base are described in the given work. It is shown, that increase of mechanical strength of nano-composition samples, obtained in the modes of slow cooling is connected with increase of interphase interaction of composition components, and increase of nano-particle sizes is connected with increase of coagulation probability of Fe₃O₄ particles.

Last time the magnetic nano-structures are successfully used for the high-density magnetic record of information, pigmentation, in the micro-wave coverings, at magnetic cooling and other technique spheres.

The nano-composite properties are defined by the chemical nature of polymeric matrix, structure of interfaces, the part of which is too large in nano-composites, and also by the interaction between nano-particles and polymer matrix. The temperature-time mode of polymer crystallization changes the physical structure of the polymeric matrix and interphase interactions between composite components that leads to the change of the composition strength properties [1-5].

The investigation results of the influence of temperature-time crystallization mode on the microstructure and strength properties of compositions on PVDF+Fe₃O₄ base are described in the given work. The magnetic polymeric nano-composites are obtained by the following way. The Fe₃O₄ nano-particles are added to the PVDF solution in dimethylformamide. The nano-particle size is 4-10nm. The mixture is mixed at the temperature 343K up to the emulsion formation, the water solution is added and Fe₃O₄, consisting PVDF, is steamed and further is dried in vacuum safe. The nano-composite samples are obtained from the compound by the method of hot pressing at PVDF melting point under the pressure 15MPa during 10 minutes with further cooling up to room temperature at various velocities.

The microstructures of PVDF+Fe₃O₄ compositions are investigated on the scanning atomic force microscope (AFM).

The mechanical strength properties of nano-composition samples are defined at temperature 293K. The mechanical strength of nano-composition samples, obtained in the modes of quick cooling (QC) $\beta=2000\text{grad/min}$ and slow cooling (SC) $\beta=4\text{grad/min}$ are studied. It is experimentally established, (fig.1) that mechanical strength of PVDF+Fe₃O₄ nano-composition, obtained in the mode $\beta=4\text{grad/min}$ bigger, than nano-composition samples have obtained in the modes $\beta=2000\text{grad/min}$. It is also shown, that the small increase of mechanical strength of PVDF+Fe₃O₄ nano-composition is observed in the dependence on the volume content of Fe₃O₄

nano-particles up to 2%v.con., after that the concentration increase takes place up to 20%v.con.

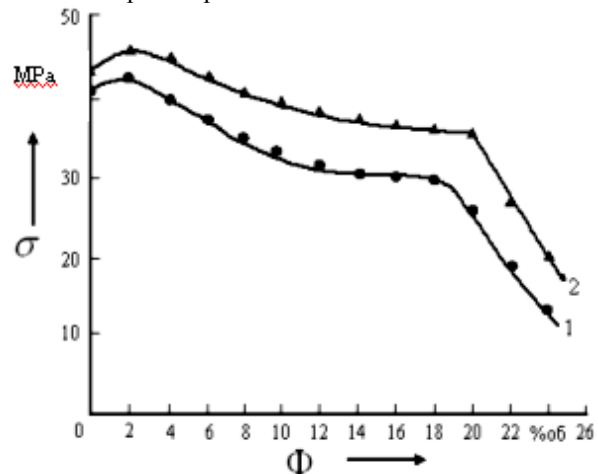


Fig.1. The dependence of mechanical strength on the filler volume content, obtained in the different cooling modes.
1. $\beta=2000\text{grad/min}$ (QC) 2. $\beta=4\text{grad/min}$ (SQ)

Further increase of nano-particle concentration leads to the strong decrease of mechanical strength of this nano-composition. From the fig.1 it is seen, that change regularity of nano-composition mechanical strength on the volume content of Fe₃O₄ is saved for the samples, obtained in the modes $\beta=4\text{grad/min}$ and $\beta=2000\text{grad/min}$.

By our opinion the small increase of nano-composition mechanical strength till 2%v.con. of Fe₃O₄ concentration is connected by the structuring of polymeric matrix. The nanoparticles play the role of crystallization center in them, if additions of Fe₃O₄ are 2%v.con.

Further decrease of mechanical strength is connected with the decrease of the part of polymeric matrix with the concentration increase of Fe₃O₄ nano-particle. The strong decrease of nano-composition mechanical strength is higher 20%v.con. that is connected with destruction of polymeric matrix.

AFM 3D image of region topography of nano-composition surface PVDF+Fe₃O₄, obtained in the modes $\beta=4\text{grad/min}$ is given on the fig.2. It is seen, that at slow-

cooled samples the nano-composition relief becomes more ordered, than at quick-cooled ones.

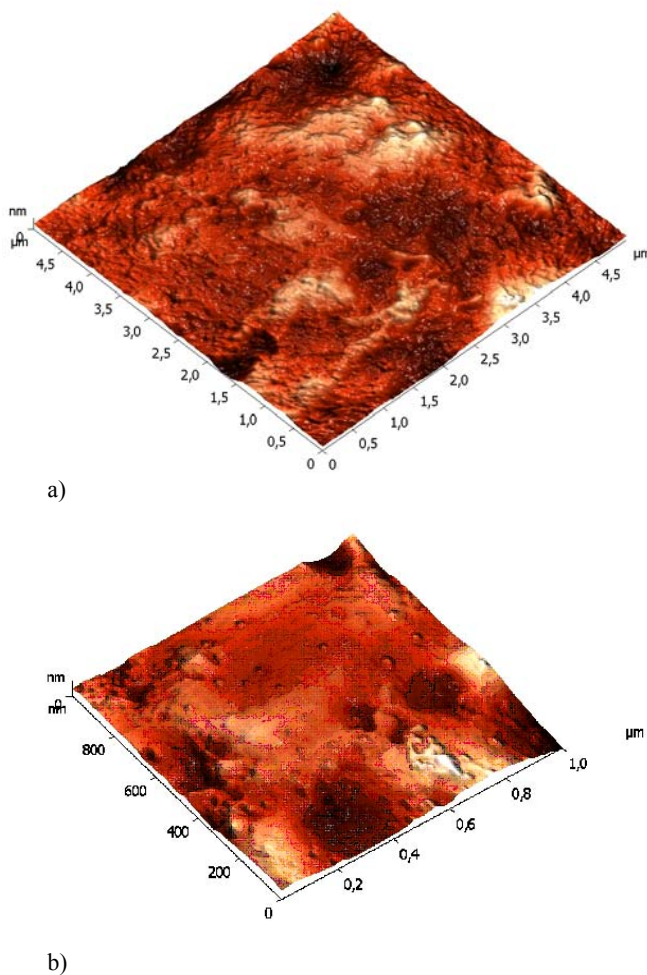


Fig.2. AFM 3D topography image of nano-composition surface region PVDF+Fe₃O₄ a) $\beta=4\text{grad/min}$. b) $\beta=2000\text{grad/min}$.

It is known, that crystallinity degree of composite materials much increases at slow cooling of polymers and composites on their base in the comparison with quick-cooled one. The decrease of crystallinity degree in the samples, obtained in the mode of quick cooling, probably can be connected with small crystal structure. By our opinion, the increase of nano-composition mechanical strength of PVDF+Fe₃O₄ samples, obtained in the modes of slow cooling is connected by the formation of more ordered structure of polymeric matrix and increase of interphase interaction of composition components.

The nano-particle sizes, the distribution topography of Fe₃O₄ nano-particle in polymeric matrix for the samples, obtained in the modes $\beta=4\text{grad/min}$ and $\beta=2000\text{grad/min}$ are given on the fig.3. AFM investigation of these samples

shows, that sizes of Fe₃O₄ nano-particle change with crystallization temperature-time mode, i.e. at $\beta=4\text{grad/min}$ is 21nm, and in the cooling modes $\beta=2000\text{grad/min}$ is 15 nm (fig.3).

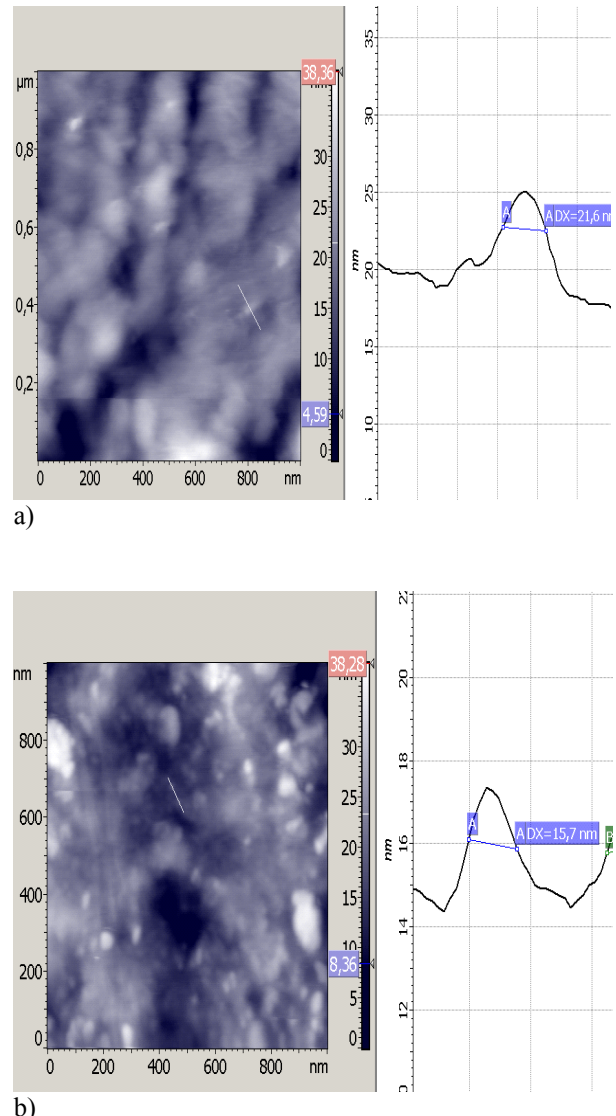


Fig.3. AFM image of nano-composition surface PVDF+Fe₃O₄ and nano-particle sizes of Fe₃O₄ a) $\beta=4\text{grad/min}$ b) $\beta=2000\text{grad/min}$.

By our opinion the increase of mechanical strength of nano-composition samples, obtained in the modes of slow cooling is connected with increase of interphase interaction of composition components, and increase of nano-particle sizes is connected with increase of coagulation probability of Fe₃O₄ particle.

-
- [1] *M.A. Ramazanov New magnetodielectric polymeric nanocomposite. Light in Nano-Size Solids 1 International Scientific Seminar Baku-2004.* p. 43-44.
 - [2] *Yu. I. Petrov. Klasteri I maliye chasticci.* M.Nauka, 1986, 124s. (in Russian).
 - [3] *L. V. Nikitin,L.S. mironova i dr. Magnitniye uprugiyie, strukturniye i magnitodeformacionniye svoystva mag-* nitoelastikov. J.VMS, t. 46(A), №3, s. 498. (in Russian)
 - [4] *A.D. Sdadnik, G.V. Kirik. Polimerniye kompoziti i nanokompoziti v magnitnikh polyax.* Sumi., 2005, 231s. (in Russian).
 - [5] *A.D. Pomogaylo, A.S. Rozenberg, I.E. Uflyand. Nano-chasticci metallov v polimerax.* Moskva. "Khimiya" 2000 г., 671s. (In Russian).

M.Ə. Ramazanov, P.B. Ağakişiyeva, S.A. Abasov, R.A. Əlizadə

KRİSTALLAŞMANIN TEMPERATUR - ZAMAN REJİMİNİN PVDF+Fe₃O₄ ƏSASINDA POLİMER MAQNİT NANOKOMPOZİTLƏRİNİN MEXANİKİ MÖHKƏMLİYİNƏ VƏ QURULUŞUNA TƏSİRİ

Bu işdə kristallaşmanın temperatur - zaman rejiminin PVDF+ Fe₃O₄ əsasında polimer maqnit nanokompozitlərinin mexaniki möhkəmliyinə və quruluşuna təsirinin tədqiqinin nəticələri şərh olunmuşdur. Göstərilmişdir ki, yavaş soyuma rejimində alınmış nanokompozit nümunələrinin mexaniki möhkəmliyinin artması kompozitin komponentləri arasında fazalararası qarşılıqlı təsirin artması ilə əlaqədardır, nanohissəciklərin ölçülərinin artması isə Fe₃O₄ hissəciklərinin koagulyasiya ehtimalının yüksəlməsi ilə əlaqədardır.

М.А. Рамазанов, П.Б. Агакишиева, С.А. Абасов, Р.А. Али-Заде

ВЛИЯНИЕ ТЕМПЕРАТУРНО-ВРЕМЕННОГО РЕЖИМА КРИСТАЛЛИЗАЦИИ НА МЕХАНИЧЕСКУЮ ПРОЧНОСТЬ И НА СТРУКТУРУ ПОЛИМЕРНЫХ МАГНИТНЫХ НАНОКОМПОЗИТОВ НА ОСНОВЕ ПВДФ+Fe₃O₄

В данной работе излагаются результаты исследования влияния температурного временного режима кристаллизации на микроструктуру и на прочностные свойства композиций на основе ПВДФ+Fe₃O₄. Показано, что увеличение механической прочности образцов нанокомпозиций, полученных в режимах медленного охлаждения, связано с увеличением межфазного взаимодействия компонентов композиций, а увеличение размеров наночастиц связано с повышением вероятности коагуляции частиц Fe₃O₄.

Received: 18.09.07

THE STRUCTURE AND FERROELECTRIC PROPERTIES IN THE SOLID SOLUTIONS WITH THE STRUCTURE OF TETRAGONAL TUNGSTEN BRONZE

R.Z. MEKHTIYEVA, A.I. MAMEDOV

*Institute of Physics of NAS of Azerbaijan,
Baku, Az -1143, H. Javid av., 33, Azerbaijan*

The investigation results of solid solution systems $K_2Ba_4Nb_{10}O_{30}$ - $K_6Li_4Nb_{10}O_{30}$ (KBN-KLN) $K_2Sr_4Nb_{10}O_{30}$ - $K_6Sr_4Nb_{10}O_{30}$ (KSN-KLN) with the structure of tetragonal tungsten bronze with the aim of revealing of influence of tetragonal position filling on the system structural parameters and electrophysical properties, in which the morphotropic phase transitions with the storage of the similar cell symmetry in whole interval of solid solution existence of tetragonal-tetragonal type ($T-T'$), accompanying by the clear anomalies on the concentration dependencies of structural and electrophysical parameters are given in the given work.

Introduction

The study of oxide solid solutions with the structure of tetragonal tungsten bronze (TTB), having the essential electrophysical properties (ferro-, antiferro-, ferroelastic and others) is presented actual both from scientific point of view, that is the order establishments, caused by their complex hierarchical construction and practical one, that is the use of accompanying structural instabilities of extreme material properties.

The aim of the given work is the revealing influence of filling of triangular positions on the system structural parameters and electrophysical properties, in which the morphotropic phases transitions (MPhT) with the storage of similar cell symmetry in the whole interval of solid solution existence (SS) of tetragonal-tetragonal type ($T-T'$), accompanying by clear anomalies on the concentration dependence of structural and electrophysical parameters in double systems of solid solutions with TTB structure [5].

Experimental part

The samples of TR systems $K_2Sr_4Nb_{10}O_{30}$ - $K_6Li_4Nb_{10}O_{30}$ (KSN-KLN) and $K_2Ba_4Nb_{10}O_{30}$ - $K_6Li_4Nb_{10}O_{30}$ (KBN-KLN) are obtained by the solid-phase synthesis from the stoichiometric oxide mixtures or carbonates of corresponding elements in two stages (with intermediate grinding) at annealing temperature in the interval from 1150 up to 1475K and duration from 2 up to 6 hours. The disk samples of high-density ceramics for the measurement of dielectric and piezoelectric parameters ($\varepsilon_{33}/\varepsilon_0$, $tg\sigma$, d_{31} , K_p and Q_M) on the techniques, described in [6] are prepared by the method of hot pressing.

The symmetry and parameters of elementary cell of the samples are defined on the powder roentgenograms (diffractometer DRON-3.0, CuK_α is filtered radiation).

The results and their discussion

The compounds of solid solutions with TTB structure with the limited solubility $K_6Li_4Nb_{10}O_{30}$ (80 mol%) [4,5] are obtained by addition introductions. The ceramic properties of solid solution compounds, which are close to KBN and KSN, which aren't baked in the pure form are investigated.

The morphotropic phase transitions (MPhT) with the storage of the similar cell symmetry in the whole interval of TR existence of tetragonal-tetragonal ($T-T'$) type, accompanying by the clear anomalies on the concentration dependencies of structural and electrophysical parameters are observed in the systems of solid solutions (TR) $K_2Ba_4Nb_{10}O_{30}$ -

$K_6Li_4Nb_{10}O_{30}$ (KBN-KLN) $K_2Sr_4Nb_{10}O_{30}$ - $K_6Li_4Nb_{10}O_{30}$ (KSN-KLN) with the structure of tetragonal tungsten bronze (TTB), also as in the system of solid solutions $K_2Pb_4Nb_{10}O_{30}$ - $Na_2Pb_4Nb_{10}O_{30}$ (KPN-NPN) with TTB structure and rhombic symmetry of extreme component ($P_1 - P'1$).

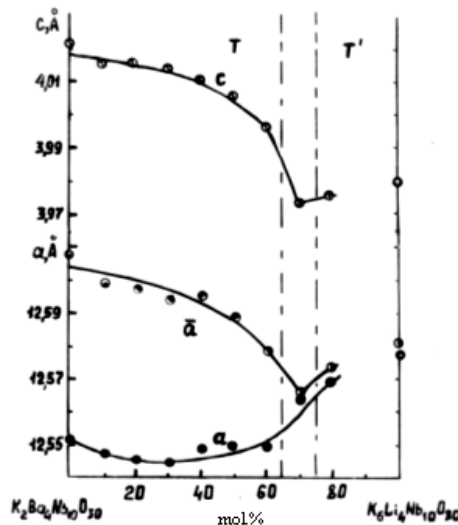


Fig.1. The concentration dependencies of structural parameters in the system of solid solutions $K_2Ba_4Nb_{10}O_{30}$ - $K_6Li_4Nb_{10}O_{30}$.

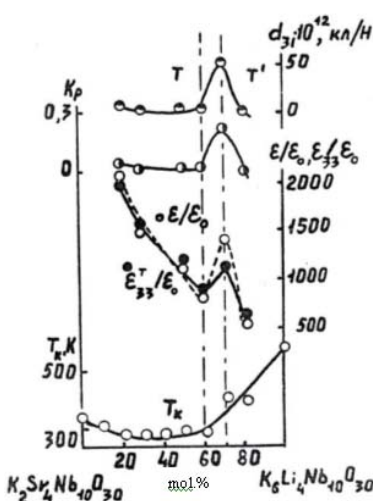


Fig.2. The concentration dependencies of electrophysical parameters in the system of solid solutions $K_2Sr_4Nb_{10}O_{30}$ - $K_6Li_4Nb_{10}O_{30}$.

MPhT $T-T'$ in these systems reveals in the anomalous behavior of elementary cell parameters: bend in the going of

average parameter \bar{a} ($\bar{a} = c^3 \sqrt{10a^2c}$, average cell parameter, is equivalent one on the volume with “ideal” [1,2]) in KSN-KLN system (table), minimum on the curves of parameter changes \bar{a} , c (KBN-KLN system, fig.1); the bend in KSN-KLN system in the going of average parameter \bar{a} is accompanied by the clear maximums of dielectric and piezoelectric parameters at 70% KLN (fig.2).

The solid solutions with the structure, which is similar to the KLN(T') structure [7] form in KBN-KLN system (fig.1) in the interval $0,7 \leq \chi \leq 0,8$ (χ -KLN), i.e. at the content of three and more Li ions on the elementary cell, and at solid

solutions on KBN(T) basis form at $0 \leq \chi \leq 0,7$. As it is seen, the a parameter in the tetragonal phase T almost doesn't change. This can be explained by the fact, that the ion average radius in A-position in KBN and KLN almost doesn't differ ($R(K^{+}) - 1,64\text{\AA}$ (c.c. 12) and $1,70\text{\AA}$ (c.c. 15); $R(Ba^{2+}) - 1,6\text{\AA}$ (c.c. 12) $1,72\text{\AA}$ (c.c. 15)) [5,7].

In KSN-KLN system the parameters of elementary cell increase with the increase of KLN content (table), as ion average radius in A-position in KSN is smaller, than in KLN ($R(Sr^{2+}) - 1,44\text{\AA}$ (c.c. 12)) [4,7].

Table
Structural parameters of double system of solid solutions $K_2Sr_4Nb_{10}O_{30}-K_6Li_4Nb_{10}O_{30}$.

KSN(%)	KLN(%)	Lattice parameters			
		a , \AA	C , \AA	\bar{a} , \AA	$\sqrt[3]{a^2c}$
90	10	12,4864	3,944	12,483	8,505
80	20	12,513	3,942	12,494	8,513
70	30	12,527	3,943	12,507	8,523
60	40	12,5460	3,9531	12,542	8,544
50	50	12,553	3,958	12,539	8,543
40	60	12,566	3,966	12,557	8,554
30	70	12,568	3,965	12,558	8,556
20	80	12,569	3,989	12,583	8,574
0	100	12,5784	3,9796	12,5803	8,572

The bent changes of piezomodule d_{31} and coefficient of electromechanical bond K_p go through the maximum on the area boundary MPhT; are accompanied by the increase of Curie temperature values (530K). The permittivity has the maximum on MPhT boundary, to which the compound with minimum value of mechanical quality Q_m is equal (fig.2).

In these systems the compound change is accompanied by the gradual filling of positions by Li ions in triangular canals and observable MPhT, probably, is connected with different filling character of these positions: with ordering or shifting from polyhedron center with coordination number 9 in the one from two incorrect octahedrons, consisting it.

- | | | |
|-----|---|--|
| [1] | V.A. Isupov. FTT, 1980, t.22, v.1, s.25-28. (in Russian) | Russian) |
| [2] | L.A. Rezničenko, R.Z. Mekhtieva, L.A. Šilkina, A.I. Mamedov. AMEA-nın Xəbərləri, fiz.-riyaz. və t.e. bül., 2003, 5(1), S.53-57. | V.Q. Krishtop, R.U. Devlikanova, O.A. Bunina, V.S. Filipev. Izv. AN SSSR. Neorgan. materiali. 1988. T.24. №9. S.1513–1515. (in Russian). |
| [3] | R.Z. Mekhtieva, V.G. Krishtop, E.N. Sidorenko, R.U. Devlikanova. Izv. AN SSSR. Ser. fiz. – 1990, t.54, № 6, s.1167-1170. (in Russian) | [7] QOST 12370-80. Materiali pyezokeramicheskie. Metodi ispitaniy. M.: Izd-vo standartov; 1982. 30 s. |
| [4] | R.Z. Mekhtieva, R.U. Devlikanova, G.I. Stepovoy i dr. | [8] V.A. Isupov, A.B. Lutsevich, A.U. Sheleg, T.N. Urban. Izv. AN SSSR. Ser. fiz. 1983, t.47, №4, S.813-815. (in Russian) |
| [5] | Neorgan. materiali. 1991, t.27, №.7, c.1483-1487. (in | |

R.Z. Mehdiyeva, Ə.İ. Məmmədov

TETRAQONAL-VOLFRAM TUNC STRUKTURLU BƏRK MƏHLULLARIN STRUKTURU VƏ SEQNETOELEKTRİK XASSƏLƏRİ

Bu işdə üçbucaq kanalların doldurulmasının tetraqonal-tetraqonal ($T-T'$) tipli bərk məhlulların bütün mövcud intervalında özəyin vahid simmetriyasının saxlanılması ilə morfotrop faza keçidləri müşahidə olunan sistemlərin elektrofiziki xüsusiyyətlərinə və struktur parametrlərinə təsirinin öyrənilməsi məqsədilə tetraqonal volfram tunc strukturlu $K_2Ba_4Nb_{10}O_{30}-K_6Li_4Nb_{10}O_{30}$ (KBN-KLN) $K_2Sr_4Nb_{10}O_{30}-K_6Li_4Nb_{10}O_{30}$ (KSN-KLN) bərk məhlulların tədqiqat sistemlərinin natiqələri göstərilmişdir.

P.3. Mekhtieva, A.I. Mamedov

СТРУКТУРА И СЕГНЕТОЭЛЕКТРИЧЕСКИЕ СВОЙСТВА В ТВЕРДЫХ РАСТВОРАХ СО СТРУКТУРОЙ ТЕТРАГОНАЛЬНОЙ ВОЛЬФРАМОВОЙ БРОНЗЫ

В данной работе приводятся результаты исследований систем твердых растворов $K_2Ba_4Nb_{10}O_{30}-K_6Li_4Nb_{10}O_{30}$ (KBN-KLN) $K_2Sr_4Nb_{10}O_{30}-K_6Li_4Nb_{10}O_{30}$ (KSN-KLN) со структурой тетрагональной вольфрамовой бронзы с целью выяснения влияния заполнения треугольных позиций на структурные параметры и электрофизические свойства систем, в которых наблюдаются морфотропные фазовые переходы с сохранением одинаковой симметрии ячейки во всем интервале существования твердых растворов, типа тетрагональная-тетрагональная ($T-T'$), сопровождающиеся четкими аномалиями на концентрационных зависимостях структурных и электрофизических параметров.

Received: 25.09.07

THE CONCEPTIONS OF THE FRACTAL IN THE PHYSICS OF SUPRAMOLECULAR EUTECTICS

F.K. ALESKEROV, S.Sh. KAKHRAMANOV

*Scientific-manufacture consortium "Selenium" of National Academy of Sciences of Azerbaijan,
Az-1143, Baku, F. Agayev str., 14*

E.D. MOROYDOR, M.G. PISHKIN

*Stambul Technical University "Yildiz", chemical-engineering faculty, Davutpasha,
Merter, 342, Stambul, Turkey*

The main statements of the theory of inorganic eutectic systems, evidencing in the proof of the supramolecular conception and taking into consideration the interaction of fractal super-assemblies are considered. The experimentally observable geometric samples-fractales are given; the nature of interphase interaction of fractal aggregate with matrix is shown. The above mentioned is proved by the example of regular eutectic systems of $A^{IV}B^{VI}$ – NiSb type and fractal dendritic structures.

Introduction

The structures, widely used in the technique of eutectic alloys, and also eutectic supramolecular conception taking into consideration the interaction of inadequate substructures and opening the formation mechanisms of supramolecular assemblies in boundary layers ("non-autonomous phases") are considered in the given article. The ability of such self-organizing supramolecular objects to the molecular recognition is their main property. The component recognition proposes the "complementarity", i.e. the mutual interaction of assembly participants both geometric one and on the level of intermolecular bond formation [1-2].

The structural peculiarities of eutectic nature, i.e. the interconnection between phase crystalline structure and phase boundary structure and peculiarities of electron structure of eutectic components are usually considered for its understanding [3-4].

The formation of fractal structures in the result of evolution of any physico-chemical systems is possible. Their formation in the macro- and nanosystems is connected with revealing of dissipative self-organization. Many materials, including dendritic structures, have fractal dimensionality on the different stages of their obtaining [5]. It would be interesting to analyze the morphology of known eutectic alloys from the point of view of their fractal character with the use of fractal aggregate conception once again. There are enough such objects in the capacity of examples.

The consideration of eutectic structures from fractales point of view can introduce the some progress in the description of both regular and irregular aggregates. However, it isn't enough only to describe the forms, it is desirable to understand the formation of internal mechanism of fractal eutectic systems. The series of eutectic aggregates has the character fiber-like structure with fuzzy edges [6]. The analogous structures are obtained in the other systems, for example PbTe – NiSb and PbS – NiSb. They are similar with fractal formations on appearance [3-4]. The investigations on the distribution of inclusion grains in the general matrix (for example, NiSb fibers into PbTe) are necessary. This leads to the consideration of fractal dimensionality. It is necessary to reveal how much the eutectic growth mechanism is able to reproduce the fractal structure, satisfying the demands, required to them. The

perceptions of fractale and fractal dimensionality are given in the works [7-8].

The nonfractal and fractal granular microstructures are schematically presented in the work [7]. The broken granule boundaries are fractal ones and are caused by the fractional fractal surface dimensionality $2 \leq D \leq 3$. Such structure is character for the high-deformed boundaries.

Here, the formations of dendrite-like structures are well known. The fractal dimensionalities of forming dendrites correspond to fractal dimensionalities in two- and three-dimensional systems, obtained at computational modeling [5-7]. The information about microscopic picture of dendrite growth is necessary for the further consideration of eutectic morphology. The eutectic crystallization is always dendrite one, meaning that granules of eutectic phases, consisting in colony, develop in the form of thin-branched dendrites in the connection of specifics of dual growth. The eutectic colonies themselves transform into two-phase dendrites in the growth process [6].

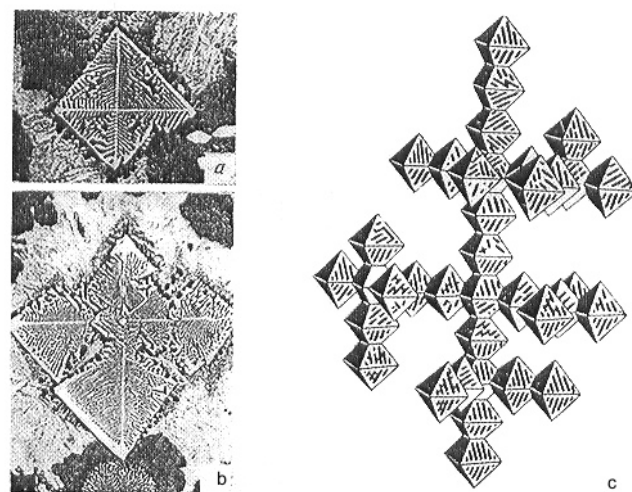


Fig. 1. The formation stages of dendrite growth of $Fe+(M_0, Fe)C$ is (a,b), model projection is (c) [6].

For us it is important to know, that each cell grows in the form of eutectic octahedron and first stages of dendrite formation (for example, in eutectic $Fe+(M_0, Fe)_6C$) reproduce the corresponding stages of the formation of leading phase dendrite (fig. 1 a,b,c) [6].

The three-dimensional eutectic dendrite, the branches of which are presented themselves the element chains of cube directions of octahedron form, quasi planted one on another along cube direction [6]. The model projection, constructed on the data of stoichiometric analysis is shown in [6] on the fig.1 c.

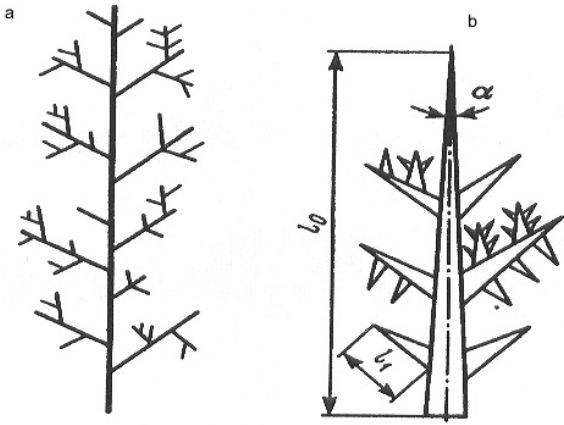


Fig.2. The irregular structure of high-dispersion dendrite particles (a) and junction model of dendrite structure of iron high-dispersion alloys (b) [7]; l is the length of particle main stem.

Thus, the dendrite formations in eutectics are integrally similar hereditary fractal structures on the structure as their leading phase. Here it is need to compare the above mentioned results with irregular structures of high-dispersion iron dendrite particles, given in the monograph [7]. The practical use of irregular structures for identification of structures of natural fractals on data [7] is illustrated on the fig.2. The irregular structure, generalizing the model of high-dispersion dendrite particles is shown on the fig.2a. The projection of junction model of dendrite particle on the electron microscope screen, constructed from isosceles triangles of decreasing sizes (at angle of α) is shown on the fig.2b. The procedure of its construction is given in the [7], here the main stem of particle by length l_0 and square $S_0 = 0,5l_0^2 \sin \alpha$ is divided into some totality of more fine gauges. The series from K_1 trigonal branches of first order by length $l_1 = l_0/K_1$ is formed. The considered models of particle space structure of high-dispersion ferromagnetic alloys allow obtaining the qualitative characteristics of their branching degree and fractional fractal dimensionalities [7].

The consideration of eutectic compositions, which are inadequate on all three crystallographic directions in extreme case in the terms of supramolecular chemistry, allows obtaining the answers on many questions and eliminating vaguenesses, mentioned at the discussion of existing eutectic conceptions [2-3].

That's why we here also pay attention on the study of microstructure morphology peculiarities of eutectic alloys with the aim of revealing of nature of interphase interaction of fractale with matrix.

The revealing of phase fractality features in inorganic eutectic suprastructures of $A^{IV}B^{VI}$ - NiSb type is the aim of the given work.

The investigation techniques

The eutectic alloys of the following systems: (PbTe) - Sb, (PbTe) - NiSb are grown by Bridgman method at the velocity

$V=3\text{mm/h}$ at $T=1200^\circ\text{K}$ and temperature gradient $\Delta T=100^\circ$ between the heaters.

The microstructures are investigated on the raster electron microscope (REM) JSM-50A with the device for local X-ray analysis and on electron microscope JSM-2000 in the beams of electron secondary emission, in the beams of transmitted electrons, roentgen images in the beams: Te, S, Ni, Sb. The spatial resolution of the mode is $\sim 0,1\text{ mc}$. The results of these investigations are presented on the fig.2-6.

The fractal dimensionality is calculated by the method, described in the work [8] – (fig.7). D dimensionality is defined by the way of sector (or cell) calculation, which are necessary for the covering of collection in the dependence on sector dimension and it is called sector dimensionality.

The result discussion

The fractal suprastructures in eutectics

The previous investigations show that structures in PbTe - NiSb, SnTe - NiSb, PbS - Ni systems are similar. First of all, let's consider the crystallization in PbTe - NiSb and PbS - NiSb systems.



Fig.3. The longitudinal section of PbTe - NiSb eutectic surface.

PbTe - NiSb eutectic (fig.3) has the fiber structure, PbS - NiSb eutectic has plate structure and composition PbTe 92mol%-NiSb 8mol%. The eutectics of (PbS - Sb), PbTe - Sb systems can be related to anomalous, limited by rod ones with leaf structure of rods and plates. The eutectic PbS - NiSb can be related to normal ones on the form and phase distribution, i.e. to "regular". Each substructure grows with unite strongly delineated solidifying interface, the surface of subblock contact legibly reveals. The definite crystallographic relations, which are character for the given systems exist between phases in the normal microstructures, investigated by us, that isn't observed in anomalous eutectics. The atom interaction of eutectic suprastructures is that indirect physical reason, which supplies the fractal accretion on the definite more energetically profitable directions and supplies the high stability of interphase boundary.

The notion about fractals was firstly used for the measurement of irregular lines, composed from the sections of constant length ε . The length of this kinked curve $L(\varepsilon)$ was accepted for approximate length of monitored object [8]. The dependence of its length on the section dimension in the case of curved line has the form: $L(\varepsilon) = a\varepsilon^{1-D}$ (1), where $a>1$ is L value for nonfractal curve; $D>1$ is fractal dimensionality.

The oriented microstructure, characterized by strong regularity of whole "supramolecular assembly" is obtained in

the process of directed crystallization. The microstructure of transversal section of oriented eutectic sample of PbTe - NiSb system is presented on the fig.4 (a,b). The composition of eutectic assembly is following: 92mol% PbTe - 8mol% NiSb. The solubility regions are observed in the solid solution on component base.

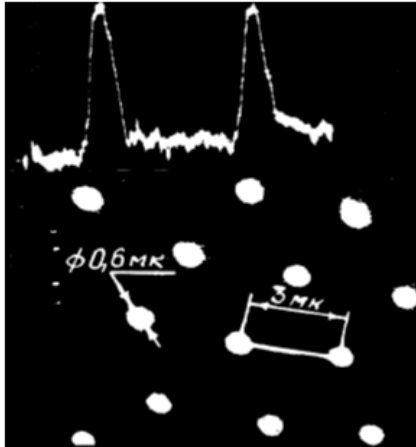


Fig.4. a) the element distribution; b) eutectic transversal section.

The microstructure regularity is reflected on the periodic potential stroke of whole eutectic crystal integrally, and namely: periodic potential of one lattice is rebladed by periodic potential of another one with some period, which is constant for the given eutectic and bigger, than constant lattice of each phase [3].

The morphology analysis of lamellar eutectic of system PbS - NiSb [3-4] and data about electron structure of eutectic alloys allows interpreting the directly oriented eutectic compositions as class of suprastuctural crystalline substances, having the fractal structure. The bond between atoms of different phases [4] appears in the eutectic on the conjugation boundary. Such bond character should be inherited to many eutectic systems according to investigation results. Probably, this leads to the boundary degradation between fractal and matrix.

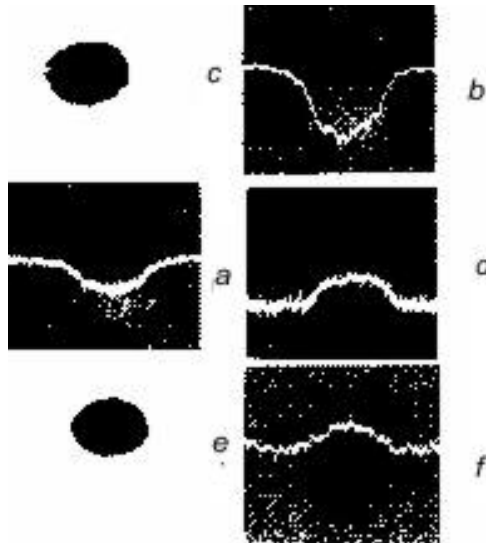


Fig.5. The photos of local X-ray analysis (XLRA) of transversal cut of (LXRA) mode-fractal structure of PbTe - NiSb eutectic in the different modes: a) SE; b) XLRA in characteristic beams Sb with linear image Sb (x14000); c)The same for Ni; d)The same in NiSb beams;e)XLRA in Te beams towards with linear distribution Te; f) SE-mode.

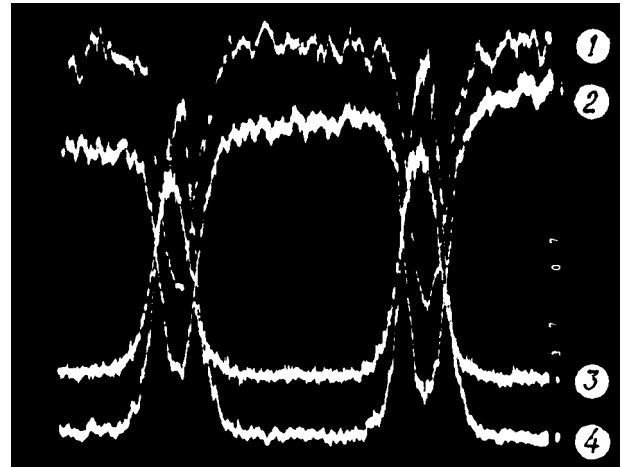


Fig.6. The element distribution in the fractal transversal section (of PbTe - NiSb eutectic).

LXRA photos of transversal section of oriented eutectic PbTe 92 mol% - NiSb 8mol% are presented on the fig.5. The roentgen images in characteristic beams Pb, Te, Ni and Sb towards with their linear distribution obviously evidence about density change particle distribution (fig.5 (a, b, c, d)). The matrix and fractals-inclusions present themselves the limited solid solutions. Each phase is the independent crystal in the system. Moreover, the length of fibers-fractales in PbTe - NiSb vibrates in the limits from 200 nm up to 700 nm at the diameter (160÷180) nm. The fractals have the irregular cigar-shaped form with thickening on the one edge and the needle-shaped sharpening on another one. Each eutectic fractal grows towards with matrix by unite solidifying interface. The boundaries of contact surfaces satisfy the conditions of fractal growth (slow transition of zigzag character). The photos of element distribution in eutectic fractal PbTe - NiSb, obtained by local X-ray analysis (LXRA) in the one granule are given on the fig.6. As it is seen from distribution of Pb, Te, Ni, Sb particles in the fractal, the signal fall from Pb and Te and signal increase from Ni and Sb take place in the granule; the distribution densities of Ni and Sb are maximum in the middle and decrease to the edges in NiSb region. The distribution maximum falls on Pb and Te in the matrix and coincides with minimum content of nickel and stibium. The images, obtained in characteristic beams of all four atoms show, that both matrix (PbTe) and inclusions (NiSb) present themselves the limited solid solutions on the base of both components. All data, including (LXRA) are in the total agreement with state diagram of PbTe - NiSb system.

The distortion of matrix and fractal lattices takes place on the interphase boundaries. Here the interaction of force field atoms, which supply the high adhesion and are able to change the complex parameters in the near-boundary series of atoms, takes place.

Thus, the eutectic alloys can be considered as phase (fractale) supramolecular assemblies in the matrix, having the distinctive feature in the comparison with artificially obtained mechanical mixtures, and namely with small distances between fractal dispersion phases and strong interphase bond [3].

It is possible to conclude, that the some chemical interaction takes place in the eutectics on the interphase boundaries that agrees with work results [2-4].

All this says about the fact, that eutectic presents itself the special class of fractal systems, in which the changes of initial component morphology take place in the comparison with them. The appearance of these or that eutectic properties is the result of the character of their chemical bond. This is proved by the morphology of structural fractales.

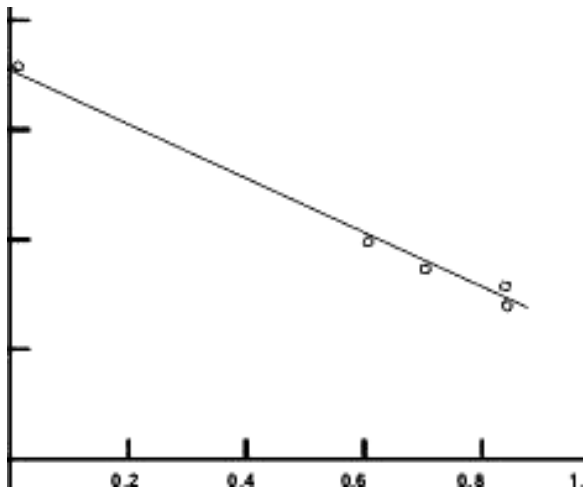


Fig.7. The curve graphical chart in logarithmic scale, corresponding to the $L(\epsilon)=a\epsilon^{1-D}$ dependence.

Let's consider the definition questions of fractal dimensionality of investigated phase boundaries in eutectic systems (for example in PbTe - NiSb). In the given case we use the method of region covering by equal square grid with the length of square side r (fig.7) for the definition of boundary (fractale) fractal dimensionality. It is calculated, that (as in the work [8]) the square number N , the sides of which cross of superblock boundaries even one time; number $N=46$ for $\epsilon=1mm$ (emphasized fourth fractale in the middle) on the given figure 3; the value $1,45\pm0,01$ is obtained for D .

This dependence in the logarithmical coordinates is linear (fig.7). The line of slope ratio corresponds to fractal dimensionality. This dimensionality is the dimensionality of only longitudinal cross-section of cigar-like fractale (PbTe - NiSb).

The description of structure geometry with the help of only one value of fractal dimensionality isn't enough. It is followed to find its reason in eutectic nature itself, which is connected with suprastructure interphase interaction. This interaction distorts the lattice on the phase boundary, containing the eutectic: the interatomic bond inside fractale itself, being in the matrix weakens. The lattice elastic deformation is maximal on the boundary and exponentially decreases in the depth of fractal phase. Along with it, the bonds between atoms in the near-boundary region inside phases should cause to the decrease of structure ordering in the given region. The fractal phases PbTe - NiSb, obtained in the eutectic, as it seen from the fig.3 and 6 differ by that property, that their densities decrease on the law, described

by the coefficient in the relation particle number – radius [8]. This is the one from the features of fractality revealing of different macro- and nanoparticles. The another characteristic is the fact, that (as it is seen from the fig.3) the fractale here occupy whole matrix object space PbTe, being the part of unite supramolecular assembly in the eutectic. These fractales consist of the parts, which are similar each other in some means.

We here have defined the phase fractal dimensionality by only one object cross-section. However, as we see, the structure of one phase PbTe - NiSb has cigar-like form and it is in elastic-resistant state; phase lattices are elastically distorted, matrix lattices are pressed on the boundary and fibers-fractals are extended. There are no lattice distortions in the transversal direction [3].

The above mentioned experimental results make the use of fractale conceptions in the case of non-self-repeating structures possible. For example the self-affine fractale, the structure of which is invariant one after simultaneous, but qualitatively different gauge change along different directions in the space. In order to totally character its properties, it is need that how fractal dimensionalities exist, how independent directions are. The self-affine fractales can be obtained by the way of simple expansion of self-repeating fractales, i.e. the relation of expansion values in the different directions should depend on the dimension. In the definite systems the particle aggregates have the brightly emphasized form anisotropy. Such aggregates are called not self-similar, but self-affine ones. In this case it is possible to introduce two fractal dimensions: longitudinal and transversal ones for the description of fractal aggregates [5,8].

The longitudinal fractal dimensionality we have already calculated. It is possible to calculate the transversal dimensionality. The consideration of fractal features of different eutectic systems is the subject of our future investigations.

Conclusion

The analysis and experimental data of physico-chemical processes, taking place in eutectic of PbTe - NiSb system show, that second phase has the fractal structure (with longitudinal fractal dimensionality $D_p=1,45$). This fractale has the fiber cigar-like form, consisting of the limited solid solution PbTe - NiSb, distributed in the matrix of stibium telluride (moreover, PbTe matrix consists of the limited solid solution PbTe - NiSb). Besides, the boundaries of fractal structures in the whole supramolecular assembly are in elastically-resistant state. The chemical bond, leading to the fractal structure formation appears on the fractale contact boundary. This gives to us the foundation for the consideration of regular eutectic structures as the essential class of supramolecular assemblies, on which the fractal conceptions can be distributed.

-
- | | |
|---|--|
| [1] J.M. Len. Supramolekulyarnaya khimiya. Konceptii i perspektivi. Nauka, Novosibirsk. 1998, s.115. (in Russian). | [3] K.Sh. Kagrananov, S.Sh. Kagrananov, E.D. Moroydor, M.G. Pishkin. Fizika Baki, Elm, 2006, c. XII, №3, p.38. |
| [2] V.S. Pervov, I.D. Mikheykin, E.B. Makhonina, V.D. Buckiy. J. Uspekhi khimii. 2003, 72 (9), c.852. (in Russian). | [4] K.Sh. Kagrananov, V.V. Didik. J. Metallofizika. I. "Nauka-Dumka" (Ukraina), 1981, №2, t..3, s. 31. (in Russian). |

- [5] V.I. Roldugin. J. Uspekhi khimii, RAN, 2003, 72 (10), c.931.(in Russian).
[6] Yu.N. Taran. Kiyev, Naukova-Dumka, 1970, c. 321. (in Russian).
[7] V.S. Ivanova, A.S. Balankin, I.J. Bunin, A.A. Okso-
chonov. Sinergetika i fraktali v materialovedenii. Moskow, "Nauka", 1994, c.43. (in Russian).
[8] Feder Jens. Fractals., Plenum Press.New York and London, p.258.

F.K. Өләсгәров, С.Ш. Қахраманов, Е.Д. Моройдор, М.Г. Пишкин

SUPRAMOLEKULYAR EVTEKTİKALAR FİZİKASINDA FRAKTAL KONSEPSİYASI

Neorganik evtektik sistemlerin supramolekulyar konsepsiyası nəzərdən keçirilib. Eksperimental alınan geometrik fraktal fiqurlar analiz olunub. Göstərilib ki, fraktallar matritsa ilə genetik əlaqədədir. Deyilənlər $A^{IV}B^{VI}$ -NiSb evtektikada və fraktal dendrit strukturlarda özünü əks edib.

Ф.К. Алескеров, С.Ш. Каҳраманов, Е.Д. Моройдор, М.Г. Пишкін

КОНЦЕПЦИИ ФРАКТАЛА В ФИЗИКЕ СУПРАМОЛЕКУЛЯРНЫХ ЭВТЕКТИК

Рассмотрены основные положения теории неорганических эвтектических систем, свидетельствующие в пользу supramolekulyarной концепции и учитывающие взаимодействие фрактальных суперансамблей. Приведены экспериментально наблюдаемые геометрические образцы-фрактали, показана природа межфазного взаимодействия фрактального агрегата с матрицей. Вышеизложенное подтверждено на примере регулярных эвтектических систем типа $A^{IV}B^{VI}$ -NiSb и фрактальных дендритных структур.

Received: 24.10.07

THE OBTAINING AND STUDYING OF ELECTRET PROPERTIES OF PELD+*x* vol.% TlGaTe₂(TlInSe₂) COMPOSITIONS

**E.M. GODJAYEV, Sh.A. ZEYNALOV, S.S. OSMANOVA,
E.A. ALLAKHYAROV, O.A. GUMBATOV**

Azerbaijan Technical University

Baku, Az-1073, H. Javid av., 25

The obtaining technology, investigation technique of polyethylene of low density with the additions of semiconductor compounds TlInSe₂, TlGaTe₂ are processed in the presented work and the investigation results of electric properties of these composition materials are described.

The wide distribution of polymer materials, conquered the positions in all regions of human activity is the one of the character elements of technical advancement. It is well known, that the most essential advantages of this type of materials, to which the small specific gravity, the ability to transform into complex configurations products with the help of high-production and accessible methods, the infusion possibility of complex valued technical properties to them, and also the presence of wide source of raw materials are related to.

The good agreement of physicomechanical and electric properties of polymer materials allows to more widely use them in the capacity of electric isolation and dielectrics in cable manufacture, and also in the manufacture of electric machines, apparatuses and compensators. It is necessary the deep studying of polymer electric properties in the dependence from their construction and exploitation conditions for rational polymer application.

Note, that polymers with different additions are studied well enough, however, information about influence of additions of inorganic nature on electric properties of these materials is very scanty. The influence of additions of semiconductor origin on polymer properties isn't considered at all. There is some information of foreign [1-3] and domestic investigators [4,5]. The information about obtaining of polyethylene polymer compositions (PELD) of low density with addition of semiconductor compound TlInSe₂ is recently appeared. It is revealed, that it is possible to increase the life time of electret materials from PELD on 4.5÷6 times with the help of additions TlInSe₂.

From above mentioned, the obtaining technology of composition material PELD with TlGaTe₂ and TlInSe₂ additions, the investigation technique of electret materials and some electrophysic properties of these composition materials are described in the present work.

The samples for the investigation are obtained by the following method: polymer powder is mixed with TlGaTe₂ (TlInSe₂) powder. Further, the films 100 mcm at melting point of polymer matrix and pressure 10÷15 MPa between aluminum foil are pressed from the mixture. The samples, obtained by such methods, are suitable for studying of electret properties.

Note that coronoelectrets are obtained in the fields of less intensity. The cusped electrodes, being on some distance from the surface of charged dielectric are applied for this. The corona discharge takes place between nib and surface, correspondingly air ionization and displacement of charge carriers, which are electrons and ions, to electret surface. The

charge carriers stay mainly in dielectric near-surface layer. The field intensity in polymer at this is low one that is lower than polymer puncture strength. The charge values are limited by puncture strength of environment. The charging speed can be big enough and the charges are equally distributed on the surface.

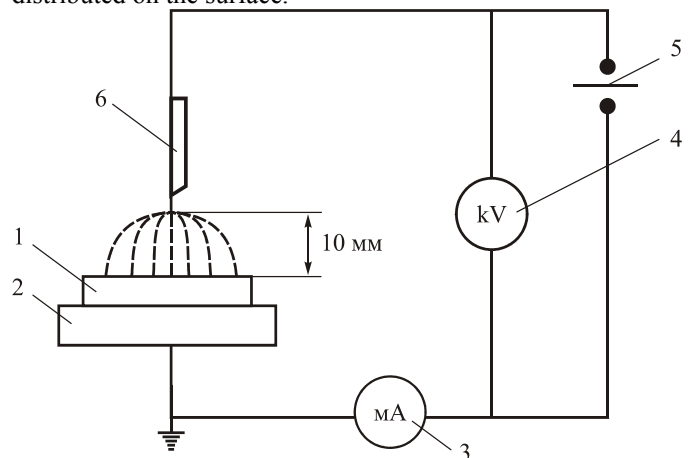


Fig.1. The installation for electret obtaining in corona discharge.

The installation scheme for electret obtaining in the corona discharge is presented on the fig.1. The polymer film 1 is put on the low grounded electrode 2 under the nib needle-electrode 6, being on the distance 10 mm under the film surface. The upper needle-electrode is connected to high-voltage edge of power supply 5. The needle potential is defined with the help of kilovoltmeter 4, and also efflux at corona discharge with the help of milliammeter. The film polarization is carried out at constant voltage 6 kV during 5 min.

Further the voltage injection is stopped. Later the polarized sample is put into cell, where the surface potential is defined by contact-free induction method. The installation scheme for the measurement of surface density of electret charges with periodical screening of measuring electrode is given on the fig.2. The device consists of massive metallic cylindrical body, on which the electromotor 1 is fixed. The one impeller 2, having four arms is fixed on the electromotor shaft. The impeller is between the low ground electrode, and upper measurement one, on which the sample is fixed. The screening of upper measurement electrode from the field, formed by electret takes at impelling rotation, that it is equivalent to the appearance of variable signal in the chain, which has the concatenation with oscilloscope 4 electrodes. The compensating voltage is injected from the source of

constant voltage 3, supplied by slow voltage regulator and is registered by oscillograph. The sign of charge surface densities is defined on the sign of compensating voltage, injected by voltmeter.

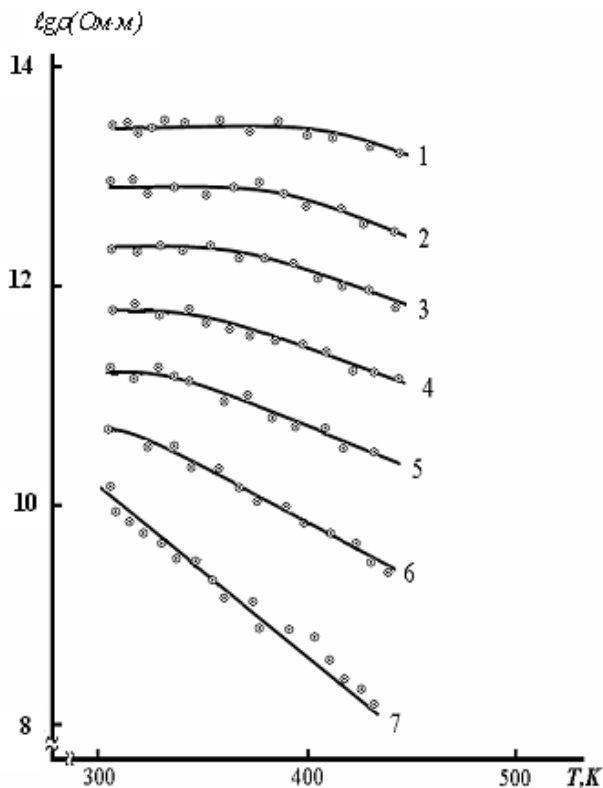


Fig.2. The temperature dependence of specific resistance for compositions PELD+X vol.% $TiInSe_2$, where 1- $x=0$; 2- $x=3$; 3- $x=5$; 4- $x=10$; 5- $x=20$; 6- $x=30$; 7- $x=40$.

The surface density of electret charge is measured by induction method with compensation and is defined on the formula:

$$\sigma_{eff} = \frac{\epsilon \epsilon_0 U_k}{d}$$

where σ_{eff} is charge surface density (Kl/m^2), ϵ is sample permittivity, $\epsilon_0=8.85 \cdot 10^{-12} F/m$ is electric constant, U_k is compensating voltage (V), d is electret sample thickness (m).

We define the life time on the formula

$$\tau = \frac{t_{xp1} - t_{xp2}}{\ln \sigma_2 - \ln \sigma_1}$$

by the working of experimental results $\sigma_{eff}=f(t_{xp})$, where σ_1 and σ_2 are charge surface densities, corresponding to retention times t_{xp1} and t_{xp2} , correspondingly.

In the given work we investigate the temperature dependence of specific resistance of compositions PELD+x vol.% $TiInSe_2$. The investigations are carried out in the temperature interval 300-450K.

As it is followed from the figure 2, the resistance decrease with temperature increase is character for all compositions. This, probably, is connected with storage of PELD structure. However, the decrease amplification of specific resistance in the dependence on the composition is observed with increase of $TiInSe_2$ content in composition compounds. The relatively essential and linear dependencies in the whole investigated temperature interval are observed for the composition PELD+40vol.% $TiInSe_2$.

- [1] P.M. Borsenberger. C. Appl. Phys. 68(12), 15 Desember 1990. p. 6263-6273.
- [2] P.M.Borsenberger. C. Chem. Phys.95(2), 15 Culy 1991, p.1258-1265.
- [3] Damodar M. Pai and B.E.Springett. Reviewis of Modern Physics, ol.65, №1, Canuary 1993, p.163-190
- [4] E.M.Gocayev, R.M.Sardarli, N.A.Eyubova, E.A.Allahya-

- rov,S.S.Osmanova. Fizika, 2005, cild XI, №3, p.3-6
- [5] E.A. Allakhyarov, T.P. Musaev, I.G. Gamdullaeva, S.S. Osmanova. Novie elektretne materiali tipa PGNP+x ves% $TiInSe_2(Ga, In, Tl)$. Sbornik trudov Mejdunarodnoy konferentsii «Amorfnie i mikrokristallicheskie poluprovodniki». Sankt-Peterburg, 19-21 iyunya 2006 g. s.316. (in Russian).

E.M. Qocayev, Sh.A. Zeynalov, S.S. Osmanova, E.A. Allahyarov, O.A. Hümbətov

ASPE+x həcm% $TiGaTe_2(TiInSe_2)$ KOMPOZİSİYALARININ ALINMASI VƏ ELEKTRET XASSƏLƏRİNİN ÖYRƏNİLMƏSİ

Təqdim olunan işdə $TiGaTe_2$ və $TiInSe_2$ əlavəli aşağı sıxlıqlı polietilenin alınma texnologiyası işlənilmiş, elektrik xassələrinin ölçülməsi üçün metodika seçilmiş və elektrik xassələri öyrənilmişdir.

Э.М. Годжаев, Ш.А. Зейналов, С.С. Османова, Е.А. Аллахяров, О.А. Гумбатов

ПОЛУЧЕНИЕ И ИЗУЧЕНИЕ ЭЛЕКТРЕТНЫХ СВОЙСТВ КОМПОЗИЦИЙ ПЭНП+х об.% $TiGaTe_2(TiInSe_2)$

В представленной работе разработана технология получения, методика исследования полиэтилена низкой плотности с добавками полупроводниковых соединений $TiInSe_2$, $TiGaTe_2$ и изложены результаты исследования электрических свойств этих композиционных материалов.

Received: 15.07.07

THE COMPOSITE GAS SENSITIVITY ON THE BASIS OF POLYMERS AND Cu₂S AND CdS NANOPARTICLES

M.B. MURADOV, G.M. EYVAZOVA

Baku State University, Z.Khalilov str., 23, Az-1073, Baku, Azerbaijan

M.A. NURIYEV

Institute of Radiation Problem of NAS of Azerbaijan, F. Agayev str., 9, Az-1143, Baku

The gas sensitivity of the samples gelatin/Cu₂S and gelatin/CdS at the influence of the steams of different solvents and ethyl alcohol is investigated. It is shown, that the composites on polymer base with Cu₂S and CdS nano-particles are sensitive on the steams of different solvents. The gas sensitivity of nano-composites depends on the population of matrix and chemical data of tested gas. These materials can be applied in the capacity of sensitive element of different gas sensors and sensing elements.

The demand of environment and ecology control always stimulates investigations on the working of gas sensors. These sensors are necessary at technological control of chemical-metallurgical and gas-, oil-producing industry. There are different gas-sensitive sensors, differing on industry action and technology. The solid-body sensors, which differ by the construction and portability simplicities, are the one from the sensor varieties. The electric signals, manufactured by such portative sensors allow obtaining the information about substance content and its physical parameters. The workings in this region lead to the formation of multi-functional devices [1] on their base. The different semiconductor devices are sensitive elements in gas sensors [2].

The nano-composites are the one of materials, presenting the big interest at formation of gas sensors. In these materials the nano-composite interaction processes with molecules of gas phase are determinant ones. Nowadays, the sensors of resistive type [3, 4] on the polymer base with metallic filler have wide distribution. The polymer composites with semiconductor particles present the essential interest. The nano-heterogeneous polymer composites consist of polymer matrix with ultra-disperse particles by dimensions 20-100 nm and distances between them of the same order [5]. Such systems have the unusual photo and gas sensitive properties, which are defined by the charge redistribution process because of external interactions. The electroconductivity of these systems changes very strongly even at room temperature in the result of adsorption of different steams and gases [6]. The electroconductivity change of nano-composites at sorption of different gases depends on many factors: population of polymer matrix with semiconductor particles, inter-particle space, and interphase interaction between matrix and semiconductor particles [7]. In this connection the nano-particle formation technology of chalcogenide semiconductors in the volume of polymer matrix with the help of ion sandwich chemical absorption allows goal-seeking changing the particle concentration and inter-particle distance in nano-composites [8].

The aim of presented work is the study of composite gas sensitivity on the basis of gelatin polymer matrix and cuprum sulfide particles (gelatin/Cu₂S) and cadmium sulfide (gelatin/CdS) at the influence of steams of different solvents and ethyl alcohol.

Experimental part

The sample, on the surface of which the electrodes are situated parallel, is put in measured cell for gas sensitivity testing. The resistance change with time at the definite

pressure in the different gaseous mediums is registered by automatic recorder through teraohmmeter E6-13A. The measurements are carried out by two methods: 1) the volume is evacuated up to vacuum 10⁻¹ atm (76 torr) and the sample sensitivity to given gas is defined after lap of tested gas or steams on the change of resistance value the gas sensitivity of samples on the steams of ethyl alcohol and acetone; 2) the vessel with tested substance (alcohol or solvent) is put in the duar and previously cooled with the help of liquid nitrogen. After freezing the vacuum system with measured cell and vessel are evacuated up to vacuum 10⁻² atm. Further the vessel with tested substance is heated in different modes. The pressure in the measured cell increases up to pressure of saturated steams of given liquid at given temperature and registration of resistance change with pressure change is carried out. The gas sensitivity is defined on the following formula:

$$\gamma = (R_1 - R_0) / (P_1 - P_0) = \Delta R / \Delta P , \quad (1)$$

where P₀ and R₀ are initial values of pressure and resistance; P₁ and R₁ are final values of pressure and resistance; ΔP and ΔR are changes of pressure and resistance.

Result discussion.

The resistance change with time for samples gelatin/Cu₂S 15 cycles (a) and 30 cycles (b) of formation after lap of ethyl alcohol (fig.1.a) and acetone (fig.1.b) is shown on the fig.1. As it is seen from the dependence the resistance increases with further saturation at the lap of gas or steams.

The influence of nano-composite content and composition on gas sensitivity kinetics is also studied, i.e. the nano-composite resistance change with different content of Cu₂S and CdS nano-particles with time in ethyl alcohol steam medium is studied. It is seen, that stabilization of resistance volume for samples gelatin/15 cycles Cu₂S takes place quicker, than for samples gelatin/30 cycles Cu₂S (~3 min. and ~20 min., correspondingly). This is said about the fact, that particles at 15 formation cycles have the relatively small dimensions, the distances between them is enough for free adsorption of gas or steam, and at 30 formation cycles the increase of concentration and nano-particle dimensions makes difficult the gas penetration and the velocity of resistance change decreases correspondingly.

The time dependence of nano-composite change gelatin/15 cycles Cu₂S, gelatin/15 cycles CdS and gelatin/30 cycles CdS in the air at normal pressure 1 atm (760 torr) (region 1), after evacuation up to 10⁻¹ atm (76 torr), after air lap (region 3), after repeated evacuation up to 10⁻¹ atm (region 4) and after the lap of ethyl alcohol steams (region 5), when the pressure in the cell changes from 76 torr up to 117 torr.

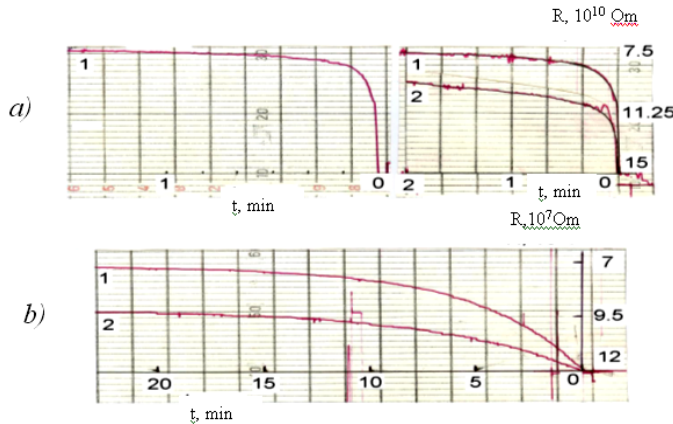


Fig.1. The resistance change of the film gel./Cu₂S at the lap of ethyl alcohol (1) and acetone (2) steams; a) gel./Cu₂S – 15 cycles; b) gel./Cu₂S – 30 cycles.

It is seen, that values of initial resistance and resistance, corresponding to the pressure 10⁻¹ atm (760 torr) with time don't change, i.e. they are relatively stable. But resistance change at the ethanol lap after evacuation up to 10⁻¹ atm has the different values for different compositions. The best gas sensitivity at the lap of ethyl alcohol steams is observed for nano-composites gelatin/15 cycles CdS (9,5x10¹⁰Om/torr).

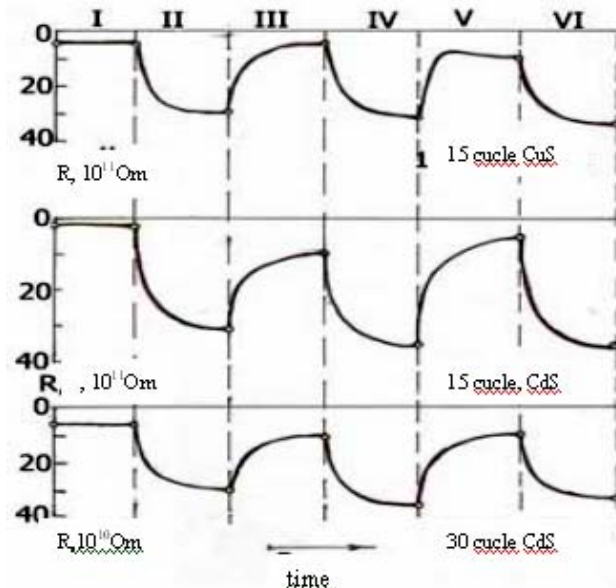


Fig.2. The kinetics change of specific surface resistance with time for nano-composites ge./15c. Cu₂S, gel./15c. CdS and gel./30c. Cds.

The second method is used for the definition of gas sensitivity of samples gelatin/15 cycles CdS.

On the fig.3 it is seen, that the samples resistance gelatin/15 cycles CdS changes with pressure value change of ethyl alcohol steams. The measurements are carried out at vessel heating with different velocity; steams of warm water, steams of hot water and the vessel are put in the warm water.

The same dependence, is shown on the fig. 4, but heating rate is changed: the vessel is heated independently at room temperature (c.1), by warm water with temperature 36 °C (c.2), with water temperature 47 °C (c.3) and with water temperature 60-65 °C (c.4).

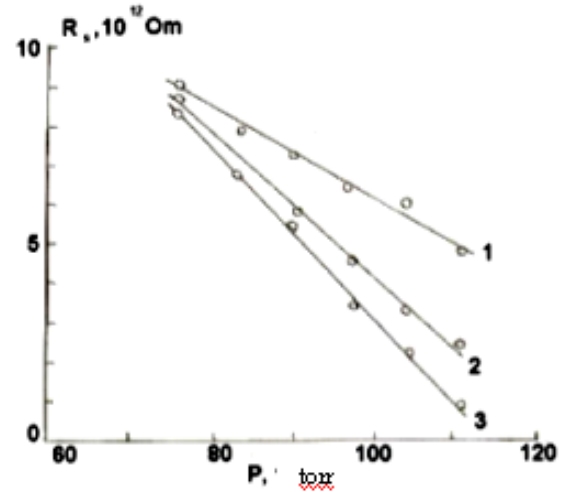


Fig.3. The resistance dependence on the change of ethyl alcohol steam pressure for the samples gel./15c. CdS at heating: 1 – warm water steams; 2 – hot water steams; 3 – the vessel in the warm water.

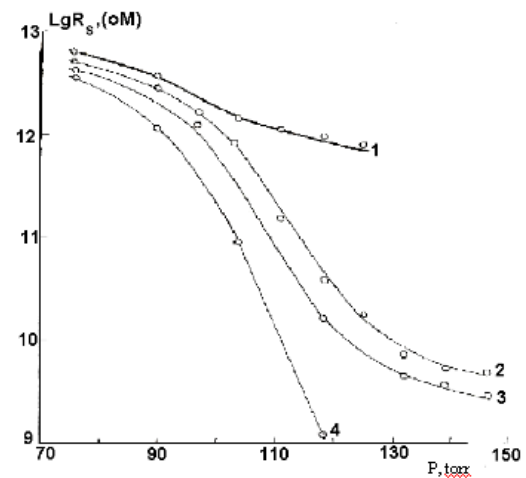


Fig.4. The resistance dependence with change of alcohol steam pressure for the samples gel./15c. CdS at the heating: 1- at room temperature; 2 – with water temperature 36°C; 3 – 47°C; 4 – 60-65°C.

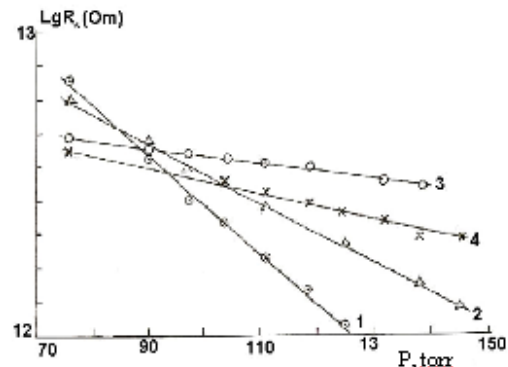


Fig.5. The resistance dependence with change of alcohol steam pressure for the samples gel./15c. CdS: 1 – alcohol; 2 - acetone; 3 – dichloroethane; 4 – methyl ethyl ketone.

THE COMPOSITE GAS SENSITIVITY ON THE BASIS OF POLYMERS AND Cu₂S AND CdS NANOPARTICLES

From the fig.4 it is seen that the curve inclination angle, which says about the increase of steam saturation velocity changes with heating rate increase. This is equivalent to increase of alcohol molecule energy. The molecule energy increase leads to the increase of sample sensitivity in the result of more deep steam adsorption.

The resistance variation of samples gelatin/15 cycles

CdS on saturated steam pressure of ethyl alcohol (c.1), acetone (c.2), dichlorethane (c.3) and methyl ethyl ketone (c.4) is shown on the fig.5. On the dependence inclination it is possible to say that the best gas sensitivity is observed at the lap of ethyl alcohol steams. Such changes of sensitivity will be understandable, if the chemical data of these solvents are compared.

Table

Stems	Ethyl alcohol	Acetone	Methyl ethyl ketone	Dichlorethane
Structure	C ₂ H ₆ O	C ₃ H ₆ O	C ₄ H ₈ O	Cl ₂ C ₂ H ₄
Molecular weight	46	58	72	99
Boiling point, °C	78	56	83	79.6
P ₀ , torr	76	76	76	76
P ₁ , torr	125	146	146	139
R ₀ , 10 ¹² Om	1	2	3.5	5.3
R ₁ , 10 ¹² Om	8,5	8	6.5	6.8
ΔR, 10 ¹² Om	7.5	6	3	1.5
ΔP, 10 ¹² Om	49	70	70	63
γ, 10 ⁻¹⁰ Om	15,3	8.6	4.3	2.38

The chemical structure, the boiling point and molecular weight of used solvents and gas sensitivity for the sample gelatin/15 cycles CdS, calculated on the formula (1) from the dependence, presented on the fig.5 is shown in the table. From the comparison it is seen, that the ethyl alcohol molecules have the least molecular weight among these materials and the best gas sensitivity is observed at the influence of its steams. The gas sensitivity consistency of the samples to the steams of these solvents should coincide with consistency of their molecular weight decrease. It is possible to say that the best adsorption and correspondingly, the best gas sensitivity is observed in the steams and gases with

relatively less molecular weight at the sample contact with the steams of these solvents. This is proved by the obtained results. Thus, the carried out investigations show that composites on the basis of polymer with cuprum sulfide and cadmium sulfide nano-particles are the sensitive ones on the steams of different solvents. The nano-composite gas sensitivity depends on the matrix population and on the chemical data of tested gas. These materials can be applied in the capacity of sensitive element of different gas sensors and sensing elements.

The given work is carried out at the support USTC, grant №3486.

-
- [1] T. Moriizum. Thin Solid Films, 1988. № 160. p. 413.
 - [2] T.A. Temofonte,K.E. Schoch. J.Appl. Phys., 1989,v.65. № 3,p, 1350.
 - [3] L.I.Traxtenberg, G.N. Gerasimov,I.K. Potapov,T.N. Rostovshikova,V.V. Smirnova,V.Yu. Zufman. Vesti.Mosk. Un-ta, ser. 2. Khimiya, 2001,t. 42, № 5, s. 325. (In Russian).
 - [4] Ye.I. Grigoryev,P.S. Zavyalov, S.N. Chvalun. «Pisma v Jet», 2003, t. 28, № 20, s.15. (In Russian).
 - [5] P.S. Voroncov, G.N. Gerasimov,Ye.N. Golubeva,Ye.I. Grigoyev,S.A. Zavyalov, L.M.Zavyalova, L.I. Traxten- berg. J. Phys. Khimiya. 1998. t. 2, № 10.s.1912. (In Russian).
 - [6] A.V. Udaratin,M.I. Fedorov. Sensor, 2003, № 1, s. 50. (In Russian).
 - [7] O.V. Anisimov,N.K. Maksimova,N.G. Filonov, L.S. Khludkova,Ye.V. Chernikov. Sensor, 2003, № 1,s. 40. (In Russian).
 - [8] V.V. Klechkovskaya,V.S. Maslov,M.B. Muradov. Kristallografiya, 34, №1,1989,182. (In Russian).

M.B. Muradov, M.A. Nuriyev, Q.M. Eyvazova

POLİMER VƏ Cu₂S , CdS NANOZƏRRƏCİKLƏRİ ƏSASINDA OLAN KOMPOZİTLƏRİN QAZA HƏSSASLIĞI

Jelatin/Cu₂S və jelatin/CdS nümunələrinin etil spirti və müxtəlif həlləedicilərin buxarlarında qaza həssaslığı tədqiq edilmişdir. Müəyyən edilmişdir ki, polimer və Cu₂S , CdS nanozərrəcikləri əsasında olan kompozitlər müxtəlif həlləedicilərin buxarlarına həssasdırlar. Nanokompozitlərin qaza həssaslığı matrisin dolma dərəcəsindən və test olunan qazın kimyəvi göstəricilərindən asılıdır. Bu materiallardan müxtəlif qaz sensorlarında həssas element kimi istifadə etmək olar.

М.Б. Мурадов, М.А. Нуриев, Г.М. Эйвазова

ГАЗОЧУВСТВИТЕЛЬНОСТЬ КОМПОЗИТОВ НА ОСНОВЕ ПОЛИМЕРОВ И НАНОЧАСТИЦ Cu₂S и CdS

Исследована газочувствительность образцов желатин/Cu₂S и желатин/CdS при воздействие паров различных растворителей и этилового спирта. Показано, что композиты на основе полимера с наночастицами Cu₂S и CdS являются чувствительными на пары различных растворителей. Газочувствительность нанокомпозитов зависит от степени заполнения матрицы и от химических данных тестируемого газа. Эти материалы могут быть применены в качестве чувствительного элемента различных газовых сенсоров и датчиков.

Received: 15.07.07

THE VOLT-AMPERE CHARACTERISTICS OF AMORPHOUS SOLID SOLUTIONS OF Se-S SYSTEM

N.Z. DJALILOV, G.M. DAMIROV, N.R. MAMEDOV

*Institute of Physics of NAS of Azerbaijan,
AZ-1143, Baku, H. Javid av., 33*

The volt-ampere characteristics (VAC) of film amorphous solid solutions of Se-S system, obtained by the method of hot wall are investigated. The current for all investigated samples increases at the change of voltage value V_x - transition from ohmic region into quadratic one, i.e. the injected current appears in the investigated samples. The increase of concentrations of local states in Se-S system samples with the increase of sulfur content is explained by structural differences of the investigated samples.

The glasses are called chalcogenide ones, in the composition of which Se, S, Te [1] are included. The systems on Se, S, Te are widely used in the additions and the experiments besides the pure ones. The glasses of more complex composition [2-4] are widely used. The chalcogenide and chalcogene glasses are used in the electron diffraction investigation (xerography), for the recording of optical information, in electric changers and storage devices [5-8].

Selenium, sulfur and solid solutions on their base are close to chalcogenide glasses on their physical properties. However, as it is known Se is semiconductor, whereas, S is good isolator. Consequently, this system promotes the interest peculiarity in the change from semiconductor up to isolator.

The homogenous solutions at the crystallization of which the series of solid solution precipitates form in melted state between sulfur and selenium. Taking into consideration, that there are many general things in sulfur and selenium behavior, it is possible to propose, that they are able to form the mixed molecules of SSe type [9].

Though Se and Te have properties, which are analogical to chalcogenide properties [10], they contain the structural units with molecular properties and are considered separately.

The structural model of binary system presents itself the continuous grid, in which the coordination "rule 8-N" for both components at any their relation is carried out. The hetero- and homeopolar bonds are possible between atoms. The hexagonal crystalline Se consists of helical chains, set parallel each other. The chemical bond inside chains has the covalent character and it is very strong, but the bond between the chains is the weak one of Van der Waals type. In liquid phase it is possible to consider, that chains are oriented occasionally. At quick alloy cooling the viscosity becomes very high before chains have time to redirect and glassy state appears [11].

The Te addition into selenium liquid solution leads to chain shorting, as Se-Te bond is weaker, than Se-Se one and crystallization at cooling becomes easier. At S addition into melt, it can be said, that the vice versa takes place, as Se-S bond is stronger, than Se-Se one. The amorphous selenium presents itself the mixture of molecules (closed rings) and polymer chains. S, Se and Te have the coordination number, which is equal to 2. The average mole energies in S, Se and Te series decrease and melting point and density increase. This shows that the more bonds are in the chain, the less bonds between them [12].

Nowadays it is established, that it is possible to directly change the electron properties of chalcogene and

chalcogenide glassy semiconductors by the change of chemical composition and also by impurity introductions. Moreover, the change of concentration of charged defect centers (U^1) in them takes place and thus it is possible to manage by their electric, optic and photoelectric properties, that it is very important for practical use [11].

The given work contains the investigation results of volt-ampere characteristics of film amorphous samples of $\text{Se}_{100-x}\text{S}_x$ ($x=5; 30; 40$) system.

The selenium by B_5 purification and pure rod sulfur, suspended with accuracy up to 0,0001g are taken for the obtaining of solid solutions selenium-sulfur. The vibration method is used for better melt homogenization. The ampoules during 3 hours are treated by shaking at temperature 280°C, i.e. on 60°C higher the selenium melting point.

The films by width 3 mcm are obtained by thermal spraying in vacuum, by the method of hot wall, on the substrates from cover glass. Te, marked by evaporation in vacuum is used in the capacity of injected contact. Al is used in the capacity of general contact [13].

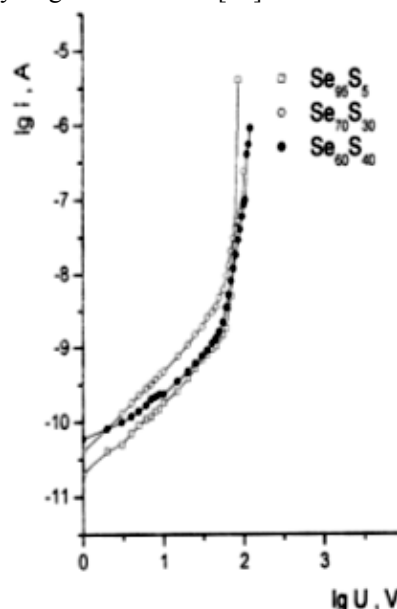


Fig.

The measurement results of VAC of investigated samples are presented on the figure.

As it is seen from the figure, VACs of investigated samples consist of ohmic and quadratic regions. The current of injected electrons, limited by recombination, begins to dominate under the current of thermally excited holes.

The voltage of V_x transition from Ohm law up to “trap” quadratic law [14] in $1/\theta$ times exceeds the transition voltage for without-trap case, defined by the formula

$$V_x \approx \frac{en_0 L^2}{\varepsilon} \quad (1)$$

If the concentration of free electrons doubles in the result of injection, then expression for the concentration of nonequilibrium electrons, picked on fin traps, has the form n/θ , moreover

$$V_x \approx \frac{en_0 L^2}{\theta \varepsilon} \quad (2)$$

The current for the sample of Se_{95}S_5 composition strongly increases at the voltage transition of V_x -transition from ohmic region into “trap” quadratic one. The current

increase from the voltage is observed for the samples of $\text{Se}_{70}\text{S}_{30}$, $\text{Se}_{60}\text{S}_{40}$ compositions, i.e. the injected current appears in the investigated samples.

It is observed, that inclinations from ohmic going in VAC for Se_{95}S_5 , $\text{Se}_{70}\text{S}_{30}$, $\text{Se}_{60}\text{S}_{40}$ samples take place at the values $V_x \approx 60$, 25; 54,95; 48, 97V, correspondingly. By this values the concentrations of local states, which are equal for given compositions: $4,75 \times 10^{19}$; $3,85 \times 10^{19}$; $3,25 \times 10^{19} \text{ cm}^{-3}$ are calculated on the formula, correspondingly [14].

$$N_t = 1,1 \times 10^6 \varepsilon \frac{V_x}{L^2} \quad (3)$$

Thus, the increase of local state concentrations in the samples of Se-S system with increase of sulfur content can be explained by the structural differentiations of the investigated samples.

- [1] A.Meden, M. Sho. Fizika i promenenie amorfikh poluprovodnikov. “Mir”, M., 1991, (In Russian).
- [2] K.Shimakawa, A.Kolobov. Adv.Phys. 1995, 44, 537.
- [3] K.L.Bhatia, G.Partasarathy. E.S.P.Gopal. J. Non-Cryst. Sol. 1985, 69, 189.
- [4] I.A. Chaban. FTT, 2007, t.49, v.3, s.405. (In Russian).
- [5] L.A.Wahab, M.B.El-Den, M.S.Youssef. Egypt. J. Sol., 2000, v.23, No.1, 71.
- [6] S.R.Ovshinsky. Phys. Rev. Letters, 1988, 21, 1450.
- [7] L.A. Wahab. Proceeding of the Second International Conference (Science & Development & Environment) Cairo, 1997, 215.
- [8] A.F.Maged, L.A.Wahab, I.A.El Kholy. J. Materials Science. 1998, 33, 3331.
- [9] D.M. Chijikov, V.P. Schastliviy. Selen i selenidi. “Nauka”, M.1964. (In Russian).
- [10] H.Mott, E. Devis. Elektronniye processi v nekristallicheskikh veshhestvakh.” Mir”, M. 1982. (In Russian).
- [11] N.Z. Dzhalilov, S.I. Mekhtiyeva, G.M. Damirov i dr.. Izv.NAN Azerb., ser. fiz.-mat. i tekhn., fiz. i astr. 2007, (v pechati). (In Russian).
- [12] S.D. Baranovskiy, E.A. Lebedev. FTP, 1985, t.19, v.6, 1035. (In Russian).
- [13] N.Z. Dzhalilov, G.M. Damirov. IX Mejdunarodnaya konferenciya “Opto-nanoelektronika, nanotekhnologii i mikrosistemi”, Ulyanovsk, 2007. (In Russian).
- [14] M. Lampert, P. Mark. Injekcionniye toki v tverdikh telakh. “Mir”, M., 1973. (In Russian).

N.Z. Cəlilov, Q.M. Dəmirov, N.R. Məmmədov

**Se-S SİSTEMİNİN AMORF BƏRK MƏHLULLARININ
VOLT-AMPER XARAKTERİSTİKASI**

Qaynar divar üsulu ilə alınmış Se-S sisteminin bərk məhlullarının volt-amper xarakteristikası tədqiq edilmişdir. Cərəyanın qiyməti V_x keçid gərginliyini (omik oblastdan kvadratik oblasta keçid) keçdikdən sonra bütün nümunələrdə artır, yəni tədqiq olunan nümunələrdə injeksiya cərəyanı baş verir. Tərkibindəki kükürdün artması ilə Se-S sisteminin nümunələrindəki lokal halların konsentrasiyasının artması tədqiq olunan nümunələrin struktur müxtəlifliyi ilə izah olunur.

Н.З. Джалилов, Г.М. Дамиров, Н.Р. Мемедов

**ВОЛЬТ-АМПЕРНЫЕ ХАРАКТЕРИСТИКИ АМОРФНЫХ ТВЕРДЫХ
РАСТВОРОВ СИСТЕМЫ Se-S**

Исследовались вольт-амперные характеристики (ВАХ) пленочных аморфных твердых растворов системы Se-S, полученные методом горячей стенки. При переходе напряжения значения V_x -переход из омической в квадратичную область-ток для всех исследованных образцов увеличивается, т.е. в исследованных образцах возникает инжекционный ток. Увеличение концентрации локальных состояний в образцах системы Se-S с увеличением содержания серы объясняется структурными различиями исследованных образцов.

Received: 16.07.07

THE INFLUENCE OF ELECTROTHERMOPOLARIZATION ON THE MICROSTRUCTURES AND COMPOSITION STRENGTH PROPERTIES ON THE BASIS OF POLYPROPYLENE AND MnO₂

M.A. RAMAZANOV, F.V. GADGIYEVA

Baku State University

Baku, Az 1145, Z.Khalilov str.23

A.S. GUSEYNOVA

Institute of Physics of NASA,

AZ-1143 Baku, Azerbaijan, H. Javid ave. , 33

The investigation results of polarization influence on the microstructure and composition strength properties on the base of polypropylene and low-molecular addition MnO₂ are described in the given work. It is established, that the change of strength properties of composition samples PP+MnO₂ after electrothermopolarization is connected with change of charge state and formation of order physical composition structures.

It is known, that the composition dielectrics have electret properties [1-2] after electrothermopolarization. It is also known, that charge carriers in polarization process are accumulated on the phase interface and in heterogeneities [3-4].

The composition electrothermopolarization changes its charge state. The accumulation of charge carriers on the phase interface changes the interphase interactions, and this can lead to the change of composition strength properties [5].

In the given work the investigation results of polarization influence on the microstructures and composition strength properties on the base of polypropylene and low-molecular addition MnO₂ are described. The compositions PP+MnO₂ are obtained from the PP solution by the way of mixture of PP solution and MnO₂ with the further solubility moving away. The concentration MnO₂ varies from 0 up to 5%. The obtaining of sample composite is carried out by the method of hot pressing at polymer melting point and pressure 15 MPa during 10 minutes with further cooling under the pressure up to room temperature.

The microstructures of PP+MnO₂ compositions are investigated on the scanning atomic force microscope (AFM).

The strength characteristics of sample compositions are defined at temperature 293K.

It is established, that the mechanical and electric strengths of the investigated samples increase with the increase of

electric field intensity of (E_p) polarization, achieves the maximum at $E_p=7 \cdot 10^6$ V/m, and later the decrease of the values of electric and mechanical strengths take place.

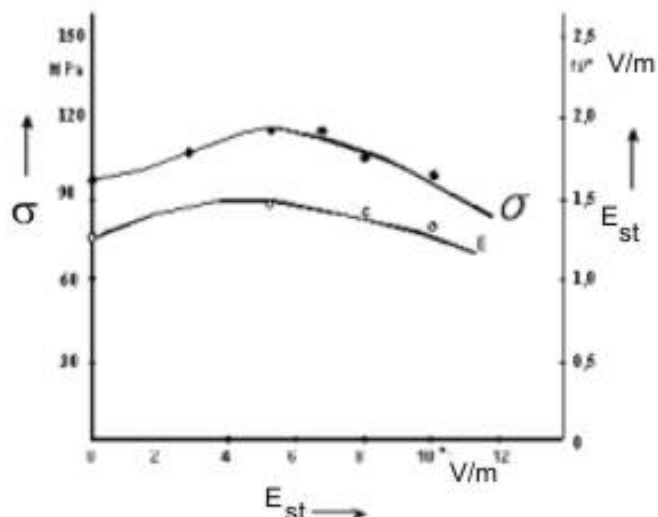


Fig.1. The dependence of electric and mechanical strengths of PP+MnO₂ composition, polarized at the temperature $T_p=373$ K on the polarization field intensity.

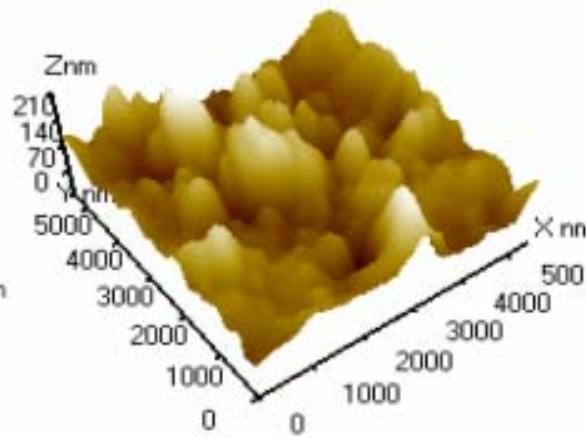
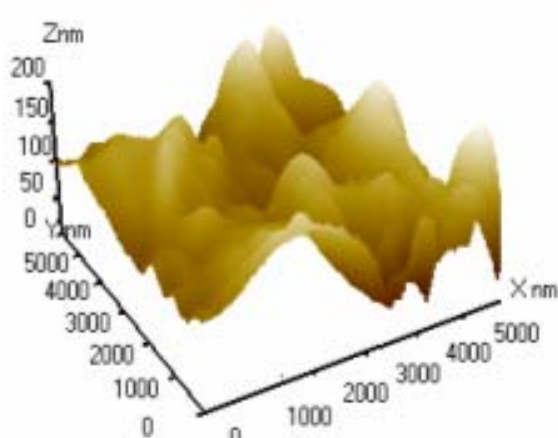


Fig.2. AFM image of PP+MnO₂ composition before and after electrothermopolarization: a) unpolarized sample; b) polarized sample $E_p=7 \cdot 10^6$ V/m, $T_p=373$ K, $t_p=1$ h.

The charges, accumulated on the phase interface of composite components increase with the increase of electric field intensity of polarization. First of all, the charge accumulation changes the interphase interaction between composite components. The increase of interphase interactions leads to the increase of composition strength properties. The decrease of the values of electric and mechanical strengths higher $E_p=7 \cdot 10^6$ V/m, probably, is connected with the charge dispersion in the composition volume, which leads to the decrease of composition strength properties. These results are well agreed with work results [3].

AFM 3D image of composition relief PP+MnO₂ before and after electrothermopolarization are given on the fig.2. AFM investigation of sample relief of PP+MnO₂ compositions shows that relief of sample compositions strongly changes after electrothermopolarization, i.e. sample relief becomes uneven. It is seen, that structural changes take

place after electrothermopolarization on the surface of composition samples.

The histogram of the element values of image and mean-square roughness of composition surface PP+MnO₂ is shown on the fig.3. The histogram of surface heterogeneity shows, that composition relief becomes relatively uneven after polarization under the influence of electric field. It is also shown, that mean-square roughness of composition surface for the unpolarized samples is 90-130 nm, and for polarized ones is 110-160 nm. The distribution of Fourier-analysis shows, that relief heterogeneities are distributed on the surfaces uniformly.

From the fig.2 and fig.3 it is seen, than the blending of surface heterogeneities takes place after electrothermopolarization, i.e. physical structure of PP+MnO₂ composition changes. It is also seen, that microstructure change leads to the change of composition strength properties.

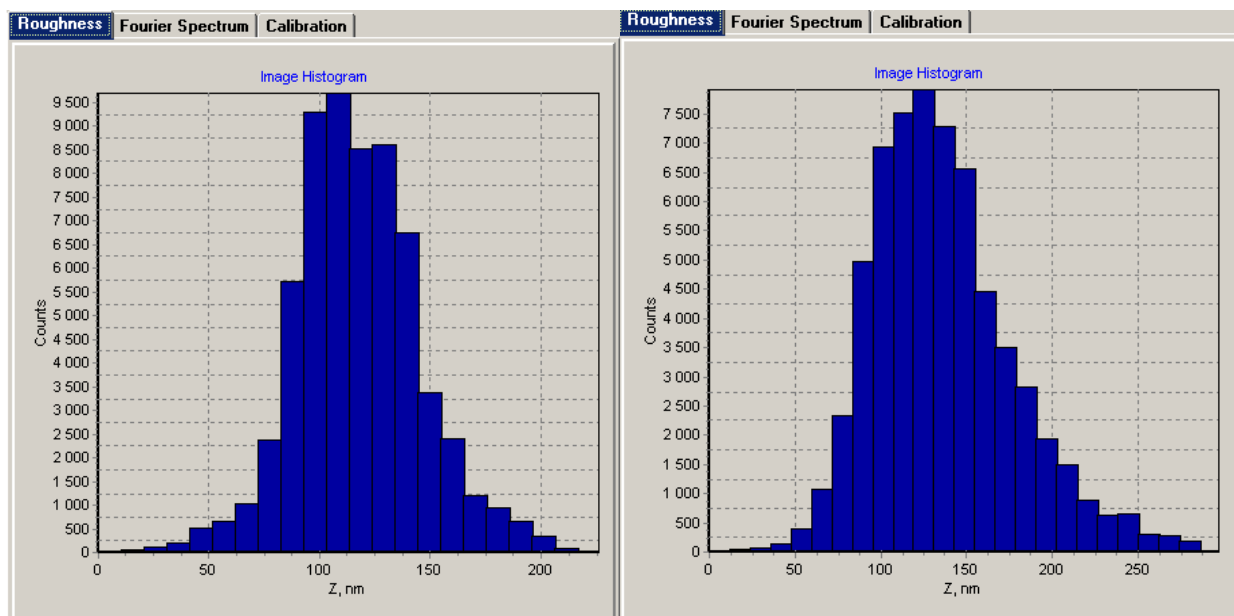


Fig.3. The analysis of surface properties of PP+MnO₂ compositions and histogram of values of image elements: a) unpolarized sample; b) polarized sample $E_p=7 \cdot 10^6$ V/m, $T_p=373$ K, $t_p=1$ h.

Thus, the change of strength properties of sample compositions PP+MnO₂ after electrothermopolarization is

connected with the change of charge state and formation of order physical composition structure.

- [1] M.A. Ramazanov, A.S. Guseynova. J. Plasticheskiye massi, 2007 № 3, Moskow, s. 13-16. (in Russian).
 - [2] Elektreti. Pod. red. G. Seslera, Moskow, Mir, 1983, 488s. (in Russian).
 - [3] M.A. Ramazanov, S.A. Abasov, Z.E. Mustafayev. Novye Technologii-21 vek. 2001, №6, s.26-29. (in Russian).
 - [4] M.A. Ramazanov, Kh.S. Ibragimova, S.A. Abasov, A.M. Gasanov. J. Elektronnaya obrabotka materialov, 2005,
 - [5] №4, Kishinyov, s. 57-62. (in Russian).
- M.A. Ramazanov, A.S. Guseynova, S.I. Mekhtiyeva, S.A. Abasov. "Vliyaniye elektrotermopoliarizacii na prochnostniye svoystva poliolefinov, modifikasirovannikh dobavkami nizkomolekulyarnikh krasiteley". Sbornik statey Mater. Mejdunarodnaya konferenciya Fizika-2005 7-9 iyun 2005, Baku, s. 509-510. (in Russian).

M.A. Ramazanov, A.C. Hüseynova, F.V. Hacıyeva

POLİPROPİLEN VƏ MnO₂ ƏSASINDA ALINMIŞ KOMPOZİSİYALARIN MİKROQURULUŞUNA VƏ MÖHKƏMLİK XASSƏLƏRİNƏ ELEKTROTERMOPOLYARLAŞMANIN TƏSİRİ

Bu məqalədə polipropilen və MnO₂ əsasında alınmış kompozisiyaların mikroquruluşuna və möhkəmlik xassələrinə elektrotermopolyarlaşmanın təsirinin tədqiqinin nəticələri verilmişdir. Göstərilmişdir ki, PP+MnO₂ əsasında alınmış kompozisiyaların möhkəmlik xassələrinin elektrotermopolyarlaşmadan sonra dəyişməsi yüksək halının və nizamlı fiziki quruluşun yaranması ilə əlaqədardır

M.A. RAMAZANOV, A.S. GUSEYNOVA, F.V. GADGIYEVA

М.А. Рамазанов, А.С. Гусейнова, Ф.В. Гаджиева

**ВЛИЯНИЕ ЭЛЕКТРОТЕРМОПОЛЯРИЗАЦИИ НА МИКРОСТРУКТУРЫ И
ПРОЧНОСТНЫЕ СВОЙСТВА КОМПОЗИЦИЙ НА ОСНОВЕ ПОЛИПРОПИЛЕНА И MnO₂**

В данной работе излагаются результаты исследования влияния поляризации на микроструктуры и прочностные свойства композиций на основе полипропилена и низкомолекулярной добавки MnO₂. Показано, что изменение прочностных свойств образцов композиций ПП+ MnO₂ после электротермополяризации связано с изменением зарядового состояния и образованием упорядоченной физической структуры композиций.

Received: 12.07.07

THE MECHANICAL PROPERTIES OF RAPID-HARDENED MULTI-COMPONENT ALLOYS ON TiNi BASIS NEAR CRYSTALLIZATION TEMPERATURE

M.B. BABANLI

*Azerbaijan Technical University
H. Javid ave., 25, Baku, Azerbaijan*

The systematic investigations of mechanical properties of rapid-hardened tapes of multi-component alloys on TiNi basis of two types: *A* and *B* are carried out. The first lot is *A*, where only Cu in the samples $Ti_{32}Hf_{18}Ni_{50-x}Cu_x$ (where $x=0; 5; 15; 25; 35; 45$ at.%) varies in the composition. The second lot is *B* (Ti, Hf, Zr) (Ni, Cu, Co, Ag, Pd), where the doping elements Hf, Zr, Pd, Ag, Co, Cu vary on NiTi basis. All alloys with amorphous, mixed amorphous and crystalline phases demonstrate the elastic behavior before destruction moment in the “after obtaining” state.

Introduction.

The technique modern development requires more and more new perfect materials. The unit loads, the exploitation temperature conditions and medium aggressiveness increase. The question about the decrease of construction weight, durability increase, reliability and stability of material properties remains very acute. Meanwhile, the resource of property increase of standard alloys practically settles itself. That's why nowadays the materials with heterogeneous and metastable structures are widely used in increasing frequency.

The structure and phase composition of obtained material can strongly differ from equilibrium ones at alloy solidification (both metallic and non-metallic) with cooling rates on the level $10^5 - 10^6$ K/c. The more typical effects are: the formation of new metastable phases (amorphous and crystal), the widening of solubility limits of doping elements, the decrease of granule and inclusion dimensions. In spite of many experimental and theoretical works, there is no total clearness about formation of rapid-hardened material structure up to now. The two questions are very important from practical point of view: how to obtain the material in the amorphous state (to suppress the crystallization) and how to carry out diffusionless crystallization.

The systematic investigation of structural changes of rapid-hardened straps of multi-component alloys on TiNi base in our previous works [1-5] had carried out by the methods of X-ray analysis, translucent microscopy and calorimetry.

The systematic investigations of mechanical properties of rapid-hardened tapes of multi-component alloys on TiNi base at different temperatures and especially the interest results by our opinion are obtained near the temperatures T_g and T_x are carried out in the present work.

The material choice and experiment technique. The choice of chemical composition for multi-component alloys with shape memory effect on TiNi base, which further will be obtained by super rapid hardening from the melt, is based on two principles. Firstly, the chemical composition should be related to amorphization at super rapid hardening from the melt; secondly, the alloy should have the martensate transformations in the massive state (before super rapid hardening from the melt).

The multi-component alloys on TiNi base of two plots: *A* and *B* are chosen for the investigation. First plot is *A*, where only Cu in the composition varies in the samples $Ti_{32}Hf_{18}Ni_{50-x}Cu_x$ (where $x=0; 5; 15; 25; 35; 45$ at%). The

second plot is *B* (Ti, Hf, Zr)(Ni, Cu, Co, Ag, Pd), where the doping elements Hf, Zr, Pd, Ag, Co, Cu vary on TiNi base.

The rapid-hardened tapes (foils) obtained from “master” alloys, the solidification from the melt; by Planar Flow Jasting are investigated in our work. In this method the distance between disk and melt is constant in the quartz crucible (less than 1 mm, in our case the distance is from 0,15 up to 0,2mm). The melt from the crucible proceeds from crack by the width 0,3-0,35mm and thickening 7-10mm, that allows obtaining the more wide tapes, than in our previous works. The cylindrical pieces of alloy (from 0,5 up to 15g) are stirred in quartz tube with the melt and are heated by inductive method. The melt temperature is controlled by pyrometer. The temperature, at which the gutter began, is 50-150K, that is higher than liquidus temperature and depends on the melt viscosity. The melt is put on the disk under argon pressure 0,2MPa. The disk by diameter 200 mm is produced from cuprum alloy Cu(Co – Be). The disk spinning rate is from 5 up to 30 m/c, the gas pressure is 0,2 MPa in the helium atmosphere [1].

The choice of the given alloys, obtained by super rapid hardening from the melt allows obtaining the different structural states after hardening at once (in initial state), and also investigating the evolution of structure and mechanical properties at the heating, the characteristics of martensate transformations after crystallization.

The nominal chemical composition of investigated rapid-hardened tapes of *A* plot ((Ti, Hf) (Ni, Cu) and *B* plot (Ti, Hf, Zr) (Ni, Cu, Co, Ag, Pd), the melt temperature at the output T_q and the width of obtained foils d are given in the tables 1 and 2.

Table 1.
The nominal chemical composition of rapid-hardened foils of *A* plot (T, Hf) (Ni, Cu), the melting point at the output T_q and foil width d .

Alloy	Nominal chemical composition (at%)				T_q (°C)	d (mcm)
	Ti	Hf	Ni	Cu		
A0	32	18	50	-	1380	30
A1	32	18	45	5	1296	30
A2	32	18	35	15	1285	30
A3	32	18	25	25	1300	30
A4	32	18	15	35	1200	30
A5	32	18	5	45	1100	30

The differential scanning calorimeter (DSC) Mettler DSC 30 and Mettler DSC 822e is used for the investigation of thermodynamic properties. These installations allow carrying

out the investigations in temperature interval from -150°C up to 700°C with heating rate 10-100K/c and cooling rate 10-20K/c. The sample mass from 5 up to 10mg, the bays type, in which the samples are situated: aluminum or platinum ones.

Table 2.
The nominal chemical composition of rapid hardened foils of B plot (Ti, Hf, Zr)(Ni, Cu, Co, Ag, Pd), melt temperature at the output T_q and foil width d .

Alloy	Nominal chemical composition (at%)					T_q (°C)	d (mcm)
	Ti	Hf ore Zr	Ni	Cu	others		
B0	50	-	25	25	-	1280	
B3	47	Hf-3	23	24.5	Pd-2 Ag-0.5	1320	30
B5	48	Zr-2	23	23	Pd-2 Ag-2	1280	30
B8	48	Zr-7	18	23	Pd-2 Ag-2	1320	30
B12	48	Zr-7	18	25	Co-2	1280	30
B20	27	Hf-18	50	5	-	1300	30
B21	27	Hf-18	40	15	-	1230	40
B22	27	Zr-18	50	5	-	1250	30
B23	27	Zr-18	40	15	-	1230	40
B24	40	Hf-15	8	37	-	1100	20
B25	40	Hf-15	3	42	-	1100	20

The machine for mechanical tests Test GmbH is used for investigation of mechanical properties of rapid-hardened foils. The given machine is additionally supplied by heating camera, that allows to us carrying out the investigations in the wide temperature interval from 20 up to 700°C with regulation of temperature and heating rate.

The investigated samples have the following dimensions: the length is ~40mm, width is 6-8, 4mm, the work part is 10mm.

The experiments are carried out on the following schemes:

1. The main mechanical properties (strength limit σ_f , Yung module E , maximum deformation before destruction ε_{max}) and deformation behavior of rapid-hardened tapes in the state “after obtaining” at room temperature (without heating). The mode “hard” machine is used. The program assigns the rate to the deformation ε' , which varies in the range $8.3 \cdot 10^{-4} - 8.3 \cdot 10^{-4} \text{ c}^{-1}$.

2. The investigations of the main mechanical properties and deformation behavior of rapid-hardened tapes in the state “after obtaining” at high temperatures (higher than room one) are carried out on the same scheme, described in the item 1, the only difference consists in the fact, that investigation temperature is varied in the interval from 20 up to 700°C (but each following experiment is carried out at constant given temperature).

3. The investigations of deformation behavior of rapid-hardened foils in the state “after obtaining” at the heating, i.e. investigation of superplasticity effect on the scheme “constant dynamic loading”: the “hard” machine mode is used. The sample is loaded up to the definite value (200-500MPa), further, the machine supports the given loading value; moreover, deformation rate is constant. After it, the sample is heated with the rate 100K/min and the deformation graphical

charts “loading – deformation” and “deformation – temperature” are written. The data about deformation behavior of amorphous and amorphous-crystal samples in temperature interval T_g-T_x can be obtained with the help of this mode, which the mode of “hard” machine.

The results and their discussion. The curves “voltage – deformation” for the investigated alloys are presented on the fig.1. The main mechanical properties for multi-component foils on TiNi base in the initial state (“after obtaining”) are given on the table 3. All samples, which are in the initially amorphous state, demonstrate $\sigma_f=740 \div 1110$ MPa (for A plot), $810 \div 1410$ MPa (for B plot), $E=15 \div 39$ MPa (for both plots); $\varepsilon_{max}=2,4 \div 7,3\%$ (for both plots).

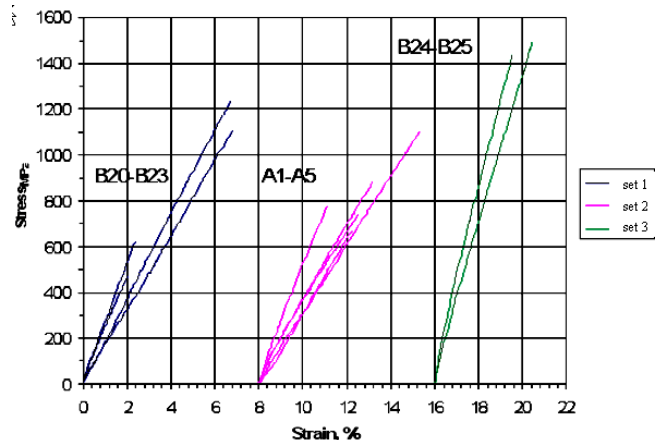


Fig.1. The curve “voltage – deformation” for the multi-component foils on TiNi base in the initial state (“after obtaining”) at $T=20^\circ\text{C}$.

The samples with mixed (amorphous-crystalline) structure show the values: $\sigma_f=480 \div 1080$ MPa; $\varepsilon_{max}=2 \div 6,8\%$ and $E=16 \div 28$ MPa (for both plots). All alloys of plots A and B with totally amorphous structure demonstrate the higher strength limit, than alloys with mixed structures.

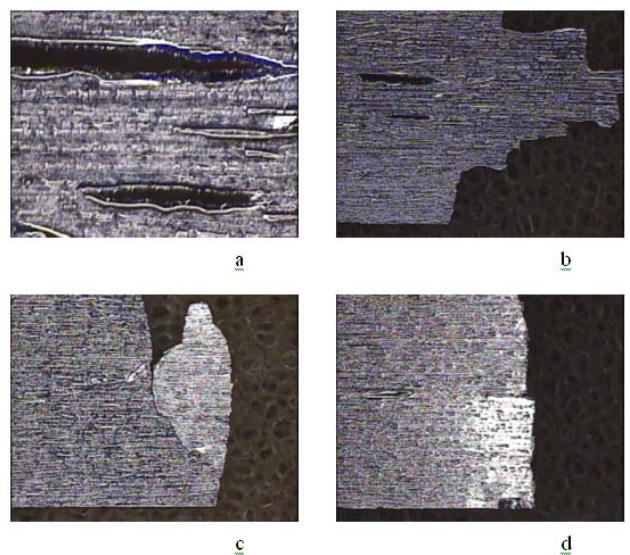


Fig.2. The surface of rapid-hardened foils after mechanical tests at $T=20^\circ\text{C}$, obtained with the help of light microscopy; a is A2 alloy after mechanical tests at $T=20^\circ\text{C}$ (pore development); b are “icles” of A2 alloy; c are cracks of B5 alloy; d are perpendicular directions to the axis of applied loading of B12 alloy.

Table 3.

The main mechanical properties for multi-component foils on TiNi basis in the initial state (“after obtaining”) at $T=20^{\circ}\text{C}$:
 σ_f is breaking point; E is Yung module; ε_{\max} is deformation before destruction.

Alloy, nom. ch. comp., at.%	Relations A:B	Structure “after obtaining”	σ_f , MPa	E , GPa	ε_{\max} , %
A1-Ti32Hf18Ni45Cu5	50:50	Amorph.+Cr.	680	16,6	4,2
A2-Ti32Hf18Ni35Cu15	50:50	Amorph.	740	15,4	4,6
A3-Ti32Hf18Ni25Cu25	50:50	Amorph.	1110	15,0	7,3
A4-Ti32Hf18Ni15Cu35	50:50	Amorph.	890	16,4	5,2
A5-Ti32Hf18Ni5Cu45	50:50	Amorph.	790	22,3	3,1
B20-Ti27Hf18Ni50Cu5	45:55	Amorph.+Cr.	480	22,1	2,0
B21-Ti27Hf18Ni40Cu15	45:55	Amorph.+Cr.	1120	16,2	6,8
B22-Ti27Zr18Ni50Cu5	45:55	Amorph.	630	25,6	2,4
B23-Ti27Zr18Ni40Cu15	45:55	Amorph.	1240	18,6	6,8
B24-Ti40Hf15Ni8Cu37	55:45	Amorph.	1460	38,7	3,6
B25-Ti40Hf15Ni3Cu42	55:45	Amorph.	1510	32,5	4,5
B3-Ti47Hf3Ni23Pd2Cu24,5Ag0,5	50:50	Amorph.+Cr.	1200	19,6	6,1
B5-Ti48Zr2Ni23Pd2Cu23Ag2	50:50	Amorph.+Cr.	810	19,0	4,2
B8-Ti48Zr7Ni18Pd2Cu23Ag2	55:45	Amorph.	1410	21,0	6,9
B12-Ti48Zr7Ni18Cu25Co2	55:45	Amorph.+Cr.	980	18,9	5,1

The inclination of alloy chemical composition from relation $A:B=50:50$ leads to the increase of alloy durability level. This result well agrees with liquidus point: the highest liquidus temperature is fixed for the relation 50:50 and decreases at the inclination from this relation. The liquidus temperature influences on temperature interval of co-existence of liquid and crystalline phases, atom diffusion activity, containing in the composition, cooling rate, that exchanges the alloy structure in the initial state (“after obtaining”) and their mechanical properties. The foil surface in the process of mechanical influences is investigated by optical microscopy and scanning electron microscopy in order to establish the possible deformation mechanisms in the foils with different initial structures. The following surface peculiarities are fixed: 1) The pore development at loading of A2 alloys, if they are present before deformation (fig.2, a); 2) The stairs, formed by the shift with orientation approximately 45° in the relation to axis of applied loading, if the destruction surface is practically perpendicular to loadings (fig.2, A2 alloy); 3) The tracks, formed by the shift with orientation approximately 45° in the relation to loading axis (B5 alloy), if the destruction surface is practically perpendicular to loading axis for B5 and B12 alloys (fig.2).

The application of term “shift” in the materials with amorphous structure doesn’t mean that the shift of one atom square in the relation to another one takes place, this is impossible in the materials with amorphous structure. For the given materials the term “shift” means the shift of one material part relatively another one (in mane cases at angle of 45° to axis of applied voltage).

The images of destruction surface on the fig.3, obtained with the help of scanning electron microscopy, show the presence of “branched” pattern in B12 alloy samples at room temperature after expansion. It is well known, that the presence of this pattern is character peculiarity for the material destruction surface with amorphous structure: it forms in the result of the fact that whole information accumulated in shift thin bands [1].

The micropores appear in these tapes, they expand and fill the spaces along shift s and further the isolation of atomic distances takes place. Moreover, the “branched” pattern is observed on the surface. These data show that the destruction has viscous character at the loading; the behavior of shift tapes is similar to the behavior of thin viscous full sphere between two parallel plates, that isn’t practically deformed with formation of “branched” pattern. This is specific feature for destruction of metals and alloys with amorphous structure.

The destruction mechanism, which shows the formation of so-called “liquid drops”, is supposed by authors of work [6]. The authors of work [6] suppose the alloy decomposition mechanism with amorphous structure, the essence of which consists in the fact that the material in the local regions (shift tapes) is heated in the result of transformation adiabatic process by accumulated deformation energy into warmth. This process leads to alloy local crystallization with amorphous structure (formations of “liquid drops”) and to the destruction in the result it. The microstructure surface analysis in destruction region doesn’t reveal the presence of “liquid drops”, i.e. the supposed destruction mechanism isn’t proved on our alloys neither with the help of optical electron microscope, nor with the help of scanning electron one. On the other hand, the series of experiments and calculations is carried out for the possibility designation of this destruction mechanism.

The information about deformation rate on the basis of mechanical properties for model alloys B23 and B25 can be critic one for the possible decomposition mechanism. Both alloys have the initial amorphous structure. The deformation rate for these alloys in the wide interval 0,5-500 nm/min doesn’t practically influence on strength limit and Yung module. The elastic behavior of all alloys up to decomposition moment is the one from the reasons of the given result, and another one consists in the fact that foils have the big external surface and small width, that’s why the warmth, which possible forms at the deformation, is transformed very quickly into environment.

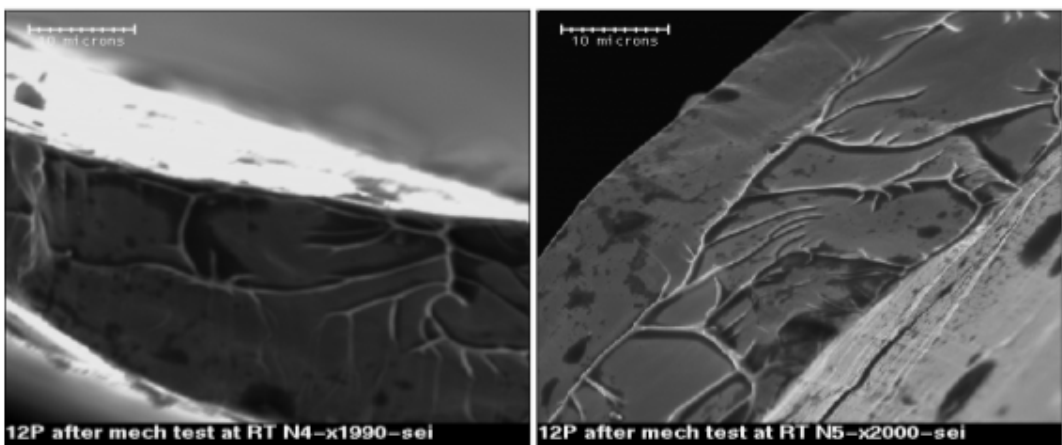


Fig.3. The destruction surfaces (scanning microscopy) of B12 alloy after mechanical tests at $T=20^{\circ}\text{C}$.

It is necessary to note the some difficulties, which appear at the definition of mechanical properties of rapid-hardened foils. These problems are connected with the presence of technological defects in the material, such as: the pores and irregularity to foil width. Moreover, this irregularity is fixed in two directions of cut: lengthwise and transversally foil length and has the form “wave” surface. Before testing the samples are investigated with the help of optical microscope, and also the measurement statistics is constructed in order to decrease the influence of these defects on the measurement results.

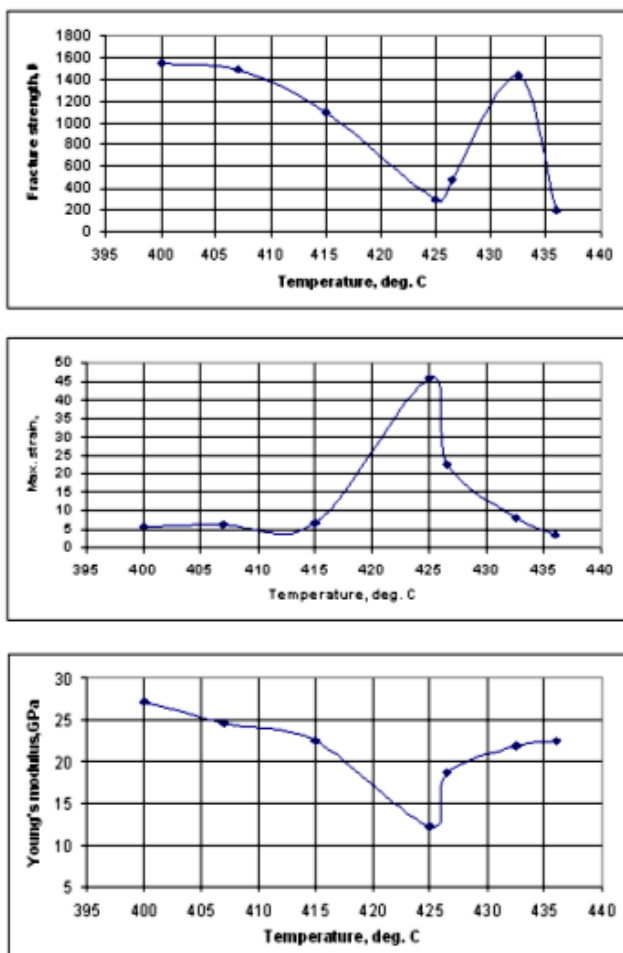


Fig.4. The dependence of the main mechanical properties (σ_f , E and ε_{max}) on the temperature of B24 alloy.

The alloys with different structural states “after obtaining” are investigated for the study of deformation behavior at temperatures, which are higher, than room ones. The dependencies of main mechanical dependencies (durability limit σ_f , Yung module E , maximum deformation up to destruction ε_{max}) on the temperature for B24 alloy, strain rate $\varepsilon=5\text{mm/min}$ are presented on the fig.4.

The alloy deformation with amorphous structure can be conditionally divided into two types: homogeneous and nonhomogeneous [7-13]. The deformation type changes from nonhomogeneous up to homogeneous one at some critical temperature T_c with temperature increase. The critical temperature T_c depends on alloy strain rate [8,9]. The critical temperature for B24 alloy is $\sim 415^{\circ}\text{C}$, the strength strongly decreases at temperature increase higher than T_c , increasing with temperature increase.

The maximum deformation before deconstruction increases. The peak appears at the deformation of homogeneous alloys of amorphous types with temperature increase, and further, decreases at crystallization process leaking. The increase of maximum deformation up to destruction well agrees with temperature dependence of alloy viscosity [8, 14-18].

Yung module decreases with at temperature increase, forming the minimum and after it increases at crystallization process leaking. This result shows, that force of interatomic interaction becomes less in T_g region. This result hasn't the clear physical explanation yet [7]. The alloy durability level decreases at more high temperatures, which are higher than T_g at formation of crystalline granules in the amorphous matrix. The deformation scheme: “constant dynamic loading” is worked for the study of deformation behavior and high durability effect in rapid-hardened foils. The high plasticity is the effect, which is character for amorphous structure at glass-transition temperatures T_g . The dependencies “deformation – voltage” and “deformation – temperature”, obtained in the experiment result on the scheme “constant dynamic loading” for A1, A2, 3P, B12, B23 alloys are presented on the fig.5. The samples demonstrate the different maximum deformation before destruction ε_{max} , for example, for A1 alloy is 19%, for A2 alloy is 62%. These results show that alloys with mixed structure (amorphous-crystalline) also have the high plasticity effect and maximum deformation depends on volume part of crystalline phase in amorphous matrix.

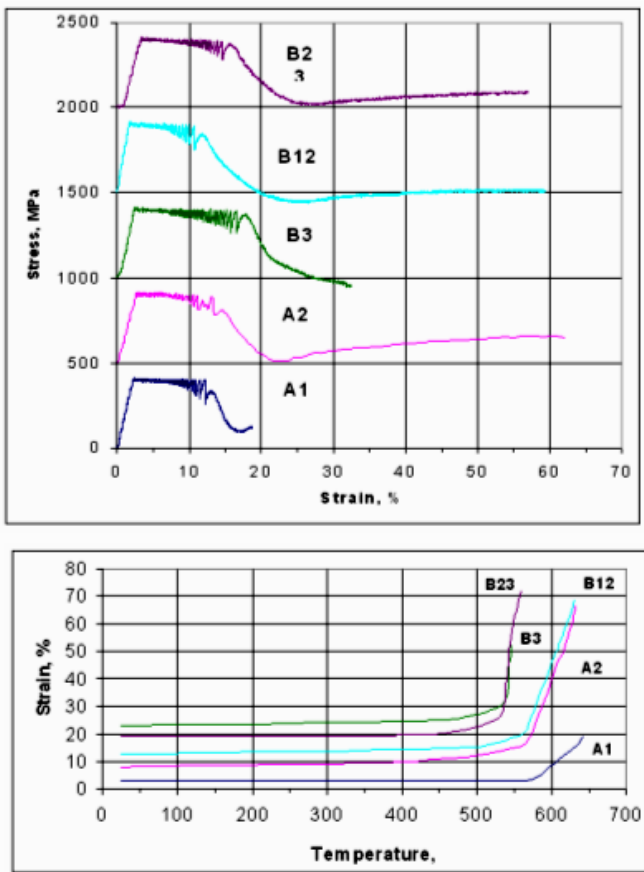


Fig.5. The dependencies “deformation - voltage” and “deformation – temperature” for alloys A_1 , A_2 , B_3 , B_{12} and B_{23} , obtained in the result of experiments on the scheme “constant dynamic loading”.

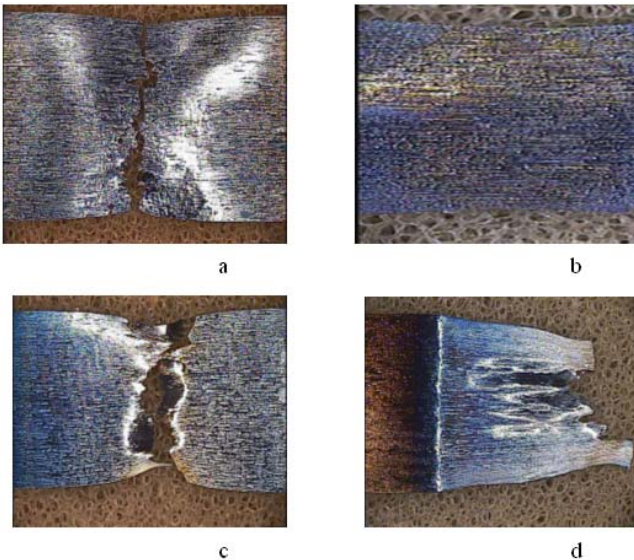


Fig.6. The foil surfaces (optical microscope) after experiment on the scheme “constant dynamic loading” 1 a is A_1 alloy; b is A_2 alloy; c is B_3 alloy; d is B_{12} alloy.

The surface images of rapid-hardened foils of A_1 , A_2 , $3P$, B_{12} alloys after investigation on the scheme “constant dynamic loading” are presented on the fig.6. These images are obtained with the help of optical microscope. All

samples have the constrictions in the middle work part that is the result of material viscous deformation.

The transition of deformation nonhomogeneous type up to homogeneous one is accompanied by the fact that the maximum, so-called “tooth” (fig.7) appears on curves “voltage – deformation”. The “tooth” height $\Delta\sigma$ is the difference between maximum voltage σ_p and concealed voltage σ_s , which decreases at temperature increase and strain rate decrease [7]. It is impossible to explain the “tooth” phenomenon with the help of dislocation theory (as dislocations are absent in amorphous structure) [7], and it can be result of viscous-elastic behavior of amorphous alloys, where the role of viscous concealed voltage becomes essential at more high temperatures and less strain rates in the relation to elastic behavior (at room temperature).

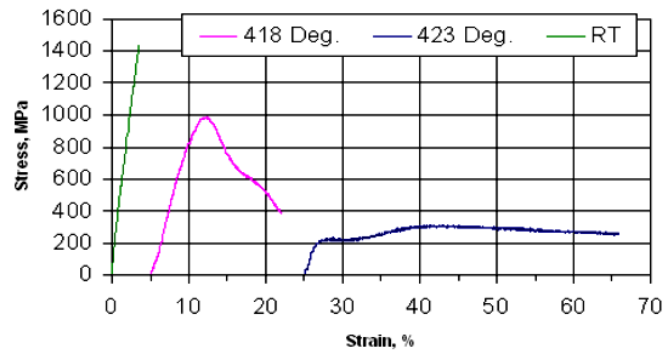


Fig.7. The deformation behavior of B_{24} alloy in the dependence on the temperature (“voltage – deformation”).

The influence of strain rate on maximum deformation up to B_{23} alloy destruction is presented on the fig.5. The maximum deformation before destruction ε_{max} increases, forming the peak at critical strain rate ε_c^I and after it decreases at increase of strain rate.

The influence of strain rate on the value of concealed voltage σ_{flow} and viscosity η for B_{23} alloy are presented on the fig.8. The material viscosity is calculated with the help of the formula (1) [8]:

$$\eta = \sigma_{flow} / 3\varepsilon'. \quad (1)$$

The viscosity stays practically constant value for strain rate, but doesn't exceed the critical ε_c^I and decreases at deformation rates, which exceeds the critical one. The value of critical deformation rate ε_c^I is responsible for cut point of dependencies $\eta=\Phi(\varepsilon')$ and divides the deformation mode into low- and high-speed ones.

The concealed voltage σ_{flow} linearly increases with increase of deformation rate and forms “plateau” at deformation rate, which exceeds the critical one. The critical deformation rate at constant temperature is the one of important deformation parameters, as it shows the maximum deformation before destruction, which is possible to achieve. The amorphous alloy demonstrates Newton type of concealed voltage at low-speed deformation mode and non-Newton one at high-speed deformation mode.

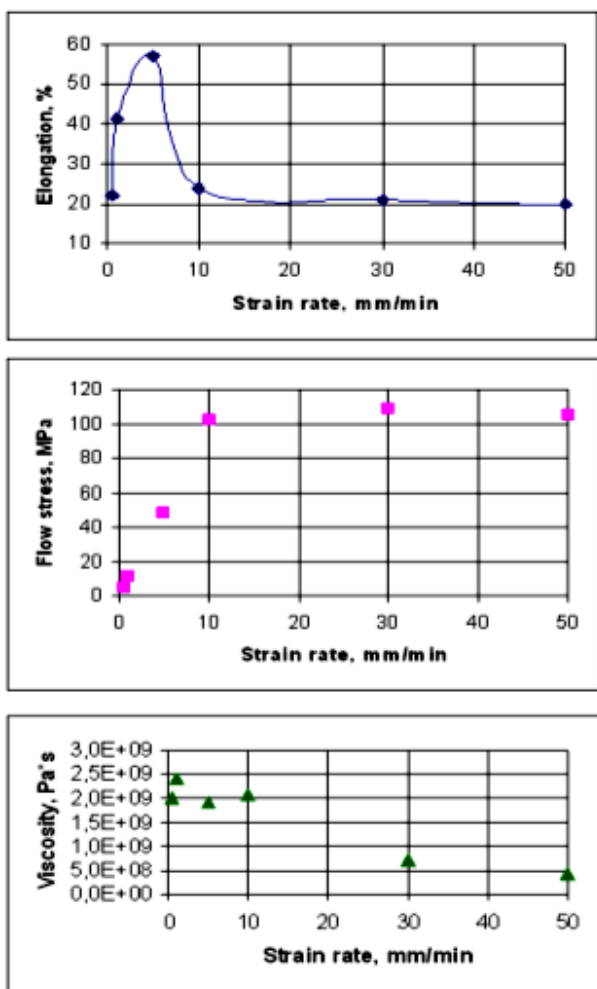


Fig.8. The dependencies of maximum deformation, voltage and viscosity of B23 alloy before destruction on the strain rate.

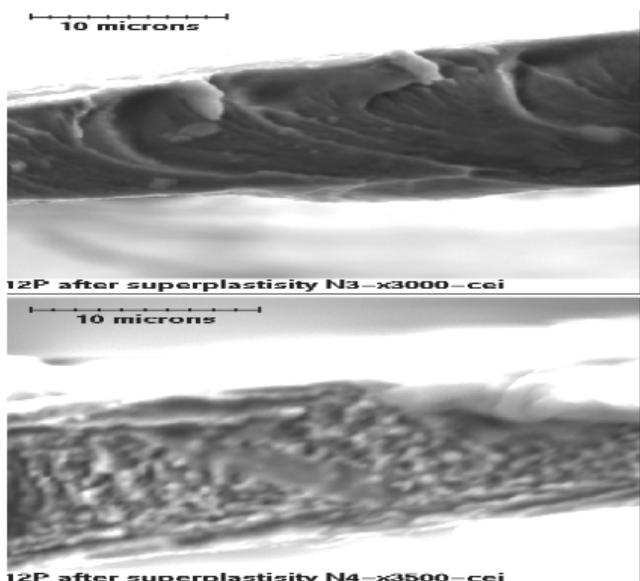


Fig.9. The destruction surface of B12 alloy after the test on the scheme "constant dynamic loading".

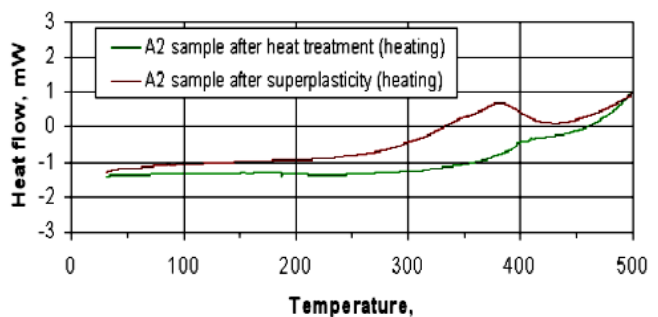


Fig.10. The calorimetric curves of rapid-hardened foils of A2 alloy after the superplasticity effect and thermal working at 630°C during 10 minutes in "free state" (without loading).

The destruction surface image of B12 alloy sample after high plasticity effect is presented on the fig.9. As it is seen from the fig.9., the microstructure of destruction surface isn't homogeneous one: the regions with intergranular destruction type and regions with "sudino-like" type, which is character for destruction of amorphous phase, are presented. The some volume part of material stays amorphous after high plasticity effect. The calorimetric curves for A2 and B3 alloys are presented on the fig.10 and 11, correspondingly. The calorimetric curves for foils of A2, which have the different pre-histories after high plasticity and thermal working in "free" state (without loading), at similar thermal conditions 630 °C during 10 minutes, are shown on the fig.10. The following result is obtained: the some alloy part stays amorphous after high plasticity effect after thermal working in "free" state. The analogous result is obtained for B3 alloy.

Conclusion. Thus, A:B relation inclinations from 50:50 up to 55:45 and 45:55 in alloy chemical composition in many cases lead to appearance of foil strength level in the state "after obtaining". This result well agrees with liquidus temperature variation, which is fixed exactly for relation "A:B" 50:50 and decreases at the inclination from this relation. It is established, that doping element variation: the introduction of Zr instead of Hf, changes the structure in the state "after obtaining" from mixed amorphous-crystalline phases to totally amorphous one. As a result, the alloys of TiZrNiCu system demonstrate the highest durability level, than alloys of TiHfNiCu system.

All alloys with amorphous and mixed crystalline phases in the state "after obtaining" demonstrate the elastic behavior up to the destruction moment. It is shown, that both normal and sufficient voltages influence on the destruction of rapid-hardened foils (the destructions have viscous nature with formation of "sudino-like" pattern, which is typical for materials with amorphous structure).

The strain rate in wide interval 0,5-500 mm/min doesn't influence on strength limit and Yung module for the alloys of amorphous and mixed amorphous-crystalline structures in the state "after obtaining".

The rapid-hardened foils on TiNi basis with amorphous and mixed (amorphous-crystalline) structures demonstrate high plasticity effect near glass-transition temperatures T_g .

- [1] M.B. Babanli. Bistrozakalenniye splavi. Baku: «ELM», 2004, 441s. (in Russian).
- [2] M.B. Babanli. Zavisimost vozniknoveniya amorfno-go sostoyaniya ot koncentracii medi i skorosti

zakalki iz rasplava v splava TiNiCu. Sb. statey Fiziko-xim. analiz i neorgan. materialovedeniye, Baku, 1997, s.184-187. (in Russian).

- [3] M.B. Babanlı, V. Kolomicev, A. Sezonenko. Fazoviye i strukturniye sostoyaniya voznykayushie v splavakh TiNiCu. Sb. stately Fiziko-khim. analiz i neorqan. materialovedeniye, Baku, 2002, s.240-246. (in Russian).
- [4] V. Kolomytsev, M. Babanly, R. Musienko, A. Sezonenko, P. Ochin, A. Dezellus, P. Plaindoux, R. Portier, P. Vermaut. The transformation kinetics of the multikomponent TINI based melt spun ribbons from the amorphous to nanocrystalline state .Metallofizika I noveysie texnoloqii Kiev, 2001, v..23, p. 124 – 137.
- [5] V. Kolomytsev, M. Babanly, R. Musienko, A. Sezonenko. Structure and functional properties of some multicomponent TiNi- dased Shape Memory melt-spun ribbons. Sb. stately «Fundamentalniye i prikladniye problemi fiziki» g. Ternopol (Ukraina), 2000, p.159-160.
- [6] L.Q. Xing, C. Bertrand.,J.P. Dallas, M. Cornet. Nanocrystal evolution in bulk amorphous Zr₅₇Cu₂₀Al₁₀Ni₈Ti₅ alloys and ist mechanical properties. Materials Science and Engineering, 1998, A241, p.216 - 225 .
- [7] R. Bush. JOM, 2000, 52(7), p.39 – 42.
- [8] H. Kato, Y. Kawamura, A. Inoue, H.S. Chen. Appl. Phys. Lett., 1998, v.73, p.3665-3667.
- [9] Y. Kawamura, T. Shibata, A. Inone, T. Masumoto. Appl. Phys. Lett., 1997, v.71 (6), p.779 – 781.
- [10] M.B. Babanlı, V.A. Lobodyuk. Osobennosti perekhoda iz amorfnoqo v kristallicheskoye sostoyaniye v splavakh TiNiCu. Sbornik nauchnikh trudov «Fiziko-khimicheskiy analiz i neorqanicheskoye materialovedeniye». Baku, 1996. s.109-112. (in Russian)
- [11] M.B. Babanlı. Texnoloqiya polucheniya mnoqokomponentnih splavov (Ti,Hf)₅₀(Ni,Cu)₅₀ i (TiHf,Zr)₅₀[(Ni,Co)(Cu,Ag)]₅₀ /Sb. stately Fiziko-khim. analiz i neorqan. materialovedenie, Baku, 1999, s. 218-223
- [12] M.B. Babanly, V.A. Lobodyuk, N.M. Matveeva. Proc. Conf. “Martensite-91”, Kiev, 1992, pp. 338-341.
- [13] M.B. Babanly, V.A. Lobodyuk, N.M. Matveeva. Izvestiya Academy of Sciences USSR, Metals 5 (1993) 171-177.
- [14] M.B. Babanli. Splavi s effektom pamjati formi. Baku:«ELM»,2006, 280s.
- [15] M.B. Babanli, V. Kolomitsev, A. Sezonenko. Oso-bennosti vliyaniya termomekhanicheskoy obrabotki na kharakteristiki martensitnoqo prevrasheniya v splavakh TiNiCu. Sb. stately Fiziko-khim. analiz i neorqan. materialovedenie, Baku, 2002, s.235-239
- [16] M.B. Babanli, V. Kolomitsev, A. Sezonenko. Fazovie i strukturnie sostoyaniya voznykayushie v splavakh TiNiCu /Sb. stately Fiziko-khim. analiz i neorqan. materialovedenie, Baku, 2002, s.240-246.
- [17] M.B. Babanli, Z.E. Salimov. Strukturnie izmeneniya v splavakh na osnove TiNi. Sb. nauch. tr. konfer. AzTU, Baku, 2001, s.217-219.
- [18] M.B. Babanli. Nekotorie voprosi polucheniya amorfnikh i nanokristallicheskikh materialov. Sb. nauch. tr. konfer. AzTU, Baku, 2006, s.153-156.
- [19] M.B. Babanli. Martensitnie prevrasheniya v splavakh TiNiZr //Uchenie zapiski AzTU, №4, 2004, s. 31-34.

M.B. Babanlı

İFRAT SÜRƏTLƏ TABLANDIRILMIŞ TiNi ƏSASLI ÇOXKOMPONENTLİ ƏRİNTİLƏRİNDE KRİSTALLAŞMA TEMPERATURU YAXINLIĞINDA MEXANİKİ XASSƏLƏR

İfrat sürətlə tablandırılmış TiNi əsası çoxkomponentli ərintilərin mexaniki xassələri iki seriyada sistemli şəkildə tədqiq edilmişdir: A və B. Birinci, A seriyada tərkibdə yalnız Cu Ti₃₂Hf₁₈Ni_{50-x}Cu_x (x=0; 5; 15; 25; 35; 45 at. %)əvəz edilmişdir. İkinci V (Ti, Hf, Zr)(Ni, Cu, Co, Ag, Pd) seriyada isə NiTi sistemi tərkibində Hf, Zr, Pd, Ag, Co, Cu kimi leqirleyici elementlər dəyişdirilmişdir. Məlum olmuşdur ki, öyrənilmiş ərintilərdə «ilkin vəziyyətdə» amorf və amorf – kristallik quruluşa malik təbəqələr dağılmaya qədər elastiliklik xassələri göstərir.

М.Б. Бабанлы

МЕХАНИЧЕСКИЕ СВОЙСТВА БЫСТРОЗАКАЛЕННЫХ МНОГОКОМПОНЕНТНЫХ СПЛАВОВ НА ОСНОВЕ Ti-Ni ВБЛИЗИ ТЕМПЕРАТУРЫ КРИСТАЛЛИЗАЦИИ

Проведены систематические исследования механических свойств быстrozакаленных лент многокомпонентных сплавов на основе TiNi двух серий: А и В. Первая серия А, где в составе варьируется только Cu в образцах Ti₃₂Hf₁₈Ni_{50-x}Cu_x (де x=0; 5; 15; 25; 35; 45 ат. %). Вторая серия В (Ti, Hf, Zr)(Ni, Cu, Co, Ag, Pd), где варьировались легирующие элементы Hf, Zr, Pd, Ag, Co, Cu на базе NiTi. Все сплавы с аморфной и со смешанной аморфной и кристаллической фазами в состоянии «после получения» демонстрируют упругое поведение до момента разрушения.

Received: 12.09.07

GENERALIZED TODA MODELS

M.A. MUKHTAROV

*Institute of Mathematics and Mechanics
370602, Baku, F. Agaev str. 9, Azerbaijan*

The group theoretical approach has been developed for one-dimensional generalized non-abelian conformal affine Toda models.

1. The study of classical and quantum non-linear integrable models is of great interest in Mathematics and especially in High Energy Physics, where such models have been used as laboratories to develop methods to explore the non-linear perturbative aspects of gauge theories, gravity and string theory. In particular, they could help in understanding some stable classical solutions, like monopoles, which must have an important role in the quantum theory, and which cannot be understood by the existing methods.

Within the integrable models in 1+1 dimensions, the investigation of the different Toda Field Theories has recently received a lot of attention. According to their underlying algebraic structure, they can be divided into three categories; each one exhibiting nice characteristic properties. First, associated to the finite simple Lie algebras, there are the Conformal Toda models, which are conformally invariant 1+1 field theories. Even more, they permit the construction of extensions of the Virasoro algebra including higher spin generators, namely W-algebras. The second class of theories

At the same time the problem of constructing of the solutions of self-dual Yang-Mills (SDYM) model and its dimensional reductions, the one dimensional WZNW model in our case, in the explicit form for arbitrary semisimple Lie algebra, rank of which is greater than two, remains important for the present time. The interest arises from the fact that almost all integrable models in one, two and (1+2)-dimensions are symmetry reductions of SDYM or they can be obtained from it by imposing the constraints on Yang-Mills potentials [10-27].

Two effective methods of generating of the exact solutions, the Riemann Hilbert Problem formalism [20] and the discrete symmetry transformation method [22], have been applied to Toda like systems. This work is devoted to construct a group theoretical background of earlier considerations.

2. The two-loop WZNW model was introduced in [6] as the generalization of the ordinary WZNW model to the affine case. Its equations of motion are given by

$$\partial_+(\partial_-\hat{g}\hat{g}^{-1})=0 ; \quad \partial_-(\partial_+\hat{g}\hat{g}^{-1})=0 , \quad (2.1)$$

where ∂_{\pm} are derivatives with respect to the light-cone variables $x_{\pm} = x \pm t$, and \hat{g} is an element of the group G formed by exponentiating an untwisted affine (real) Kac-Moody (KM) algebra \hat{G} . Its generators T_a^m , D and C satisfy the commutation relations

are the Affine Toda models, based on loop algebras, which can be regarded as a perturbed Conformal Toda model where the conformal symmetry is broken by the perturbation while the integrability is preserved [1]. One of their main properties is that they possess soliton solutions. These two classes of models are called abelian or non-abelian referring to whether their fields live on an abelian or non-abelian group [2, 3, 4, 5]. Finally, the conformal symmetry can be restored in the abelian Affine Toda models just by adding two extra fields which do not modify the dynamics of the original model; one of these fields is a connection whose only role is to implement the conformal invariance. These are the so called Conformal Affine Toda models [6, 7], and they are based on a full Kac-Moody algebra; moreover, they are integrable [8], and have soliton solutions [9]. In fact, many properties of the Affine Toda models can be more easily understood by considering them as the Conformal Affine Toda models with the conformal symmetry spontaneously broken.

$$[T_a^m, T_b^n] = f_{ab}^c T_c^{m+n} + m C g_{ab} \delta_{m+n,0} \quad (2.2)$$

$$[D, T_a^m] = m T_a^m, \quad [C, D] = [C, T_a^m] = 0 \quad (2.3)$$

where f_{ab}^c are the structure constants of a finite (real) semisimple Lie algebra G , n and m are integers, and g_{ab} is the Killing form of G , i.e., $g_{ab} = \text{Tr}(T_a T_b)$, T_a being the generators of G . The non-degenerate bilinear form of \hat{G} is defined as

$$\text{Tr}(T_a^m T_b^n) = \delta_{m+n,0} \text{Tr}(T_a T_b), \quad \text{Tr}(C, D) = 1$$

$$\text{Tr}(C, T_a^m) = \text{Tr}(D, T_a^m) = 0 \quad (2.4)$$

and we will use the same notation, Tr , for both the Killing form of G and the bilinear form of \hat{G} .

The two-loop WZNW model is invariant under left and right translations

$$\hat{g}(x_+, x_-) \rightarrow \hat{g}_L(x_-) \hat{g}(x_+, x_-), \quad \hat{g}(x_+, x_-) \rightarrow \hat{g}(x_+, x_-) \hat{g}_R(x_+) \quad (2.5)$$

The corresponding Noether currents are the components of $\partial_- \hat{g} \hat{g}^{-1}$ and $\hat{g}^{-1} \partial_+ \hat{g}$, and they generate two commuting copies of the so called two-loop Kac-Moody algebra, defined by the relations

$$[J_a^m(x), J_b^n(y)] = f_{ab}^c J_c^{m+n}(x) \partial(x-y) + g_{ab} \delta_{m,-n} (k \partial_x \partial(x-y) + m J^C(x) \partial(x-y)) \quad (2.6)$$

$$[J^D(x), J_a^m(y)] = m J_a^m(y) \partial(x-y) \quad (2.7)$$

$$[J^C(x), J^D(y)] = k \partial_x \partial(x-y) \quad (2.8)$$

$$[J^C(x), J_a^m(y)] = 0 \quad (2.9)$$

The left and right currents satisfying the above relations are related to the group element \hat{g} in eq.(2.1) by

$$F_R(x_+) = k \hat{g}^{-1} \partial_+ \hat{g} = \sum_{ab} \sum_{n=-\infty}^{\infty} g^{ab} J_{R,a}^{-n}(x_+) T_b^n + J_R^D(x_+) C + J_D^C(x_+) D \quad (2.10)$$

$$F_L(x_-) = -k \partial_- \hat{g} \hat{g}^{-1} = \sum_{ab} \sum_{n=-\infty}^{\infty} g^{ab} J_{L,a}^{-n}(x_-) T_b^n + J_L^D(x_-) C + J_D^C(x_-) D \quad (2.11)$$

where g^{ab} is the inverse of the Killing form g_{ab} defined above. The different meaning of the two central extensions in eqs.(2.6)-(2.9) algebra is clarified by expressing the algebra as

$$[Tr(UF(x)), Tr(VF(y))] = Tr([U, V] F(x)) \partial(x-y) + k Tr(UV) \partial_x \partial(x-y) \quad (2.12)$$

where U, V are two elements of the Kac-Moody algebra \hat{G} , F is either F_R or F_L , and Tr is the invariant bilinear form of \hat{G} .

Consider now a gradation of the Kac-Moody algebra \hat{G}

$$\hat{G} = \bigoplus_s \hat{G}_s \quad (2.13)$$

with

$$[\hat{G}_s, \hat{G}_r] \subset \hat{G}_{s+r} \quad (2.14)$$

The reduction presented in this section does not require that this gradation is integer; it just needs that the grades s take zero, positive and negative values, i.e.,

$$\hat{G} = \hat{G}_+ \oplus \hat{G}_0 \oplus \hat{G}_- \quad (2.15)$$

with

$$\hat{G}_+ = \bigoplus_{s>0} \hat{G}_s, \quad \hat{G}_- = \bigoplus_{s<0} \hat{G}_s \quad (2.16)$$

We now consider those group elements that can be written in a “Gauss decomposition” form

$$\hat{g} = NBM \in G \quad (2.17)$$

where N, B and M are group elements formed by exponentiating elements of \hat{G}_+ , \hat{G}_0 and \hat{G}_- respectively.

Using eq.(2.17), we can write the equations of motion (2.1) as

$$\partial_- K_R = [K_R, \partial_- MM^{-1}] \quad (2.18)$$

$$\partial_+ K_L = [K_L, N^{-1} \partial_+ N] \quad (2.19)$$

where we have introduced

$$K_L = N^{-1} \partial_- \hat{g} \hat{g}^{-1} N = N^{-1} \partial_- N + \partial_- BB^{-1} + B \partial_- MM^{-1} B^{-1} \quad (2.20)$$

$$K_R = M \hat{g}^{-1} \partial_+ \hat{g} M^{-1} = B^{-1} N^{-1} \partial_+ NB + B^{-1} \partial_+ B + \partial_+ MM^{-1} \quad (2.21)$$

Although the quantities $K_{L/R}$ are not chiral, they have a simpler structure than the currents and will be very useful in what follows. We will reduce the two-loop WZNW model by imposing constraints not directly on the currents but on $K_{L/R}$. We impose the constraints

$$B^{-1} (N^{-1} \partial_+ N) B = \Lambda_l \quad (2.22)$$

$$B (\partial_- M) M^{-1} B^{-1} = \Lambda_{-l} \quad (2.23)$$

where $\Lambda_{\pm l}$ are constant elements of $\hat{G}_{\pm l}$. These constraints reduce the two-loop WZNW model to a theory containing only the fields corresponding to the components of B and to

the components of N and M associated to the generators whose grade is $< l$ and $> l$ respectively.

To obtain the equations of motion for such model one notices that the constraints (2.22) and (2.23) imply that

$$N^{-1} \partial_+ N \in \hat{G}_l \quad (2.24)$$

$$(\partial_- M) M^{-1} \in \hat{G}_{-l} \quad (2.25)$$

Therefore the only terms of zero grade on the right hand side of (2.19) are coming from $[\Lambda_{-l}, N^{-1} \partial_+ N] = [\Lambda_{-l}, B \Lambda_l B^{-1}]$. So we get

$$\partial_+(\partial_- BB^{-1}) = [A_{-l}, B A_l B^{-1}] \quad (2.26)$$

which can also be written as

$$\partial_-(B^{-1} \partial_+ B) = -[A_l, B^{-1} A_{-l} B] \quad (2.27)$$

These are the equations of motion of what we call the generalized non-abelian conformal affine Toda models.

3. The one dimensional reduction of self duality equations obtained in [20] are the equations for the element f , taking values in the semisimple algebra,

$$\begin{aligned} & \frac{\partial^2 f}{\partial r^2} + 2 \frac{\partial f}{\partial r} - [H, [H, f]] - 2[X^-, [X^+, f]] - 2[X^+, [X^-, f]] + \\ & + 2[[\frac{\partial}{\partial r} - H, f], [X^+, f]] = 0 \end{aligned} \quad (3.1)$$

Here H, X^\pm are generators of $A_1(SL(2, C))$ algebra

$$[X_M^+, X^-] = H, [H, X^\pm] = \pm 2X^\pm$$

embedded to gauge algebra in the half-integer way.

Let's rewrite (3.1) in the equivalent form:

$$\begin{aligned} & [\frac{1}{2}(\frac{\partial}{\partial r} + H) - [X^+, f], -\frac{1}{2}[\frac{\partial}{\partial r} - H, f] + X^-] - \\ & - \frac{1}{2}[\frac{\partial}{\partial r} - H, f] + X^- = 0 \end{aligned}$$

This equation after changing the variable $t = \ln r$ has the following form

$$\begin{aligned} & [\frac{\partial}{\partial t} + \frac{1}{2}H - [X^+, f], -\frac{\partial f}{\partial t} + \frac{1}{2}[H, f] + X^-] - \\ & - \frac{\partial f}{\partial t} + \frac{1}{2}[H, f] + X^- = 0 \end{aligned} \quad (3.2)$$

Introducing the notation

$$\tilde{F} = e^{\frac{1}{2}Ht} (-\frac{\partial f}{\partial t} + \frac{1}{2}[H, f] + X^-) e^{-\frac{1}{2}Ht}, \quad (3.3)$$

multiplying (2) from the left side by $e^{\frac{1}{2}Ht}$ and from the right side by $e^{-\frac{1}{2}Ht}$, we obtain

$$\frac{\partial \tilde{F}}{\partial t} - [[e^{\frac{1}{2}Ht} X^+ e^{-\frac{1}{2}Ht}, e^{\frac{1}{2}Ht} f e^{-\frac{1}{2}Ht}], \tilde{F}] + \tilde{F} = 0$$

Due to the evident equality

$$e^{\frac{1}{2}Ht} X^+ e^{-\frac{1}{2}Ht} = e^t X^+$$

the last equation can be rewritten in a form

$$\frac{\partial \tilde{F}}{\partial t} - e^t [[X^+, \tilde{f}], \tilde{F}] + \tilde{F} = 0, \quad (3.4)$$

where $\tilde{f} = e^{\frac{1}{2}Ht} f e^{-\frac{1}{2}Ht}$.

In terms of these notations we have from (3.3) the following expression

$$\tilde{F} = -\frac{\partial \tilde{f}}{\partial t} + [H, \tilde{f}] + X^- e^{-t} = 0$$

Let's introduce the notation

$$F = e^t \tilde{F} = -e^t \frac{\partial \tilde{f}}{\partial t} + e^t [H, \tilde{f}] + X^- = 0$$

Then (3.4) has a form

$$\frac{\partial F}{\partial t} + [A, F] = 0, \quad (3.5)$$

where $A = -e^t [X^+, \tilde{f}]$.

The equation (5) is one-dimensional evolution equation defined by Lax pair operators and it is one of the principal criteria of equations integrability.

From the presentation (3.5) it is followed that

$$\frac{\partial}{\partial t} s p F^n = 0, \text{ for } \forall n$$

and solution of the equations can be found in a form

$$F = \varphi F_0 \varphi^{-1}, \quad (3.6)$$

where $\varphi(t)$ takes values in the corresponding Lie group and $F_0 = F|_{t=0}$.

From equation (5) and presentation (6) it is directly followed the expression for the operator A :

$$A = \varphi' \varphi^{-1} \quad (\varphi' = \frac{\partial \varphi}{\partial t}) \quad (3.7)$$

Let's consider the commutator of F with X^+ :

GENERALIZED TODA MODELS

$$\begin{aligned}
 [X^+, F] &= [X^+, X^-] - e^t \frac{\partial}{\partial t} [X^+, \tilde{f}] + e^t [X^+, [H, \tilde{f}]] = \\
 &= H - e^t \frac{\partial}{\partial t} [X^+, \tilde{f}] - 2e^t [X^+, \tilde{f}] + e^t [X^+, [H, \tilde{f}]] = \\
 &= H - \frac{\partial}{\partial t} (e^t [X^+, \tilde{f}]) - e^t [X^+, \tilde{f}] + [H, e^t [X^+, \tilde{f}]].
 \end{aligned}$$

Taking into account (3.6) and (3.7) the last expression can be rewritten in a form

$$[X^+, \varphi F_0 \varphi^{-1}] = H - (\varphi' \varphi^{-1})' - \varphi' \varphi^{-1} + [H, \varphi' \varphi^{-1}].$$

Making the substitution $\varphi = e^{Ht} q$ and introducing a new variable $\tau = e^{-t}$, we have

$$\frac{\partial}{\partial \tau} \left(\frac{\partial q}{\partial \tau} q^{-1} \right) = [q F_0 q^{-1}, X^+] \quad (3.8)$$

Equation (3.8) is one-dimensional generalized non-abelian conformal affine Toda model as it is obviously seen from eq. (2.26). The group-theoretical approach derived for this equation in paragraph 2 gives reasonable opportunities to obtain the exact solutions for arbitrary semisimple algebra and that will be the subject of the further publications.

-
- [1] *T.Eguchi and S-K.Yang*, Phys. Lett. 224B (1989) 373-378; *T.J. Hollowood and P. Mansfield*, Phys. Lett. 226B (1989) 73-79.
 - [2] *A.N. Leznov and M.V. Saveliev*, Commun. Math. Phys. 89 (1983) 59-75; Theor. Mat. Phys. 54 (1983) 209-217.
 - [3] *A.N. Leznov and M.V. Saveliev*, Group Theoretical Methods for Integration of Non Linear Dynamical Systems; Progress in Physics 15 (Birkhauser, Basel, 1992).
 - [4] *J.L. Gervais and M.V. Saveliev*, Phys. Lett. 286B (1992) 271.
 - [5] *J. Underwood*, Aspects of non abelian Toda theories, hep-th/9304156.
 - [6] *H. Aratyn, L.A. Ferreira, J.F. Gomes and A.H. Zimerman*, Phys. Lett. 254B (1991) 372-380
 - [7] *O. Babelon and L. Bonora*, Phys. Lett. 244B (1990) 220-226.
 - [8] *A. Aratyn, L.A. Ferreira, J.F. Gomes and A.H. Zimerman*, The conserved charges and integrability of the Conformal Affine Toda Models, to appear in Mod. Phys. Lett. A, hep-th/9308086.
 - [9] *H. Aratyn, C.P. Constantinidis, L.A. Ferreira, J.F. Gomes and A.H. Zimerman*, Nucl. Phys. B406 [FS](1993) 727-770
 - [10] *R.S. Ward*, Phil. Trans. R. Soc. Lond. A315, 451 (1985); Lect. Notes Phys., 1987, 280, 106; Lond. Math. Soc. Lect. Notes Ser., 1990, 156, 246.
 - [11] *L.J. Mason and G.A. Sparling*, Phys. Lett., 1989, A137, 29; J. Geom. and Phys., 1992, 8, 243.
 - [12] *S. Chakravarty, M.J. Ablowitz and P.A. Clarkson*, Phys. Rev. Lett., 1990, 1085.
 - [13] *Bakas and D.A. Depireux*, Mod. Phys. Lett., 1991, A6, 399.
 - [14] *M.J. Ablowitz, S. Chakravarty and L.A. Takhtajan*, Comm. Math. Phys., 1993, 158, 1289.
 - [15] *T.A. Ivanova and A.D. Popov*, Phys. Lett., 1992, A170, 293.
 - [16] *L.J. Mason and N.M.J. Woodhouse*, Nonlinearity 1, 1988, 73; 1993, 6, 569.
 - [17] *M. Kovalyov, M. Legare and L. Gagnon*, J. Math. Phys., 1993, 34, 3425.
 - [18] *M. Legare and A.D. Popov*, Pis'ma Zh. Eksp. Teor. Fiz., 1994, 59, 845.
 - [19] *A.A. Belavin and V.E. Zakharov*, Phys. Lett., 1978, B73, 53.
 - [20] *A.N. Leznov and M.A. Mukhtarov*, J. Math. Phys., 1987, 28 (11), 2574; Prepr. IHEP, 1987, 87-90. Prepr. ICTP 163, Trieste, Italy, 1990; J. Sov. Laser Research, 13 (4), 284, 1992.
 - [21] *A.N. Leznov*, IHEP preprint-92/87, 1990.
 - [22] *A.N. Leznov, M.A. Mukhtarov and W.J. Zakrzewski*, Tr. J. of Physics 1995, 19, 416.
 - [23] *M.A. Mukhtarov*, Fizika, 2002, v. 5, N 2, 38
 - [24] *M.A. Mukhtarov*, Fizika, 2002, v. 5, N 3, 3
 - [25] *V.G. Knizhnik and A.B. Zamolodchikov*, Nucl. Phys. B247 (1984) 83.
 - [26] *F. Bastianelli*, Nucl. Phys. B361 (1991) 555.
 - [27] *A.A. Tseytlin*, Nucl. Phys. B411 (1994) 509.

M.A. Muxtarov

TODANIN ÜMÜMİLƏŞDİRİLMİŞ MODELİ

Todanın birölcülü qeyri-abel konform affin modeli üçün qruplaşmış nəzəri yanaşma işlənmişdir.

М.А. Мухтаров

ОБОБЩЕННЫЕ МОДЕЛИ ТОДА

Теоретико групповой подход разработан для одномерных неабелевых конформных аффинных моделей Тода.

Received: 22.09.07

Ag_{2-x}Cu_{0+x}S ($x=0.45; 0.8; 1.07$) BİRLƏŞMƏSİNDE POLİMORF ÇEVRİLMƏLƏR

Y.İ. ALIYEV, A.Q. BABAYEV, F.Q. MƏHƏRRƏMOVA

*Azərbaycan MEA Fizika İnstitutu,
Bakı, Az-1143, H. Cavid pr., 33*

Ag_{1.55}Cu_{0.45}S, Ag_{1.2}Cu_{0.8}S, Ag_{0.93}Cu_{1.07}S birləşmələri sintez edilmiş, Brümen üsulu ilə monokristalları alınmışdır. Yüksəktemperaturlu rentgendifraktometrik metodla kristallardakı polimorf çevrilmələr tədqiq edilmişdir.

Ag₂S-Cu₂S sistemi birləşmələrinin termik, mikrostruktur və yüksəktemperaturlu rentgenanaliz metodları ilə tədqiq edilməsi haqqında məlumatlar [1-6] işlərdə verilmişdir. Göstərilmişdir ki, yüksək temperatur oblastında Ag₂S və Cu₂S birləşmələrinin hər ikisi ÜMK strukturlu olub, kəsilməz bərk məhlul sırası təşkil edir. α -Ag₂S

kristalinin aşağıtemperatur modifikasiyasının α -Cu₂S-də həllolması, əksinə, çox cüzi olub, 340K temperaturda 1.87mol% təşkil edir. Cədvəl 1-də Ag₂S və Cu₂S binar birləşmələrinin strukturu və polimorfizmi haqqında məlumatlar verilmişdir.

Cədvəl 1.

Ag₂S və Cu₂S birləşmələrinin kristal strukturu və modifikasiyaların keçid temperaturu.

Modifikasiya və kecid temperaturu	Kristal qefəsin parametrləri					Fəza qrupu	ρ_x q/sm ³	Ədəbiyyat
	a(Å)	b(Å)	s(Å)	β	Z			
Ag ₂ S-Monoklin	4.236	6.909	7.888	99.35°	4	P2 ₁ /C	7,243	
	452 K							
	4.864				2	$O_h^g - 1m3m$	7,107	7-11
Ag ₂ S-ÜMK	873K							
	6.269				4	Fm3m	5,815	
Cu ₂ S-Monoklin	15.246	11.884	13.494	116.35°	48	P2 ₁ /n	5,8	
	373 K							
	3.961		6.722			P2 ₁ /mmC	5,785	12-17
Cu ₂ S-ÜMK	738 K							
	5.725				4	Fm3m	5,632	

İş [3]-də qeyd edilmişdir ki, bərk halda Ag_{1.55}Cu_{0.45}S, Ag_{1.2}Cu_{0.8}S, Ag_{0.93}Cu_{1.07}S tərkibli aralıq fazalar yaranır və homeogenlik oblastı Ag_{1-x}Cu_{1+x}S ($0 \leq x \leq 1$) düsturu ilə ifadə olunur ki, AgCuS (50mol% Ag₂S) birləşməsi də həmin oblastda yerləşir. AgCuS, Ag_{1.55}Cu_{0.45}S, Ag_{1.2}Cu_{0.8}S və Ag_{0.93}Cu_{1.07}S birləşmələrinin polimorf modifikasiyalarının strukturu və çevrilmə temperaturları haqqında ədəbiyyat məlumatları cədvəl 2-də verilmişdir.

AgCuS üçqat birləşməsi otaq temperaturunda, elementar qefəsin parametrləri $a=4,06\text{ \AA}$, $b=6,66\text{ \AA}$, $s=7,99\text{ \AA}$, fəza qrupu D_{2h}^{17} -Cmcm, $Z=4$ olan ortorombik qefəsdə kristallaşır [3]. AgCuS birləşməsinin aşağıtemperatur ortorombik modifikasiyasının Ag₂S birləşməsinin monoklin strukturu ilə bəzi oxşarlığı var [7]. AgCuS birləşməsinin strukturundakı kükürd və mis atomlarından təşkil olunmuş laylar Ag₂S birləşməsindəki kükürd-gümüş laylarına çox bənzəyir. Bu laylarda hər bir mis atomu $\sim 2.28\text{ \AA}$ məsafədə yerləşən kükürd atomları ilə əhatə olunmuşdur. Laylar gümüş atomları vasitəsilə birləşir və kükürd-gümüş məsafəsi $\sim 2.28\text{ \AA}$ -dir.

Qeyd etmək lazımdır ki, AgCuS birləşməsi defektli struktura malikdir və güman etmək olar ki, mis atomları strukturda çatışmayan Ag atomlarını qismən əvəz edirlər.

AgCuS birləşməsindəki polimorf çevrilmələr [19]-da tədqiq edilmiş və göstərilmişdir ki, aşağıtemperatur ortorombik modifikasiya 400K temperaturda β -Cu₂S ilə [12] identik olan heksaqaonal modifikasiyaya, bu modifikasiya isə $705 \pm 2\text{ K}$ -də yüksəktemperatur ÜMK modifikasiyasına keçir (Cədvəl 6).

Təqdim olunan işdə yüksəktemperaturlu rentgen metodu ilə Ag_{1.55}Cu_{0.45}S, Ag_{1.2}Cu_{0.8}S, Ag_{0.93}Cu_{1.07}S monokristallarında polimorf çevrilmələr öyrənilmişdir.

TƏCRÜBİ HİSSƏ.

Ag_{1.55}Cu_{0.45}S, Ag_{1.2}Cu_{0.8}S, Ag_{0.93}Cu_{1.07}S birləşmələrinin sintezi və monokristallarının alınması.

Göstərilən tərkiblərin sintezi üçün Ag və Cu təmizlik dərəcəsi 99,999% olan və «B5» markalı S komponentlərindən istifadə edilmişdir. İçərisində müvafiq tərkiblər olan ampulalar sobanın temperaturu stabil olan zonasında yerləşdirilmiş, sonra sobanın temperaturu kükürdün ərimə temperaturuna ($T_{sr}=393\text{ K}$) qədər qaldırılmış və kükürd, gümüş və mis arasında reaksiyanın getməsi üçün 3 saat müddətində sobanın temperaturu sabit saxlanılmışdır. Sonra temperatur 50K/saat sürətlə AgCuS-in ərimə temperaturundan ($T_{sr}=1357\text{ K}$) yuxarı qaldırılmışdır. Hə-

min temperaturda 3 saat saxlanıldıqdan sonra soba ampulalarla birlikdə 20K/saat sürətlə otaq temperaturuna qədər soyudulmuşdur.

Alınmış nümunələrin bırsazalılığını müəyyən etmək üçün mikrostruktur və rentgen-faza analizi aparılmışdır.

$\text{Ag}_{1.55}\text{Cu}_{0.45}\text{S}$ birləşməsinin tozundan alınmış difraktoqram tetraqonal (cəd.3), $\text{Ag}_{1.2}\text{Cu}_{0.8}\text{S}$ birləşməsinin tozundan alınmış difraktoqram monoklin (cəd.4), $\text{Ag}_{0.93}\text{Cu}_{1.07}\text{S}$ birləşməsinin tozundan alınmış difraktoqram isə ortorombik (cəd.5) qəfəs parametrləri əsasında indekslənmişdir.

Sintez edilmiş təkiblərin monokristalları Bricmen üsulu ilə alınmışdır. Hər bir tərkib xirdalanmış halda, rüşeymləri seçməyə imkan verən iti uclu ampulaya yerləşdirilmişdir. Ampulaların havası 10^{-3}Pa təzyiqə qədər sorulmuş,

hər ampula növbə ilə sobanın yuxarı hissəsində yerləşdirilmiş və 1400K-dən yuxarı temperatura qədər qızdırılmışdır. Bundan sonra ampulalar 1.5mm/saat sürətlə sobanın temperatur qradienti zonasından keçirilmişdir.

Bu şərtlər daxilində yüksək temperatur modifikasiyasının kristalları almır. Ampulalar sobanın temperatur qradientindən keçərkən soyuduqda kristallar yüksək temperatur modifikasiyasından aşağı temperatur modifikasiyasına keçirlər. Gərginlik və deformasiyanı aradan qaldırmaq məqsədilə aşağı temperatur modifikasiyasının kristalları 48 saat ərzində sobanın 3-cü zonasında kecid temperaturundan aşağı temperaturda saxlanılmışdır.

Bələliklə, alınmış kristallar təqdim olunan işin tədqiqat obyektləri olmuşdur.

Cədvəl 2.

AgCuS , $\text{Ag}_{1.55}\text{Cu}_{0.45}\text{S}$, $\text{Ag}_{1.2}\text{Cu}_{0.8}\text{S}$ və $\text{Ag}_{0.93}\text{Cu}_{1.07}\text{S}$ birləşmələrinin kristal strukturu və kecid temperaturları haqqında ədəbiyyat məlumatları.

Modifikasiya və kecid temperaturu	Kristal qəfəsin parametrləri					Fəza qrupu	ρ_x q/sm ³	Ədəbiyyat
	$a(\text{\AA})$	$b(\text{\AA})$	$s(\text{\AA})$	β	Z			
AgCuS -Ortorombik	4.06	6.66	7.99		4	Cmcm	6.30	
	366K							
	Heksagonal	4.005	6.806		2	P6 ₃ /m mc	6.350	1-5, 19
$\text{Ag}_{1.55}\text{Cu}_{0.45}\text{S}$ -Tetraqonal	705K							
	ÜMK	5.729			4	Fmcm	7.186	
	>373 K							
$\text{Ag}_{1.2}\text{Cu}_{0.8}\text{S}$	HMK	8.673	11.756		16		6.8	
	424 K							1-5
	ÜMK	4.825			2		6.736	
$\text{Ag}_{0.93}\text{Cu}_{1.07}\text{S}$ -Ortorombik	424 K	-	-	-	-	-	-	
	ÜMK	5.999						1-5
	~373K							
$\text{Ag}_{0.93}\text{Cu}_{1.07}\text{S}$ -Ortorombik	Heksagonal	4.066	6.628	7.972		4	Cmcm	6.194
	~453K							
	HMK	4.138	7.105		2			1-5
		5.961			2			

$\text{Ag}_{1.55}\text{Cu}_{0.45}\text{S}$, $\text{Ag}_{1.2}\text{Cu}_{0.8}\text{S}$, $\text{Ag}_{0.93}\text{Cu}_{1.07}\text{S}$ kristallarının yüksək temperatur difraktometrik tədqiqi.

Yüksək temperaturlu difraktometrik tədqiqatlar 10^{-3}Pa vakuum almağa imkan verən yüksək temperaturlu «URVT-2000» əlavəsi olan DRON-3M (CuK_α -şüa, Ni-filtr) difraktometrində aparılmışdır. Difraksiya xətlərinin yazılışında bucaq ayrıdetməsi $\approx 0.1^\circ$, bucaqların təyinindəki xəta $\Delta\theta = \pm 0.02^\circ$ -dir.

1. **$\text{Ag}_{1.55}\text{Cu}_{0.45}\text{S}$.** Kristallik $\text{Ag}_{1.55}\text{Cu}_{0.45}\text{S}$ birləşməsindən otaq temperaturunda (293K) ixtiyari istiqamətli $5 \times 5 \times 2$ mm ölçülü nümunə kəsilmişdir. Bu nümunə üçün $10^\circ \leq 2\theta \leq 100^\circ$ bucaq intervalında 15 aydın difraksiya xətləri qeydə alınmışdır (Cədvəl 3-də onlar ulduzla işarələnmişdir). Cədvəl 3-də göstərildiyi kimi, qeydə alınmış bütün

xətlər toz nümunəsindən alınmış xətlərlə üst-üstə düşür və tetraqonal qəfəs parametrləri ilə dəqiqlik indekslənirlər.

Otaq temperaturunda difraktoqram çəkildikdən sonra soba işə salınmış və hər 30K-dən sonra difraksiya xətləri çəkilmişdir. Hər çəkilmədən əvvəl nümunənin temperaturu 30 dəqiqə ərzində sabit saxlanılmışdır. Bu zaman 403K temperaturda alınmış difraktoqramdakı xətlərin sayıda və intensivliyində dəyişiklik olmamışdır. Yalnız 493K-də əvvəlki bucaq intervalında 7 difraksiya xətti qeydə alınmışdır.

Bu xətlər qəfəs parametrləri $a=4.833X$, $Z=2$, $\rho_x=6.704$ q/sm³ olan HMK strukturunda birqiyəmətli indekslənirlər. Nümunəni 673K-ə qədər qızdırıldıqda HMK modifikasiya parametrləri $a=5.951X$, $Z=4$, $\rho_x=7.179$ q/sm³ olan ÜMK modifikasiyaya keçir.

Cədvəl 3.
Ag_{1.55}Cu_{0.45}S kristalının müxtəlif temperaturlarda alınmış rentgenqramlarının hesabı.

<i>T, K</i>	<i>d_{eksp.}(X)</i>	<i>I/I₀</i>	<i>d_{hex.}(X)</i>	<i>h k l</i>	Kristal qəfəsin parametrləri
1	3	2	4	5	6
293	6,933	30	6,9410	101	Tetraqonal <i>a</i> =8,673 X <i>c</i> =11,576 X <i>Z</i> =16 ρ =6,981 q/sm ³
	4,812	40	4,8143	102	
	4,319*	60	4,3365	200	
	4,064	40	4,0609	201	
	3,878	30	3,8787	210	
	3,673	40	3,6777	121	
	3,480*	40	3,4705	202	
	3,222	20	3,2221	212	
	3,065	40	3,0664	220	
	2,892	40	2,8910	300	
	2,802*	100	2,8049	301	
	2,746	100	2,7452	104	
	2,484*	60	2,4785	312	
	2,432*	100	2,4072	204	
	2,353*	100	2,3552	321	
	2,164*	40	2,1683	400	
	2,103	20	2,1035	140	
	2,030	30	2,0305	042	
	1,991	20	1,9907	134	
	1,930*	20	1,9276	332	
	1,838	40	1,8389	242	
	1,742*	40	1,7352	404	
	1,677*	20	1,6828	151	
	1,611	40	1,6111	424	
	1,566*	20	1,5569	415	
	1,487	30	1,4878	434	
	1,442*	40	1,4406	532	
	1,388*	40	1,3882	505	
	1,327*	40	1,3229	534	
	1,278	30	1,2780	543	
	1,219	10	1,2197	551	
	1,168	10	1,1689	553	
	1,146*	20	1,1458	329	
	1,083	20	1,0838	555	
385	4,331	60	4,3334	200	Tetraqonal <i>a</i> =8,667 X <i>c</i> =11,778 X <i>Z</i> =16 ρ =6,951 q/sm ³
	3,490	40	3,4900	202	
	2,805	100	2,8061	301	
	2,488	60	2,4853	312	
	2,437	100	2,4354	204	
	2,356	100	2,3551	321	
	2,168	40	2,1667	400	
	1,931	20	1,9302	332	
	1,745	40	1,7453	404	
	1,679	20	1,6822	151	
	1,567	20	1,5684	415	
	1,443	40	1,4411	532	
	1,396	40	1,3962	505	
	1,328	40	1,3269	534	
	1,147	20	1,1493	329	
573	2,438	60	2,4380	200	HMK <i>a</i> =4,876 X <i>Z</i> =2 ρ =6,526 q/sm ³
	1,991	100	1,9906	211	
	1,724	40	1,7239	220	
	1,542	20	1,5419	310	
	1,407	60	1,4076	222	
	1,303	50	1,3032	321	
	1,219	40	1,2190	400	
673	2,974	40	2,9753	200	ÜMK <i>a</i> =5,951 X <i>Z</i> =4 ρ =7,179 q/sm ³
	2,103	60	2,1034	220	
	1,793	100	1,7940	311	
	1,717	80	1,7169	222	
	1,487	60	1,4876	400	
	1,365	90	1,3644	331	

2. Ag_{1.2}Cu_{0.8}S. Sintez edilmiş Ag_{1.2}Cu_{0.8}S nümunəsinin tozundan alınmış difraktoqramda qeydə alınmış 26 difraksiya xətti Cu_{1.96}S tərkibinə məxsus olan monoklin qəfəs parametrləri əsasında indekslənir: $a=26,897\text{\AA}$, $b=15,745\text{\AA}$, $c=13,565\text{\AA}$, $\beta=90^{\circ}13'$, $Z=8$, fəza qrupu P2₁/n [12, 15].

Qeyd etmək lazımdır ki, 26 difraksiya xəttindən 13-ü Ag₂S-in monoklin qəfəs parametrləri ilə də indekslənirlər.

Temperatur tədqiqatları üçün polimorf keçiddən alınmış yüksəktemperatur modifikasiyasının kristalından istifadə edilmişdir. Ag_{1.2}Cu_{0.8}S-dən otaq temperaturunda ixtiyari istiqamətli $4\times4\times2$ mm ölçülü nümunə kəsilmişdir. Bu nümunə üçün $10^{\circ}\leq2\theta\leq100^{\circ}$ bucaq intervalında 15 aydın di-

fraksiya xətləri qeydə alınmışdır (Cədvəl 4-də onlar ulduzla işarələnmişdir). Cədvəl 4-də göstərildiyi kimi, qeydə alınmış bütün xətlər toz nümunədən alınmış rentgenqramla üst-üstə düşür.

Ag_{1.2}Cu_{0.8}S nümunəsinin otaq temperaturunda ikifa-zalılığı müəyyən edildikdən sonra, nümunənin istiqamətini dəyişmədən soba işə salılmış və 4-cü cədvəldən göründüyü kimi, 372K-də əvvəlki bucaq intervalında 15 difraksiya xətti əvəzinə yalnız 8 xətt qeydə alınmışdır. Bu difraksiya xətləri Cu_{1.96}S və Ag₂S-in qəfəs parametrləri ilə indekslənirlər. Difraksiya xətlərinin sayının azalması, görünür, nümunələrin qızdırılması ilə əlaqədardır.

Cədvəl 4.
Ag_{1.2}Cu_{0.8}S kristalinin müxtəlif temperaturlarda alınmış rentgenqramlarının hesabı.

T, K	$d_{eksp.}(X)$	I/I ₀	Cu _{1.96} S [12]		Ag ₂ S [12]		Kristal qəfəsin parametrləri
			$d_{hes.}(X)$	h k l	$d_{hes.}(X)$	h k l	
293	6,809	20	6,8089	021	-	-	Cu _{1.96} S <u>Monoklin</u> $a=26,897\text{ X}$ $b=15,745\text{ X}$ $c=13,565\text{ X}$ $\beta=90.13^{\circ}$ $Z=8\text{Cu}_{31}\text{S}_{16}$ f.q. P2 ₁ /n $\rho_x=7,854\text{ q/sm}^3$
	6,050	20	6,0504	202	-	-	
	4,812	30	4,8150	131	-	-	
	3,882*	40	3,8788	123	3,8801	002	
	3,051*	60	3,0502	433	-	-	
	2,861*	60	2,8684	911	-	-	
	2,607*	100	2,6010	10 11	2,6031	121	
	2,564*	40	2,5646	161	-	-	
	2,522*	40	2,5217	552	-	-	
	2,500*	20	2,4983	022	-	-	
	2,407*	60	2,4055	461	-	-	
	2,307*	60	2,3076	054	2,3178	122	
	2,186*	40	2,1893	271	-	-	
	2,164*	40	2,1656	126	-	-	
	2,090*	40	2,0903	815	2,0931	122	
	2,070*	60	2,0690	164	2,0707	023	
	2,009*	40	2,0081	173	-	-	
	1,947*	60	1,9466	944	1,9400	004	
	1,882	30	1,8817	027	-	-	
	1,801	20	1,8010	237	1,8168	114	
	1,720	40	1,7207	291	1,7202	033	
	1,681	40	1,6806	292	1,6862	041	
	1,486	60	1,4858	309	1,4838	034	
	1,393	30	1,3927	468	1,3987	143	
	1,262	20	1,2614	488	1,2630	152	
	1,126	20	1,1254	499	1,1256	054	
373	2,539	40	2,5371	253	-	-	Cu _{1.96} S <u>Monoklin</u>
	2,127	40	2,1281	172	-	-	
	2,071	100	2,0730	11 2 3	2,0707	023	
	2,034	40	2,0344	472	2,0163	130	
	1,981	100	1,9812	11 0 4	1,9806	032	Ag ₂ S <u>Monoklin</u>
	1,919	60	1,9189	555	1,9144	131	
	1,443	30	1,4436	767	1,4440	142	
	1,097	20	1,0972	5 14 1	1,0965	225	
424	2,998	40	2,9986	200			ÜMK $a=5,997\text{ X}$ $Z=4$, f.q. Fm3m $\rho_x=6,532\text{ q/sm}^3$
	2,119	100	2,1204	220			
	1,808	60	1,8083	311			
	1,733	20	1,7313	222			

373K-də difraksiya xətləri çəkildikdən sonra nümunənin qızdırılması davam etdirilmiş və 424K-də əvvəlki bucaq intervalında 4 yeni difraksiya xətti qeydə alınmışdır ki, bunlar parametrləri $a=5,997\text{\AA}$ olan ÜMK yüksəktemperatur modifikasiyasına mənsubdur. Keçid dönen keçidir və nümunə soyuduqda birləşən ÜMK modifikasiya əvvəlki ikifazalı hala qayıdır.

3. Ag_{0.93}Cu_{1.07}S. Ag_{0.93}Cu_{1.07}S kristalından otaq temperaturunda (293K) ixtiyari istiqamətli $5\times5\times2$ mm ölçülü nümunə kəsilmişdir. Bu nümunə üçün $10^{\circ}\leq2\theta\leq90^{\circ}$ bucaq intervalında 18 aydın difraksiya xətləri qeydə alınmışdır (Cədvəl 5-də onlar ulduzla işarələnmişdir).

5-ci cədvəldən göründüyü kimi, qeydə alınmış difraksiya xətlərinin hamısı toz nümunəsindən alınmış rentgen-

qramdakı xətlərlə üst-üstə düşür və tetraqonal qəfəs parametrləri ilə dəqiq indekslənilər.

Otaq temperaturunda difraktoqram çəkildikdən sonra soba işə salınmış və nümunə tədricən qızdırılmışdır. 373K-də əvvəl qeydə alınmış 18 difraksiya xətlərinin həmisi yox olmuş və əvvəlki bucaq intervalında 6 yeni xətt yaranmışdır. Bu xətlər, Ag₂S-in ikinci modifikasiyası olan

heksaqaonal qəfəsin parametrləri ilə indekslənilər. Heksagonal modifikasiya 469K-də qəfəs parametri $a=5,962\text{\AA}$ olan yüksəktemperatur ÜMK modifikasiyasına keçir. Bütün keçidlər döndəndir, yəni nümunə soyudulduğda Ag_{0,93}Cu_{1,07}S kristalı ilkin vəziyyətinə qayıdır.

Cədvəl 5.

Ag_{0,93}Cu_{1,07}S kristalının müxtəlif temperaturlarda alınmış rentgenqramlarının hesabı.

<i>T, K</i>	<i>d_{eksp.} (X)</i>	<i>I/I₀</i>	<i>d_{hes.} (X)</i>	<i>h k l</i>	Kristal qəfəsin parametrləri
293	3,982*	20	3,9860	002	Ortorombik $a=4,063 \text{ X}$ $b=6,628 \text{ X}$ $c=7,974 \text{ X}$ $Z=4$ f.q. Cmcm $\rho_x = 6,194 \text{ g/sm}^3$
	3,630*	20	3,6226	101	
	3,458	40	3,4666	110	
	3,309*	60	3,3140	020	
	3,056	40	3,0737	021	
	2,615*	100	2,6153	112	
	2,546	60	2,5579	022	
	2,110*	25	2,1087	113	
	2,071*	40	2,0730	023	
	2,031*	60	2,0330	200	
	1,994*	60	1,9930	004	
	1,884*	60	1,8861	131, 211	
	1,745*	60	1,7453	132, 212	
	1,733	40	1,7333	220	
	1,728*	40	1,7275	114	
	1,709*	40	1,7077	024	
	1,693	40	1,6939	221	
	1,588*	40	1,5893	222	
	1,567	40	1,5690	213	
373	1,451	40	1,4528	223	
	1,422*	60	1,4261	204	
	1,306*	40	1,3077	224	
	1,258*	40	1,2598	312, 150	
	1,239*	40	1,2392	116, 321	
	1,142	20	1,1433	331	
469	2,522	100	2,5222	102	Heksagonal $a=4,138 \text{ X}$ $c=7,090 \text{ X}$ $Z=2$ $\rho_x = 6,329 \text{ g/sm}^3$
	2,067	100	2,0690	110	
	1,971	100	1,9753	103	
	1,809	40	1,7917	200, 112	
	1,773	40	1,7714	004	
	1,737	40	1,7387	201	
469	2,979	40	2,9812	200	ÜMK $a=5,962 \text{ X}$ $Z=4, f. q. Fm3m$ $\rho_x = 6,277 \text{ g/sm}^3$
	2,108	50	2,1080	220	
	1,797	100	1,7977	311	
	1,720	60	1,7212	222	
	1,491	40	1,4906	400	

ALINMIŞ NƏTİCƏLƏR VƏ ONLARIN MÜZAKİRƏSİ.

Qeyd edildiyi kimi, AgCuS birləşməsinin kristal strukturunun Ag₂S kristalının strukturu ilə bəzi oxşarlığı var. Bu oxşarlıq, AgCuS-in strukturunun β oxu, Ag₂S-in isə β oxu boyunca proyeksiyalarının müqayisəsində daha aydın nəzərə çarpır. Buna baxmayaraq, AgCuS və Ag₂S-dəki modifikasiyaların sayı və kecid temperaturları biribirindən fərqlənir.

Cədvəl 6-dan göründüyü kimi, tədqiq olunmuş tərkiblərdən yalnız Ag_{0,93}Cu_{1,07}S kristal strukturuna və polimorf kecidlərinə görə AgCuS kristalına uyğun gelir. Lakin heksaqaonal modifikasiyanın ÜMK modifikasiyasına keçidi Ag_{0,93}Cu_{1,07}S kristalında, AgCuS kristalına nisbətən aşağı temperaturda (236K) baş verir.

Ag_{1,55}Cu_{0,45}S kristalında aşağı temperatur tetraqonal modifikasiya 425K-də HMK modifikasiyaya, bu modifikasiya isə 673K temperaturda ÜMK modifikasiyaya keçir.

Ag_{1,2}Cu_{0,8}S kristalı otaq temperaturunda ikifazalıdır. Fazalardan biri Cu_{1,96}S kristalının monoklin qəfəsinin parametrlərini, digəri isə Ag₂S-in monoklin qəfəsinin parametrlərini qəbul edir. 424K temperaturda hər iki modifikasiya eyni vaxtda yüksəktemperatur ÜMK modifikasiyasına çevirilir.

Beləliklə, yüksəktemperatur rentgendifraktometrik metodla Ag_{1,55}Cu_{0,45}S, Ag_{1,2}Cu_{0,8}S, Ag_{0,93}Cu_{1,07}S kristallarında polimorf çevrilmələr tədqiq edilmişdir. Alınmış nəticələr cədvəl 6-da verilmişdir.

$\text{Ag}_{2-x}\text{Cu}_{0+x}\text{S}$ ($x=0.45; 0.8; 1.07$) BİRLƏSMƏSİNDE POLİMORF ÇEVİRİLMƏLƏR

Cədvəl 6.

AgCuS , $\text{Ag}_{0.93}\text{Cu}_{1.07}\text{S}$, $\text{Ag}_{1.55}\text{Cu}_{0.45}\text{S}$ və $\text{Ag}_{1.2}\text{Cu}_{0.8}\text{S}$ kristallarının qəfəs parametrləri və keçid temperaturları.

Modifikasiya və keçid temperaturu	Kristal qəfəsin parametrləri				Z	Fəza qrupu	ρ_x q/sm ³
	a(Å)	b(Å)	s(Å)	β			
AgCuS- Ortorombik Heksagonal ÜMK	4,06	6,66	7,99	-	4	Cmcm	6,30
	4,005	-	6,806	-	2	P6 ₃ /mmc	6,350
	5,729	-	-	-	4	Fm3m	7,186
$\text{Ag}_{0.93}\text{Cu}_{1.07}\text{S}$ -Ortorombik Heksagonal ÜMK	4,063	6,628	7,974	-	4	Cmcm	6,194
	4,138	-	7,090	-	2	P6 ₃ /mmc	6,329
	5,962	-	-	-	4	Fm3m	6,229
$\text{Ag}_{1.55}\text{Cu}_{0.45}\text{S}$ - Tetraqonal HMK ÜMK	8,673	-	11,576	-	6	-	6,951
	4,833	-	-	-	2	-	6,704
	5,951	-	-	-	4	Fm3m	7,179
$\text{Ag}_{1.2}\text{Cu}_{0.8}\text{S}$ - Monoklin Cu _{1,96} S Monoklin Ag ₂ S ÜMK	26,897	15,745	13,565	90,13°	8	P2 ₁ /n	7,859
	4,236	6,909	7,888	99,35°	4	P2 ₁ /s	7,243
	5,997	-	-	-	4	Fm3m	6,532

-
- [1] A.J.Frueh. Zeit. Krist., 1955, v.106, p.299-307.
[2] A.N.Krestovnikov, A.Yu.Mendelebur, V.M.Qlazov. Neorganicheskiye materiali, 1968, t.4, №7, s.1280-1281. (in Russian).
[3] P.Pierre, Y.Clande. Rev. Chem. Miner. 1971. V.8. №1. P.87-97.
[4] N.Valverde. Z. Phys. Chem. 1968. V.62. №1-4. P.218-220.
[5] B.J.Skinner. Economic Geology. 1966. V.61. №1.P.1-26.
[6] R.B.Graf. J. Electrochemical Soc. 1968. V.115. №4. P.433-439.
[7] A.J.Frueh. Z. Krist. 1958. V.110. P.136-144.
[8] P.Rahlfs. Z. Phys. Chem. 1936. (B)31. P.157-194.
[9] F.C.Kracek. Trans. Amer. Geophys. Union. 1946. V.27. P.364-368.
[10] E.Rickert. Z. Phys. Chem. V.21. NOF. P.432-435.
[11] G.A. Dzhabrailova, Yu.G. Asadov. Neorganicheskie materiali. 1977. T.13. №3. S.423-425. (in Russian)
[12] T.Howard, Jr.Evans. Zeit. Kristallographie. 1979. V.150. P.299-320.
[13] N.V. Belov, V.A. Butuzov. Dokl. AN SSSR. 1964. T.54. №8. S.717-720. (in Russian)
[14] S.Djurle. Acta Chem. Scand. 1958. V.12. №7. P.1415-1426.
[15] M.Z.Buerger, N.W.Buerger. Am. Mineral. 1944. V.44. P.55-65.
[16] R.Ueda. J. Phys. Soc. Japan. 1949. V.3. P.287-292.
[17] M.J.Buerger, B.J.Wuensch. Science. 1963. V.141. P.276-277.
[18] K.T. Vilke. Metodi virashivaniya kristallov, Izd-vo «Nedra», Leningrad-1968, S.423. (K.Th. Wilke. Methoden der kristallzüchtung, veb deutscher verlag der wissenschaften, Berlin. 1963).

- [19] R.B. Baykulov, Yu.G. Asadov. Materiali mejdunaro-dnoy konferentsii, posvyashennoy 85 letiyu akade-mika G.B. Abdullaeva, g. Baku. 2003. C.69-75.

Y.I. Aliyev, A.G. Babayev, F.G. Magerramova

POLYMORPHIC TRANSFORMATIONS IN $\text{Ag}_{2-x}\text{Cu}_{0+x}\text{S}(x=0.45; 0.8; 1.07)$

$\text{Ag}_{1.55}\text{Cu}_{0.45}\text{S}$, $\text{Ag}_{1.2}\text{Cu}_{0.8}\text{S}$, $\text{Ag}_{0.93}\text{Cu}_{1.07}\text{S}$ single crystals are grown by Bridgmen method and synthesized. Polymorphic transformations are investigated in them by high temperature roentgenodiffractometer method.

Ю.И. Алыев, А.Г. Бабаев, Ф.Г. Магеррамова

ПОЛИМОРФНЫЕ ПРЕВРАЩЕНИЯ В $\text{Ag}_{2-x}\text{Cu}_{0+x}\text{S}(x=0.45; 0.8; 1.07)$

Синтезированы и методом Бриджмена выращены монокристаллы составом $\text{Ag}_{1.55}\text{Cu}_{0.45}\text{S}$, $\text{Ag}_{1.2}\text{Cu}_{0.8}\text{S}$, $\text{Ag}_{0.93}\text{Cu}_{1.07}\text{S}$ и высокотемпературным рентгенодифрактометрическим методом исследованы полиморфные превращения в них.

Received: 17.09.07

TlGa_{1-x}Co_xS₂ BƏRK MƏHLULLARININ TƏDQİQİ

A.İ. HƏSƏNOV, E.M. KƏRİMÖVA, N.Z. HƏSƏNOV, K.M. HÜSEYNOVA

AMEA Fizika İnstitutu,

AZ 1143, Bakı, H. Cavid pr., 33

TlGaS₂-TlCoS₂ sistemində qarşılıqlı təsir öyrənilib və bu sistemin hal diaqramı qurulmuşdur. Otaq temperaturunda TlGaS₂ əsasında 15mol%-li TlCoS₂-nin həll olması ilə bərk məhlullar əmələ gəldiyi təyin olunub.

Geniş temperatur intervalında (77÷400K) TlGa_{0,95}Co_{0,05}S₂ birləşməsində keçiriciliyin və termo-e.h.q.-nin temperaturdan asılılığı araşdırılmış, keçiriciliyin metallik xarakter daşıdığı təyin olunmuşdur. 100K temperaturda TlGa_{0,95}Co_{0,05}S₂-də termo-e.h.q.-nin işarəsinin dəyişməsi müşahidə olunmuşdur və bu temperaturdan yuxarı qiyamətlərdə keçiricilik *n*-tipli olmuşdur.

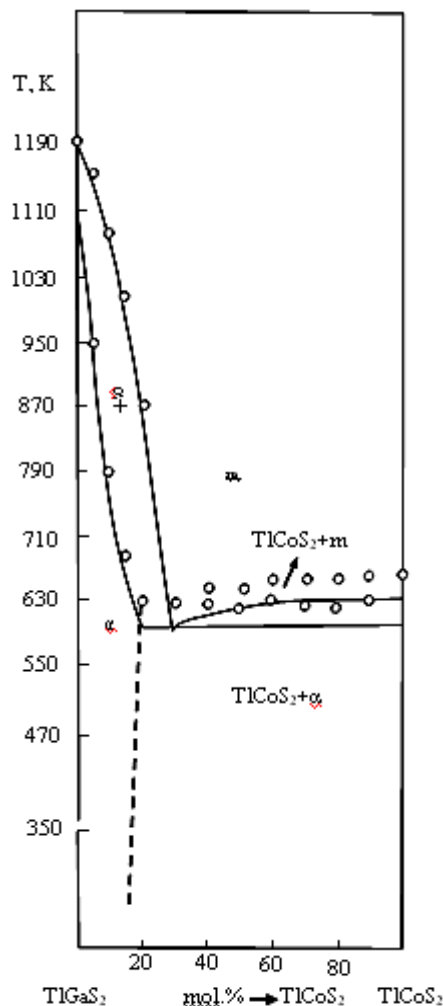
TlGa_{1-x}Co_xS₂ bərk məhlullarının udulma sərhəddi kobaltın cüzi konsentrasiyalarında düz eksiton zolağı şəklində formalasır, bu zaman $\partial E^{\text{ex}} / \partial T$ temperatur əmsalı TlGaS₂-də olduğu kimi müsbət işarəsini saxlayır, amma Ga-nin Co-la gismən əvəzlənməsi nəticəsində eksiton zolağı qısa dalgalı oblasta tərəf sürüsür.

Aşağı ölçülü maqnetiklər sinfinə aid olan TlCoS₂ birləşməsi son illərdə tədqiqatçıların diqqətini daha çox cəlb edir. İş [1]-də rentgenoqrafik analiz vasitəsilə TlCoS₂-nin heksagonal strukturaya malik olduğu təyin edilmişdir. Onun maqnit nüfuzluluğunun və maqnitlənməsinin 77÷300K temperatur intervalında ölçülülməsi göstərdiki, TlCoS₂ ferrimaqnetikdir. Küri temperaturu 112K, effektiv maqnit momenti $4,6\mu_B$ təşkil edir. İş [2]-də geyd olunur ki, TlCoS₂ 77÷225K temperatur intervalında p-tip keçiriciliyə malikdir və 225K temperatur ətrafında e.h.q.-nin işarəsinin dəyişməsi baş verir. Həmçinin TlCoS₂-nin istilik tutumu ölçülümdür, bu zaman onun maqnit hissəsinin özunu kvaziasağı ölçülü maqnetiklərə uyğun aparması müşahidə olunmuşdur.

TlCoS₂ bərk məhlullarını, daha çox öyrənilmiş TlGaS₂ yarımkəciriçi birləşmələri ilə müqayiseli şəkildə tədqiq olunması maraq doğurur. İş [1]-də göstərilmiş metod əsasında bizim tərəfimizdən TlCoS₂ birləşməsi sintez edilmişdir. TlGaS₂-TlCoS₂ sisteminin hal diaqrammasının qurulması üçün 13 nümunə hazırlanmışdır. Birləşmələrin sintez rejimi, onların ərimə temperaturalarına uyğun olaraq seçilmiştir: TlGaS₂ üçün 1180K, TlCoS₂ üçün 670K. Sintez olunmuş xəlitlərin homogenizasiya olunması üçün, 20 sutka ərzində 780K temperaturda gallium birləşməsi və 24 sutka ərzində 470K temperaturda kobaltlı xəlitlər dəmə qoyulmuşdur.

DTA metodu ilə alınmış nümunələr əsasında TlGaS₂-TlCoS₂ sisteminin hal diaqramı qurulmuşdur. Şəkil 1-dən görünür ki, diaqramın sağ tərəfində nonvariant eftetik nöqtədən TlCoS₂-yə qədərcadə eftetika əmələ gəlir. Burada nonvariant eftetik nöqtə (TlGaS₂)_{0,70}(TlCoS₂)_{0,30} tərkiblə və 633K temperatura ilə xarakterizə olunur. Diaqramın sol tərəfində nonvariant nöqtə ilə TlGaS₂ arasında bərk məhlul əmələ gəlir. Otaq temperaturunda TlGaS₂ əsasında 15mol%-li TlCoS₂-nin həll olması ilə bərk məhlullar əmələ gəlir.

Öyrənilən TlGa_{1-x}Co_xS₂ bərk məhlul monokristalları tekmilləşdirilmiş Bricmen-Stokbarger metodu ilə ərintidən yetişdirilmişdir. Butun bunlar laylı quruluşa malikdirlər. Alınmış kristalların DTA-i və difraktogramması göstərdiki, kobalt galliumu kristal qəfəsdə əvəz edir. Sintez olunmuş bərk məhlul nümunələrinin rentgenstruktur analizi, onların kristal qəfəsinin parametrlərini təyin etməyə imkan verdi. Butun bunlar, başlangıç birləşmədə daxil olmaqla, cədvəldə göstərilmişdir.



Şəkil 1. TlGaS₂-TlCoS₂ sisteminin hal diaqramması.

TlGa_{1-x}Co_xS₂ ($x=0; 0,005; 0,01$) laylı monokristallarının dielektrik xassələri iş [3]-də öyrənilmişdir və təyin olunmuşdur ki, $5 \cdot 10^4 \div 2 \cdot 10^7$ Hz tezlik oblastında bu kristallarda Fermi səviyyəsi yaxınlığında lokallaşmış hallar üzrə yüksəkdaşma hoppanma tipli mexanizmlə baş verir. Bu halların sıxlığı (N_F) və energetik paylanması (ΔE), hoppanmaların orta müddəti (τ) və məsafəsi (R) təyin edilmişdir.

TlGa_{1-x}Co_xS₂-nin kristal qəfəs parametrləri

Tərkib	Sinqoniya	Qəfəs parametri				Z	F. sim. qrup	Sixlıq q/sm ³
		a(Å)	b(Å)	c(Å)	β			
TlGaS ₂	Monoklin	10.40	10.40	15.17	100	16	P2 _{1/m}	5.560
TlCoS ₂	Heksagonal	3.726	-	22.510	-	3	-	6.026
TlGa _{0.999} Co _{0.001} S ₂	Monoklin	10.421	10.406	15.174	100	16	P2 _{1/m}	5.544
TlGa _{0.995} Co _{0.005} S ₂	Tetraqonal	7.29	-	29.90	-	16		5.650
TlGa _{0.99} Co _{0.01} S ₂	Tetraqonal	7.29	-	29.90	-	16		5.662

Maddədə yük daşıyıcılarının elektron və ya deşik tipli olmasının birbaşa təyin edən üsul termo-e.h.q.-nın ölçülməsidir. Bir tipli yükdaşıyıcılara halında halogen yarımkəcəricilər üçün termo-e.h.q.-nın düsturu aşağıdakı şəkildədir:

$$\alpha(T) = -\frac{k}{e} \left[\frac{\Delta E}{kT} + A \right] \quad (1)$$

harada ki $A \approx 1$; ΔE -keçiciliyi aktivləşmə enerjisidir (burda qəbul olunmuşdur ki, yarımkəcərici p -tipə malikdir).

Aşağıda bizim tərəfimizdən alınmış TlGa_{0.95}Co_{0.05}S₂ birləşməsinin keçiciliyinin və termo-e.h.q.-nın temperatur asılılığının tədqiqi zamanı alınmış nəticələr verilir.

Elektrik ölçmələri üçün nümunələr paralelepiped formasında hazırlanıb. Kontaktlar vurulmamışdan əvvəl nümunələr 450K temperaturada dəmələnmişdir.

Omkı kontaktlar misin elektrolitik çökdürülməsi nəticəsində alınmışdır. Nümunələrin elektrik keçiciliyi (σ) və termo-e.h.q.-nın əmsali (α) dörd zond metodu ilə 1% dəqiqliklə 78÷400K temperatur intervalında ölçülmüşdür.

Şəkil 2-də $7.91 \times 4.56 \times 2.32 \text{ mm}^3$ ölçülü TlGa_{0.95}Co_{0.05}S₂ nümunəsinin keçiciliyinin temperaturdan asılılıq əyrisi verilmişdir. Qeyd etmək lazımdır ki, TlGa_{0.95}Co_{0.05}S₂ kristalının otaq temperaturunda qaranlıq xüsusi müqaviməti $\rho \sim 5.5 \text{ Om} \cdot \text{sm}$ təşkil edir, bu isə TlCoS₂-nin qaranlıq xüsusi müqavimətindən ($\rho = 0.33 \text{ Om} \cdot \text{sm}$) 16.7 dəfə çoxdur.

Temperatura 78-dən 400K-ə qədər artıqla TlGa_{0.95}Co_{0.05}S₂ nümunəsinin keçiciliyi azalır, bu isə keçiciliyi metallik xarakterli olması ilə müşahidə olunur. Termo-e.h.q.-nın mənfi işarəli olması tədqiq olunan nümunənin bütün öyrənilən temperatur diapazonunda n-tip keçiciliyi malik olmasına təsdiq edir. Termo e.h.q.-nın "metallik" düsturuna uyğun olaraq, temperaturun artması ilə termo e.h.q.-nın mütləq qiyməti xətti olaraq artır.

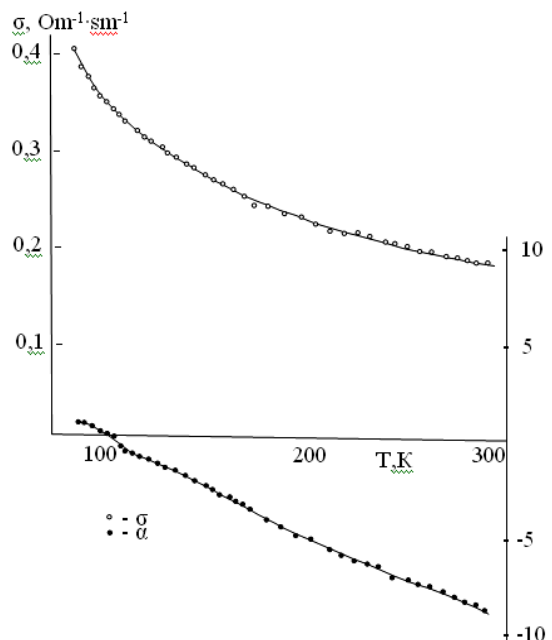
$$\alpha(T) = \frac{\pi^2}{3} \cdot \frac{k^2 T}{e} \left(\frac{\partial \ln \sigma}{\partial E} \right)_{E=E_F} \quad (2)$$

(2) düsturu ancaq $\kappa T < E_F$ olduqda doğrudur. Məlumdur ki, metallarda cərəyan daşınması (E_F) Fermi səviyyə-

si yaxınlığında qalınlığı kT tərtibində olan energetik qat-dakı yükdaşıyıcılar hesabınadır.

TlGa_{0.95}Co_{0.05}S₂-nin termo e.h.q.-nın işarəsinin dəyişmə temperaturası (100K) TlCoS₂-yə nisbətən çox aşağıdır, hardakı bu TlCoS₂ üçün 225K təşkil edir.

Belə ki, TlGa_{0.95}Co_{0.05}S₂ birləşməsi 78÷400K temperatur oblastında metallik keciciliklə xarakterizə olunur və termo-e.h.q.-nın maksimal qiyməti 10mK/V/K təşkil edir.



Şəkil 2. Ölçüləri $7.91 \times 4.56 \times 2.32 \text{ mm}^3$ olan TlGa_{0.95}Co_{0.05}S₂ nümunədə keçiciliyinin və termo-e.h.q.-nın temperaturdan asılılığı.

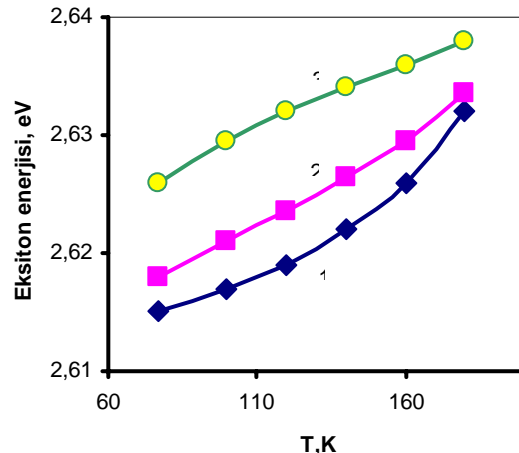
TlGa_{1-x}Co_xS₂ ($x=0; 0.005; 0.01$) tərkiblərinin udulma sərhəddinin 77÷300K temperatur intervalında bizim tərəfimizdən ölçülməsi aşağıdakılardır söyləməyə imkan verir: göstərilən bütün tərkiblərin udulma sərhəddi düz eksiton zolağı şəklində formalasılır, onların vəziyyətləri 180K temperatura qədər yüksək dəqiqliklə ayırd edilir, daha yüksək temperaturada bu zolaq cırlaşaraq pillə şəklində cevrilir və sonra silinir. Tərkibində kobalt olan bərk məhlul kristallarıda müsbət $\partial E^{ex}/\partial T$ temperatur əmsalına malikdirlər. Şəkil 3-də tətdiq olunan bütün tərkiblərin

eksiton zolağının maksimumlarının temperaturdan asılılığı gösterilmişdir. Eksitonun əlaqə enerjisinin temperaturdan asılı olaraq zəif dəyişməsini nəzərə alsaq, iddia etmək olar ki, bu kristalların qadağan olunmuş zonasının temperatur əmsali müsbət olmalıdır. Şəkilə əsaslanaraq demək olar ki, kobaltın miqdarı arttıkca $\partial E^{ex}/\partial T$ mütləq qiymətcə azalır, başqa sözlə $\partial E^{ex}/\partial T$ -də adı mənfi işarəli qiymətinə dönüşən tendensiyası müşahidə olunur. Harada ki, $\partial E^{ex}/\partial T$ -nin orta qiyməti 77÷180K temperatur intervallında TlGaS₂ üçün $1,65 \cdot 10^{-4}$ eV/K və TlGa_{0,99}Co_{0,01}S₂ üçün isə $1,16 \cdot 10^{-4}$ eV/K qədər dəyişir.

Gözlənilməz olan isə kobaltın konsentrasiyasının udulma sərhəddində eksiton zolağının maksimumunun vəziyyətinə təsiri oldu. Adətən əsas kristal-matrisaya ləğirə edici əlavə vurduqda qadağan olunmuş zonanın eninin azalması halı müşahidə olunur, hansıki bizim tərəfindən dəfələrlə qeyd olunub (bax, [5]). Bizim halda isə eksiton pikinin qısa dalgalara doğru sürüşməsi baş verir. 77K temperaturda TlGaS₂-dən TlGa_{0,99}Co_{0,01}S₂-yə keçidkən bu sürüşmə 11mēV təşkil edir. Uyğun olaraq Co atomlarının konsentrasiyasının TlGa_{1-x}Co_xS₂ bərk məhlullarında bir neçə mol faiz tərtibdə artması, bu kristalların qadağan olunmuş zonasının eninin artmasına gətirib çıxarır.

Bəsliliklə TlGaS₂ yarımkürəcili birləşmələrində Ga-nın Co-la kiçik konsentrasiyalarda əvəz olunması, bu kristalların optik xassələrinin idarə olunmasına imkan ve-

rir və buda öz növbəsində onların praktikada tətbiq olunmasına imkanı yaradır.



Şəkil 3. TlGa_{1-x}Co_xS₂ bərk məhlullarının, $x = 0; 0,005; 0,01$ qiymətlərində, sərhəd eksiton pikinin vəziyyətinin temperatur asılılığı. Harada ki, x : 1- 0; 2- 0,005; 3- 0,01.

- [1] R.Z. Sadixov, E.M. Kerimova, Yu.G. Asadov, R.K. Veliyev. Magnitnie svoystva sloistikh soedineniy TlCoS₂ i TlSoSe₂. FTT, 2000, t.42, v.8, s.1449-1450.
- [2] E.M. Kerimova, S.N. Mustafaeva, M.A. Aldjanov, A.I. Djabbarli. Temperaturnie zavisimosti provodimosti, termoeds i tephlyomnosti TlCoS₂. FNT, 2004, t.30, №4, s.395-397.
- [3] S.N. Mustafaeva, A.I. Gasanov, N.Z. Gasanov. Frequency – dependent dielectric properties of TlGa_{1-x}Co_xS₂ single crystals. Fizika, 2007, v.13, N4, p.95-97.
- [4] S.G. Abdullaeva, N.A. Abdullaev, G.L. Belenkiy, N.T. Mamedov, R.A. Suleymanov. Temperaturniy sdvig eksitonnoy polosi i deformatsionniye effekti v sloistikh kristallakh TlGaS₂. FTP, 1983, t.17, v.11, s.2068-2070.
- [5] N.Z. Gasanov, E.M. Kerimova, A.I. Gasanov, Yu.G. Asadov. Opticheskie svoystva i parametri kristallicheskoy reshetki tverdikh rastvorov TlGa_{1-x}Fe_xSe₂. FNT, 2007, t.33, №1, s.115-118.

A.I. Hasanov, E.M. Kerimova, N.Z. Hasanov, K.M. Huseynova, P.M. Iskenderova

RESEARCH OF SOLID SOLUTIONS TlGa_{1-x}Co_xS₂

It is established the interaction of system TlGaS₂-TlCoS₂ and shown the diagram of a condition of this system. It is established, that on the basis of TlGaS₂ are formed solid solutions up to 15mol. % TlCoS₂ at a room temperature.

It is investigated temperature dependences (77÷400K) of conductivity in the wide range of temperatures and thermo-e.m.f. of compounds TlGa_{0,95}Co_{0,05}S₂, and the metal course of conductivity was observed. It is established, that at 100K there is an inversion of a mark thermo e.m.f., i.e. above this temperature in TlGa_{0,95}Co_{0,05}S₂ the n-type of conductivity takes place.

It is revealed, that the edge of absorption of solid solutions TlGa_{1-x}Co_xS₂ at small concentration of cobalt is formed direct exsiton by a strip, thus the temperature factor $\partial E^{ex}/\partial T$ has a positive mark, as well as in TlGaS₂, and itself exsiton the strip direct to short-wave area at partial replacement Ga on Co.

А.И. Гасанов, Э.М. Керимова, Н.З. Гасанов, К.М. Гусейнова, П.М. Искендерова

ИССЛЕДОВАНИЕ ТВЕРДЫХ РАСТВОРОВ TlGa_{1-x}Co_xS₂

Изучено взаимодействие в системе TlGaS₂-TlCoS₂ и построена диаграмма состояния этой системы. Установлено, что на основе TlGaS₂ образуются твердые растворы до 15моль.% TlCoS₂ при комнатной температуре.

В широкой области температур (77÷400К) исследованы температурные зависимости проводимости и термо-э.д.с. соединения TlGa_{0,95}Co_{0,05}S₂, причем наблюдался металлический ход проводимости. Установлено, что при 100К происходит инверсия знака термо-э.д.с., т.е. выше этой температуры в TlGa_{0,95}Co_{0,05}S₂ имеет место n-тип проводимости.

Обнаружено, что край поглощения твердых растворов TlGa_{1-x}Co_xS₂ при небольших концентрациях кобальта формируется прямой экситонной полосой, при этом температурный коэффициент $\partial E^{ex}/\partial T$ имеет положительный знак, как и в TlGaS₂, а сама экситонная полоса сдвигается в коротковолновую область при частичной замене Ga на Co.

Received: 24.09.07

p⁺- Si ƏSASINDA YARADILMIŞ MEZOMƏSAMƏLİ SİLİSİUMDA YÜKDAŞIYICILARIN DAŞINMASI PROSESLƏRİ

H.Ə. HƏSƏNOV

MTN-in H.Əliyev adına Akademiyası

p⁺- Si əsasında yaradılmış və məsaməliliyi böyük olmayan (16÷30%) mezoməsaməli silisiumun elektrik xassələri eksperimental tədqiq edilmişdir. Alınmış nöticələr 30÷50% məsaməlilik intervalında ümumiləşdirilmişdir. Məsaməli silisium təbəqəsinin altlığa nəzərən keçiricilik tipinin dəyişilməsi effekti aşkar edilmişdir. Eksperimentin nöticələri aşqar atomlarının (bor) hidrogenlə passivləşdirilməsi modelinin köməyi ilə izah olunmuşdur. Məsaməli silisiumun elektrik xassələrinin tədqiqi zamanı istifadə olunan digər modellərin üstün cəhətləri və çatışmazlıqları araşdırılmışdır.

p - silisium altlığında formalasdırılmış mezoməsaməli strukturlu məsaməli silisium (MS) bir sıra özəl xassələrə malik olduğundan, onun tədqiq edilməsinə çoxlu sayıda işlər həsr olunmuşdur [1,2,3,4,5,6]. Verilmiş MS məsamələrinin eninə ölçüləri 1nm-dan onlarla nm-ya qədər dəyişən inkişaf etmiş sistemdir. p⁺- Si əsasında yaradılmış mezoməsaməli nümunələr p⁺- Si altlıqli mezo- və mikroməsaməli nümunələrə nisbətən daha böyük elektrik keçiriciliyinə malik olduqlarından, elektrolüminessensiya yuvacılarnın hazırlanması üçün perspektivli materiallar sayılrlar. Mezoməsaməli silisiumun strukturunu ədədi qiyməti 15÷60% intervalında dəyişən məsaməlilik göstəricisindən asılıdır. p⁺- Si əsasında yaradılmış mezoməsaməli silisiumun elektrofiziki xarakteristikalarını təyin edərkən əsas çətinliklər, birincisi, MS təbəqələrinin yüksək komplu olması, ikincisi, strukturun metal və monokristallik altlıqla sərhədlərində eksperimentin nöticələrində parametrləri nəzərə alınmalıdır olan düzləndirici keçidlərin mövcudluğudur.

Birinci mərhələdə məsaməliliyi böyük olmayan (16÷30%), sonra isə 30÷50% məsaməlilik intervalında p⁺- Si əsasında yaradılmış mezoməsaməli silisiumun elektrik xassələri eksperimental tədqiq edilmişdir.

Böyük olmayan məsaməliliyi malik olan MS nümunələri KДБ-0,03 (111) altlığında elektrokimyəvi aşılama metodu ilə plavik turşusunun 48%-li su məhlulunda $10 \frac{mA}{sm^2}$ və $15 \frac{mA}{sm^2}$ anodlaşma cərəyanı sıxlığında alınmışdır. Anodlaşma $10 \div 60$ dəqiqə müddətində aparıldığda, MS təbəqələrinin qalınlığı 15mkm-dan 60mkm-ya qədər artır. Nümunələrin çəki məsaməliliyi 16÷30% təşkil edir. Analoji anod emal rejimində plazmakimyəvi metodla formalasdırılmış «şahid» nümunələrin amortlaşmış səth təbəqəsi (AST) tamamilə ləğv edilmişdir. Beləliklə, aparılmış tədqiqatlar həm elektrofiziki parametrləri, həm də MS səthindəki amorf təbəqəni qiymətləndirməyə imkan verir. Termovakuum tozlanması metodu ilə MS və monokristallik silisiumun səthinə çəkilmiş alüminium kontakt təbəqəsi 20 dəqiqə müddətində 300°S -də təsirsiz qaz mühitində saxlanılmışdır. Çoxtəbəqəli, ölçüləri $5 \times 5 \text{mm}^2$ Al-Məs.Silisium-Monosilisium-Al test strukturları hazırlanmışdır. MS təbəqələrinin böyük fotohəssaslığını nəzərən alaraq, bütün ölçmələr qaranlıqda aparılmışdır.

MS təbəqələrinin mühüm özəlliyi onun altlığa nəzərən keçiricilik tipinin dəyişməsidir. Termozond metodu vasitəsilə aparılan ölçmələr göstərir ki, MS təbəqələr effektiv elektron keçiriciliyinə malikdirlər. Yalnız anod emalı

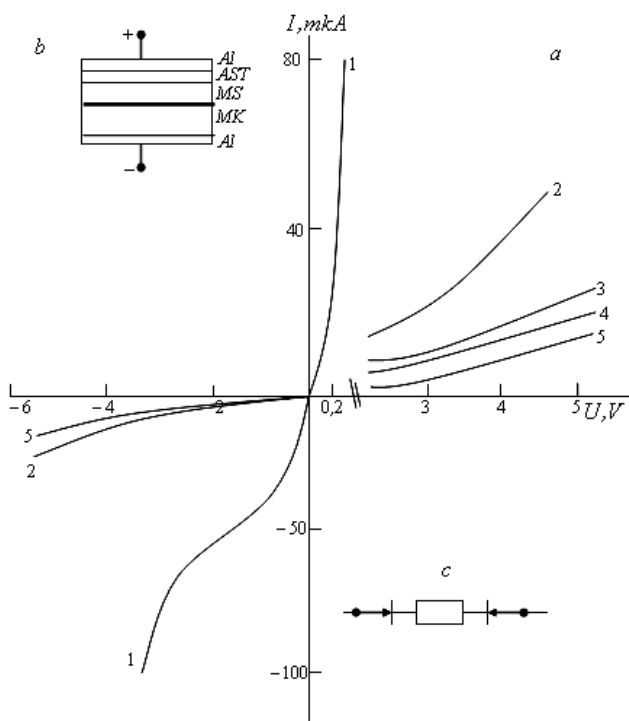
müddəti 20 dəqiqə və anod cərəyanı sıxlığı $5 \frac{mA}{sm^2}$ olan

rejimdə alınan nümunələr deşik keçiriciliyinə malik olurlar. Məhz bu cür aşağıomlu nümunələrdə Holl effektinin ölçülümləri mümkün oldu. Ölçmələr deşiklərin konsentrasiyasının başlangıç altlığa nəzərən 1-2 tərtib az olmasına aşkar çıxardı.

Anod emal zamanı MS təbəqələrinin keçiricilik tipinin dəyişməsi faktının ədəbiyyatda praktiki olaraq əksini tapmamasını qeyd etmək lazımdır. Bu barədə təkcə [11] sayılı işdə ötəri məlumatlar vardır. Effekti aşağıdakı kimi izah etmək olar. «Yumşaq» rejimdə alınan MS-in monokristallik matrisində elektrokimyəvi aşılama zamanı yükdaşıcıların konsentrasiyası azalır. Yeri gəlmışkən, Holl effektiinin ölçmələrinin nöticələri konsentrasiyanın azalması faktını təsdiq edir. MS-də deşiklərin konsentrasiyası çox sürətlə azaldıqdan, material məxsusi keçiricilik halına keçir($p \approx n$). Bu halda termo ehq-in işarəsi daha mütəhərrrik zərrəciklərin işarəsi ilə müəyyən olunur. Silisiumda elektronların yüyüklüyü deşiklərin yüyüklüyündən çox olduğundan, MS nümunələrində effektiv elektron keçiriciliyi meydana çıxır.

Al-Məs.Silisium-Monosilisium-Al strukturunun elektrik parametrlərinin təyin olunması volt-amper xarakteristikasının ölçülümləsi və təhlili əsasında yerinə yetirilmişdir. 1 sayılı şəkildə bir nümunənin misalında $120 \div 300 K$ temperatur intervalında tipik VAX göstərilmüşdür. Silisium altlığa verilən müsbət potensial düz sürüşməyə uyğun gəlir. Otaq temperaturunda düzləndirmə əmsali birdən böyük, 1V sürüşmə zamanı isə $1,3 \div 1200$ -ə bərabər olmuşdur. p-Si altlığında MS üçün bənzər VAX digər işlərdə də (məsələn, [7,8,9,10]) qeyd edilmişdir. Ancaq uzun müddət aparılan elektrokimyəvi emal zamanı ($40 \div 60$ dəq.) və amorf səth təbəqəsi (AST) ləğv edilmədikdə düzləndirmə əmsali 1-dən kiçik olur. Bundan əlavə, $25 \div 40$ dəqiqə müddətində formalasian AST-li MS-də düzləndirmə əmsali $210 K$ temperaturundan aşağı temperaturlarda 1-dən kiçik olur. Bu fakt, bir tərəfdən, AST-in strukturdan yüksəşinması prosesinə güclü təsir etməsi və Al/MS kontaktında Şottki çəpərini dəyişməsinə dəlalət edir, digər tərəfdən, strukturda bir-birinə qarşı qoşulmuş iki düzləndirici keçidin olmasından xəbər verir.

Alınmış VAX-ların tədqiqi üçün 1c sayılı şəkildə göstərilmiş ekvivalent sxemdən istifadə edilmişdir. Ekvivalent sxem iki ardıcıl birləşdirilmiş dioddan və müqavimətdən ibarətdir. Dioldardan biri MS/MK (monokristallik silisium), digəri isə Al/MS keçidlərinə uyğundur. MS/MK keçidinə müsbət gərginlik verdikdə o, düz istiqamətdə qoşulur.



Şək. 1(a). Tədqiq olunan strukturlarda VAX-in temperatur asılılıqları. MS- $j_a = 10 \frac{mA}{cm^2}$; cərəyan sıxlığında və $t_a=600$ san müddətində formalasılıb və amorf təbəqə loğv edilməyib. 1-293K, 2- 205K, 3- 160K, 4-137K, 5- 120K. b) Strukturun düz istiqamətdə qoşulması. c) Strukturun ekvivalent elektrik sxemi.

Keçidin VAX-1

$$I = j_s \cdot S \cdot \exp\left(\frac{qU_1}{nkT}\right) \quad (1)$$

düsturu ilə təsvir olunur. MS-in VAX-1

$$I = \frac{U_2}{R} = \frac{SU_2}{r} \quad (2)$$

düsturuna əsasən təyin olunur. Belə şəraitdə Şottki çöpəri tərs istiqamətdə qoşulmuşdur və generasiya-rekombinasiya mexanizmində onun VAX-1

$$I = S\beta^{-\frac{1}{2}} \cdot (\phi_0 + U_3)^{\frac{1}{2}} \quad (3)$$

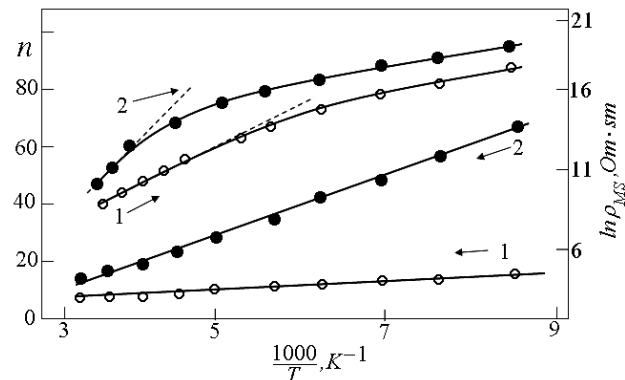
düsturu ilə müəyyən olunur. (1) və (2) düsturlarında aşağıdakı işarələrdən istifadə edilmişdir: I - strukturdan keçən cərəyan, j_s - doyma cərəyanının sıxlığı, q - elektronun yükü, n -MS/MK heterokeçidində cərəyan keçiriciliyi əmsali, U_1 - heterokeçiddə gərginlik düşgüsü, U_2 - MS təbəqəsindəki gərginlik düşgüsü, U_3 - Al/MS kontaktındakı gərginlik düşgüsü, R -MS təbəqəsinin müqaviməti, $r=RS$, β -aşqar atomların konsentrasiyası, MS-in dielektrik nüfuzluğu, yüksəkdaşıyıcıların yaşama müddətindən asılı olan əmsaldır. Al/MS kontaktı omik hesab olunur və aktiv müqavimət MS təbəqəsinin müqavimətinə (plazmakimyəvi aşilanmaya məruz qalmamış nümunələr üçün) və ya MS

təbəqəsi ilə AST-nin birgə müqavimətinə bərabərdir. Nəzərə alınmışdır ki, təbəqənin müqaviməti dar sürüşmələr intervalında sabitdir, lakin xarici gərginliyin artması zamanı dəyişir. (1)-(3) düsturlarından alınır ki, struktura verilən U gərginliyi

$$U = \left(\frac{nkT}{q} \right) \cdot \ln\left(\frac{I}{S}\right) + r\left(\frac{I}{S}\right) + \beta\left(\frac{I}{S}\right)^2 - \alpha \quad (4)$$

düsturu vasitəsilə təyin olunur. Burada,

$$\alpha = \left(\frac{nkT}{q} \right) \cdot \ln J_S + \varphi_0. \quad (5)$$



Şək. 2. AST ləğv edilmiş iki nümunədə xüsusi müqavimət və cərəyan keçiriciliyi əmsalının tipik temperatur asılılıqları.

Verilmiş halda funksional i -yə görə 1-dən s -ə qədər olan cəmə bərabər olur:

$$\Phi = \sum_{i=1}^s \left(U_i - \left(\frac{nkT}{q} \right) \ln\left(\frac{I_i}{S}\right) - r\left(\frac{I_i}{S}\right) - \beta\left(\frac{I_i}{S}\right)^2 + \alpha \right)^2. \quad (6)$$

Burada, s -VAX üzərindəki eksperimental nöqtələrin sayıdır.

VAX-in nəzəri və eksperimental qiymətlərinin üst-üstə düşdürüyü ən yaxşı şərt nəzəri qiymətlərin eksperimental qiymətlərdən meyl etməsinin kvadratından tərtib olunan funksionalın minimum olmasıdır. Funksional minimumun zəruri şərtləndən

$$\frac{\partial \Phi}{\partial r} = 0; \frac{\partial \Phi}{\partial \beta} = 0; \frac{\partial \Phi}{\partial \alpha} = 0; \frac{\partial \Phi}{\partial n} = 0 \quad (7)$$

dörd xətti tənlikdən ibarət sistem alınır. Sistemi həll etməklə (r , β , n , α) kəmiyyətləri təyin olunur. Bu kəmiyyətlərdən r və n birbaşa fiziki mənaya malikdirlər. MS-in xüsusi müqaviməti

$$\rho_{MS} = \frac{r}{d_{MS}} \quad (8)$$

düsturuna əsasən təyin olunur. Hesablamaların aparılması üçün VAX-in düz budagında eksperimental və nəzəri

asılılıqların müqayisəsindən MS-in ρ xüsusi müqaviməti, MS/MK keçidində n cərəyan keçiriciliyi əmsalını təyin etməyə imkan verən *POR* programı hazırlanmışdır. Adı çəkilən program vasitəsilə eksperimental nəticələrin təhlili göstərir ki, nəzəri və eksperimental asılılıqlar yaxşı uyğunlaşır və xəta 4%-dən böyük olmur.

AST-siz təbəqələrin təhlili göstərir ki, 15÷60 dəqiqə müddətində formalşmış MS-in xüsusi müqaviməti otaq temperaturunda, $2V$ -a qədər sürüşmələrdə $(1,4 \div 8,4) \cdot 10^5 \text{ Om} \cdot \text{sm}$ -ə bərabər olub, elektrokimyəvi emal müddətindən zəif asılıdır. Kiçik emal müddətində ρ_{MS} zalır və 10 dəqiqə anod-aşma müddətində $5 \cdot 10^3 \text{ Om} \cdot \text{sm}$ -ə bərabər olur. MS təbəqədə nazik dielektrik qat yaradan AST, xüsusi müqaviməti 1÷2 tərtib artırır. AST-in müqaviməti anod emali müddətindən asılı olub, 10 Kom-dan 40 Mom-a qədər dəyişir.

Böyük sürüşmələr oblastında VAX-in təhlili göstərdi ki, tədqiq olunmuş MS nümunələrinin xüsusi müqaviməti identik nümunələrin kiçik sürüşmələr oblastındakı xüsusi müqavimətindən bir tərtib az olur. Bu fakt böyük sahələr oblastındaki xarici sürüşmələrin artması ilə azalmağa doğru gedən MS təbəqəsi müqavimətinin qeyri-xətti xarakterinə dəlalət edir. *p-Si* əsasında MS təbəqəsinin müqavimət modulllaşması Pul-Frenkel modeli əsasında [4] sayılı işdə, fəza yükleri ilə məhdudlaşmış cərəyanlar nəzəriyyəsinə əsasən ətraflı izah edilmişdir. Birinci halda keçiriciliyin qeyri-xətti xarakteri

$$\sigma_F = \sigma_0 \cdot \exp\left(\frac{E_a}{kT}\right) \cdot \exp\left(\frac{F}{F_0}\right)^{-\frac{l}{2}}; F_0^{-\frac{l}{2}} = \frac{\left(\frac{kT}{q}\right)^{\frac{l}{2}}}{\pi \varepsilon \varepsilon_0} \quad (9)$$

düsturu ilə müyyəyən olunur. Burada, F -xarici elektrik sahəsidir. İkinci halda cərəyanın gərginlikdən qeyri-xətti asılılığı

$$I = \frac{\gamma(T)U^n}{d_{nk}^m} \quad (10)$$

düsturu vasisəsilə təsvir olunur. Burada, $\gamma(T)$ -daşıyıcıların yüyrükliyünün dəyişməsini xarakterizə edən və temperaturdan asılı olan əmsaldır. 2 sayılı şəkildə temperaturun otaq temperaturundan $120\text{ K}-ə$ qədər azalması zamanı n əmsalının və MS-in xüsusi müqavimətinin tipik dəyişmələri göstərilmişdir. Şəkildən görünür ki, $300\div200\text{K}$ temperatur intervalında xüsusi müqavimətin dəyişməsi aktivləşmiş xarakter daşıyır:

$$\rho_{MS} \sim \exp\left(-\frac{E_a}{kT}\right). \quad (11)$$

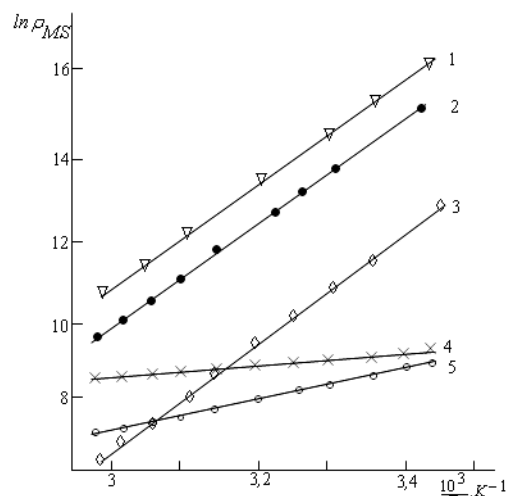
Bu düsturda E_α aktivləşmə enerjisi $200\div800\text{MeV}$ intervalında döyişir. 3 sayılı şəkildə bir neçə nümunə üçün $295\div340K$ temperatur intervalında ρ_{MS} -in temperatur asılılıqları təsvir olunmuşdur. Asılılıq əyriləri keçiriciliyin aktivləşmiş xarakterini təsdiq edir. Aktivləşmə enerjisi üçün alınan nəzəri qiymətlər azməsaməli MS nümunələri üçün [12, 13, 14] sayılı islərdə alınan nəticələrlə yaxşı uyğunlaşır.

$\rho_{MS}(T)$ -nin müşahidə olunan aktivləşmiş xarakteri yüksək məsaməli ($P>50\%$) MS-də Meyer–Neydel qaydalarını ödəmir.

AST ləğy edilmiş MS-də n cərəyan keçiriciliyi əmsalı $1,9 \div 8,3$, AST-li MS-də isə $1 \div 2,9$ intervalında dəyişir. n tətbiq olunan gərginlikdən asılı olur və gərginlik, $1,5V$ -dən $7V$ -ya qədər artanda, $2 \div 3$ dəfə artır. Temperatur aşağı düşdükdə n -in anomal yüksək qiymətlərə qədər artması müşahidə olunur (şək.2). Bu hadisənin səbəbi deşiklərin silisium allığıdan MS-yə injeksiyasının yüksək səviyyəsi ola bilər. Belə injeksiya MS təbəqəsinin müqavimətini modullaşdırır, sərhəddə lokal hallar və MS sahəsində qeyri-bircinslliliklər yaradır.

Tədqiq olunan nümunələrdə lokal elektrik sahəsinin yaranması qeyri-adi hadisələr kateqoriyasına aiddir. MS səthindəki müxtəlif kontaktlar arasında qiyməti $10 \div 100\text{mV}$ intervalında dəyişən və işıqlanmadan güclü asılı olan e.h.q. yaranır. [3] sayılı işdə bənzər hadisəni müəllif materialın qeyri-bircins strukturuna mikrosahələrin əlavə qosulması ilə izah edir.

Alınmış eksperimental nöticələr aşağıda göstərilmiş model çərçivəsində təsvir oluna bilər. p^+ -Si əsasındaki az məsaməli mezoməsaməli silisiumda məsamələr arasındakı arakəsmə 5nm-dan böyük ölçüyə malikdirlər. Bu cür kris-tallitlərdə kvant ölçü effekti olmur və yükdaşıyıcıların da-şınması klassik elektrodinamika qanunlarına uyğun ola-raq baş verir. Eyni zamanda silisium kristallik matrisində Fermi səviyyəsi qadağan olunmuş zonanın ortasına düş-dükə, yükdaşıyıcıların məxsusi keçiricilik halina gətirib çıxara bilən yoxsullaşması həyata keçir. Azməsaməli nü-munələrdə məsamələrin səth boyunca qeyri-bərabər paylanması nöticəsində dərəcələri müxtəlif olan yoxsul-laşmış oblastlar yarana bilər. Məsaməlilik göstəricisi art-dıqca MS məxsusi keçiricilik halına daha da yaxınlaşır.



Sək.3. Otaq temperaturu oblastında tədqiq olunan MS təbəqələri kecicilikinin aktivləşmiş xarakteri

$$1-j = 10 \frac{mA}{sm^2}; t_a = 20 \text{ dæq.} \quad 2-j = 15 \frac{mA}{sm^2}; t_a = 10 \text{ dæq.}$$

$$3-j = 10 \frac{mA}{sm^2}; t_a = 60 \text{ dəq.} \quad 4-j = 10 \frac{mA}{sm^2}; t_a = 10 \text{ dəq.}$$

$$5-j = 15 \frac{mA}{2}; t_a = 20 \text{ døq.}$$

$\sigma = \sigma_0 \cdot \exp\left(\frac{E_a}{kT}\right)$ asılılığının parametrləri belədir:

- 1- $\sigma_0=3 \cdot 10^{10} \text{ Om}^{-1} \text{ sm}^{-1}$; $E_a=0.8 \text{ eV}$,
- 2- $\sigma_0=4 \cdot 10^{10} \text{ Om}^{-1} \text{ sm}^{-1}$; $E_a=0.7 \text{ eV}$,
- 3- $\sigma_0=2 \cdot 10^9 \text{ Om}^{-1} \text{ sm}^{-1}$; $E_a=0.8 \text{ eV}$,
- 4- $\sigma_0=2 \cdot 10^2 \text{ Om}^{-1} \text{ sm}^{-1}$; $E_a=0.3 \text{ eV}$,
- 5- $\sigma_0=1 \cdot 10^{-1} \text{ Om}^{-1} \text{ sm}^{-1}$; $E_a=0.4 \text{ eV}$.

Yoxsullaşma effekti MS-in xüsusi müqavimətinin kifayət qədər yüksək qiymətlərini izah edir ($10^5 \text{--} 10^6 \text{ Om} \cdot \text{sm}$). Belə sistemdəki daşınma prosesləri valent və keçiricilik zonalarının potensial relyefinin fluktasiyalarına malik olan qeyri-bircins yarımkəcəricilər modeli çərçivəsində izah edilmiş bilər [15].

p^+ -Si əsasında formalasdırılmış azməsaməli mezoməsaməli silisiumda məsamələr arasında arakəsmənin deşiklər tərəfindən yoxsullaşdırılması müləhizəsi hazırda ədəbiyyatda ciddi müzakirə olunur, ancaq hələlik konkret nəticə yoxdur. Təklif edilən hipotezlərdən 4-ü öz təsdiqini daha çox tapır. Bunlardan birincisi aşqar atomların (bor) hidrogenlə passivləşdirilməsi metodudur. Təqdim olunmuş işdə, [3, 4] sayılı işlərdə məhz bu model tətbiq olunmuşdur. Mezoməsaməli silisium halında anodlaşmanın hətta azacıq müddəti hidrogen atomlarının arakəsmələrə daxil olaraq Si-H-B neytral kompleksini yaratmasına Kifayət edir. Belə yanaşma yüksək passivləşmə səviyyəsi, termik emal zamanı MS-in keçiriciliyinin dəyişməsini yaxşı izah etsə də, bəzi MS təbəqələrinin infraqırmızı buraxma spektrində, 1900 cm^{-1} oblastında, Si-H-B neytral kompleksinin xarakterik udulma pikinin olmaması bu metodun əleyhinədir. MS/MK ikitəbəqəli strukturunda belə pik müşahidə olunmuş və MS təbəqəni altlıqdan ayırdıqda yaranan istilik və ya deformasiya zərbəsi nəticəsində aşqar atom-hidrogen kompleksi məhv edilmişdir. Son illərdə aşqar atomlarının elektrik xassələrini fəallıqdan məhrum edən ionlaşma enerjisinin artması effekti əsasında yaradılan model intensiv tətbiq olunur. Ölçüsü A olan sferik nanozərrəcikdə yükdaşıyıcısının aşqar atomundan qopması üçün lazım olan E_b enerjisi

$$E_b = \left(\frac{1}{\varepsilon_{mdn}} + \frac{1,44}{\varepsilon_{sdn}} \right) \cdot \left(\frac{e^2}{A} \right) \quad (12)$$

düsturuna əsasən təyin olunur. Burada, ε_{sdn} - silisium monokristallitlərinin dielektrik nüfuzluluğu, ε_{mdn} - ətraf mühitin dielektrik nüfuzluluğudur. Belə yanaşma [16] sayılı işin müəllifləri tərəfindən p^+ -Si əsasındaki mezoməsaməli silisiumda elektrik keçiriciliyinin məsamələri dielektrik nüfuzluluğu artan mühitlərlə doldurluqda (vakuum üçün 1-dən etanol üçün 24-ə qədər) böyüməsini izah etmək üçün tətbiq edilmişdir. Quptanın işlərində [17] elektron

paramaqnit rezonansının tədqiqi sayəsində aşqar bor atomlarının MS-də elektrik fəallığını itirməsinin başqa bir səbəbi də təklif olunmuşdur. Göstərilmişdir ki, məsamə yaranması prosesini müşayiət edən mexaniki gərginliklər aşqar bor atomlarını düyünlərarası fəzadan çıxararaq, onları passiv hala salmağa qadirdirlər. Aşqar bor atomlarının MS-də passivləşməsinin dördüncü hipotezi aşqar atomların elektrik fəallığına kristallitlərin səthinin təsiri ilə əsaslandırılır.

18 sayılı işdə göstərilmişdir ki, elektrokimyəvi emal zamanı bor atomları məsamə səthində yaxın yerləşdikdə (1-3 atom təbəqələri) silisiumun lokal aşilanması dayanır. Səthə Bor radiusundan yaxın məsafədə yerləşən aşqar atomları akseptor xassələrini itirirlər. Baxılan 4 hipotezin hər birinin həm müsbət, həm də mənfi cəhətləri vardır və çox güman ki, MS-də yoxsullaşma yaranan universal vahid səbəb axtarmaq mənasızdır. MS-in struktur xarakteristikaları rəngarəng olduğundan, yoxsullaşmanı bir səbəb və ya bir neçə səbəbin birlikdə yaratması mümkünür.

Sonrakı eksperimentlər göstərdi ki, azməsaməli ($P < 30\%$) silisium strukturları üçün nəzərdə tutulan ikiçəpərli model daha böyük məsaməliliklərdə də ($P < 50\%$) mezoməsaməli silisiumun xassələrini təsvir edə bilər. Tədqiq olunan $3 \div 11 \text{ mkm}$ qalınlıqlı MS nümunələri plavik turşusunun 40%-li su məhlulu və izopropil spirtinin 1:1 nisbətindəki qarışığında alınmışdır. (111) oriyentasiyalı KDB-0,03, KDB-1 markalı silisium altlıqlardan istifadə edilmişdir. Nümunələrin məsaməliliyi 30-50% təşkil edir. MS səthinə ölçülüri $1 \times 1 \text{ mm}^2$ olan alüminium və indium kontaktlar çəkilib. In/MS/MK/Al və Al/MS/MK/Al strukturlarının VAX-1 qaranlıq şəraitdə $295 \div 350 \text{ K}$ temperatur intervalında çəkilmişdir. VAX qeyri-xəttiliyi və qeyri-simetrikliliyi ilə xarakterizə olunur; düzləndirmə əmsali (MS-dəki + müsbət sürüşmə kimi götürülür) eyni strukturun müxtəlif metallarla kontaktında vahiddən kiçik və ya böyük qiymətlər ala bilir. Cox-Strek metodunun ölçmələri ilə indium və alüminium kontaktların omik olmaması isbat edilmişdir. İkiçəpərli model və POR kompüter programının tətbiqi göstərdi ki, nəzəri və eksperimental asılılıqdar arasındaki fərq 10%-i aşmir. Müxtəlif metallar üçün VAX-in fərqli görünüşü olsa da, eyni MS təbəqəli In/MS/MK/Al və Al/MS/MK/Al strukturların xüsusi müqavimətləri eyni qiymətə malik olur. Bu fakt seçilmiş modelin düzgünlüyü və ρ_{MS} qiymətlərinin həqiqiliyinə dəlalət edir. Verilmiş eksperimentdə MS təbəqələrinin xüsusi müqaviməti $10^5 \div 10^7 \text{ Om} \cdot \text{sm}$ təşkil edir. ρ_{MS} -in temperatur asılılığı və $320 \div 680 \text{ meV}$ intervalında qiymətləndirilən aktivləşmə enerjisi aktivləşmiş xarakterə malikdirlər. Azməsaməli mezoməsaməli silisium halında olduğu kimi, $\rho_{MS}(T)$ asılılığının da aktivləşmiş xarakteri yüksəkməsaməli silisium üçün Meyer-Neldel qaydasından fərqlənir.

-
- [1] R.C.Anderson, R.S.Muller, C.W. Tobias. *Investigations of the electrical properties of porous silicon // J. Electrochem. Soc.- 1991.- V.138.- P.3406-3411.*
 - [2] L.A.Balagurov, D.G.Yarkin, E.A. Petrova. *Electronic transport in porous silicon of low porosity made on a p+ substrate // Mater. Sc. and Engin.- 2000.- V.B69-70.- P.127-131.*
 - [3] C. Cadet, D. Deremes, D. Vuillaume et al. *Appl. Phys.Lett.- 1994.- V.64.- P.2827-2829.*
 - [4] M. Ben-Chorin, F. Muller, F. Koch. *Phys. Rev. B.- 1994.- V.49.- P.2981-2984.*
 - [5] J.J. Mares, J. Kristofik, J. Pangras et al. *Appl. Phys. Lett.- 1993.- V.63.- P.180-182.*
 - [6] J.T.Lue, C.S.Chang, C.Y. Chen et al. *Thin Sol. Films.- 1999.- V.399.- P.294-298.*
 - [7] Д.Г. Яркин ФТП.- 1999.- Т.33.- С.211-214.
 - [8] M.Ben-Chorin, A.Kux, I.Schechter. *Appl. Phys. Lett.- 1994.- V.64.- P.481-483.*

Н.Э. НӘСӘНОВ

- [9] A.B.Жерзев, В.Х.Кудоярова, А.В.Медведев и др. Письма в ЖТФ.- 1993.- Т.19, вып.23.- С.87-90.
- [10] E.C.Yen, J.H.Chan, T.H. Shien et al. Phys. Stat. Sol. (a).- 1998.- V.165.- P.63-65.
- [11] J.I.Pankove, P.J.Zanzucchi, C.W. Magee et al. Appl. Phys. Lett.- 1985.- V.46.- P.421-423.
- [12] V.Lehmann, F.Hofmann, F. Muller et al. Thin Sol. Films.- 1995.- V.255.- P.20-22.
- [13] A.Diligenti, A.Nannini, G. Pennelli et al. Appl. Phys. Lett.- 1996.- V.68.- P.687- 689.
- [14] R.Schwarz, F.Wang, M.Ben-Chorin et al. Thin Sol. Films.- 1995.- V.255.- P.23-26.
- [15] Б.И.Шкловский, А.Л.Эфрос. Электронные свойства легированных полупроводников.- М.: Наука, 1979.- 416с.
- [16] V.Yu. Timoshenko, V.Lysenko, Th. Dittrich et al. Phys. Stat.Sol (a).- 2000.- V.182.- P.163-168.
- [17] C.L. Gupta. J. Appl. Phys.- 1994.- V.76.- P.4800-4804.
- [18] G.Polisski, D.Kovalev, G.Dollinger et al. Physica B.- 1999.- V.273-274.- P.951-954.

H.A. Hasanov

TRANSITION OF CHARGE CARRIERS CHARGEHOLDERS IN MEZOPOROUS SILICON MADE ON BASE OF p^+ -Si

In this article the electrical properties of mezoporous silicon which is made on the base of p^+ -Si and having not broad porosity (16÷30%), were researched experimentally. Acquired results have been summarized between 30-50% interval of porosity. The change effect of conductivity type relative to base has been detected. The results of experiment were explained by passivation model of admixture atoms with hydrogen. The advantages and areas of improvement of other models used to study electrical properties of porous silicon were analyzed.

Г.А. Гасанов

ПЕРЕНОС НОСИТЕЛЕЙ ЗАРЯДА В МЕЗОПОРИСТОМ КРЕМНИИ НА ОСНОВЕ p^+ -Si

Приведены результаты экспериментального исследования электрических свойств мезопористого кремния на основе p^+ -Si подложек на слоях с невысокой пористостью (16-30%), а затем эти результаты были распространены на диапазон пористости 30-50%. Важная особенность изучаемых слоев ПК заключалась в смене типа проводимости по сравнению с исходной подложкой. Результаты экспериментов обоснованы на основе модели пассивации примесных атомов (бор) водородом. Анализированы преимущества и недостатки других моделей, применяемых при изучении электрических свойств пористого кремния.

Received: 15.11.07

Fizika

**Azərbaycan Milli Elmlər Akademiyası
Fizika-Riyaziyyat və Texnika Elmləri Bölməsi
Fizika İnstitutu**

M ÜNDƏRİ CAT

Yüksək gərginlikli qisa impulsların bərk cisim halında olan dielektriklərə və yüksək sıxlıqlı qazlara təsiri zamanı elektronların hərəkətinin lokal və qeyri-lokal kriteriyaları.....	3
.....E.D. Qurbanov, I.P.Kujekin, A.M.Həşimov, A.S.Bondyakov	
Kompleks sindırma əmsallı əks etdirməyən optik örtüklerin spektral xarakteristikaları.....	9
.....R.Ə. Kərəməliyev, R.M. Qasimov	
Ge/Ge _{1-x} Si _x geterostrukturlarında kombinasion səpilmə spektrləri.....	12
.....Ş.M. Abbasov, A.S. Baysar, Z.A. İbrahimov, G.T. Ağaverdiyeva, L.A.Taibov, U.F. Fərəcovə	
İnversiya zonasında Pb _{1-x} Sn _x Te heteroquruluşlarının faza keçidi.....	
.....A.A. Ağasiyev, E.S.Qarayev, S.N.Sərməsov	15
Nəmişliyin nazik təbəqəli məsaməli silisiyumun optik və elektrik xassələrinə təsiri	
.....T.D. Cəfərov, S. Aydın, C. Oruc Lus	17
Bioloji sistemlərdə UB şüaların piqmentə təsiri və piqmentin rolü.....	
.....R.B. Aslanov, R.L. Məmmədova	21
“Zəif qeyri-abelizasiya yaxınlaşmasında mezonların paylanması funksiyaları və $F_K(Q^2)$ -ə üstlü düzəlişlər.....	24
.....Y.V. Məmmədova	
Faza kvazisinxronizm rejimində işləyən yüksək effektli lazer tezlik çeviriciləri	
.....Z.H.Tağıyev, N.V. Kərimova, R.C. Qasimova, Q.Ə. Səfərova, M.Ə. Məmmədov	29
Aqar gelinin özlü-elastik xassələrinin rebinder üsulu ilə öyrənilməsi.....	
.....E.Ə. Məsimov, A.R. İmaməliyev, K.M. Budaqov	32
Paylanması əmsalı vahiddən böyük olduqda yeni üsulla düzəldilmiş xəlitənin başlangıcının qidalandırıcının başlangıcı götürməklə bərk məhlul monokristallarının alınması.....	
.....V.İ. Tahirov, Z.Ə. Ağamalıyev, Z.Y. Həsənov, Ə.F. Quliyev, N.F. Qəhrəmanov	35
Tərkibində samarium aşqarı olan Se ₉₅ As ₅ - şüşəvari halkogenid yarımkeçirici sistemlərində fəza yükleri ilə məhdudlanmış cərəyanlar.....	
.....A.İ. İsayev, S.İ. Mehdiyeva, N.Z. Cəlilov, R.İ. Ələkbərov	41
Fotoyarımkeçiricinin mikrozərrəciklərinin səthə yaxın oblastının xlor atmosferində termik işləməklə leqirə edilməsinin triqonal Se-nin əlaqələndiricidə EF laylarının parametrlərinə təsiri.....	
.....N.İ. İbrahimov, V.H. Ağayev	45
Kristallaşmanın temperatur - zaman rejiminin PVDF+Fe ₃ O ₄ əsasında polimer maqnit nanokompozitlərinin mexaniki möhkəmliyinə və quruluşuna təsiri.....	
.....M.Ə. Ramazanov, P.B. Ağakışiyeva, S.A. Abasov, R.A. Əlizadə	47
Tetraqonal-volfram tunc strukturlu bərk məhlulların strukturu və seqnetoelektrik xassələri.....	
.....R.Z. Mehdiyeva, Ə.İ. Məmmədov	50
Supramolekulyar evtektikalar fizikasında fraktal konsepsiyası.....	
.....F.K. Ələsgərov, S.Ş. Qəhrəmanov, E.D. Moroydor, M.Q.Pişkin	52
ASPE+x həcm% TlGaTe ₂ (TiInSe ₂) kompozisiyalarının alınması və elektret xassələrinin	

öyrənilməsi. . E.M. Qocayev, Ş.A. Zeynalov, S.S. Osmanova, E.A. Allahyarov, O.A. Hümbətov Polimer və Cu ₂ S , CdS nanozərrəcikləri əsasında olan kompozitlərin qaza həssaslığı.	57
.....M.B. Muradov, M.A. Nuriyev, Q.M. Eyvazova Se-S sisteminin amorf bərk məhlullarının volt-amper xarakterisi.	59
.....N.Z. Cəlilov, Q.M. Dəmirov, N.R. Məmmədov Polipropilen və MnO ₂ əsasında alınmış kompozisiyaların mikroquruluşuna və möhkəmlik xassələrinə elektrotermopolyarlaşmanın təsiri. M.A. Ramazanov, A.C. Hüseynova, F.V. Hacıyeva İfrat sürətlə tablandırılmış TiNi əsaslı çoxkomponentli ərintilərində kristallaşma temperaturu yaxınlığında mexaniki xassələr. M.B. Babanlı	62
Todanın ümumiləşdirilmiş modeli. M.A. Muxtarov Ag _{2-x} Cu _{0+x} S (x=0.45; 0.8; 1.07) birləşməsində polimorf çevrilmələr. Y.İ. Aliyev, A.Q. Babayev, F.Q. Məhərrəmovə TlGa _{1-x} Co _x S ₂ bərk məhlullarının tədqiqi	64
.....A.İ. Həsənov, E.M. Kərimova, N.Z. Həsənov, K.M. Hüseynova, P.M. İsgəndərova p ⁺ -Si əsasında yaradılmış mezoməsaməli silisiumda yükdaşıyıcıların daşınması prosesləri. H.Ə. Həsənov	67
.....	74
.....	78
.....	85
.....	88

СОДЕРЖАНИЕ

Локальный и нелокальный критерии убегания электронов в плотных газах и твердых диэлектриках при воздействии коротких импульсов высокого напряжения.	3
.....Э.Д. Курбанов, И.П. Кужекин, А.М. Гашимов, А.С. Бондяков	
Спектральные характеристики антиотражающих оптических покрытий с комплексным показателем преломления. Р.А.Карамалиев, Р.М.Касимов	9
Спектры комбинационного рассеяния в гетероструктурах Ge/Ge _{1-x} Si _x	
.....Ш.М. Аббасов, А.С. Байцар, З.А. Ибрагимов, Г.Т. Агавердиева, Л.А. Таиров, У.Ф. Фараджова	12
Поведение фазового перехода в Pb _{1-x} Sn _x Te вблизи инверсии зон.	
.....А.А. Агасиев, Э.С.Гараев, С.Н. Сармасов	14
Влияние влажности на оптические и электрические свойства тонких пленок пористого кремния. .	
.....Т.Д. Джадаров, С.Айдын, Дж. Орудж Лус	17
Воздействие уф сета на пигмент в биологических системах и роль пигмента.	
.....Р.Б. Асланов, Р.Л. Мамедова	21
Функции распределения мезонов в приближении «наивной неабелизации» и степенно-подавленные поправки к $F_K(Q^2)$ Е.В. Мамедова	24
Высокоэффективные преобразователи частоты лазерного излучения в режиме фазового квазисинхронизма. З.А. Тагиев, Р.Дж. Касумова, Г.А. Сафарова, М.А. Мамедов, Н.В. Керимова	29
Изучение упруговязких свойств гелей агара методом Ребиндера.	
.....Э.А. Масимов, А.Р. Имамалиев, К.М. Будагов	32
Получение бинарных твёрдых растворов монокристаллов использованием начала новым методом полученного подпитывающего слитка как начала подпитки при k>1.	
.....В.И. Тагиров, З.А. Агамалыев, З.Ю. Гасанов, А.Ф. Гулиев, Н.Ф. Гахраманов	35
Токи, ограниченные пространственными зарядами в халькогенидных стеклообразных полупроводниках системы Se ₉₅ As ₅ содержащие примеси самария.	
.....А.И. Исаев, С.И. Мехтиева, Н.З. Джалилов, Р.И. Алекперов, В.З. Зейналов	41
Влияние легирования приповерхностных областей микрочастичек фотополупроводника отжигом в атмосфере хлора на электрофотографические (EF) параметры слоёв тригонального Se в связующем. Н.И. Ибрагимов, В.Г. Агаев	45
Влияние температурно-временного режима кристаллизации на механическую прочность и на структуру полимерных магнитных нанокомпозитов на основе ПВДФ+Fe ₃ O ₄	
.....М.А. Рамазанов, П.Б. Агакишиева, С.А. Абасов, Р.А.Али-Заде	47
Структура и сегнетоэлектрические свойства в твердых растворах со структурой тетрагональной вольфрамовой бронзы. Р.З. Мехтиева, А.И. Мамедов	50

Концепции фрактала в физике супрамолекулярных эвтектик	52
..... Ф.К. Алескеров, С.Ш. Каҳраманов, Е.Д. Моройдор, М.Г. Пишкин	
Получение и изучение электретных свойств композиций ПЭНП+х об.% TlGaTe ₂ (TlInSe ₂)	
..... Э.М. Годжаев, Ш.А. Зейналов, С.С. Османова, Е.А. Аллахяров, О.А. Гумбатов	57
Газочувствительность композитов на основе полимеров и наночастиц Cu ₂ S и CdS	
..... М.Б. Мурадов, М.А. Нуриев, Г.М. Эйвазова	59
Вольт-амперные характеристики аморфных твердых растворов системы Se-S	
..... Н.З. Джалилов, Г.М. Дамиров, Н.Р. Меммедов	62
Влияние электротермополяризации на микроструктуры и прочностные свойства композиций на основе полипропилена и MnO ₂	
..... М.А. Рамазанов, А.С. Гусейнова, Ф.В. Гаджиева	64
Механические свойства быстрозакаленных многокомпонентных сплавов на основе Ti-Ni вблизи температуры кристаллизации	
..... М.Б. Бабанлы	67
Обобщенные модели Тода	
..... М.А. Мухтаров	74
Полиморфные превращения в Ag _{2-x} Cu _{0+x} S(x=0.45; 0.8; 1.07)	
..... Ю.И. Алыев, А.Г. Бабаев, Ф.Г. Магеррамова	78
Исследование твердых растворов TlGa _{1-x} Co _x S ₂	
..... А.И. Гасанов, Э.М. Керимова, Н.З. Гасанов, К.М. Гусейнова, П.М. Искендерова	85
Перенос носителей заряда в мезопористом кремнии на основе p ⁺ -S	
..... Г.А. Гасанов	88

CONTENTS

Local and nonlocal criterions of runaway electrons in solid gases and dielectrics under action of high voltage pulses by short wavefront	3
..... E.D. Gurbanov, I.P.Kuzhekin, A.M. Hashimov, A.S. Bondyakov	
Spectral characteristics of antireflective optical coatings with complex refractive indexes	
..... R.A. Karamaliyev, R.M. Kasimov	9
Raman spectra in heterostructures Ge/Ge _{1-x} Si _x	
..... Sh.M. Abbasov, A.S. Baytsar, Z.A. Ibrahimov, K.T. Agaverdiyeva, L.A. Taibov, U.F. Farajova	12
Behavior of phase transition in near inversion zone of Pb _{1-x} Sn _x Te	
..... A.A. Aqasiyev, E.S. Garayev, S.N. Sarmasov	15
Effect of humidity on optical and electrical properties of free standing porous silicon films	
..... T.D. Dzhafarov, S. Aydin, C. Oruc Lus	17
The effect of uv light on pigmented in biological systems and the role of pigment	
..... R.B. Aslanov, R.L. Mamedova	21
Mesons distribution functions in the “naive-non-abelianization” approximation and power-suppressed corrections to F _K (Q ²)	
..... Y.V. Mamedova	24
High efficiency laser radiation frequency converters in quasi-phase –matched regime	
..... Z.H. Tagiev, R.J. Kasumova, G.A. Safarova, M.A. Mamedov, N.V. Kerimova	29
The investigation of elastoviscous properties of agar gels by Rebinder’s method	
..... F.A. Masimov, A.R. Imamaliyev, K.M. Budagov	32
Obtaining of binary solid solution single crystals using the beginning of the feeding ingot as replenishment beginning at k>1 by new method	
..... V.I. Tagirov, Z.A. Agamaliyev, Z.Y. Hasanov, A.F. Quliyev, N.F. Qahramanov	35
The currents, limited by the space charges in chalcogenide vitreous semiconductors of Se ₉₅ As ₅ system, containing the samarium impurities	
..... A.I. Isayev, S.I. Mekhtiyeva, N.Z. Jalilov, R.I. Alekperov, V.Z. Zeynalov	41
The doping influence of near-surface regions of photosemiconductor microparticles by annealing in chlorine atmosphere on the electrophotographical (EF) parameters of trigonal Se layers in the bonding solution	
..... N.I. Ibragimov, V.G. Agayev	45
The influence of temperature – time crystallization mode on the mechanical strength and on the structure of polymeric magnetic nano-composites on pvdF+Fe ₃ O ₄ basis	
..... M.A. Ramazanov, P.B. Agakishiyeva, S.A. Abbasov, P.A. Ali-zade	47
The structure and ferroelectric properties in the solid solutions with the structure of tetragonal tungsten bronze	
..... R.Z. Mekhtiyeva, A.I. Mamedov	50

The conceptions of the fractal in the physics of supramolecular eutectics.....	52
..... F.K. Aleskerov, S.Sh. Kakhramanov, E.D. Moroydor, M.G. Pishkin	
The obtaining and studying of electret properties of PELD+x vol.% TlGaTe ₂ (TlInSe ₂) compositions.....	57
..... E.M. Godjayev, Sh.A. Zeynalov, S.S. Osmanova, E.A. Allakhyarov, O.A. Gumbatov	
The composite gas sensitivity on the basis of polymers and Cu ₂ S and CdS nanoparticles.....	59
..... M.B. Muradov, G.M. Eyvazova, M.A. Nuriyev	
The volt-ampere characteristics of amorphous solid solutions of Se-S system.....	62
..... N.Z. Djalilov, G.M. Damirov, N.R. Mamedov	
The influence of electrothermopolarization on the microstructures and composition strength properties on the basis of polypropylene and MnO ₂	64
..... M.A. Ramazanov, F.V. Gadgiyeva, A.S. Guseynova	
The mechanical properties of rapid-hardened multi-component alloys on tini basis near crystallization temperature.....	67
..... M.B. Babanli	
Generalized Toda models.....	74
..... M.A. Mukhtarov	
Polymorphic transformations in Ag _{2-x} Cu _{0+x} S(x=0.45;0.8; 1.07).....	78
..... Y.İ. Aliyev,A.G. Babayev, F.G. Magerramova	
Research of solid solutions TlGa _{1-x} Co _x S ₂	85
..... A.I. Hasanov, E.M. Kerimova, N.Z. Hasanov, K.M. Huseynova, P.M. Iskenderova	
Transition of charge carriers in mezoporous silicon made on base of p ⁺ -Si.....	88
..... H.A. Hasanov	